Modélisation de l'infiltration chimique en phase vapeur, CVI isotherme et isobare : étude de l'infiltration d'un pore rectiligne par diverses céramiques

Roland Fédou

N° d'ordre : 792

THÈSE

PRESENTÉE A

L'UNIVERSITÉ DE BORDEAUX I

POUR OBTENIR LE GRADE DE

DOCTEUR

SPÉCIALITÉ : SCIENCES DES MATÉRIAUX

PAR

Roland FÉDOU

INGÉNIEUR E.N.S.C.P.B.

MODÉLISATION DE L'INFILTRATION CHIMIQUE EN PHASE VAPEUR (CVI) ISOTHERME ET ISOBARE. ÉTUDE DE L'INFILTRATION D'UN PORE RECTILIGNE PAR DIVERSES CÉRAMIQUES

Soutenue le 27 février 1992, devant la Commission d'Examen :

MM.	P. HAGENMULLER	*Président*
	M. DUCARROIR	
	J.-P. CALTAGIRONE	
	H. GASPAROUX	*Examinateurs*
	F. CHRISTIN	
	R. NASLAIN	
	F. LANGLAIS	

- 1992 -

A Florence,

A ma Mère, A mon Père,

A mon Frère, A ma Famille,

Témoignage de ma profonde
affection et reconnaisance.

A mes amis,
A tous ceux qui me sont chers.

Tout homme qui dirige, qui fait quelque chose, a contre lui ceux qui voudraient faire la même chose, ceux qui font précisément le contraire et surtout la grande armée des gens plus sévères, qui ne font rien.

Claretie Jules, romancier et auteur dramatique français né à Limoges 1840-1913

Ce travail a été réalisé au Laboratoire de Chimie du Solide du CNRS puis au Laboratoire des Composites Thermostructuraux (Unité Mixte de Recherche 47 CNRS-SEP-Université de Bordeaux 1)

Je remercie vivement Monsieur le Professeur Paul HAGENMULLER pour l'intérêt scientifique qu'il a porté à ce travail, et pour avoir accepté d'être le Président de mon jury de thèse.

Monsieur Michel DUCARROIR, Directeur de Recherches du CNRS à l'Institut de science et de génie des Matériaux et Procédés (I.M.P.) du CNRS, a bien voulu me faire l'honneur de juger mon travail. Je le prie d'accepter l'expression de ma respectueuse reconnaissance.

Monsieur Jean-Pierre CALTAGIRONE, Professeur à l'Ecole Nationale Supérieure de Chimie et de Physique de Bordeaux (E.N.S.C.P.B.) et responsable du Laboratoire de Modélisation Avancée des Systèmes Thermiques et des Écoulements Réels m'a fait l'honneur d'examiner ce travail. Je tiens à lui exprimer mes remerciements les plus vifs.

Monsieur le Professeur Henry GASPAROUX, Directeur de l'Ecole Nationale Supérieure de Chime et de Physique de Bordeaux (E.N.S.C.P.B.), m'a fait l'honneur de participer à mon jury de thèse. Il m'est particulièrement agréable de lui adresser mes remerciements les plus sincères.

Monsieur François CHRISTIN, Chef du Département Développement Matériaux à la Société Européenne de Propulsion, après avoir suivi avec intérêt ce travail, a aimablement accepté de participer à mon jury de thèse, qu'il reçoive ici l'expression de mes vifs remerciements.

Monsieur le Professeur Roger NASLAIN, Directeur du Laboratoire des Composites Thermostructuraux m'a accueilli au sein de son équipe de recherche. Qu'il trouve ici

le témoignage de ma profonde gratitude.

Monsieur Francis LANGLAIS, Chargé de Recherches au CNRS, a dirigé ce travail. Il m'a permis de mener à bien cette étude grâce à ses compétences scientifiques, sa pondération et ses qualités humaines. Travailler avec lui fut un grand plaisir. Je tiens à lui assurer ma très profonde gratitude.

C'est avec un grand plaisir que j'exprime de sincères remerciements aux membres passés et présents du L.C.S. et du L.C.T.S., qui ont contribués par leur collaboration amicale, leur sympathie et leur bonne humeur, à créer une ambiance de travail agréable.

Je tiens à remercier, particulièrement, Monsieur Claude PRÉBENDÉ pour ses conseils et son enseignement précieux sur l'installation de CVD. J'aimerais également citer Monsieur Didier LESPIAUX, Mademoiselle Fabienne LOUMAGNE, Messieurs Stéphane PROUHET, Olivier DUGNE et Didier MOCAER. Ma gratitude va aussi à ceux qui ont plus particulièrement collaboré à ce travail : Etienne SIPP et Francis REBILLAT pour l'étude de l'infiltration des oxydes et Pascal DUPEL pour l'étude de l'infiltration de pyrocarbone.

Je ne saurais oublier Monsieur Louis ALBINGRE, pour son assistance technique et sa gentillesse, lorsque j'étais au Laboratoire de Chimie du Solide.

Mes remerciements s'adressent aussi à Mesdames Monique GEORGY, Josette FORGET et Florence DUCASSE toujours disponibles avec le sourire. Je tiens également à remercier Josette FORGET et Cécile DUPOUY pour leur contribution à la réalisation de ce mémoire.

J'adresse aussi mes remerciements à la SEP, au Ministère de l'Education Nationale de la Jeunesse et des Sports (MENJS) et à la Communauté Européenne (Contrat EURAM) pour leur soutien, grâce auquel cette étude a été menée.

SOMMAIRE

Chapitre 2 :A MODELING OF THE ISOTHERMAL ISOBARIC CHEMICAL VAPOR INFILTRATION IN A STRAIGHT CYLINDRICAL PORE PART 2 - APPLICATION TO THE CVI OF SiC

Chapitre 3 :A MODELING OF THE ISOTHERMAL/ISOBARIC CHEMICAL VAPOR INFILTRATION IN A STRAIGHT CYLINDRICAL PORE PART 3 : APPLICATION TO THE CVI OF ZIRCONIA OR YTTRIA

INTRODUCTION GÉNÉRALE

1- LES COMPOSITES FIBREUX

1.1 *Les composites à matrice organique*
1.2 Les Composites à Matrice Métallique (CMM)
1.3 Les Composites à Matrice Céramique (CMC)

2 - ÉLABORATION DES CMC

2.1 Les différentes méthodes d'élaboration
2.2 - Procédés d'élaboration par voie gazeuse

3 - OBJECTIFS ET CONTENU DU MÉMOIRE

INTRODUCTION GÉNÉRALE

Un matériau composite est un matériau polyphasé dans lequel deux ou plusieurs constituants sont associés en vue de lui conférer un ensemble original de propriétés que les constituants, pris isolément, ne permettent pas d'atteindre [1]. Cette idée consistant à associer plusieurs matériaux en contact intime à l'échelle microscopique n'est pas nouvelle : il existe depuis longtemps dans la nature des structures composites comme le bois, et ce n'est que très récemment que l'homme a élaboré des matériaux composites synthétiques. Il existe une grande variété de composites se différenciant par (i) la morphologie d'un ou de plusieurs de ses constituants (sphères, trichites (whiskers), fibres, filaments), (ii) la nature respective de ses constituants (matériau organique, verre, alliage métallique, céramique), (iii) leur agencement relatif (distribution aléatoire, planaire, alignements parallèles (1D) ou tissages 2D, ..nD), et (iv) la nature des propriétés recherchées (électriques, magnétiques, optiques, mécaniques ...). Les propriétés de ces matériaux proviennent non seulement des propriétés intrinsèques des constituants, mais aussi des couplages (e.g. de type mécanique) existant au niveau des interfaces entre deux constituants ayant des propriétés ou des caractéristiques différentes. Le présent mémoire est plus particulièrement consacré à une étude concernant l'élaboration de composites appartenant à la famille des composites dits structuraux, pour lesquels on cherche sans cesse à améliorer les caractéristiques mécaniques spécifiques, et à élargir le domaine d'application et d'utilisation (température, atmosphère chimiquement agressive, ...). Les composites structuraux associent le plus couramment (i) un renfort, généralement constitué de fibres, principalement destiné à supporter les charges mécaniques appliquées au matériau, et (ii) une matrice dont le rôle principal est de permettre un bon transfert des charges sur le renfort, mais qui doit aussi assurer un rôle de liant et de protection du renfort contre les diverses agressions extérieures (chimiques comme l'oxydation, mécaniques, ...). C'est ainsi que les matrices métalliques sont renforcées par des fibres en céramique afin d'être rigidifiées alors que les matrices céramiques peuvent être associées à des fibres métalliques pour pallier leur fragilité. Le concept composite permet ainsi d'obtenir des matériaux de plus en plus performants.

1- LES COMPOSITES FIBREUX

Les composites fibreux peuvent être classés suivant la nature de leur matrice,

chacune correspondant à une gamme de températures d'utilisation : les composites à matrice organique, métallique, et céramique.

1.1 *Les composites à matrice organique*

Ce sont les matériaux composites les plus répandus. Ils représentent plus de 90% des applications des composites. La matrice organique (polyester, polyépoxyde ...) de ces composites est renforcée par des fibres de verre, de carbone ou de nature organique (e.g. polyamide aromatique). Ces matériaux présentent des résistances mécaniques spécifiques (i.e ramenées à l'unité de masse) excellentes. De par leur facilité de mise en oeuvre et leur faible coût (en comparaison avec les autres types de composites), leur application couvre un large évantail allant du secteur des articles de sport (raquette de tennis, ...) et des loisirs (coque des bateaux de plaisance), à l'industrie aéronautique et spatiale en passant par l'automobile (carrosserie, ...). Cependant, la plupart de ces matrices donnent lieu sous vide à des dégazages relativement importants, et leur stabilité thermique limite toujours le domaine d'utilisation prolongée à des températures inférieures à $\approx$ 250 °C.

1.2 Les Composites à Matrice Métallique (CMM)

L'utilisation de composites à matrice métallique permet d'étendre ce domaine d'utilisation jusqu'à des températures proches de 600 °C. Afin d'obtenir des caractéristiques spécifiques intéressantes, ces matrices (généralement des alliages d'aluminium, de magnésium ou de titane) sont renforcées par des fibres de carbone, de carbure de silicium ou d'alumine. En raison de la difficulté de leur élaboration et de leur coût, l'industrialisation de ces matériaux reste limitée. Cependant, la mise au point et l'amélioration de nouveaux procédés tels que le forgeage liquide [2-4], leur ouvrent de nouvelles perspectives (e.g. pièces de moteur pour automobile).

1.3 Les Composites à Matrice Céramique (CMC)

Pour les applications à hautes températures (aubes de turbines à gaz, matériaux de structure pour les parties portées à haute température par la rentrée dans l'atmosphère de la navette Hermès), les seuls matériaux envisageables sont les céramiques. Les CMC ont aussi quelques applications plus particulières comme le blindage (à cause de leur dureté alliée à une ténacité proche de celle des alliages légers), les prothèses ou les disques de freins. Les céramiques présentent une excellente réfractairité, de hauts modules d'élasticité, une dureté élevée, des densités relativement faibles, et pour certaines d'entre elles une bonne inertie chimique (le carbure de

silicium, par exemple, résiste en atmosphère oxydante au-delà de 1400 °C) et sont généralement des isolants électriques [5,6]. Les liaisons fortes, covalentes ou iono-covalentes au sein de ces matériaux expliquent leurs propriétés. Le principal défaut bien connu des céramiques est leur extrême fragilité, qui donne à leur rupture un caractère catastrophique et les rend peu fiables. Elles sont en particulier très sensibles aux effets d'entaille et aux défauts préexistants. Certaines propriétés mécaniques sont en bonne partie gouvernées par la forme, la taille et la répartition de ces défauts. La population de ces défauts étant difficilement maîtrisable, les déterminations expérimentales de la résistance à la rupture montrent une grande dispersion [7,8].

Les lois gouvernant cette dispersion montrent que la résistance à la rupture moyenne d'une céramique augmente lorsque son volume diminue. L'amélioration des caractéristiques mécaniques des céramiques passe donc (i) par une diminution du volume de la céramique et (ii) par une limitation du nombre de défauts. Cette optimisation conduit à élaborer des éléments de petit volume sous forme de trichites (whiskers) et le plus souvent sous forme de fibres de céramiques de faible diamètre (quelques µm). Ces fibres peuvent atteindre 3 GPa pour la contrainte à la rupture et des allongements à la rupture de l'ordre de 1% [9]. Leur fragilité conduit souvent à les protéger en les enrobant à l'aide d'ensimage lorsqu'elles sont à l'état élémentaire, puis à les enrober au sein d'une matrice dans les composites. Les architectures d'assemblage de ces fibres sont adaptées au type de sollicitation mécanique auquel sera soumise la pièce. Ainsi, la structure sera unidirectionnelle (composite 1D) lorsque le chargement sera axial, et pourra être multidirectionnelle (composite nD) dans le cas de sollicitations plus complexes. L'enrobage de ces assemblages aboutit à des matériaux réfractaires (le renfort et la matrice étant des céramiques) ayant des caractéristiques mécaniques telles que l'on peut les utiliser en tant que matériau de structure à hautes températures : ces matériaux sont alors appelés composites thermostructuraux. La grande liberté de choix permise par la nature des divers constituants ainsi que par le type d'architecture utilisé permet l'obtention d'une pièce aux propriétés exactement adaptées aux spécifications requises lors de la conception de la pièce.

Les premiers composites thermostructuraux ayant débouché sur une application industrielle significative sont les composites carbone-carbone.. A l'origine, ils ont été développés pour les tuyères d'engins propulsifs et les boucliers thermiques des corps de rentrée. Ces matériaux sont aussi utilisés pour leurs propriétés tribologiques (friction) dans divers systèmes de freinage (Airbus, Rafale, Formule 1) ainsi que pour leur biocompatibilité dans les prothèses osseuses et vasculaires en chirurgie. En revanche, le carbone s'oxyde à l'air à partir de 500 °C, ce qui limite l'emploi prolongé des composites carbone-carbone aux seules atmosphères non oxydantes. En vue d'obtenir

des CMC pour des applications hautes températures en atmosphère oxydante, des recherches furent conduites pour remplacer tout ou partie de la matrice carbonée. Le choix s'est tout d'abord porté sur le carbure de silicium dont les propriétés de résistance à l'oxydation sont bien connues. Les recherches sur le carbure de silicium [10], ont été étendues à d'autres carbures : TiC [11], B_4C [12], à des nitrures : BN [13], et plus récemment à des oxydes : Al_2O_3 [14] et ZrO_2 [15]. Parallèlement, la nature des fibres céramiques commercialisées s'est étendue (carbone, carbure de silicium, alumine). Cette diversité de combinaison fibre-matrice permet d'élargir les applications à hautes températures.

2 - ÉLABORATION DES CMC

2.1 Les différentes méthodes d'élaboration

Les composites à matrice céramique peuvent être élaborés selon trois mode de préparation, i.e par voie solide, liquide ou gazeuse.

La première voie utilise des techniques de métallurgie des poudres (frittage) et s'applique essentiellement aux composites à fibres courtes. Elle nécessite l'application de hautes températures et/ou de hautes pressions qui détèriorent les fibres, ce qui entraîne une diminution des caractéristiques mécaniques des matériaux ainsi élaborés.

La réfractairité élevée des céramiques interdit tout procédé d'imprégnation directe à partir de céramique fondue. Le procédé d'élaboration par voie liquide consiste, dans un premier temps, à imprégner la préforme fibreuse par une barbotine, un précurseur organométallique (e.g. un polycarbosilane pour le carbure de silicium) ou un hydrosol. Le pré-imprégné ainsi obtenu est séché, puis pyrolysé et densifié par compression à chaud. Pour réaliser le composite final, la séquence imprégnation-séchage-pyrolyse est répétée jusqu'à l'obtention du taux de matrice désiré. Cette technique permet d'élaborer des matériaux comportant une porosité résiduelle pouvant être très faible (typiquement $< 5\%$). Cette voie semble prometteuse, car les temps d'élaboration sont relativement courts en comparaison de ceux qui sont pratiqués par le procédé en phase gazeuse. Cependant, l'application en cours d'élaboration d'une pression et la répétition de nombreux cycles thermiques et de retraits issus de la pyrolyse de la matrice altèrent le renfort et détèriorent les caractéristiques mécaniques finales.

Avant densification, les préformes fibreuses constituent des milieux poreux complexes. La voie gazeuse consiste à les densifier à l'aide d'un dépôt résultant d'une réaction chimique hétérogène gaz-solide se produisant sur toute la surface interne de leur réseau de pores.

2.2 - Procédés d'élaboration par voie gazeuse

L'infiltration chimique par voie gazeuse (CVI pour Chemical Vapor Infiltration) est la technique d'élaboration la plus utilisée pour les CMC. Ce procédé dérive du dépôt chimique en phase vapeur (CVD pour Chemical Vapor Deposition). Le procédé CVD a été principalement développé et industrialisé dans le secteur de la microélectronique pour l'élaboration de couches minces semi-conductrices (Si, AsGa ...), isolantes (SiO_2, Al_2O_3, BN, ...), ou conductrices (W, WSi_2, ...) dans les circuits intégrés et des dispositifs optoélectroniques [16]. Récemment, le carbure de silicium a été envisagé en tant que semi-conducteur à cause de sa stabilité thermique et de son inertie chimique. Des études récentes ont permis de synthétiser par CVD des matériaux comme le diamant [17] ou des supraconducteurs [18]. Un des intérêts majeurs de cette méthode réside dans le fait que sa mise en oeuvre s'effectue à des températures très inférieures à celle de la fusion ou de la décomposition de la céramique à déposer (e.g. $\approx$ 1000°C au lieu de 2500 °C pour le carbure de silicium). Dans le cas de l'élaboration de composites à matrice céramique, cela évite une dégradation du renfort fibreux, et donc une diminution des caractéristiques mécaniques du matériau finalement obtenu. C'est la raison pour laquelle la CVI est le procédé de choix pour l'élaboration des CMC.

La faisabilité de ce procédé a été établie pour une grande variété de matrices incluant le carbone (ou pyrocarbone), des carbures (SiC, TiC, B_4C, ..), des nitures (BN, Si_3N_4, ...) et des oxydes réfractaires (Al_2O_3, ZrO_2, ...) [10-15]. Le procédé classique de CVI mis en oeuvre au plan industriel pour infiltrer une matrice de carbone ou de carbure de silicium s'effectue selon un procédé isotherme/isobare[(1)] (ICVI pour Isothermal/ isobaric CVI). Les conditions opératoires doivent être choisies de sorte que la cinétique des réactions de dépôt soit faible (en comparaison des vitesses de transfert de matière dans la préforme poreuse), afin d'éviter une fermeture prématurée du pore par le dépôt. En effet, ce dernier se forme préférentiellement à l'entrée du pore, ce qui implique des cycles de densification/écroutage relativement longs et l'obtention de matériaux comportant une porosité résiduelle. Néanmoins, ce procédé permet d'infiltrer simultanément de nombreuses pièces de géométrie complexe, ce qui n'est pas le cas si l'on applique un gradient de température et/ou de pression à la préforme dans le but d'accroître la vitesse de densification (procédé FCVI pour Forced CVI), variante du procédé ICVI[(2)] [19].

---

(1) Développé par la Société Européenne de Propulsion sur la base de recherches conduites au Laboratoire de Chime du solide

(2) Développé par Oak Ridge National Laboratory

Enfin, deux nouvelles études en cours visent à améliorer l'homogénéité du dépôt et/ou la vitesse de densification en jouant sur l'alimentation des gaz. La première consiste à appliquer à la préforme un gradient en concentration sur au moins deux réactifs, tout en maintenant la pression totale constante (CVI par réactifs séparés pour l'infiltration d'oxydes par hydrolyse de chlorures) [20]. La deuxième applique successivement à la préforme des séquences de très courtes durées : alimentation en gaz réactifs/pompage des gaz produits (CVI pulsée) [21,22].

La synthèse par CVD d'un solide est un processus extrèmement complexe. La **réaction chimique globale** peut se résumer à une simple décomposition (e.g. dépôt de carbone par CH_4), une hydrolyse (e.g. dépôt de zircône à partir du mélange $ZrCl_4$-H_2-CO_2), une réduction (e.g. de $SiCl_4$ par l'hydrogène pour le dépôt du silicium). L'activation de cette réaction est le plus souvant d'origine thermique (chauffage du mélange gazeux et/ou du substrat). Une partie de cette activation peut aussi être fournie sous la forme d'un plasma généré par un champ électrique de haute fréquence (CVD assisté par plasma), ou par excitation d'une onde électromagnétique (CVD assisté par laser). Ces deux techniques ne sont cependant pas applicables à la densification d'une préforme. Le procédé CVD permet de déposer des corps simples (carbone, silicium, ...), des combinaison binaires (SiC, TiC, BN, Al_2O_3, Si_3N_4, B_4C, ZrO_2, ...) ou même des mélanges polyphasiques (e.g. codépôt SiC + C ou SiC + Si).

Plusieurs précurseurs permettent d'obtenir une céramique donnée. Par exemple, le carbure de silicium peut être formé dans le système élémentaire Si-C-H-Cl à partir des mélanges $SiCl_4$-CH_4, $SiHCl_3$-C_3H_8 ou CH_3SiCl_3-H_2. L'état physique dans les conditions normales de température et de pression des précurseurs est variable (CH_4 est gazeux, $SiCl_4$ liquide et $ZrCl_4$ solide). L'usage de précurseurs organométalliques (OMCVD pour OrganoMetallic CVD) s'intensifie, car il permet d'abaisser fortement la température de dépôt. En CVI, les chlorures simples leur sont préférés, car ils sont moins onéreux et ils diffusent plus rapidement dans les milieux poreux.

La partie centrale du dispositif de synthèse des céramiques par le procédé CVD est le réacteur. Il en existe deux types. Dans les **réacteurs à parois froides**, seul le substrat est chauffé, ce qui (i) limite les réactions en phase homogène et les dépots sur les parois, et qui (ii) induit de forts gradients thermiques, rendant ainsi difficile le contrôle de la composition de la phase gazeuse à la surface du substrat. Dans un **réacteur à parois chaudes** (type de réacteur utilisé dans le cadre de cette étude), l'existence d'une zone isotherme permet d'avoir une phase gazeuse plus homogène. Ce type de réacteur favorise les réactions en phase homogène et induit la production d'un dépôt parasite sur les parois internes de la chambre de dépôt. Ces réacteurs de CVD à parois chaudes sont conçus de manière à permettre un contrôle aisé des paramètres

opératoires du dépot, à savoir : la température de la chambre de réaction, la pression totale prise en aval du réacteur et les divers débits gazeux introduits en amont du réacteur. Dans un tel réacteur, la synthèse par CVD d'un solide met en jeu les séquences suivantes [23,24] (fig.1) :

1- transport par convection forcée du mélange gazeux introduit en amont du réacteur vers la zone chaude

2 - élévation de la température de ce mélange induisant un ensemble de réactions en phase homogène entre les constituants initiaux. Ces réactions forment une nouvelle phase gazeuse ("bulk") composée d'espèces intermédiaires (stables à haute température et basse pression), complètement différente de la phase gazeuse introduite en amont du réacteur.

3 - transport depuis le bulk par convection, puis diffusion à travers la couche limite de certaines espèces intermédiaires (les espèces réactives) vers la surface du substrat

4 - réactions chimiques hétérogènes de ces espèces faisant intervenir :

a) adsorption des espèces réactives

b) réactions à la surface

- entre espèces adsorbées
- entre espèces adsorbées et espèces présentes dans le phase gazeuse

c) désorption des espèces adsorbées et en particulier des espèces produites par les réactions à la surface

5- transport par diffusion à travers la couche limite des gaz produits de la surface du substrat vers le bulk

6 - transport par convection forcée des gaz produits et des gaz n'ayant pas réagi de la zone réactionnelle vers la sortie du réacteur.

Ces étapes sont toutes plus ou moins interdépendantes et sont régies par des mécanismes physiques (étapes 1, 3, 5 et 6) ou chimiques (2 et 4). La compréhesion de ces mécanismes necessite des connaissances variées (i) en transfert de chaleur (par conduction et rayonnement) et de matière, (ii) en mécanique des fluides, (iii) en cinétique homogène et hétérogèns, et, dans une moindre mesure, (iv) en thermodynamique. La **vitesse du processus global** de CVD se traduit expérimentalement par la vitesse de dépôt exprimée en terme de prise de masse par unité de temps et de surface ($kg.s^{-1}.m^{-2}$) ou en terme de vitesse de croissance de l'épaisseur du dépot ($m.s^{-1}$). Elle peut être **limitée** soit par les **transferts de matière** (intervenant aux étapes 3 et 5), soit par les **réactions de surface** (étapes 4). Il a été montré au laboratoire que la densification d'une préforme poreuse par une céramique (CVI) doit au moins être réalisée dans des conditions opératoires correspondant au régime cinétique pour les réactions de surface.

Cette condition implique généralement que le dépôt soit réalisé à basse température et à basse pression (les conditions opératoires dépendant très fortement du comportement de la cinétique des réactions de surface). Lorsque l'on utilise le procédé CVI pour densifier des préformes, des étapes supplémentaires se rajoutent à celles précédemment décrites (fig.2). Les étapes (1) et (2) de CVD ne sont pratiquement pas modifiées, et imposent la composition de la phase gazeuse entourant la préforme. Au lieu de diffuser seulement à travers la couche limite, les espèces réactives doivent maintenant diffuser à travers tout le réseau de pores de la préforme pour parvenir au coeur de celle-ci. L'étape 3 devient ainsi une étape primordiale du processus, et elle est de plus couplée à l'étape 4 en tout point de la surface interne des pores de la préforme. Le rôle de l'étape 5 se renforce aussi car les produits de la réaction doivent diffuser depuis le coeur de la préforme jusqu'à l'extérieur. L'étape 5 peut même jouer un rôle important si les espèces gazeuses produites à l'intérieur de la préforme agissent sur la cinétique des réactions de surface (e.g. en tant qu'inhibiteur).

3 - OBJECTIFS ET CONTENU DU MÉMOIRE

La brève description précédente montre la grande complexité des phénomènes intervenant au cours de la densification par CVI de composites à matrice céramique. Cette complexité explique pourquoi, malgré l'expérience acquise, l'optimisation des conditions opératoires d'infiltration reste encore empirique. Il est donc apparu souhaitable - après avoir initié l'industrialisation de l'élaboration de certains composites thermostructuraux - d'effectuer un retour vers l'amont, dans le but (i) d'approfondir les connaissances et la compréhension des mécanismes d'infiltration (modes de transport de matière dans le pore, couplages entre transferts de matière et cinétique des réactions de surface), ainsi que (ii) de construire des modèles prévisionnels dont le but final est de permettre l'optimisation à la fois de la qualité des composites obtenus (e.g. diminution de la porosité résiduelle) et de leur coût (augmentation de la vitesse de densification). Le présent mémoire se propose d'aborder pleinement le premier objectif et d'entamer le second, en développant un modèle prévisionnel de l'infiltration d'un pore rectiligne. L'inconvénient de ce type de modèle réside dans le fait qu'il ne s'applique pas directement à l'infiltration d'une préforme réelle donnée (ce qui est l'objectif ultime de la modélisation). Par contre, le modèle développé dans le cadre de cette étude présente plusieurs avantages par rapport à d'autres modèles préexistants (cf. chapitre 1) :

- il peut s'appliquer à n'importe quel système chimique (gazeux et/ou solide),
- il peut prendre en compte n'importe quelle loi cinétique pour les réactions hétérogènes,

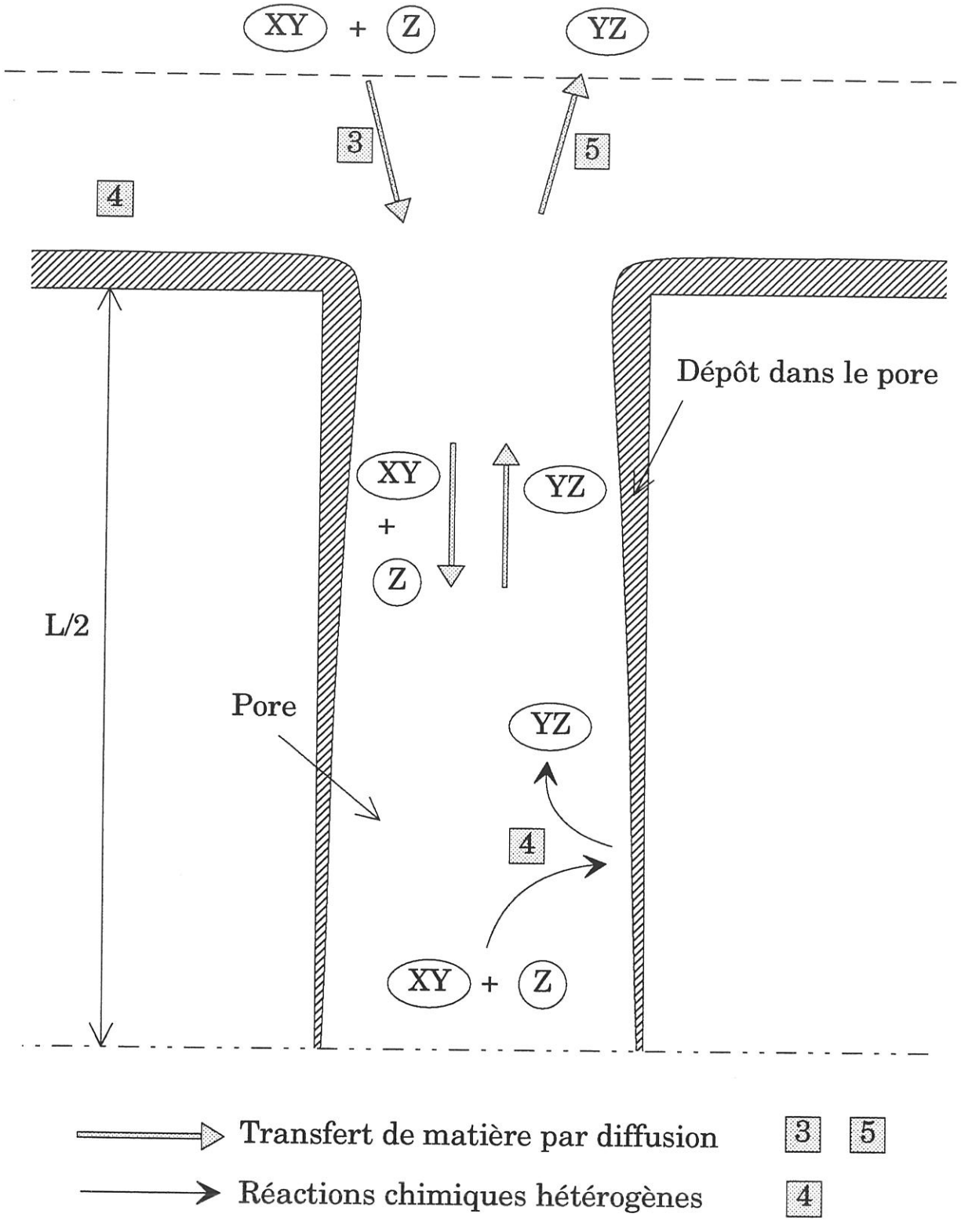

Fig. 2 : Etapes supplémentaires dans le processus d'infiltration d'un solide X dans un pore , par rapport au processus de dépôt sur la surface, à partir de l'espèce gazeuse source XYZ

$$XYZ_{(g)} \longrightarrow X_{(s)} + YZ_{(g)}$$

- il peut servir de base pour une modélisation de la densification de toute une préforme, et enfin

- la géométrie simple des pores modèles qu'il considère permet, si l'on parvient à élaborer de tels pores, une comparaison quantitative aisée avec l'expérience.

Des études récentes, demandant de lourds calculs et décrivant l'infiltration dans des milieux poreux modèles avec un réactif unique et une loi cinétique du premier ordre [25,26], montrent que l'évolution de la densification dépend fortement de la représentation géométrique du milieux poreux. Elles montrent aussi que l'influence des conditions opératoires semble qualitativement identique pour divers mileux poreux modèles.

Le travail décrit dans ce mémoire est consacré à la compréhension des mécanismes élémentaires de l'infiltration et fait abstraction des problèmes liés à la représentation géométrique des préformes. Il s'attache en particulier à montrer l'influence de tous les paramètres opératoires et permet de mettre en évidence les données quantitatives qu'il faut acquérir pour pouvoir élaborer des modèles prévisionnels concernant la densification d'une préforme réelle. Il met en relief les différences de comportement existant entre divers systèmes chimiques et permet d'avoir une idée de la capacité à obtenir une bonne infiltration d'une préforme pour tel ou tel système chimique.

Le mémoire s'articule autour de **deux publications**. La première est scindée en **trois parties**, correspondant chacune à un chapitre. La deuxième publication publication forme le dernier chapitre. Le premier chapitre contient la **description** détaillée **de la modélisation** de l'infiltration d'un pore rectiligne cylindrique, la méthode de résolution du système d'équations différentielles non linéaires posé par le modèle, ainsi qu'une validation numérique, par comparaison, dans des cas bien particuliers, à des modèles préexistants. Le deuxième chapitre concerne l'**application du modèle** au cas de l'**infiltration de carbure de silicium dans un pore cylindrique**. Ce chapitre comporte une étude théorique approfondie de l'influence des divers paramètres sur l'infiltration, suivie d'une confrontation avec des expériences menées dans un réacteur CVD/CVI décrit dans l'**annexe A**. Le chapitre 3 montre l'aptitude du modèle à prendre en compte des cinétiques complexes, en l'appliquant au cas de l'**infiltration de deux oxydes dans un pore cylindrique**, sur la base de cinétiques proposées par E. Sipp [27]. Le dernier chapitre traite de l'**extension du modèle** au cas du **pore rectiligne à section rectangulaire**, et de l'application de cette extension au cas de l'**infiltration de pyrocarbone** à partir de propane dans un tel pore. Quelques annexes viennent compléter ce mémoire. Une discussion sur les modes de transport dans un pore et sur l'estimation des coefficients de diffusion est présentée en **annexe B**. Une justification de l'hypothèse du régime stationnaire est donnée en **annexe C**. Quant aux **annexes**

D et E, elles traitent de méthodes numériques liées à la résolution du système d'équations différentielles engendré par le modèle. Une partie de ce travail a déjà fait l'objet d'une communication au congrès international de CVD XI, à Seattle en Octobre 1990 (**annexe F**) et un poster a été presenté dans le cadre de journées BRITE/EURAM (Bruxelles, Février 1989).

REFERENCES

[1] R. Naslain, "Introduction aux Matériaux Composites 2- Matrices Métalliques et Céramiques", Ed. du CNRS/IMC, Bordeaux, 1985

[2] F. Girot, Thèse N° 100, Université de Bordeaux I, 1987

[3] F. A. Girot, R. Fédou, J.-M. Quenisset, R. Naslain, "On the Squeeze Casting Conditions of Aluminium Matrix Composite Materials", Journal of Reinforced Plastics and Composites, Vol. 9, pp. 456-469, 1990

[4] S. Schamm, R. Fédou, J.-P. Rocher, J.-M. Quenisset, R. Naslain, "The K_2ZrF_6 Wetting Process : Effect of Surface Chemistry on the Ability of a SiC-Fiber Preform to be Impreganted by Aluminium", Metallurgical Transactions A, Vol. 22A, pp. 2133-2139, 1991

[5] W. D. Kingery, H. K. Bowen, D. R. H. Uhlmann, "Introduction to Ceramics", J. Wiley and Sons eds., New York, 1989

[6] J. L. Chermant, "Les Céramiques Thermomécaniques", Presses du CNRS, Paris, 1989

[7] R. Labbens, "Introduction à la Mécanique de la Rupture", Editions Pluralis, Paris, 1980

[8] J. F. Knott, "Fundamentals of Fracture Mechanics", Butterworths Ed., London, 1973

[9] L. C. Sawyer, R. Arons, F. Hainback, H. Jaffe, K. D. Rappaport, "Characterization of Nicalon^{TM} : Strength, Structure and Fractography", Ceram. Eng. and Sci. Proc., Vol. 6, N° 7-8, pp. 567-575, 1985

[10] F. Christin, R. Naslain, C. Bernard, "A Thermodynamic and Experimental Approach of Silicon Carbide-CVD Application to the CVD Infiltration of Porous Carbon-Carbon Composites", Proc. 7th Int. Conf. CVD, Los Angeles, USA (1979), (T.O. Sedgwick et al., eds.), The Electrochem. Soc., Princeton, pp. 499-514, 1979

[11] J.Y. Rossignol, R. Naslain, P. Hagenmuller, L. Heraud, "New Composite Materials with a Carbon-Titanium Carbide Hybrid Matrix for High Temperature Applications", ICCM IV, Tokyo, Japan (1982), (T. Hayashi et al., eds.), pp. 1227-1237, 1982

[12] H. Hannache, F. Langlais, R. Naslain, "Kinetics of Boron Carbide Chemical Vapor Deposition and Infiltration", Proc. 5th European Conf. CVD, Uppsala, Sweden 1985), (J.O. Carlsson et al., eds.), Upssala Univ. Press, pp. 219-233, 1985

[13] H. Hannache, R. Naslain, C. Bernard, "Boron Nitride Chemical Vapor Infiltration of Fibrous Materials from BCl_3-NH_3-H_2 or BF_3-NH_3 Mixtures : a Thermodynamic and Experimental Approach", J. Less-Common Met., Vol. 95, pp. 221-246, 1983

[14] R. Colmet, I. Lhermite-Sebire and R. Naslain, "Fibrous Alumina-Alumina Composite Materials Obtained according to a CVI Technique",Adv. Ceram. Mater., Vol. 138, N° 2, p. 221, 1982

[15] J. Minet, F. Langlais and R. Naslain, "Chemical Vapor Deposition of Zirconia within the Pore Network of Fibrous Ceramics Materials from $ZrCl_4$-H_2-CO_2-Ar Gas Mixtures", Composites Sciences and Technology, Vol. 37, pp. 79-107, 1990

[16] A. Sherman, "Chemical Vapor Deposition for Microelectronics", Noyes Publications, 1987

[17] R. Messier, A.R. Badzian, T. Badzian, K.E. Spear, "From Diamond-Like Carbon to Diamond Coatings", Thin Solid Films, Vol. 153, p. 1, 1987

[18] G. Wahl, F. Schmaderer, "Chemical Vapor Deposition of Superconductors", J. Mater. Sci., Vol. 24, N° 4, p. 1141, 1989

[19] T. M. Bessmann, R.A. Lowden, D.P. Stinton, T.L. Starr, "A Method for Rapid Chemical Vapor Infiltration of Ceramic Composites", Proc. 7th European Conf. CVD, Perpignan, France (1989), (M. Ducarroir et al., eds.), Colloque de Physique, Les Editions de Physique, Colloque C5, Suppl. N° 5, Vol 50, pp. 229-239, 1989

[20] Y. Lin, K. J. De Vries, A. J. Burggraaf, "CVD Modification of Ceramic Membranes: Simulation and Preliminary Results", Proc. 7th European Conf. CVD, Perpignan, France (1989), (M. Ducarroir et al., des.), Colloque de Physique, Les Editions de Physiques, Colloque C5, Suppl. N° 5, Vol. 50, pp. 861-872, 1989

[21] K. Sugiyama, T. Nakamura, "Puse CVI of Porous Carbon", J. Mater. Sci. Lett., Vol. 6, pp. 331-333, 1987

[22] K. Sugiyama, Y. Ohsawa, "Carbon or SiC Particulate Preform Using a R.F. Heating System",J. Mater. Sci., Vol. 25, pp. 4511-4517, 1990

[23] K. E. Spear, "Thermochemical Modeling of Steady State CVD Processes", Proc. 9th

Int. Conf. CVD, Paris, France (1989), (Mc Robinson et al., eds.), The Electrochem. Soc., Pennington, pp. 81-97, 1984

[24] C. E. Morosanu, "Thin Films in Chemical vapor Deposition", Elsevier Ed., Amsterdam-Oxford-New York-Tokyo, 1990

[25] S. Middleman, B. Heble, H. C. T. Cheng, "Improved Uniformity of Densification of Ceramic Composites Trough Control of the Initial Preform Porosity Distribution", J. Mater. Res., Vol. 5, N° 7, pp. 1544-1548, 1990

[26] G.-Y. Chung, B. J. Mc Coy, "Modeling of Chemical Vapor Infiltration for Ceramic Composites Reinforced with Layered, Woven Fabric", J. Am. Ceram. Soc., Vol. 74, N° 4, pp. 746-751, 1991

[27] E. Sipp, "CVD/CVI de Céramiques à Base de Zircône Pure ou Stabilisée : Approche Thermodynamique et Expérimentale", Thèse N° 483, Université de Bordeaux I, 1990

CHAPITRE 1

Titre : A MODELING OF THE ISOTHERMAL ISOBARIC CHEMICAL VAPOR INFILTRATION IN A STRAIGHT CYLINDRICAL PORE PART 1 - DESCRIPTION OF THE MODEL

A MODELING OF THE ISOTHERMAL ISOBARIC CHEMICAL VAPOR INFILTRATION IN A STRAIGHT CYLINDRICAL PORE PART 1 - DESCRIPTION OF THE MODEL

R. FÉDOU, F. LANGLAIS (*), and R. NASLAIN
Laboratoire des Composites Thermostructuraux (UMR 47 CNRS-SEP-UB1)
Domaine Universitaire, 3 Allée La Boétie
33600 Pessac (France)

ABSTRACT : Chemical vapor infiltration is a convenient method to elaborate ceramic matrix composites by densifying porous preforms made of ceramic fibers. In order to foresee densification rate and infiltration homogeneity, a numerical model is proposed concerning (i) a cylindrical straight open-ended pore with a large aspect ratio and (ii) any chemical system, including the solid deposit and the gaseous phase (reactant species, product species and carrier gas), defined by the stoichiometry and the kinetics of the heterogeneous reaction. Three kinds of equations are considered in this 1D model : (i) the equations of mass transfer for each gaseous species, based on Fick and Knudsen diffusion and a convection term resulting from the gaseous mole number changes in the deposition reaction, (ii) the boundary conditions at the entrances and the center of the pore and (iii) the equation for the local change of pore geometry. To solve these various equations, a finite differences method is used, which permits to calculate, at any stage of the densification, and particularly at the end of the process when the pore is closed, the concentration profiles of each gaseous species and the diameter profile. A first validation of the model is given by comparing its results with those obtained from previous models.

1 - INTRODUCTION

The chemical vapor infiltration (CVI) is a very convenient technique for the processing of ceramic matrix composites (CMC). These materials are prepared by densifying refractory fibrous preforms (usually made of carbon, silicon carbide or alumina fibers) with a deposit resulting from a heterogeneous gas-solid chemical reaction taking place on the internal surface of the pore network of the preform. This technique was successfully applied to various refractory matrices such as

(*) to whom correspondence should be sent

pyrocarbon, carbides (SiC, TiC, B_4C), nitride (BN) and oxides (Al_2O_3, ZrO_2) [1-9].

In the classical isothermal isobaric technique (ICVI), infiltration temperature and pressure must be chosen in order to favour in-depth deposition with respect to external surface coating. These conditions result in decreasing the residual porosity of the so-prepared composites but also in raising the densification durations. In spite of these drawbacks, the ICVI is suitable to densify simultaneously a large number of preforms with complex and various shapes, without damaging the ceramic fibers.

With a view to accelerate the infiltration process, the use of a gradient of pressure and/or temperature through the preform has been studied. But these techniques of forced CVI (FCVI) need specific tools and are not very flexible [10]. The choice of convenient infiltration conditions, even in the case of the largely studied SiC and pyrocarbon matrices, is still empirical owing to the complexity of the actual porous substrates and the physical and chemical phenomena. A thorough study of the infiltration mechanisms, resulting in previsional models, seemed to be necessary in order to optimize both the homogeneity of CVI-processed composites and densification rates. These models need simplified geometric descriptions which simulate the actual fibrous preforms. These equivalent porous media are not yet available. So, the first model which will permit to understand the involved mechanisms, can be built up in the case of a single straight cylindrical pore. This kind of geometry has already been selected in a few studies recently published [4, 11-19].

Most recent papers in this field are based on old works carried out by Thiele in the field of theoretical studies on the efficiency of porous catalysts [11]. This author built a 1D model taking into account the diffusive transfers and the chemical reaction occurring in a straight cylindrical pore with a constant diameter. The analytical solution of mass balance equations in the steady state, resulted, for a first order kinetics with respect to the reactant species, in concentration profiles and effective reaction rates as a function of a dimensionless number (proportional to the ratio between the kinetic constant of the heterogeneous reaction and the diffusion coefficient), presently referred to as Thiele modulus. The same kind of approach was used by Petersen for etching chemical reactions, such as gasification of graphite by CO_2. The proposed model permitted to foresee the increase in radius of a cylindrical pore [12]. This author validated the quasi steady-state hypothesis, which involves that the mass transfers are very rapid with respect to the variations of the pore geometry.

In the field of CVI modelling itself, Fitzer calculated, for the first time, theoretical infiltration depths on the basis of limit values of the Thiele modulus by assuming, as in catalysts, that the infiltration efficiency is given by the ratio between the deposition rate within the pore and the deposition rate at the pore entrance [13]. Van den Brekel et al. proposed a 2D analytical modelling of the CVD process in a macroscopic cylindrical tube whose radius was assumed not to depend on time [14]. They considered, on the one hand, chemical reactions with orders close to one and, on the other hand, transfers occurring only by Fick diffusion. For a first order kinetics, they found exactly the analytical solution of the 1D model proposed by Thiele. Then Rossignol et al. applied this model to CVI in a microscopic cylinder [4]. They introduced Knudsen diffusion and assumed a reaction order equal to one and a cylindrical geometry of the pore with a time dependent diameter. Similar models, applied to the infiltration of various ceramics (SiC and Al_2O_3 for composites, ZrO_2 (Y_2O_3) for porous membranes [15]), dealt with 1D or quasi 1D calculations, under the hypothesis of the quasi steady state, taking into account Knudsen diffusion transfers.

A few authors introduced in the equations of mass conservation a convection term originating from either a gaseous mole number variation related to the heterogeneous reaction [11, 15] or a forced flow in the porous substrate [20]. In most studies, only the heterogeneous reactions are considered and assumed to be first order with respect to the precursor species [16-18, 20]. Conversely, Lin et al. showed in their model the influence of reaction orders ranging between 0 and 2, on the deposition profiles [15]. Recently, Middleman proposed an analytical modelling including, besides the heterogeneous reaction, an homogeneous reaction resulting in the formation of an intermediate species [18].

In most of the previously mentioned models, the effects of the pore geometry variations during the infiltration process were sometimes discussed but ususally they were not taken into account at all in the calucations. Nevertheless, the Knudsen diffusion coefficient and consequently the Thiele modulus depend on the pore radius, which varies as a function of both time and spatial coordinate along the pore. The aim of the present first article is to describe with some details a model which foresees gaseous species concentration profiles and diameter profiles and which includes : (i) the local pore geometry, (ii) multicomponent chemical systems, (iii) any heterogeneous kinetics and (iv) gaseous precursor not necessarily diluted. The use of this model in the case of several chemical systems (CVI of SiC and oxides such as ZrO_2 and Y_2O_3) with a few experimental comparisons, will be proposed in two related papers (Part 2 and Part 3 [21, 22]).

2 - DESCRIPTION OF THE MODEL

2.1 - Geometry of the pore

The pore considered here is a cylindrical straight open-ended pore with an initial diameter Φ_0 and a length L (fig. 1). The boundary conditions are identical at both ends, i.e. the pore is symmetrical with respect to its center and the study is thus limited to one half of the pore. Due to the symmetry with respect to its axes, the pore is assumed to remain straight during the infiltration process and any cross-section is a disc.

2.2 - Hypotheses

(1) The temperature is supposed to be constant not only versus time, but also in the whole pore volume (isothermal process).

(2) No homogeneous reaction occurs within the pore.

(3) The mass transfers within the pores are only controlled by diffusion processes, the forced convection phenomena being negligible in small pores. Nevertheless, the convection terms, which result from the mole number changes in the chemical reactions, are considered but can become zero when the reactive species are highly diluted.

(4) The mass transfers are assumed to be very rapid with respect to the rate of variation of the pore geometry, i.e. the infiltration can be considered as a series of quasi-steady states. This assumption is analytically justified by Petersen in his study of the gasification of graphite [12] and by Gupte et al. which found mass transfers at least 100 times more rapid than the variations of the pore geometry [16].

(5) The concentrations of the gaseous species are constant in a cross-section of the pore, i.e. the radial diffusional fluxes are negligible compared to the axial fluxes, which permits to reduce a 2D problem to a 1D problem. This hypothesis can be justified by (i) a large aspect ratio (L/Φ_0), (ii) the identical results analytically obtained by Van den Brekel with a 2D model [14] and Thiele with a 1D model [11] and (iii) the homogeneity of deposit thickness observed experimentally in straights pores with rectangular cross-section of a straight pore [23].

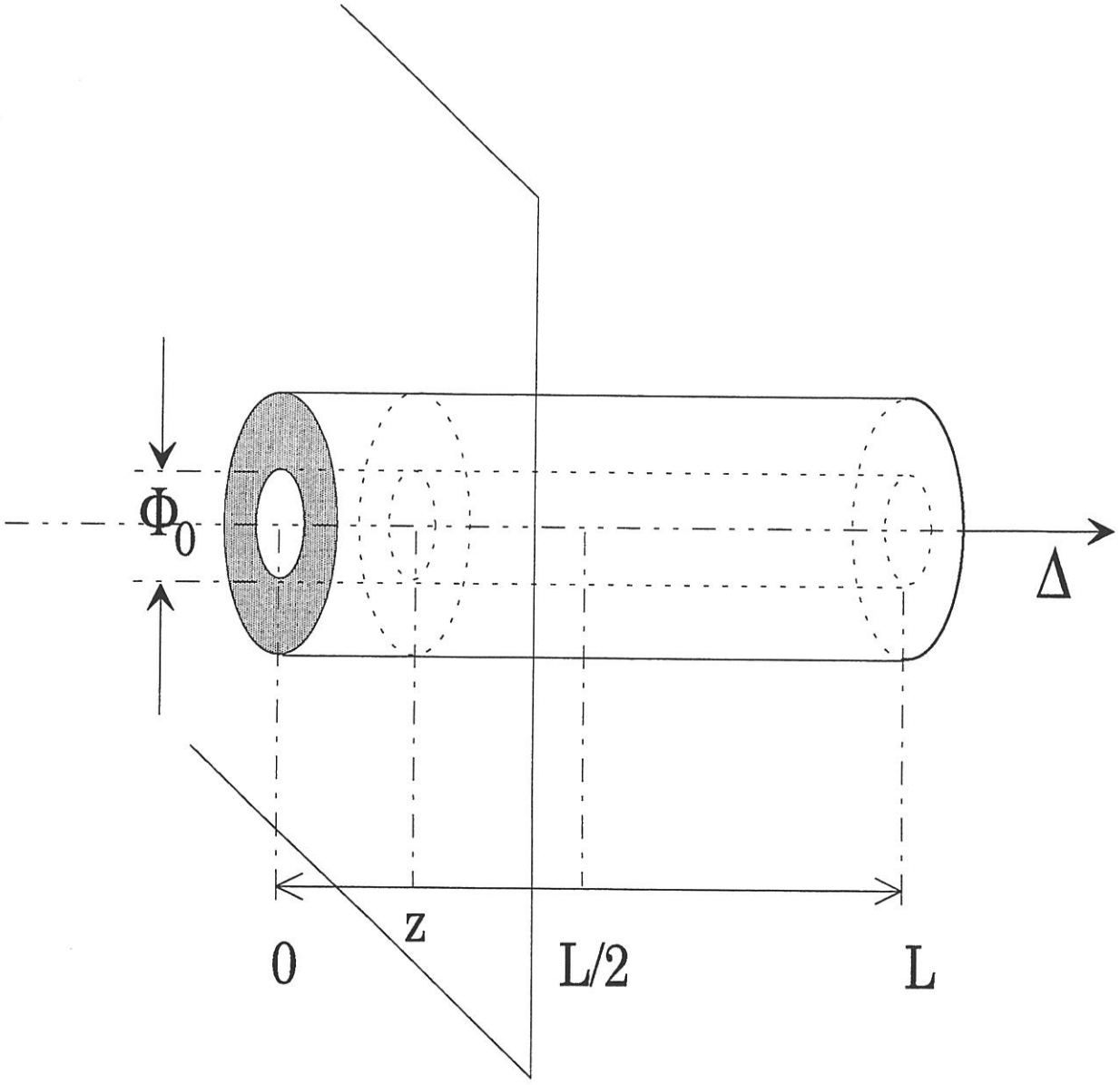

Fig. 1 - Geometrical features of the straight cylindrical model pore

2.3 - Space and time variables

The axial coordinate, named z, is defined as the distance from the nearest pore entrance (i.e. $0 \leq z \leq L/2$). The reduced infiltration depth is the adimensional variable $z' = z/L$.

The time origin ($t = 0$) is chosen as corresponding to the first mass transfer steady state, which is supposed to be set up very rapidly compared to the rate of variations of the pore diameter. The time needed to close the pore is named t_c. An adimensional time is also defined as $t' = t/t_c$.

The geometry of the pore at the time t is totally described by the function Φ (z, t) which gives the diameter of the pore for any value of z.

2.4 - Chemical system

The chemical system involved in the heterogeneous reaction of the CVI process, can be described as a set of species : a solid phase produced on the pore walls and a gaseous phase including three kinds of species, (i) those consumed at the solid surface, (ii) those produced by the deposition reaction and possibly (iii) inert species used as carrier gas such as Ar.

Generally speaking, the heterogeneous chemical reaction can be written as :

$$\sum_l \nu_l A_l = 0 \qquad (1)$$

where A_l represents gaseous or solid chemical species l,

ν_l is the stoichiometric coefficient related to species l (which is positive for the reaction products, negative for the reactants and nil for the inert species).

For a given reaction, the equation (1) can be written so that the stoichiometric coefficient is one for the deposited solid.

According to these conditions and by using the concept of the extent of reaction ξ (in mol) [24], the rate of the heterogeneous reaction for the production of one mole of solid on a unit surface, is defined as follows :

$$\vartheta = \frac{\partial \xi}{\partial t \, \partial S} \qquad (2)$$

where S is the area of the surface where the reaction occurs. ϑ can be expressed

like a molar flux in $mol.m^2s^{-1}$. Consequently, the rate of consumption or production of the gaseous species i can be written as a molar flux to or from the reaction surface:

$$N_i = \frac{\partial(\nu_i \xi)}{\partial t \, \partial S} = \nu_i \vartheta \qquad (3)$$

The reaction rate ϑ depends on the temperature, the total pressure and the pressure and the composition of the gaseous phase close to deposition surface. Species with $\nu_i = 0$ can play an important kinetic role, i.e. as catalyst or inhibitor.

2.5 - Equations of the model

2.5.1 - *Mass transfer equations*

The time variations of the concentration profiles for the various gaseous species and the deposit thickness profiles can be investigated by solving the mass balance equations for each species. The conservation equation for species i, resulting from the z-component of the general vector equation of mass transfer in cylindrical coordinates (hypothesis (5)), can be expressed in terms of molar units as follows [25]:

$$\frac{\partial C_i}{\partial t} + \frac{\partial N_i}{\partial z} = R_i \qquad (4)$$

where C_i is the concentration of species i (in $mole.m^{-3}$)
N_i is the absolute molar flux of species i (in $mol.m^{-2}s^{-1}$)
R_i is an algebraic term of source ($R_i > 0$) or sink ($R_i < 0$) for species i (in $mol.m^{-2}s^{-1}$).

According to the hypothesis (4) of quasi-steady state, this equation is obviously simplified in :

$$\frac{\partial N_i}{\partial z} = R_i \qquad (5)$$

The term R_i can be deduced from a local treatment, by writing the conservation of mole number of species i over a thin shell of pore (δz in thickness, $\mathcal{A}$ in section and $\mathcal{P}$ in perimeter) : the rate of consumption or production of species i by chemical reaction on the side wall of this shell, must be equal to the difference between the algebraic flow rate of i through the cross-section at $z + \delta z$, i.e. :

$$\nu_i \vartheta \mathcal{P} \Delta z = [\, N_i(z) - N_i(z+\Delta z) \,] \mathcal{A} \qquad (6)$$

By taking the limit as δz approaches zero, it is obtained :

$$\frac{\partial N_i}{\partial z} = \frac{\nu_i \vartheta \mathcal{P}}{\mathcal{A}} \qquad (7)$$

In the particular case of cylindrical pore, (7) is equal to :

$$\frac{\partial N_i}{\partial z} = \frac{4 \nu_i \vartheta}{\Phi} \qquad (8)$$

If this equation is summed on all the gaseous species i, it becomes :

$$\frac{\partial \mathbf{N}}{\partial z} = \frac{4 \Delta\nu \vartheta}{\Phi} \qquad (9)$$

with

$$\mathbf{N} = \sum_{i=1}^{n_g} N_i \qquad (10)$$

and

$$\Delta\nu = \sum_{i=1}^{n_g} \nu_i \qquad (11)$$

where **N** is the total gaseous molar flux

and $\Delta\nu$ the overall variation of the gaseous mole number resulting from the heterogeneous reaction.

According to the hypothesis (3), the absolute molar flux includes a pure diffusion term (i.e. first Fick law) and a convective term (which is positive if the heterogeneous reaction consumes gaseous molecules and negative in the opposite case), usually named as Stefan flow :

$$N_i = -D_i \frac{\partial C_i}{\partial z} + x_i \mathbf{N} \qquad (12)$$

where D_i is the diffusion coefficient of species i in the gaseous mixture (in $m^2 s^{-1}$)

and x_i the molar fraction of species i, defined by :

$$x_i = \frac{C_i}{\sum_{j=1}^{n_g} C_j} \qquad (13)$$

By combining equations (8) and (12) and neglecting the term including the derivative of diffusion coefficient, the mass transfer equation to be solved, results as follows :

$$D_i \frac{\partial^2 C_i}{\partial z^2} - \frac{\partial (x_i \mathbf{N})}{\partial z} + \frac{4 \nu_i \vartheta}{\Phi} = 0 \qquad (14)$$

2.5.2 - *Diffusion coefficient of species i in the gaseous mixture.*

Classically, the mass transport phenomena by Fick diffusion are controlled by the collision of the molecules between each other. In the case of CVI, where diffusion occurs at high temperature and low pressure in pores with low diameters, the mean free path of the molecules can be high with respect to the pore diameter, so the diffusion transport can be governed by the collision of the molecules on the walls: it is the Knudsen diffusion regime [26, 27]. Nevertheless, both mechanisms can occur in the CVI process and an overall diffusion coefficient must be taken into account, according to Bosanquet definition [27] :

$$\frac{1}{D_i} = \frac{1}{D_{i,F}} + \frac{1}{D_{i,K}} \qquad (15)$$

where $D_{i,K}$ is the Knudsen diffusion coefficient of species i (in $m^2 s^{-1}$)
and $D_{i,F}$ is the Fick diffusion coefficient of species i in the gaseous mixture.

The coefficient $D_{i,F}$ depends on the gaseous phase composition. By assuming that species i diffuses through a stagnant mixture, $D_{i,F}$ can be calculated with the expression :

$$\frac{1-x_i}{D_{i,F}} = \sum_{\substack{j=1 \\ j<>i}}^{n_g} \frac{x_j}{D_{i,j}} \qquad (16)$$

where $D_{i,j}$ is the Fick diffusion coefficient for the binary gaseous mixture of species

i and j. Every value of $D_{i,j}$ and consequently the value of $D_{i,F}$ are proportional to 1/P and T^{β} ($1.2 \leq \beta \leq 2$), P and T being the total pressure and the temperature of the CVI process (cf. Appendix 1).

Conversely Knudsen diffusion coefficient depends only on the temperature and the geometry of the pore according to [26] :

$$D_{i,K} = \frac{\Phi}{3}\left[\frac{8\,\boldsymbol{R}\,T}{\pi M_i}\right]^{1/2} \qquad (17)$$

where $\boldsymbol{R}$ is the ideal gas constant (8.32 $J.K^{-1}mol^{-1}$).
and M_i is the molar mass of species i (in $kg.mol^{-1}$).

2.5.3 - *Boundary conditions*

At the pore entrance, the concentration C_i is assumed to be constant and set by the phenomena occurring outside the pore :

$$C_i(0,t) = C_{i,0} \qquad (18)$$

At the center of the pore, the symmetry involves :

$$\left[\frac{\partial C_i}{\partial z}\right]_{z=L/2} = 0 \qquad (19)$$

and

$$(\mathbf{N})_{z=L/2} = 0 \qquad (20)$$

2.5.4 - *Equation for the pore geometry change*

The coefficient $D_{i,K}$ and the chemical reaction term of the mass transfer equation (14) being dependent on the pore diameter, another differential equation must be solved, which gives the diameter variations versus time for the position z (cf. Appendix 2)

$$\frac{\partial \Phi}{\partial t} = -2\,V_s\,\vartheta \qquad (21)$$

where V_s is the molar volume of the deposited solid (in m^3mol^{-1}).

3 - SOLVING METHOD

In order to solve the various partial differential equations which describe the system, it is necessary to use a numerical model which makes (i) the space, the time and (ii) the equations discrete. For the differential equations, the finite differences method [28] is used. This procedure is detailed in appendix 3.

The general calculation procedure can be described as the following loop (fig. 2) :

(1) The geometry of the pore being fixed at the time t_u, the concentration profiles are calculated for each gaseous species at the time t_{u+1} by solving the system of equations (A12), (A13) and (A15) - (A17) (appendix 3).

(2) if this concentration profiles are put in the equation (A18), the pore diameter profile can be calculated at the time t_{u+1}.

(3) As the diameter of the pore influences the chemical source or sink term and the diffusion coefficient in equations (A12) and (A15), the new concentration profiles at t_{u+2} are then calculated as in step (1) by using the diameter profile at t_{u+1}.

The procedure begins with the cylindrical pore ($\Phi_{p,o} = \Phi_o$), calculates concentration profiles and diameter profile as the infiltration is going on and is stopped when the pore is closed, usually at the entrances ($\Phi_p \leq 0$ for $p = 0$).

The step devoted to the calculation of the concentration profiles at the time t_{u+1}, on the basis of the concentration profiles and diameter profile at t_u, uses an iterative method as shown in fig. 3. For each iteration, the calculated profiles are different from those obtained at the previous step, but are considered to be better until the difference between two successive calculations is lower than a given relative difference. The procedure is stopped when the convergence criterion is verified for all concentration profiles and the last ones are assumed to be the most convenient.

The computation programme for these various procedures is written in FORTRAN [29].

4 - DATA ON THE CHEMICAL DEPOSITION PROCESS

4.1 - Molar volume of the deposited solid phase

If the solid deposited from the heterogeneous reaction is a pure phase without

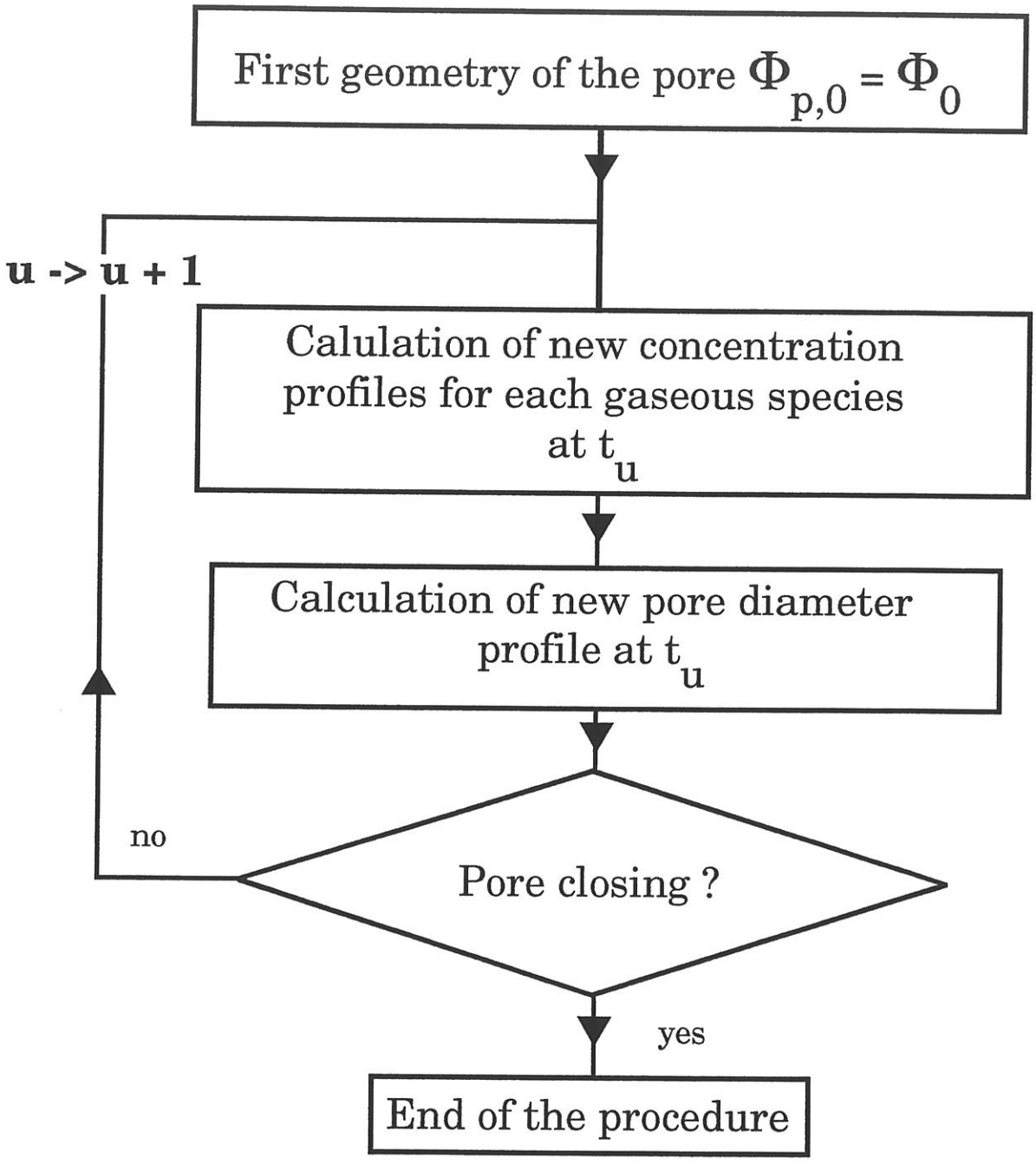

Fig. 2 - General method of resolution

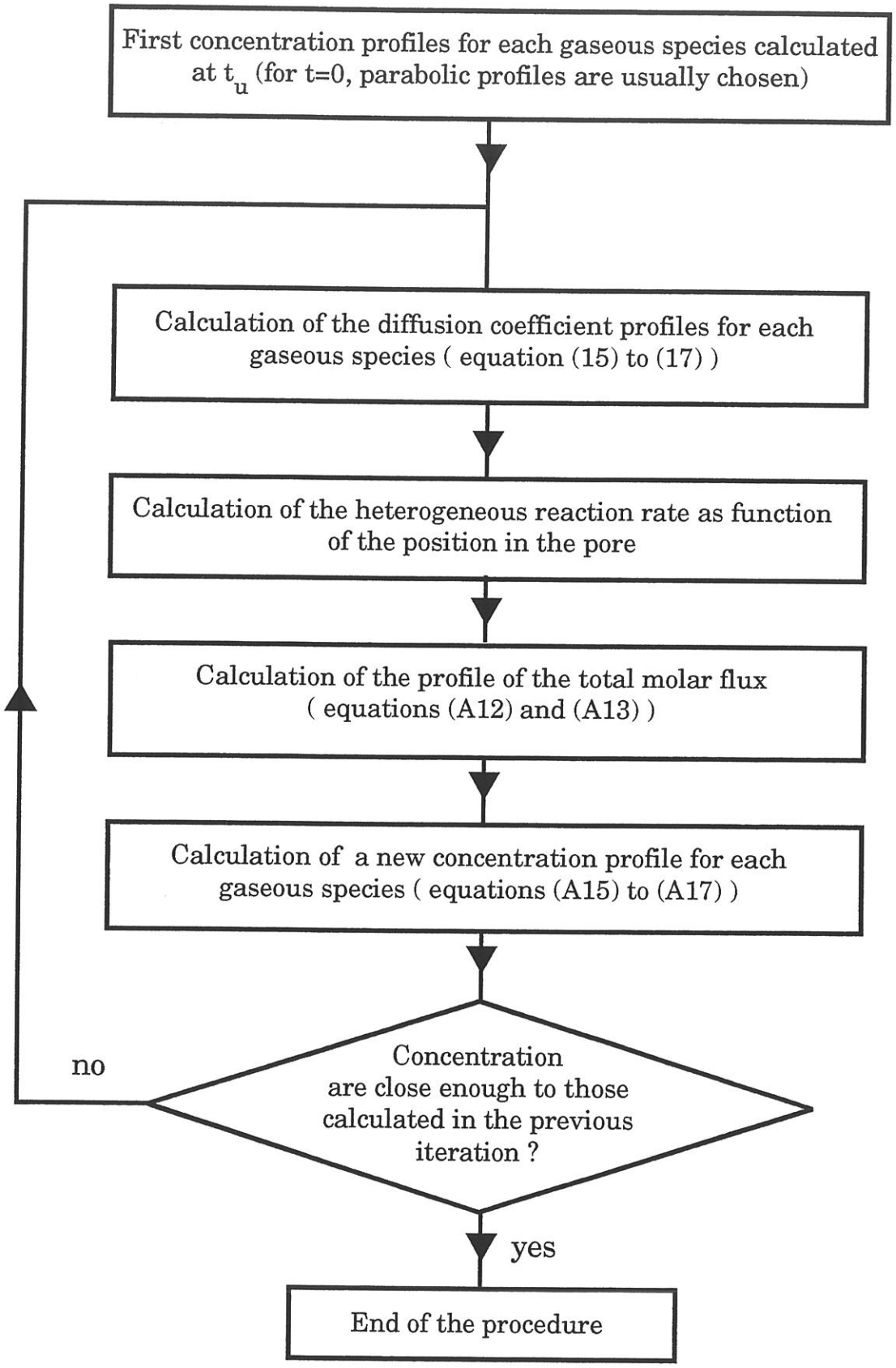

Fig. 3 - Calculation procedure of the concentration profiles for each gaseous species at the time t_u

microporosity, its molar volume (in $m^3\ mol^{-1}$) is given by :

$$V_s = \frac{M_s}{\rho_s} \qquad (22)$$

where M_s is the molar mass of the deposited phase (in $kg.mol^{-1}$)
and ρ is the specific mass of the deposited phase (in $kg.m^{-3}$).

If the chemically deposited solid is made of n_s phases, the corresponding molar volume (i.e. for an extent of reaction of one mole) can be written as :

$$V_s = \frac{1}{\sum_{w=1}^{n_s} \nu_w} \sum_{v=1}^{n_s} \nu_v \frac{M_v}{\rho_v} \qquad (23)$$

where ν_v is the stoichiometric coefficient of the solid phase v in the heterogeneous reaction (as defined in 2.4)
M_v is the molar mass of the solid phase v (in $kg.mol^{-1}$)
and ρ_v is the specific mass of the solid phase v (in $kg.m^{-3}$).

4.2 - Heterogeneous reaction rate

In the equation of mass transfer (13), the term ϑ means the rate of production of solid phase per unit area. This term is a function of the temperature, the total pressure and the composition of the gaseous phase near the deposition surface. This function, i.e. the kinetic law, can be derived from experiments on flat substrates. These experiments yield : (i) the domain where the kinetics are controlled by the chemical reactions, (ii) the activation energies by drawing Arrhenius plots and (iii) reaction orders with respect to reactant and product species. The main problem in CVI is to express the kinetic laws as a function of the intermediate species which result from homogeneous reactions occurring in the hot zone and which actually react at the solid surface (e.g. the pore wall).

For a first order kinetic law for a single precursor species I with an initial concentration C°_I (in $mol.m^{-3}$), the deposition rate ϑ (in $mol.m^{-2}\ s^{-1}$) can be expressed as :

$$\vartheta = k_a\, C^\circ_I \qquad (24)$$

where k_a is the kinetic constant of the overall reaction (in $m.s^{-1}$).

In a hot wall reactor, this precursor species I is very often decomposed into intermediates before reaching the reaction surface. If it is assumed that only one of these intermediates, the species X, yields the solid deposit and its concentration C_X is proportional to $C°_I$, then :

$$C_X = k_h C°_I \qquad (25)$$

where k_h is a constant related to the homogeneous reactions (dimensionless).

By combining (24) and (25),

$$\vartheta = \frac{k_h}{k_a} C_X = k_s C_X \qquad (26)$$

where k_s (T) is the kinetic constant of the heterogeneous reaction (in $m.s^{-1}$).

For an infiltrationprocess occuring in a cylindrical pore, the boundary conditions should take into account the gaseous phase composition at both ends of the pore, which results from the various homogeneous reactions. The quality of the densification depends on the kinetic constant of the heterogeneous reaction (e.g. k_s (T)). So it seems necessary to assess the local kinetic laws such as those given by equation (26).

5 - VALIDATION OF THE MODEL

5.1 - Comparison with Van den Brekel model

If the chemical system, including an inert species 1 and a species 2 which reacts into a solid phase, is considered under the following hypotheses, (i) no variation of the gaseous mole number in the deposition reaction ($\Delta\nu = 0$), (ii) first order heterogeneous reaction with respect to species 2 and (iii) Knudsen diffusion coefficients of species 1 and 2 very high compared to binary Fick diffusion coefficient, the previously described model can be reduced to a model very similar to those proposed by Thiele [11] and then by Van den Brekel et al. [14]. In this case, the terms containing the total molar flux can be removed (equation (9)) from mass transfer equations which are analytically solved and give the profile of species 2 along the pore :

$$\frac{C_2(z)}{C_2(0)} = \frac{\mathrm{Cosh}\left(\left(1 - 2z/L\right)\tau\right)}{\mathrm{Cosh}\left(\tau\right)} \qquad (27)$$

where

$$\tau = \sqrt{\frac{k_s L^2}{D_{1,2}\Phi_0}} \qquad (28)$$

is the Thiele modulus,

with k_s (in $m.s^{-1}$) the kinetic constant of the heterogeneous reaction (from the first order kinetic law $\vartheta = k_s C_2$),

and $D_{1,2}$ (in $m^2 s^{-1}$) the Fick diffusion coefficient related to the binary mixture of species 1 and 2.

Equation (27) shows that the concentration within the pore is more homogeneous with a smaller Thiele modulus. By introducing identical data (i.e. values of L, Φ_0, k_s, $D_{1,2}$ and τ) in both present and Van den Brekel models, very similar results were obtained with relative differences lower than 10^{-3}. This validates the present model in a first simple case, which does not take into account the local variation of the diameter and the Knudsen diffusion.

5.2 - Comparison with Rossignol model

The Rossignol model, derived from Van den Brekel model, takes partially into account Knudsen diffusion and variations of the diameter but uses first order kinetics and a binary gaseous mixture. A comparison between the present model and Rossignol model can be made on the basis of thickness profiles calculated at the end of the infiltration process when the pore is closed (i.e. at $t = t_c$), in the case of the following chemical system : (i) gaseous mixture CH_3SiCl_3 (MTS)/H_2, (ii) deposit of pure SiC with a density of 3.2 and (iii) first order kinetics with respect to MTS (which is assumed not to react in the homogeneous phase), as follows :

$$\vartheta = k_0 \exp\left(-\frac{E_a}{RT}\right) C_{MTS} \qquad (29)$$

where k_0 is the frequency factor (in $m.s^{-1}$)

and E_a is the activation energy of the reaction (in $J.mol^{-1}$).

The comparison is carried out for a various values of the parameters T, P, Φ_0

and L. A few examples of these profiles calculated from both models are given in figure 4. Similar tendencies are observed when varying e.g. the temperature but a slight shift towards a less homogeneous infiltration is obtained for the Rossignol model. This shift can be attributed to the Rossignol's hypothesis of a diameter equal to the entrance diameter (i.e. always lower than the actual diameter all along the pore), which results in an over-estimated Thiele modulus and a worse infiltration profile (cf equations (27) and (28)).

ACKNOWLEDGEMENTS

This works has been supported by EEC (EURAM program contract n° MAIE/ 0018/C) and jointly by French Ministry of Research and Technology (MRT) and SEP through a grant given to one of the authors (R. F.).

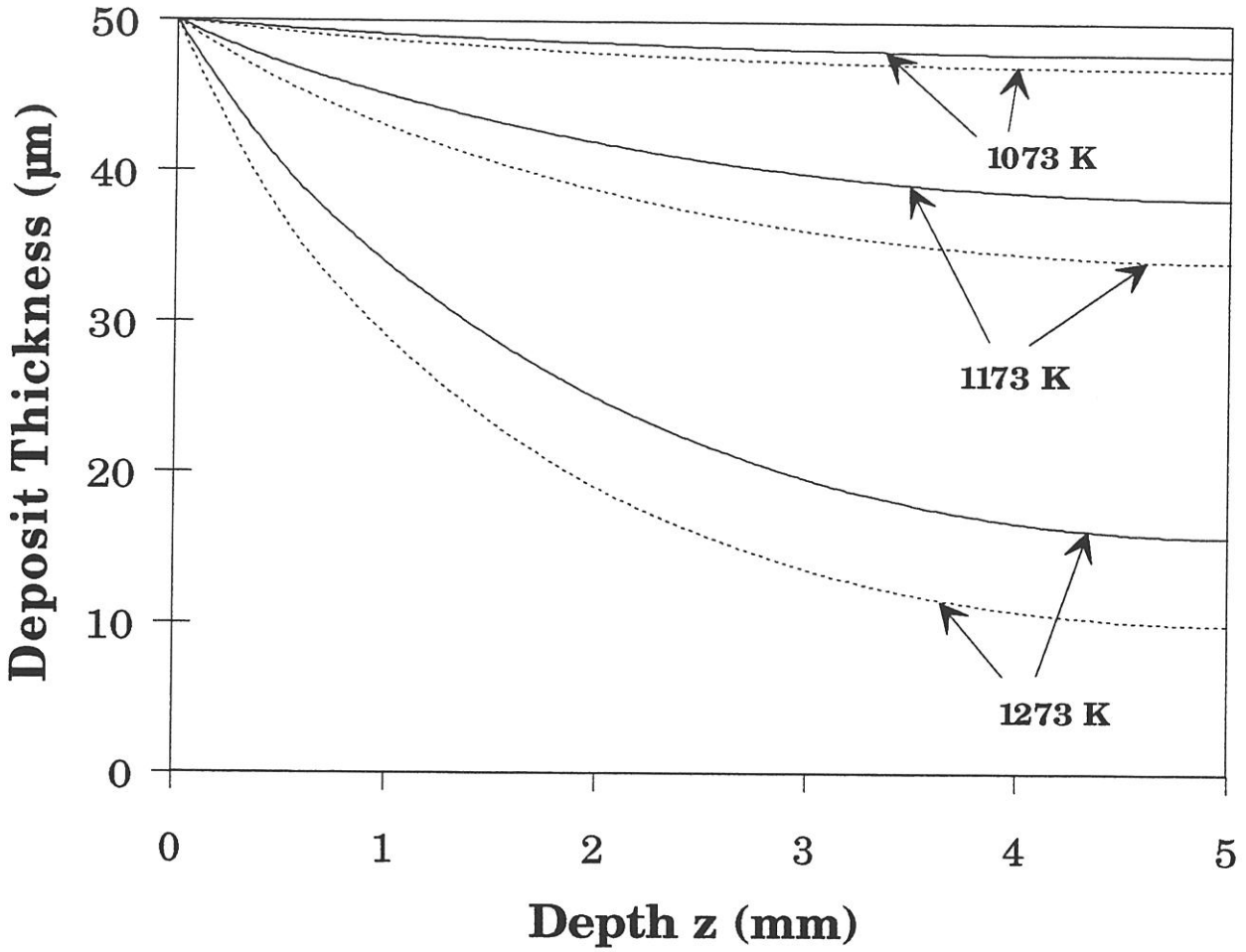

Fig. 4 - SiC thickness profiles calculated from present model (full line) and Rossignol model (dashed line) in a cylindrical straight half pore for various temperatures and P = 20 kPa, Φ_0 = 100 µm, L/Φ_0 = 100.

APPENDIX 1- Valuation of Fick diffusion coefficients

Due to the difficulties in measuring the diffusion coefficients in the gases, particularly at high temperature [30], valuation methods were proposed by various authors.

Hirschfelder formula

In order to take into account attractive and repulsive forces between molecules, Hirschfelder et al. performed various calculations on the Lennard-jones potential leading to an expression of the Fick diffusion coefficients for a binary mixture between species i and j [31] :

$$D_{i,j} = 5.876\ 10^{-24} \frac{T^{3/2}}{P\ \sigma_{i,j}^{2}\ \Omega_D} \left[\frac{1}{M_i} + \frac{1}{M_j} \right]^{1/2} \qquad \text{(A1)}$$

where $\sigma_{i,j}$ is the mean collision diameter (in m)

P is the total pressure (in Pa)

Ω_D is the Lennard-Jones collision integral (dimensionless)

M_i and M_j are the molar masses of species i and j (in $kg.mol^{-1}$)

Ω_D is a function of the adimensional factor $T^* = kT/\varepsilon_{i,j}$ where k is the Boltzman constant and $\varepsilon_{i,j}$ an energy term in the Lennard-Jones potential expression. Ω_D has been tabulated by Hirschfelder for various T* values [32]. For intermediate values of T*, linear interpolations are possible. As a consequence, it can be noticed that $D_{i,j}$ does not depend exactly on $T^{3/2}$.

The Lennard-Jones constants $\sigma_{i,j}$ and $\varepsilon_{i,j}$ for the binary mixture i, j can be determined from the characteristics of each species, according to :

$$\sigma_{i,j} = \frac{\sigma_i + \sigma_j}{2} \qquad \text{(A2)}$$

$$\frac{\varepsilon_{i,j}}{k} = \left[\frac{\varepsilon_i}{k} \cdot \frac{\varepsilon_j}{k} \right]^{1/2} \qquad \text{(A3)}$$

These individual constants can be found in tables or calculated with other formulas [25, 31]. When these various constants cannot be estimated, semi-empirical expressions are used.

Gilliland formula

Gilliland proposed a semi-empirical formula derived from the kinetic theory of gases, in order to estimate the Fick diffusion coefficient of a binary mixture i, j [33]:

$$D_{i,j} = 1.360\ 10^{-3} \frac{T^{3/2}}{P\,(v_i^{1/3} + v_j^{1/3})^2} \left[\frac{1}{M_i} + \frac{1}{M_j}\right]^{1/2} \qquad \text{(A4)}$$

where v_i and v_j are the molar volumes of species i and j at their boiling point (in $cm^3 mol^{-1}$).

APPENDIX 2- Differential equation for the pore geometry change

The required equation results from a local treatment, by writing the volume of solid δV deposited on a thin shell of pore (δz in thickness) during the time δt :

$$\delta V = \frac{\pi}{4} \left(\Phi^2(t) - \Phi^2(t+\delta t) \right) \delta z \qquad \text{(A5)}$$

This volume can also be written as a function of the rate of the heterogeneous reaction ϑ and the molar volume of the deposited solid V_s :

$$\delta V = \vartheta \, \pi \, \Phi_t \, \delta z \, \delta t \, V_s \qquad \text{(A6)}$$

Equation (A5) can be developped as follows :

$$\delta V = \frac{\pi}{4} \left(\Phi^2(t) - \left[\Phi(t) + \frac{\partial \Phi}{\partial t} \delta t \right]^2 \right) \delta z \qquad \text{(A7)}$$

or

$$\delta V = \frac{\pi}{4} \left[\Phi^2(t) - \Phi^2(t) - \left[\frac{\partial \Phi}{\partial t} \right]^2 \delta t^2 - 2 \, \Phi(t) \frac{\partial \Phi}{\partial t} \delta t \right] \delta z \qquad \text{(A8)}$$

By combining (A6) and (A8) (neglecting the second order term in (A8)) with δt approaching zero, equation (21) is deduced :

$$\frac{\partial \Phi}{\partial t} = - 2 \, V_s \vartheta \qquad (21)$$

APPENDIX 3- Discretization procedure

Space discretization

The half pore is divided in n_z identical elements with a length :

$$\Delta z = \frac{L}{2n_z} \qquad \text{(A9)}$$

which results in a network made of $n_z + 1$ points located at the abscissa :

$$z_p = p\Delta z \qquad \text{with } p = 0, 1, \ldots, n_z \qquad \text{(A10)}$$

Time discretization

The time t_c (as defined in 2.3) is divided in n_t identical periods with a duration:

$$\Delta t = \frac{t_c}{n_t} \qquad \text{(A11)}$$

which results in a network made of n_{t+1} instants t_u such as :

$$t_u = u\Delta t \qquad \text{with } u = 0, 1, \ldots, n_t$$

Discretization of the partial differential equations

The functions occurring in the equations to be solved (e.g. the diameter of the pore and the concentrations of the gaseous species) are subjected to various indices as follows : firstly, i, j, k and l for the chemical species, secondly, p for the space variable and thirdly, u for the time variable. As an example, the concentration of species i at the abscissa z_p at the instant t_u, is written $C_{i,\,p,\,u}$. By applying the finite differences method, the equations (9) and (20), which allows to calculate the profile of the total molar flux, and the mass transfer equation (14), discretized at the instant t_u, can be written as :

$$\frac{N_{p+1} - N_p}{\Delta z} = \frac{4\,(\Delta v)_p\,\vartheta_p}{\Phi_p} \qquad \text{(A12)}$$

with $\quad 0 \le p \le n_z - 1,$

$$\mathbf{N}_{n_z} = 0 \qquad \text{(A13)}$$

and

$$D_{i,p} \frac{C_{i,p+1} + C_{i,p-1} - 2C_{i,p}}{\Delta z^2} - \frac{(x_i \mathbf{N})_{p+1} - (x_i \mathbf{N})_{p-1}}{2\Delta z} + \frac{4 \nu_{i,p} \vartheta_p}{\Phi_p} = 0 \qquad \text{(A14)}$$

with $1 \leq p \leq n_z - 1$.

The last equation (A14) is equivalent to :

$$- C_{i,p-1} + 2C_{i,p} - C_{i,p+1} = \frac{4 \nu_{i,p} \vartheta_p}{D_{i,p} \Phi_p} \Delta z^2 - \frac{(x_i \mathbf{N})_{p+1} - (x_i \mathbf{N})_{p-1}}{2 D_{i,p}} \Delta z \qquad \text{(A15)}$$

The boundary conditions on the concentrations (equations (18) and (19)) become:

$$C_{i,0,u} = C_{i,e} \qquad \text{(A16)}$$

and

$$C_{i,n_z} = C_{i,n_z-1} \qquad \text{(A17)}$$

At last, discretizing between t_u and t_{u+1} the equation (21) for the diameter change, leads to :

$$\frac{\Phi_{p,u+1} - \Phi_{p,u}}{\Delta t} = - 2 (V_s)_p \vartheta_p \qquad \text{(A18)}$$

with $1 \leq p \leq n_z$ and $0 \leq u \leq n_t - 1$

REFERENCES

[1] F. Christin, R. Naslain, C. Bernard, "A Thermodynamic and Experimental Approach of Silicon Carbide-CVD Application to the CVD Infiltration of Porous Carbon-Carbon Composites", Proc. 7th Int. Conf. CVD, Los Angeles, USA (1979), (T.O. Sedgwick et al., eds.), The Electrochem. Soc., Princeton, pp. 499-514, 1979

[2] E. Fitzer, D. Hagen, J. Strohmeier, Rev. Int. Hautes Temper. Refract., Vol. 17, p. 23, 1980

[3] H. Hannache, F. Langlais, R. Naslain, "Kinetics of Boron Carbide Chemical Vapor Deposition and Infiltration", Proc. 5th European Conf. CVD, Uppsala, Sweden (1985), (J.O. Carlsson et al., eds.), Upssala Univ. Press, pp. 219-233, 1985

[4] J. Y. Rossignol, F. Langlais, R. Naslain, "A Tentative of Modelization of Titanium Carbide CVI within the Pore Network of Two-Dimensional Carbon-Carbon Composites Preforms", Proc. 9th Int. Conf. CVD, Cincinnati, USA (1984), (J. M. Blocher et al., eds.), The Electrochem. Soc., Pennington, pp. 596-914, 1984

[5] H. Hannache, R. Naslain, C. Bernard, "Boron Nitride Chemical Vapor Infiltration of Fibrous Materials from BCl_3-NH_3-H_2 or BF_3-NH_3 Mixtures : a Thermodynamic and Experimental Approach", J. Less-Common Met., Vol. 95, pp. 221-246, 1983

[6] R. Colmet, L. Lhermitte-Sebire and R. Naslain, Adv. Ceram. Mater., Vol. 138, N° 2, p. 221, 1986

[7] R. Colmet, R. Naslain, P. Hagenmuller, C. Bernard, "Thermodynamic and Experimental Analysis of Chemical Vapor Deposition of Alumina from $AlCl_3$- H_2-CO_2 Gas Phase Mixtures", J. Electrochem. Soc., Vol. 129, N° 6, pp. 1367- 1372, 1982

[8] J. Minet, F. Langlais and R. Naslain, Composites Sci. Technology, Vol. 37, pp. 79-107, 1990

[9] J. Minet, F. Langlais, R. Naslain, "On the Chemical Vapor Deposition of Zirconia from $ZrCl_4$-H_2-CO_2-Ar Gas Mixture : II An Experimental Approach", J. Less-Common Met., Vol. 132, pp. 273-287, 1987

[10] T. M. Bessmann, R.A. Lowden, D.P. Stinton, T.L. Starr, "A Method for Rapid Chemical Vapor Infiltration of Ceramic Composites", Proc. 7th European Conf. CVD, Perpignan, France (1989), (M. Ducarroir et al., eds.), Colloque de Physique, Les Editions de Physique, Colloque C5, Suppl. N° 5, Vol 50, pp. 229-239, 1989

[11] E. W. Thiele, "Relation Between Catalytic Activity and Size of Particle", Ind. Eng. Chem., Vol. 31, N° 7, pp. 916-920, 1939

[12] E.E. Petersen, "Reaction of Porous Solid", AIChE Journal, Vol. 3, N° 4, pp. 443-448, 1957

[13] E. Fitzer and R. Gadow, "Fiber-Reinforced Silicon Carbide", Am. Ceram. Soc. Bull., Vol. 65, pp. 326-335, 1986

[14] C. H. J. Van Den Brekel, R. M. M. Fonville, P. J. M. Van Der Straten, G. Verspui, "CVD of Ni, TiN and TiC on Complex Shapes", Proc. 8th Int. Conf. CVD, Paris, France (1984), (Mc D. Robinson et al., eds.), The Electrochem. Soc., Pennington, pp. 142-156, 1984

[15] Y. S. Lin, K. J. De Vries, A. J. Burggraaf, "CVD Modification of Ceramic Membranes: Simulation and Preliminary Results", Proc. 7th European Conf. CVD, Perpignan, France (1989), (M. Ducarroir et al., eds.), Colloque de Physique, Les Editions de Physique, Colloque C5, Suppl. N° 5, Vol. 50, pp. 861-872, 1989

[16] S. M. Gupte, J. A. Tsamopoulos, "Densification of Porous Materials by Chemical Vapor Infiltration", J. Electrochem. Soc., Vol. 136, N° 4, pp. 555-561, 1989

[17] N. H. Tai, T. W. Chou, "Analytical Modeling of Chemical Vapor infiltration in Fabrication of Ceramic Composites", J. Am. Ceram. Soc.,Vol. 72, N° 3, pp. 414-420, 1989

[18] S. Middleman, "The Interaction of Chemical Kinetics and Diffusion in the Dynamics of Chemical Vapor infiltration", J. Mater. Res. ,Vol. 4, N° 6, pp. 1515-1524, 1989

[19] M. F. Carolan, J. N. Michaels, "Chemical Vapor Deposition of Yttria Stabilized Zirconia on Porous Supports", Solid State Ionics, Vol. 25, pp. 207-216, 1987

[20] T. L. Starr, "Modeling of Forced Flow/Thermal Gradient CVI", Proc. Int. Conf. on Wiskers-and-Fiber-Toughened Ceramics, Oak Ridge, USA (1988), (R. A. Bradley et al., eds), ASM International, Oak Ridge, pp. 243-252, 1988

[21] R. Fédou, F. Langlais, R. Naslain, "A Modeling of Isothermal/Isobaric Chemical Vapor Infiltration in a Straight Cylindrical Pore. Part 2 : Application to the CVI of SiC", to be published

[22] R. Fédou, F. Langlais, R. Naslain, "A Modeling of Isothermal/Isobaric Chemical Vapor Infiltration in a Straight Cylindrical Pore. Part 3 : Application to the CVI of Zirconia or Yttria", to be published

[23] R. Fédou, P. Dupel, F. Langlais, R. Pailler, R. Naslain, "A Modeling of Isothermal/ Isobaric Chemical Vapor Infiltration in a Straight Pore with a Rectangular Cross Section. Application to the CVI of PyroCarbon ", to be published

[24] P. Molaës, J.C. Molaës, "Cinétique Chimique et Chimie Organique", Vuibert, Paris, 1985

[25] R.B. Bird, W.E. Stewart, E.N. Lightfoot, "Transport Phenomena", J. Wiley and sons, eds., New York, 1960

[26] M. Knudsen, "The Kinetic Theory of Gases", 3rd ed., Wiley, New York, 1950

[27] P.C. Carman, "L'écoulement des gaz à travers les milieux poreux", translated by J. Machefer, P.U.F., Paris, 1961

[28] M. Sibony, J.-Cl. Mardon, "Analyse Numérique II - Approximations et Equations Différentielles", Hermann, 1988

[29] J.P. Lamoitier, "Le Langage FORTRAN IV", Dunod Université, Paris, 1978

[30] J. Salvinien, B. Brun, J. Apell, "Mesure des coefficients de diffusion, Séparation chimique", Les Techniques de l'Ingénieur, Paris, p. 1515

[31] J.O. Hirschfelder, R.B. Bird, E.L. Spotz, Chem. Revs., Vol. 44, p. 205, 1949

[32] J.O. Hirschfelder, C.F. Curtis, R.B. Bird, "Molecular Theory of Gases and Liquid", Wiley, New York, 1954

[33] E.R. Gilliland, Ind. Eng. Chem., Vol. 26, p. 681, 1934

CHAPITRE 2

Titre : A MODELING OF THE ISOTHERMAL ISOBARIC CHEMICAL VAPOR INFILTRATION IN A STRAIGHT CYLINDRICAL PORE PART 2 - APPLICATION TO THE CVI OF SiC

A MODELING OF THE ISOTHERMAL ISOBARIC CHEMICAL VAPOR INFILTRATION IN A STRAIGHT CYLINDRICAL PORE PART 2 - APPLICATION TO THE CVI OF SiC

R. FÉDOU, F. LANGLAIS (*) and R. NASLAIN
Laboratoire des Composites Thermostructuraux (UMR 47 CNRS-SEP-UB1)
Domaine Universitaire, 3 Allée La Boétie
33600 Pessac (France)

ABSTRACT : A previously described modeling of the chemical vapor infiltration process in a straight cylindrical pore is applied to the deposition of SiC-based ceramics from CH_3SiCl_3-H_2 in the case of a first order kinetic law with respect to CH_3SiCl_3. The model gives concentrations and deposit thickness profiles along the pore at any stage of the densification and particularly at the end of the process when the pore becomes sealed. The infiltration homogeneity is predicted to be improved by decreasing the aspect ratio of the pore, the CVI temperature and, under conditions of Fick diffusion, by decreasing the total pressure and the pore diameter.The model is validated by the good fit between the deposit thickness profiles along the pore calculated after adjustment of the kinetic data and experimental profiles drawn for a 34 µm straight pore.

INTRODUCTION

Silicon carbide (SiC) is more and more prepared as thin films by chemical vapor deposition (CVD), for its interesting physical and chemical properties. Besides its electronic applications [1], SiC is used as a matrix in the fiber reinforced ceramic-ceramic composites owing to its high thermal, mechanical and chemical characteristics for applications at high temperatures in oxidizing atmospheres [2]. The chemical vapor infiltration technique (CVI), which directly derives from CVD, is well adapted to the processing of such ceramic matrix composites : it mainly consists in a densification of a porous fiber preform with the ceramic matrix deposited in-situ from a gaseous precursor [3].

(*) to whom correspondence should be sent

If specific cases are excepted [4-13], most of SiC depositions involve the Si-C-H-Cl chemical system [2, 14-26]. An organometallic compound e.g. CH_3SiCl_3 (MTS), is often used as precursor partly for its ability to be decomposed at moderate temperatures (which usually favors the CVI-process), partly for economical reasons [27, 28].

In order to understand the mechanisms involved in the CVI-process and to optimize the homogeneity and the rate of the infiltration, a model was built up in the case of a single straight cylindrical pore. A detailed description of this model was given in the previous paper, Part 1 [29]. The aim of the present second part is to apply the model to the CVI of SiC in the MTS-H_2 system, to investigate the effect of the experimental parameters on the theoretical deposit thickness and concentration profiles, on the basis of simplified hypotheses concerning the heterogeneous chemical process. Then, an experimental procedure in a hot wall reactor is proposed to validate the model and the hypotheses on the chemistry are discussed in order to fit the calculated profiles with the experimental data.

2 - DATA RELATED TO THE CH_3SiCl_3-H_2 SYSTEM

2.1 - The gaseous phase

The MTS molecule is known to be rapidly decomposed in the homogeneous phase, particularly in a hot wall reactor [30]. But data are not available, neither on the kinetics of the homogeneous reactions, nor on the actual composition of the gaseous phase close to the deposition surface. So MTS is supposed to react itself heterogeneously according to :

$$CH_3SiCl_{3(g)} \xrightarrow{H_2} SiC_{(s)} + 3HCl_{(g)} \qquad (1)$$

This SiC deposition reaction gives rise to a large amount of HCl. As a consequence, the chemical system considered in the present application of the CVI model includes the three following gaseous species : MTS, H_2, HCl.

2.1.1 - Diffusion coefficients

The Knudsen diffusion coefficient of species i is calculated by using equation (16) of Part 1 [29], which can be written as :

$$D_{i,K} = d_{i,K}\,\Phi\,T^{1/2} \qquad (2)$$

where $d_{i,K}$ is a reduced Knudsen diffusion coefficient which depends only on the molar mass of the species i (table I).

The Fick diffusion coefficients are calculated on the basis of equation (15) and appendix 1 in Part 1 [29]. For the binary mixtures including MTS molecules, it is necessary to use the Gilliland's expression (equation (A4) in [29]) rather than that of Hirschfelder (equation (A1) in [29]) because data such as collision diameter σ and reduced Lennard-Jones energy ε/k are not available for MTS. The data needed to perform the calculations of Fick diffusion coefficients are listed in tables II and III : σ, ε/k and molar volume v for each species. The molar volume of CH_3SiCl_3 is considered as the sum of the volumes of each atom [31].

2.1.2 - Heterogeneous kinetics

The reaction corresponding to equation (1) was found by a few authors to exhibit a first order kinetics with respect to MTS under specific conditions [23, 27, 28, 33]. Nevertheless, several results are not in good accordance with such an order and the surface mechanisms involved in this system are not clarified [34-36]. In the present study, a simplified kinetics is used, which assumes a direct reaction of MTS on the solid surface and first order with respect to this species. The kinetic law taken from Schoch et al. [37] is the following :

$$\vartheta = k_0 \exp\left(-\frac{E_a}{\boldsymbol{R}T}\right) C_{MTS} \qquad (3)$$

where $k_0 = 3.89\ 10^9\ m.s^{-1}$

$E_a = 296\ kJ.mol^{-1}$

$\boldsymbol{R}$ is the ideal gas constant ($8.314\ J.mol^{-1}\ K^{-1}$)

and C_{MTS} is MTS concentration in the gaseous phase near the reaction surface (in $mol.m^{-3}$).

Species i	CH_3SiCl_3	H_2	HCl
M_i ($kg.mol^{-1}$)	0.149	$2\ 10^{-3}$	$3.65\ 10^{-2}$
$d_{i,K}$ ($m.s^{-1}.K^{-1/2}$)	3.97	34.30	8.03

Table I : Values of molar masses M_i and reduced Knudsen diffusion coefficients $d_{i,K}$

Species i	H_2	HCl
σ_i (nm)	0.2827	0.3339
ε_i/k (K)	59.7	344.7

Table II : Values of σ_i and ε_i/k chosen for the calculation of Ω_D (from [31])

Species i	v_i or Σv_i $cm^3.mol^{-1}$
H_2	14.3
CH_3SiCl_3	122.7
HCl	25.3

Table III : Values of molar volume used in the Gilliland formula (from [32])

2.2 - The deposited solid

The gaseous mixture MTS - H_2 can yield a codeposition of SiC with free carbon or free silicon under specific conditions. Nevertheless, it is possible to find a large range of experimental conditions which lead to stoichiometric SiC deposit. In the present study, the deposited solid is assumed to be pure SiC without microporosity.

The molar volume V_s of SiC (which is supposed not to depend on the deposition conditions), calculated according to equation (21) from part 1 [29] with a density of 3.2, is equal to $1.25 \times 10^{-5} m^3 mol^{-1}$.

2.3 - The boundary conditions

At the pore entrances, the gaseous phase composition is assumed to be constant and the HCl concentration to be zero :

$$C_{MTS}(0,t) = C_{MTS,0} \tag{4}$$

$$C_{H_2}(0,t) = C_{H_2,0} \tag{5}$$

$$C_{HCl}(0,t) = 0 \tag{6}$$

As MTS species is not supposed to react homogeneously, the gaseous phase at the entrances of the pore can be partly defined by the ratio α between H_2 and MTS concentrations at the entrance of the reactor :

$$\frac{C_{H_2,0}}{C_{MTS,0}} = \alpha \tag{7}$$

On the other hand, the entrance total concentration can be written as a function of the temperature T and the total pressure P :

$$C_{H_2,0} + C_{MTS,0} = \frac{P}{\boldsymbol{R}\,T} \tag{8}$$

By combining (7) and (8), it is possible to calculate each entrance concentration

with respect to the experimental parameters :

$$C_{MTS,0} = \frac{1}{1+\alpha} \quad \frac{P}{\boldsymbol{R}\,T} \tag{9}$$

$$C_{H_2,0} = \frac{\alpha}{1+\alpha} \quad \frac{P}{\boldsymbol{R}\,T} \tag{10}$$

3 - CALCULATION RESULTS

The model provides the diameter of the pore and the composition of the gaseous phase for any value of the space - time coordinates (z,t) and any infiltration conditions : T, P, α-values at the pore entrance and geometry of the pore (length L and initial diameter Φ_0). The results of the simulation are mainly presented as deposit thickness profiles ((Φ_0 -Φ(z,t))/2 where Φ(z,t) is the diameter at the abscissa z and the instant t) in a half pore (i.e. for $0 \leq z \leq L/2$ with L length of the pore) at the end of the densification process, i.e. when the pore entrance becomes closed at $t = t_c$. A few examples of gaseous species concentration profiles and plots of the infiltrated volume fraction of SiC versus time are also given.

3.1 - Influence of temperature

Figure 1 shows the influence of temperature on the calculated profiles, for a total pressure of 20 kPa, an initial pore diameter Φ_0 = 100 µm, an initial aspect ratio (L/Φ_0) of 100 and a value α = 10.

The infiltration appears to be almost perfectly homogeneous at 1073 K, while at 1373 K only a very thin layer of SiC is deposited at the center of the pore. These results, which depend directly on the high activation energy of the heterogeneous kinetics, are qualitatively similar to those presented in previous works [3,26,38].

3.2 - Influence of total pressure

The influence of total pressure is shown in figures 2 and 3 for a temperature of 1223 K, an initial aspect ratio of 100, a gaseous phase composition defined by α = 10 and a respective diameter of 100 and 1 µm (which means respective length of 10 and

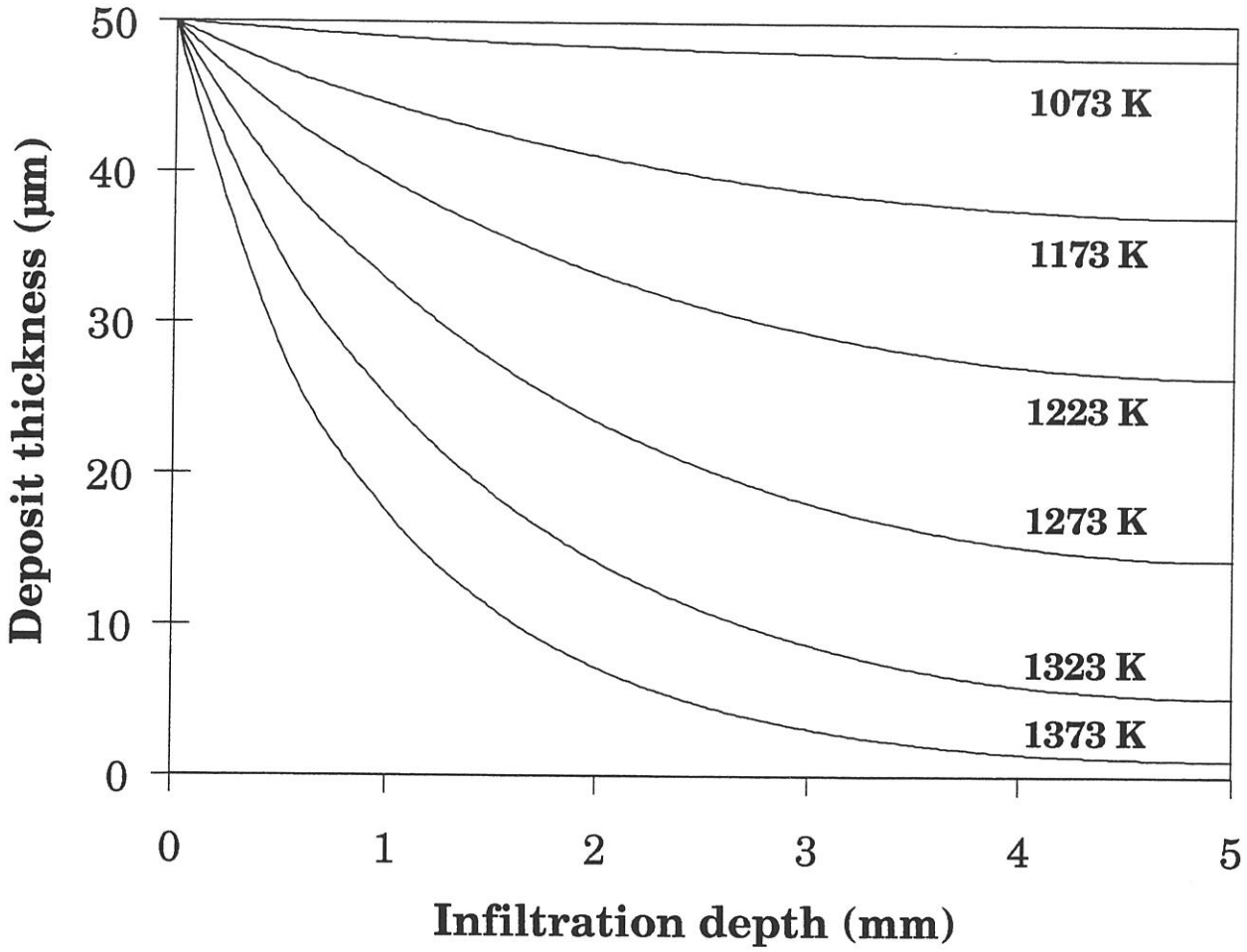

Fig. 1 : Influence of temperature on the calculated thickness profiles of a silicon carbide deposit obtained from a MTS - H_2 gas mixture with: P = 20 kPa, Φ_0 = 100 µm, L/Φ_0 = 100, α = 10

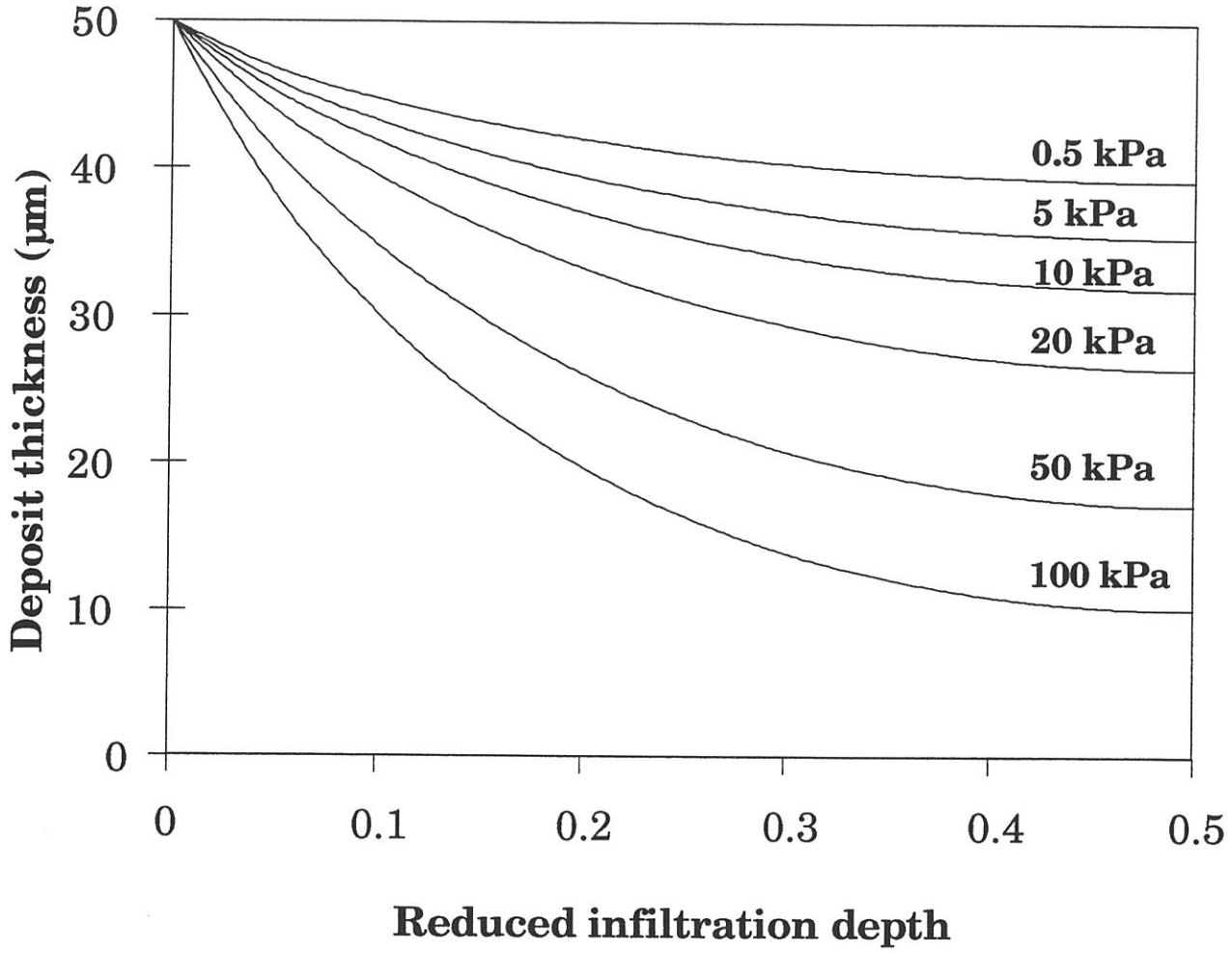

Fig. 2 : Influence of total pressure under Fick diffusion regime on the calculated thickness profiles of a silicon carbide deposit obtained from a MTS - H_2 gas mixture with : T =1223 K, Φ_0 = 100 µm, L/Φ_0 = 100, α = 10

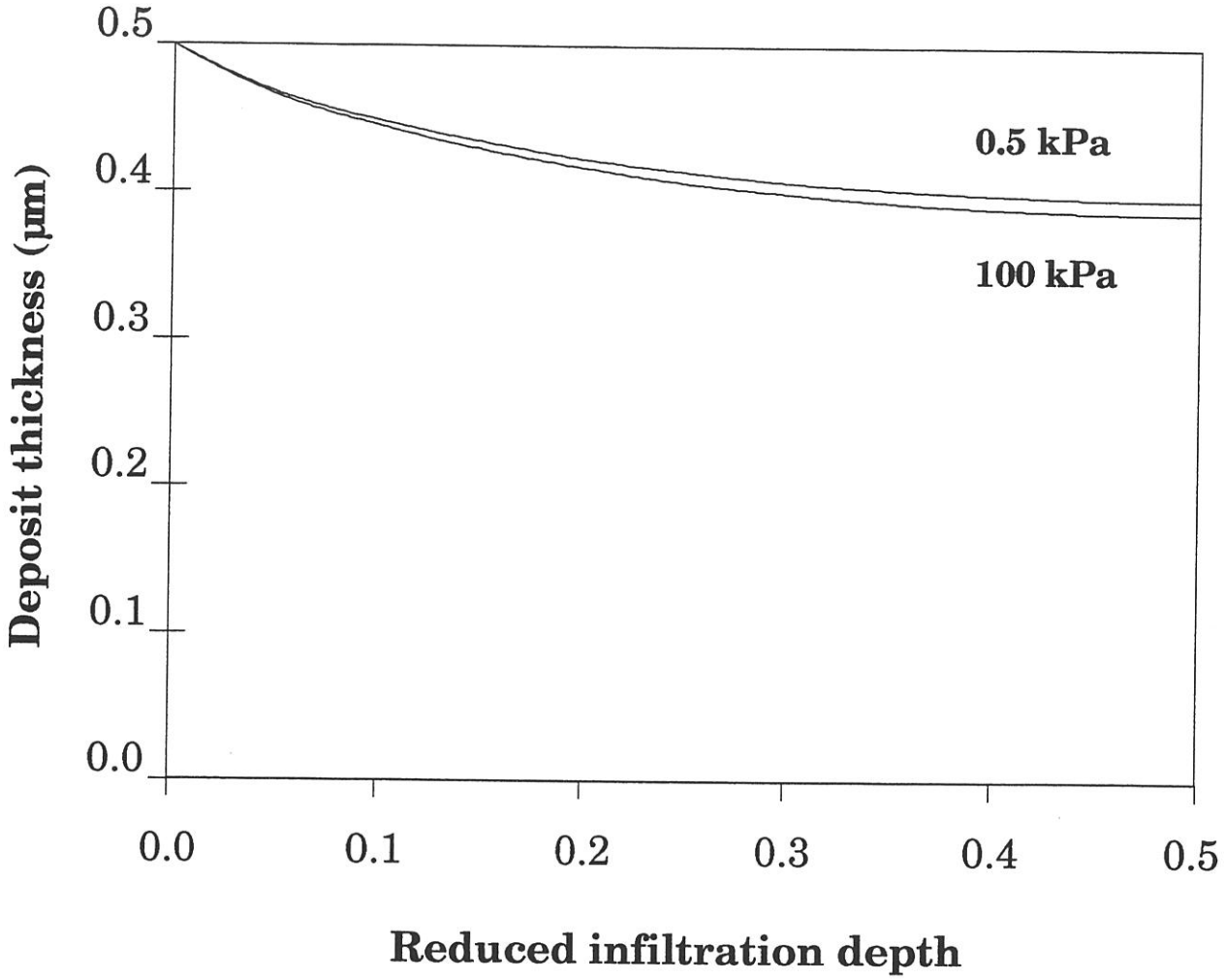

Fig. 3 : Influence of total pressure under Knudsen diffusion regime on the calculated thickness profiles of a silicon carbide deposit obtained from a MTS - H_2 gas mixture with : T =1223 K, Φ_0 = 1 µm, L/Φ_0 = 100, α = 10

0.1 mm). In order to compare the behavior of both types of pores, the use of the reduced infiltration depth z' = z/L is needed [29]. In the first case (i.e. for the large pore where the mass transfers occur mainly by Fick diffusion), a decrease of the total pressure from 100 to 10 kPa drastically improves the infiltration homogeneity, but a further decrease from 10 to 0.5 kPa should not be very usefull. This latter feature can be explained by assuming that, as the pressure decreases the Knudsen regime becomes predominant and the effect of pressure on the reaction rate and the diffusion transfer are balanced. This independence of the infiltration profiles with total pressure in Knudsen regime is confirmed in the case of small pores where a pressure decrease from 100 to 0.5 kPa results in a very low profile change. This independence can be explained on the basis of the Thiele modulus, a dimensionless number characterizing the homogeneity of a deposit in a cylindrical pore for a reaction order of one (the infiltration profiles are more homogeneous with a smaller Thiele modulus) [29] :

$$\tau = \sqrt{\frac{k_s L^2}{D\Phi_0}} \qquad (11)$$

where k_s is the kinetic constant of the heterogeneous reaction (in $m.s^{-1}$).

For Fick diffusion regime, the diffusion coefficient D is proportional to P^{-1} and τ is proportional to $P^{1/2}$. So a decrease of P leads to a decrease of τ, which means an improvement of the infiltration profile.

Under Knudsen diffusion regime, D and consequently τ do not depend on the total pressure which does not affect the infiltration profiles.

3.3 - Influence of the gas phase composition at the pore entrance

Deposit thickness profiles are plotted in figure 4 for three values of the external composition ratio α, T = 1223 K, P = 20 kPa, Φ_0 = 100 µm and L/Φ_0 = 100 (i.e. under Fick diffusion regime). The small differences between these profiles can be attributed to the dependence of the MTS Fick diffusion coefficient on the composition of the gas phase. This coefficient is a combination of the MTS-H_2 and MTS-HCl binary mixtures coefficients, with the molar fractions of H_2 and HCl, according to equation (15) in [29]. When MTS species is highly diluted in hydrogen, i.e. for a high α ratio ($10 \leq \alpha \leq 100$), D_{MTS} is very close to $D_{MTS,\ H2}$ and the calculated profile in the pore is hardly influenced by the external composition of the gas phase. For a more concentrated gaseous mixture ($1 \leq \alpha \leq 10$), HCl molar fraction within the pore is relatively high

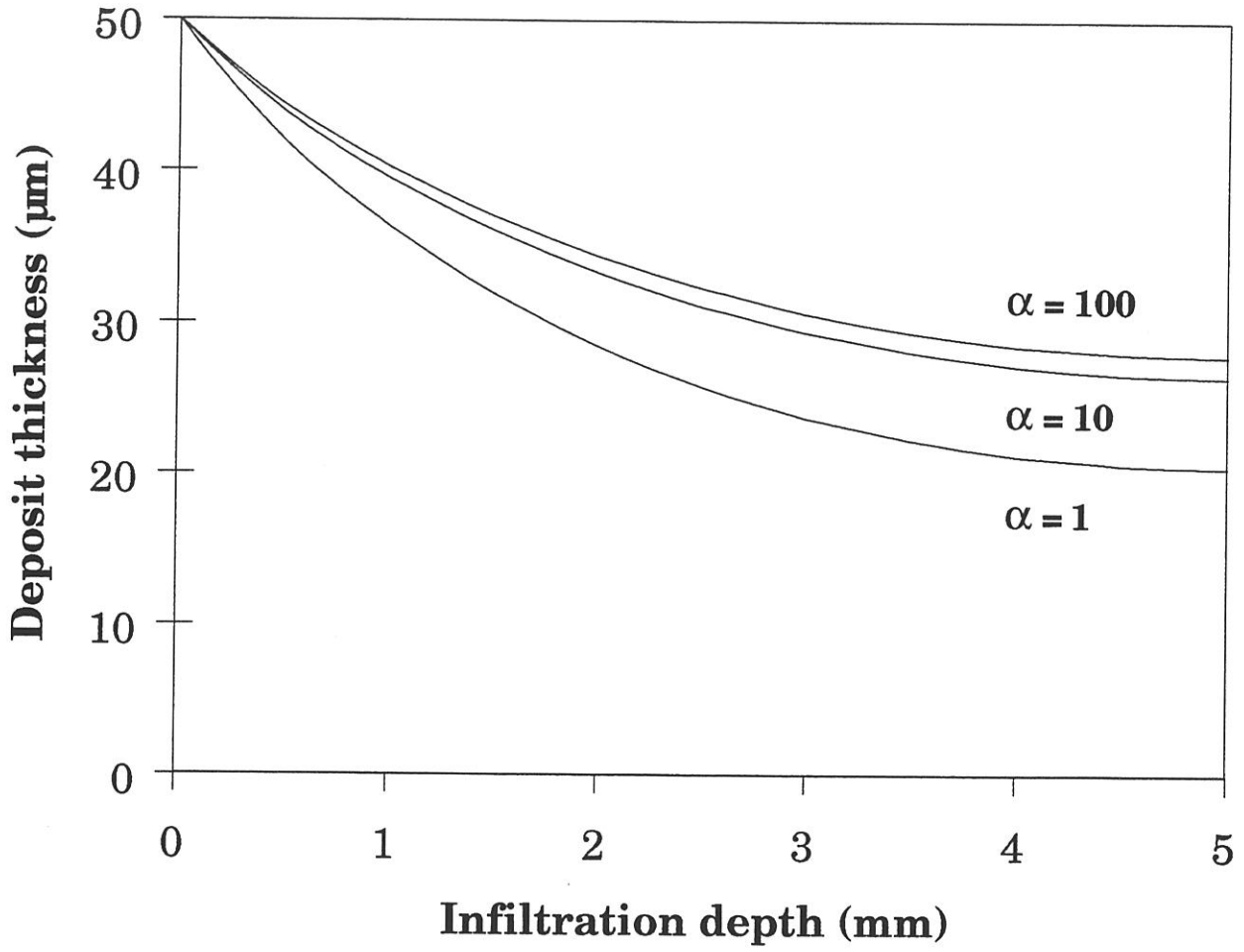

Fig. 4 : Influence of external composition of the gas phase (α ratio = $[H_2]$/[MTS]) on the calculated thickness profiles of a silicon carbide deposit obtained from a MTS - H_2 gas mixture with : T =1223 K, P = 20 kPa, Φ_0 = 100 µm, L/Φ_0 = 100, and $1 \leq \alpha \leq 100$

and $D_{MTS,\ HCl}$ which is lower than $D_{MTS,\ H2}$, must be taken into account. As α decreases from 10 to 1, an increase of HCl concentration results in a decrease of D_{MTS} and a degradation of the infiltration profile.

Generally speaking, the low dependence of the deposit thickness profiles on the gas phase composition originates in the first order of the deposition reaction rate. The case of more complex kinetic laws will be studied in one of the companion papers (Part 3 [39]).

3.4 - Influence of the pore geometry

The influence of the geometry of the pore is presented in figures 5 to 7. It can be analysed on the basis of the Thiele modulus re-expressed as follows :

$$\tau = \frac{L}{\Phi_0} \Phi_0^{1/2} \sqrt{\frac{k_s}{D}} \qquad (12)$$

with two geometrical parameters : the aspect ratio L/Φ_0 and the pore diameter Φ_0.

Figure 5 shows the influence of the aspect ratio L/Φ_0 on the calculated thickness profiles for T = 1223 K, P = 0.1 kPa, α = 10 and Φ_0 = 100 µm. As the aspect ratio increases from 10 to 1000, i.e. the pore length varies from 1 to 100 mm, the infiltration profiles (drawn with the reduced infiltration depth as abscissa) are less and less homogeneous particularly for the high values of the aspect ratio.

Figure 6 shows the variations of the deposit thickness at a given infiltration depth and at the end of the densification (i.e. for $t = t_c$), as a function of the aspect ratio, under the same conditions as those for figure 5. For the high values of the aspect ratio, the chosen infiltration depths (1 to 4 mm) are close to the entrance of the pore. The deposit thickness decreases rapidly when L/Φ_0 rises up to 500, but beyond this value the variations are rather flat, i.e. the phenomena occurring near the pore entrance are not significantly influenced by the length of the pore. The first part of these plots can be explained as follows : an increase of the aspect ratio provides a larger area available for the heterogeneous reaction, which leads to a more important consumption of MTS species per unit time, i.e. a higher MTS molar diffusional flux at the pore entrance and consequently an increase of MTS concentration and deposit thickness gradients.

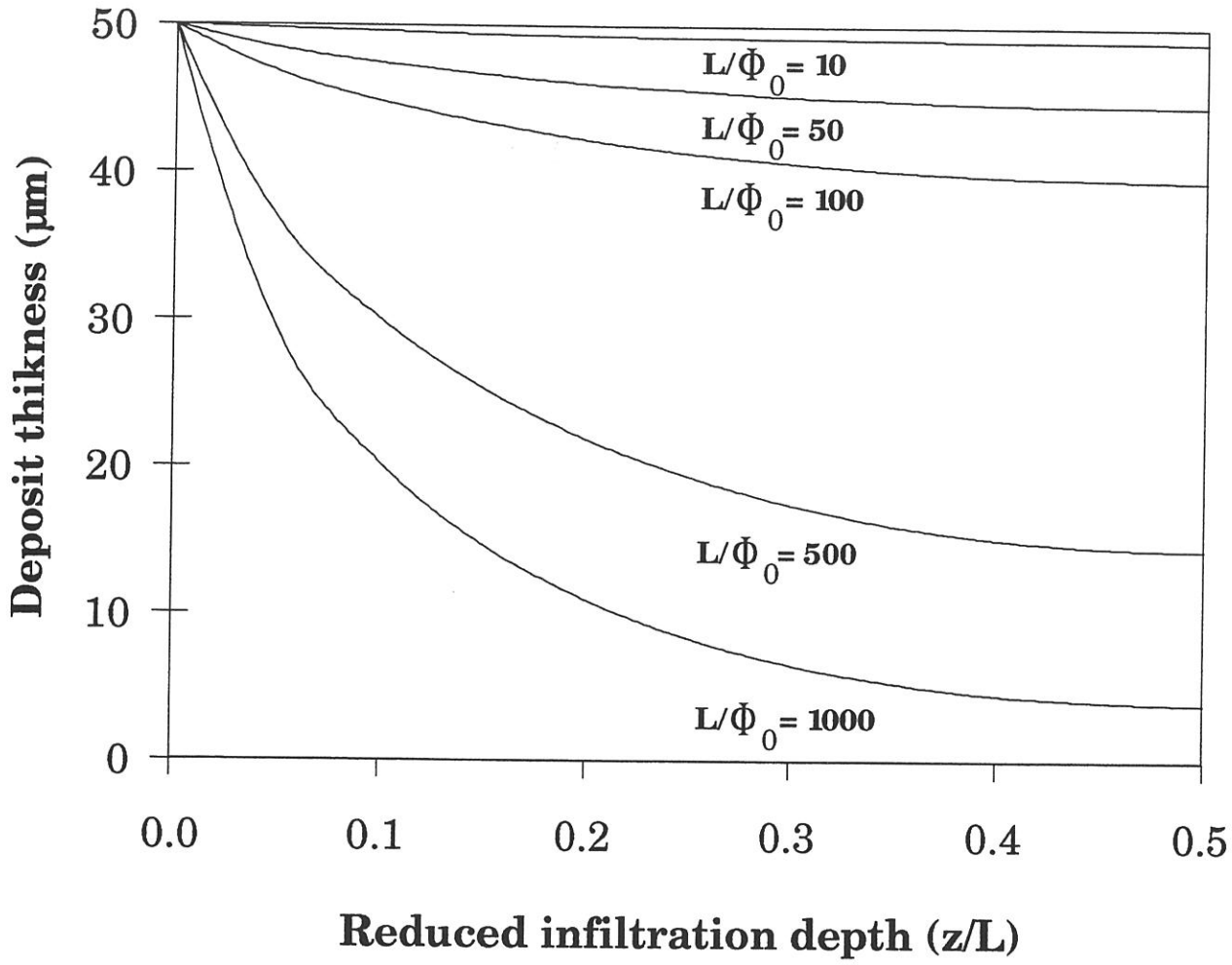

Fig. 5 : Influence of the aspect ratio on the calculated thickness profiles of a silicon carbide deposit obtained from a MTS - H_2 gas mixture with : T =1223 K, P = 0.1 kPa, Φ_0 = 100 µm, α = 10

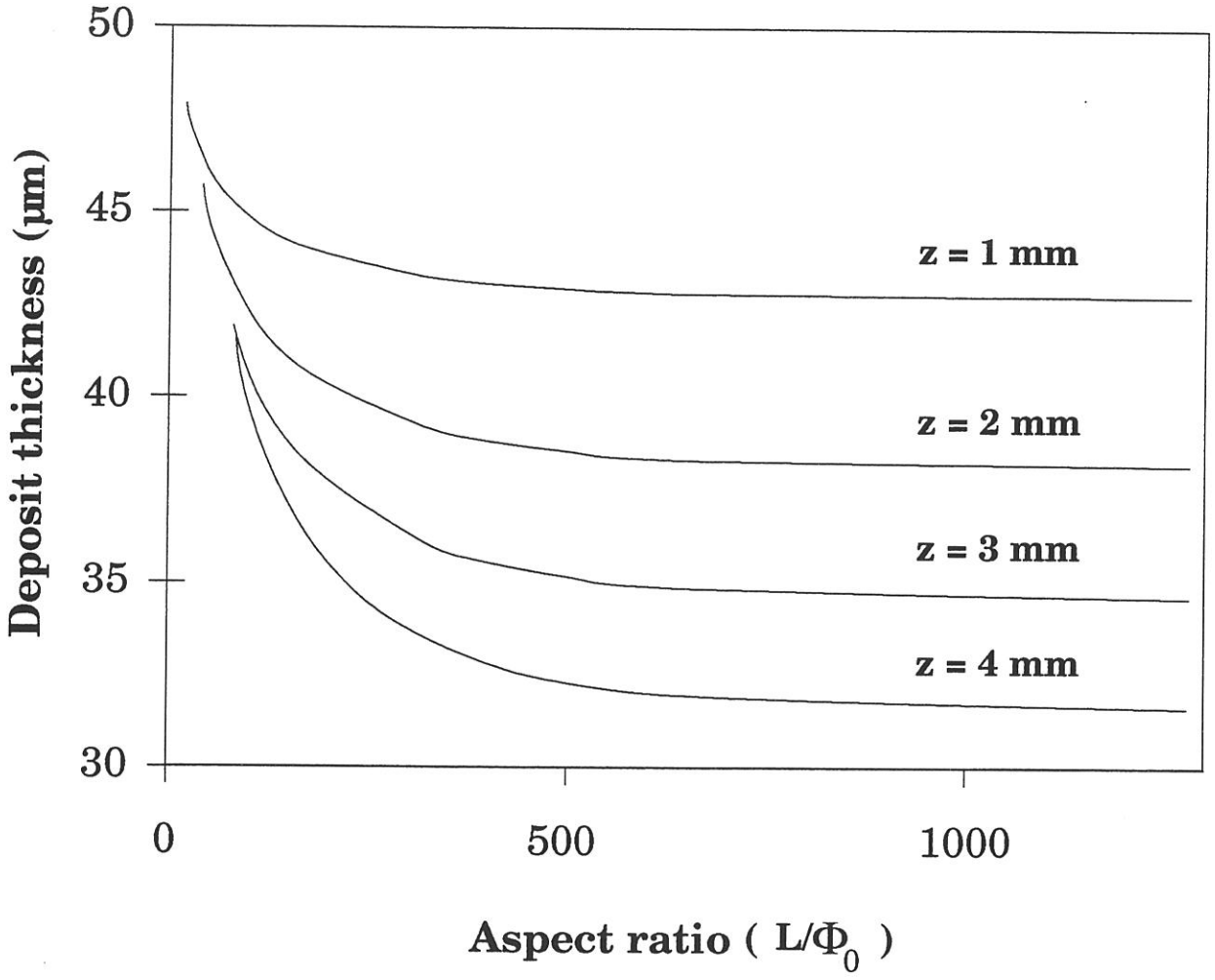

Fig. 6 : Influence of the aspect ratio on the deposit thickness at $t = t_c$ and at a given infiltration depth z (with $1 < z < 4$ mm) in a cylindrical pore for silicon carbide infiltration with :T =1223 K, P = 0.1 kPa, Φ_0 = 100 µm, α = 10

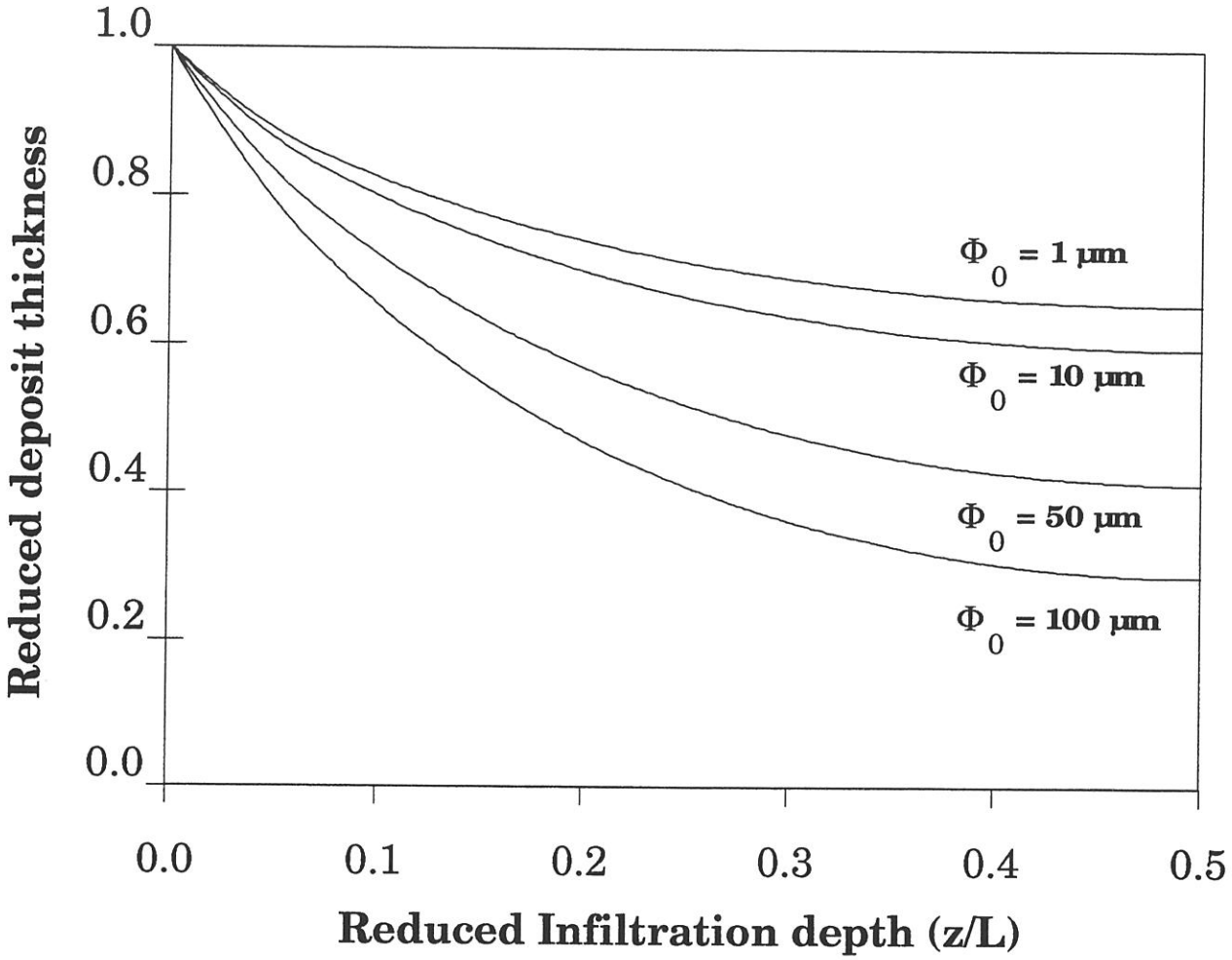

Fig. 7 : Influence of the diameter on the calculated thickness profiles of a silicon carbide deposit obtained from a MTS - H_2 gas mixture with : T =1273 K, P = 20 kPa, $L/\Phi_0 = 100$, $\alpha = 10$

The influence of the pore diameter Φ_0 (with a constant aspect ratio) on the infiltration profiles has been shown in figure 7 by plotting the reduced deposit thickness $(\Phi_0 - \Phi(z, t_c))/\Phi_0$ versus the reduced infiltration depth, under the following conditions : T = 1223 K, P = 20 kPa, α = 10 and L/Φ_0 = 100. A decrease of the pore diameter improves the homogeneity of the infiltration profile, which is in accordance with a decrease of the Thiele modulus (equation (12)), but the improvement is not so important for the small pores ($1 \leq \Phi_0 \leq 10$). In this latter case, as the pore diameter decreases, the mass transers occur more and more by Knudsen diffusion, the diffusion coefficient D becomes proportional to the diameter Φ_0 and the Thiele modulus and the infiltration profile become independent of the diameter (for a constant aspect ratio).

3.5 - Concentration and deposit thickness profiles during densification

As the model permits to calculate the deposit thickness and the gas phase concentrations at any stage of the infiltration process, it is interesting to simulate how the densification occurs as a function of time. The chosen conditions are the following : T = 1223 K, P = 100 kPa, Φ_0 = 100 µm, L/Φ_0 = 100 and α = 10.

Figure 8 shows the various profiles for four values of the infiltration time (including the last : $t = t_c$). The thickness gradient is steeper and steeper close to the pore entrance as the densification process is going on (fig. 8a). On the other hand, the gaseous species concentration profiles (fig. 8b) exhibit simultaneous decrease of MTS concentration and increase of HCl concentration from the entrance to the center of the pore. The concentration gradients are increased during the infiltration and particularly at the end of the process (i.e. between $t = 0.75\ t_c$ and $t = t_c$). Moreover, it is worthy of note that the gas phase near the center of the pore is rather poor in MTS while HCl concentration is almost as high as that of MTS at the entrance of the pore. These results are directly related to the rather poor thickness profiles shown in figure 8a.

The deposit thickness can also be plotted versus reduced time as shown in figure 9 for various infiltration depths from the entrance (z = 0) to the center (z = 5 mm) of the pore. As densification proceeds, the local deposition rate decreases within the pore and particularly at the center, while it is constant at the entrance.

Another way to simulate the pore densification is to plot versus reduced time the volume fraction of infiltrated silicon carbide, as defined by :

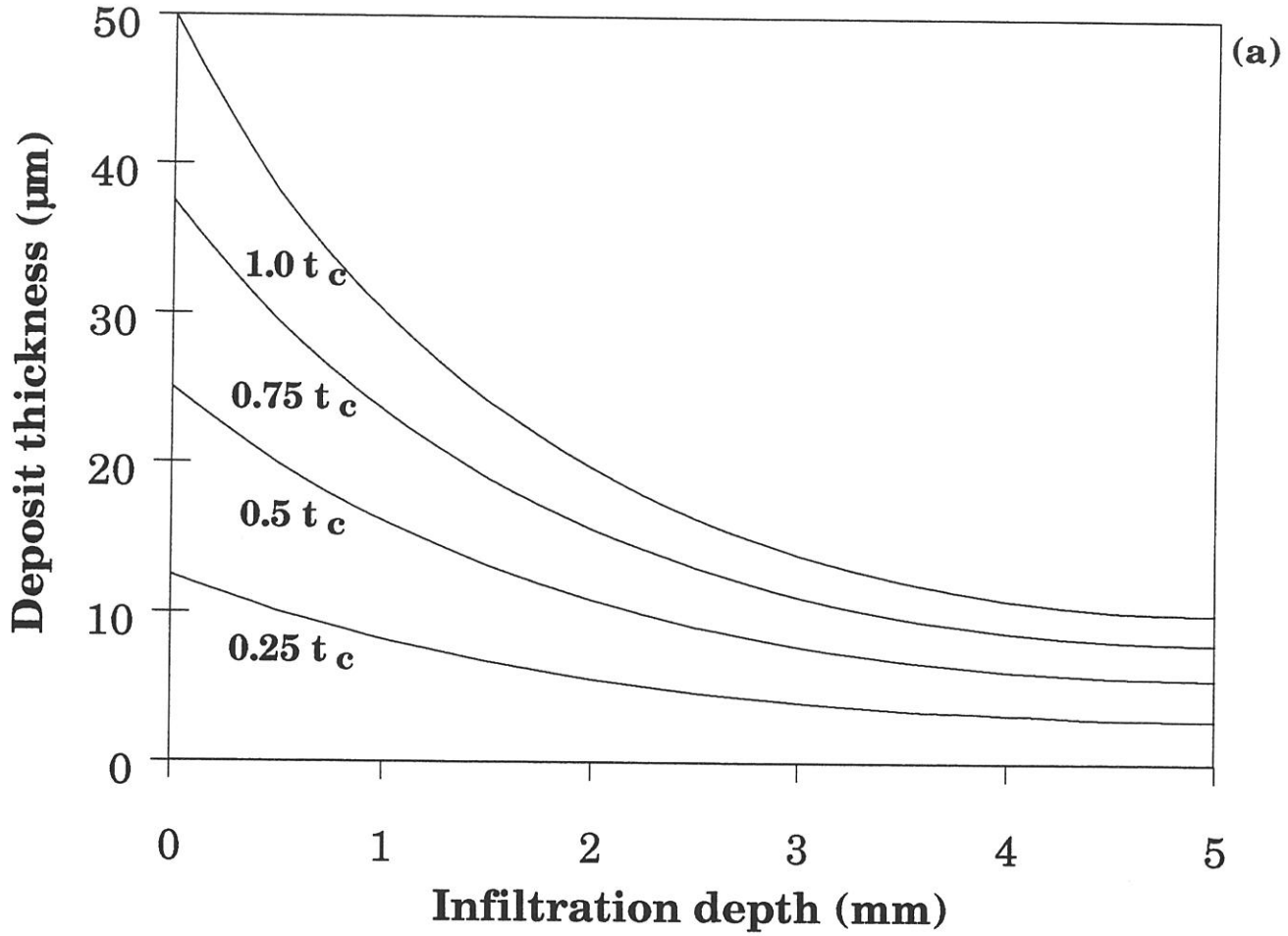

Fig. 8 : Calculations of (a) deposit thickness profile and (b) concentrations of the gaseous species profiles for a silicon carbide deposit obtained from a MTS-H_2 gas mixture and for various infiltration times between t = 0 and t = t_c with : T =1223 K, P = 100 kPa, Φ_0 = 100 µm, L/Φ_0 = 100, α = 10

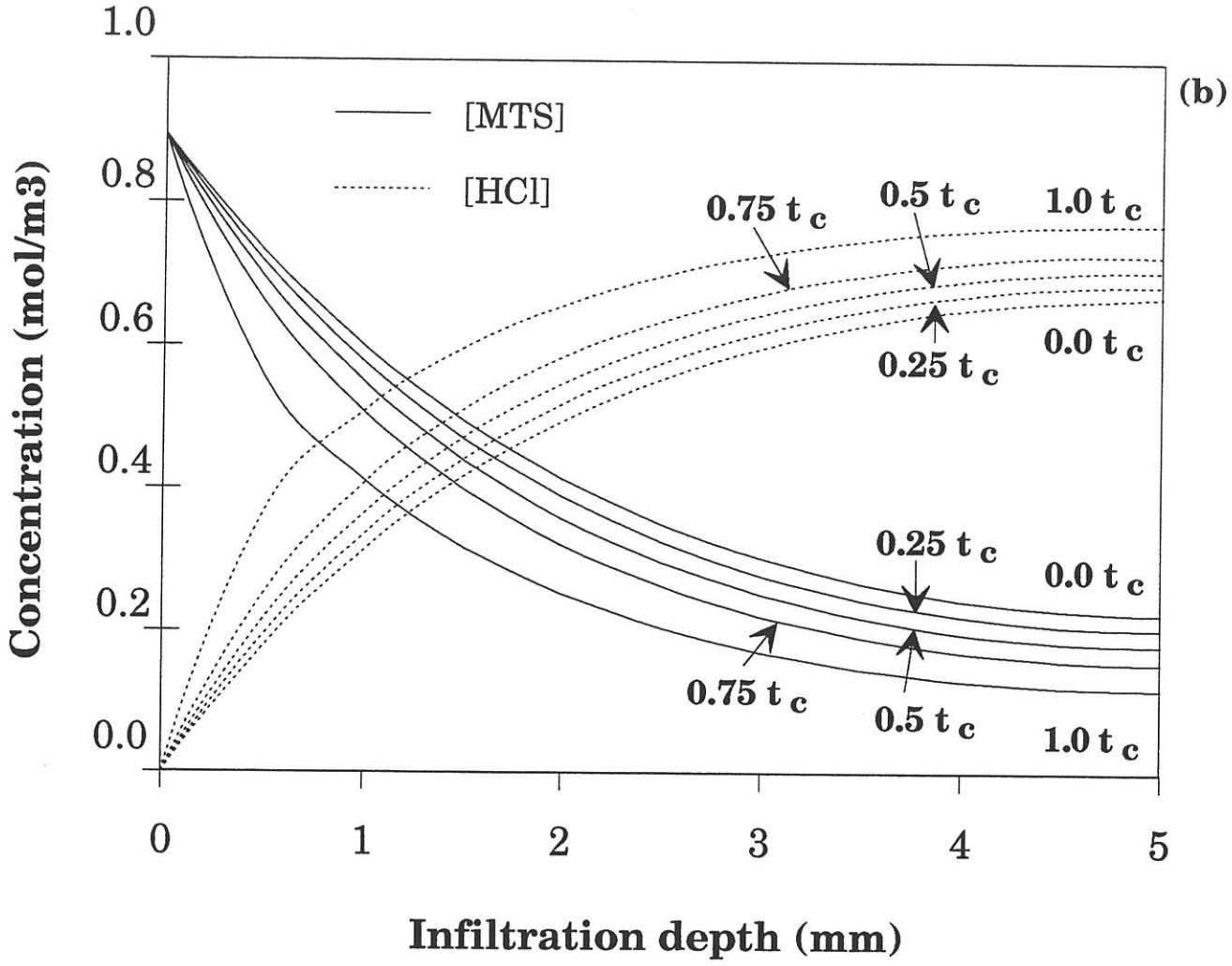

Fig. 8 : Calculations of (a) deposit thickness profile and (b) concentrations of the gaseous species profiles for a silicon carbide deposit obtained from a MTS-H_2 gas mixture and for various infiltration times between t = 0 and t = t_c with : T =1223 K, P = 100 kPa, Φ_0 = 100 µm, L/Φ_0 = 100, α = 10

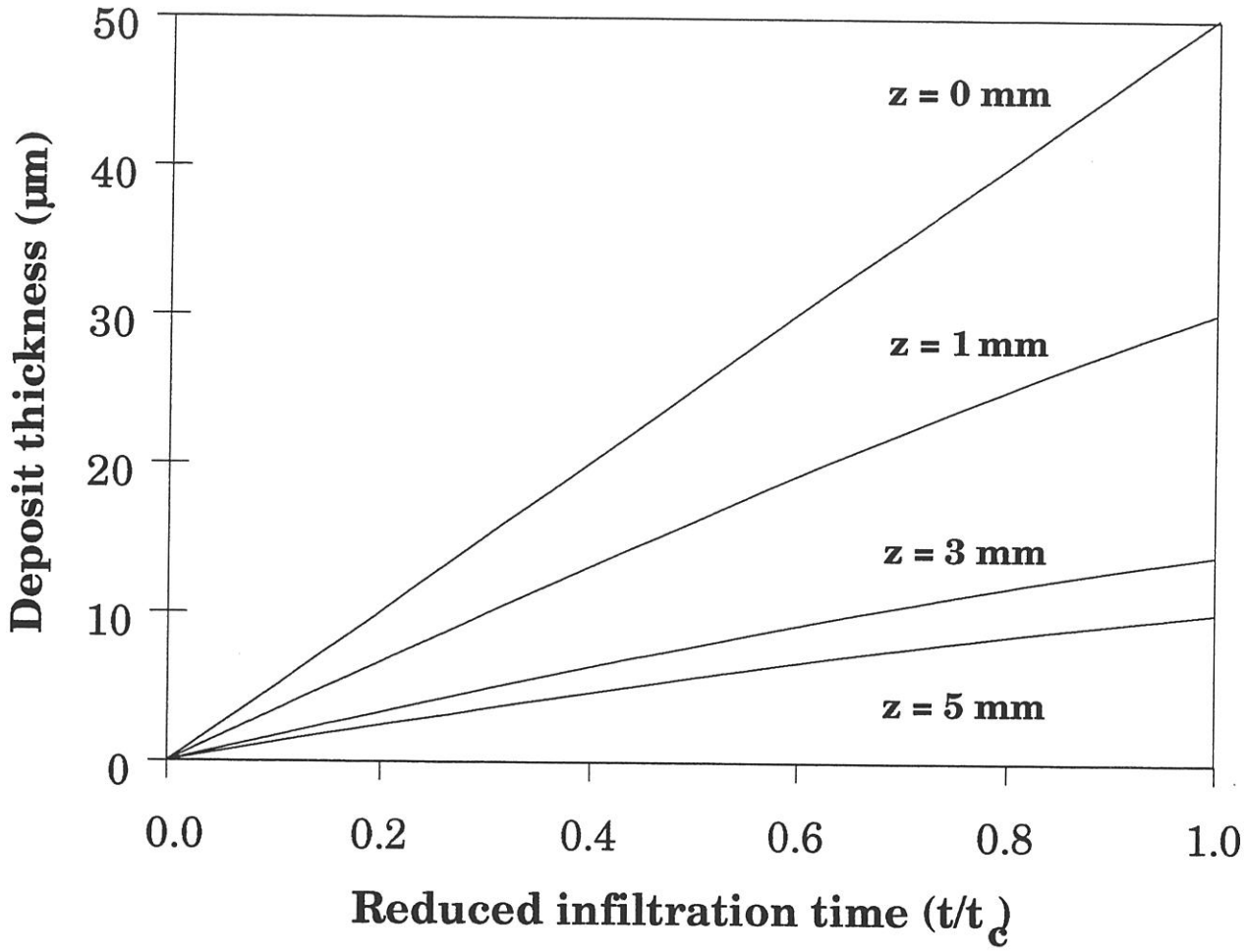

Fig. 9 : Variations of the deposit thickness with the reduced time at various infiltration depths for a silicon carbide deposit obtained from a MTS-H_2 gas mixture with : T =1223 K, P = 100 kPa, Φ_0 = 100 µm, L/Φ_0 = 100, α = 10

$$\eta(t) = \frac{2}{L} \int_0^{L/2} \frac{\Phi_0^2 - \Phi^2(z,t)}{\Phi_0^2} \, dz \qquad (13)$$

Such infiltration curves are shown in figure 10 for various values of the aspect ratio in the range 10 - 1000 and an initial diameter of 100 µm. As the aspect ratio increases, particularly from 100 to 1000, the SiC volume fraction obtained when the pore is closed, is markedly decreased, which is consistent with the degradation of the corresponding thickness profiles. Nevertheless, this type of decription of the infiltration process hides the actual shape of the profile, because many different Φ (z) functions can yield the same volume fraction of infiltrated SiC.

4 - EXPERIMENTAL STUDY

Up to now, only few papers have reported experimental thickness profiles for ceramics obtained by CVI. It is probably due to problems occurring in (i) the preparation of model pores with a well-controlled geometry and which conveniently represent the pores of the actual fibrous preforms of the ceramic matrix composites (low diameter < 100 µm and high aspect ratio > 100) and (ii) the accurate measurement of deposit thickenesses of about 1 µm. The only articles published in this field give qualitative profiles (obtained by Electron Probe for Micro Analysis) for the infiltration of TiC [38] or Zirconia [40,41] in ceramic fibrous preforms, or quantitative thickness profiles of SiC or TiC in capillary of about 1 mm in diameter with low aspect ratio (< 100) [33,42,43].

4.1 - Preparation of the model pores

The preparation route, used to obtain straight cylindrical pores, starts with cylindrical SiC-based CVD filaments(*), which consists of (i) a carbon core (32 µm in diameter), (ii) a pyrocarbon coating (about 1 µm in thickness) and (iii) a 53 µm SiC deposit. Pieces of these filaments (about 1 cm in length) were subjected to a controlled oxidation at 800°C in air for about 10 h, which resulted, by consumption of the carbon core and pyrocarbon film, in a microscopic tube with an inner diameter of 34 µm. These samples, briefly characterized by optical and scanning electronic microscopy (SEM), were found to be very regular with a smooth inner surface (fig.11). Several of

(*)SCS-2 filaments from TEXTRON, Lowell (Mass.)

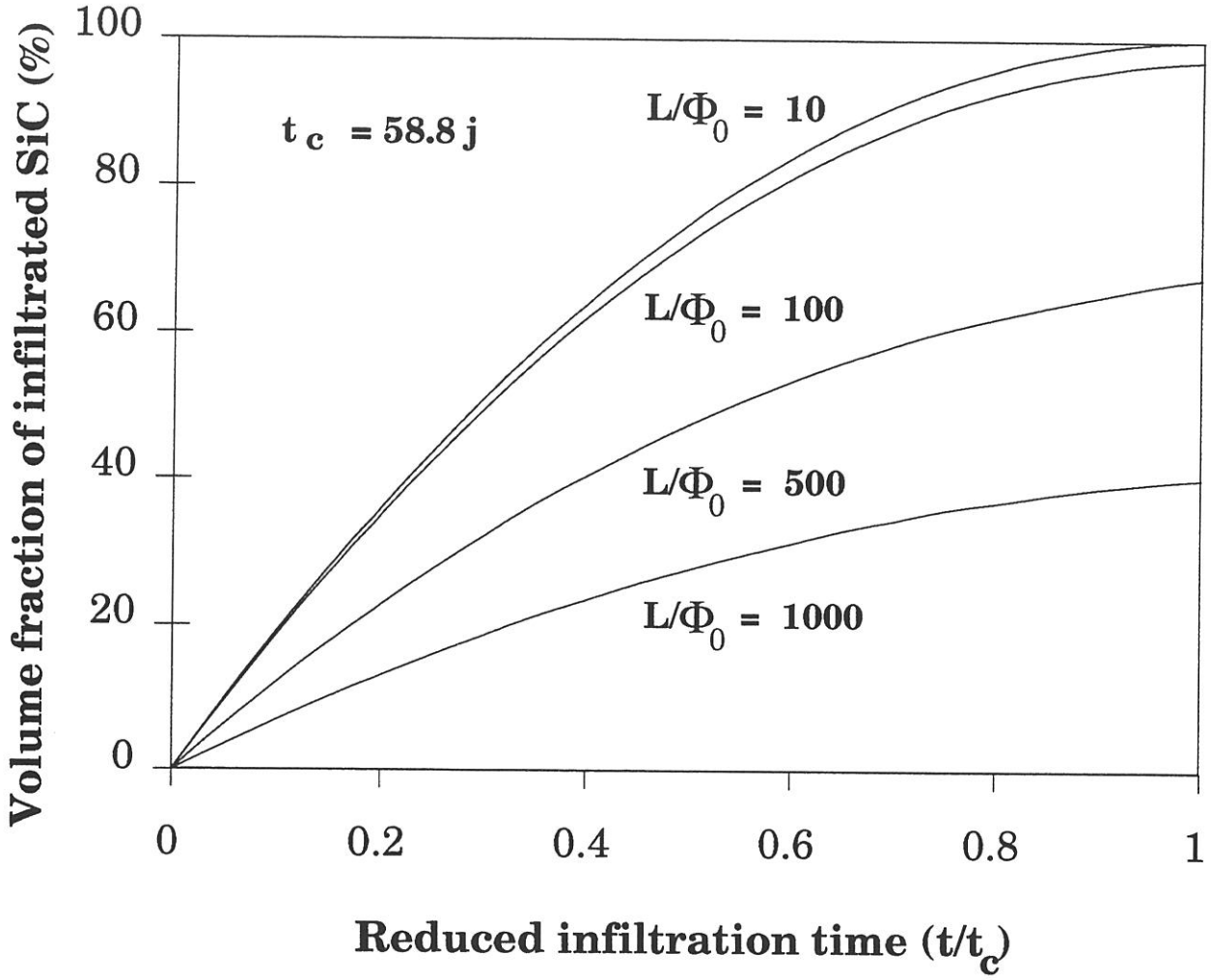

Fig. 10 : Variations of the volume fraction of infiltrated SiC with the reduced time for : T = 1223 K, P = 0.1 kPa, Φ_0 = 100 µm, α = 10 and various values of the aspect ratio

(a)

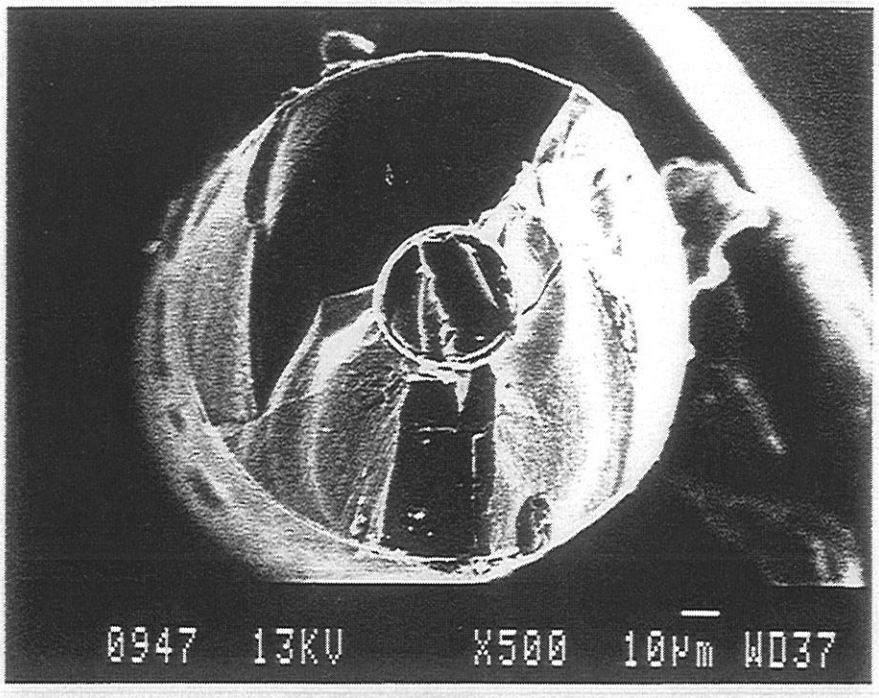

(b)

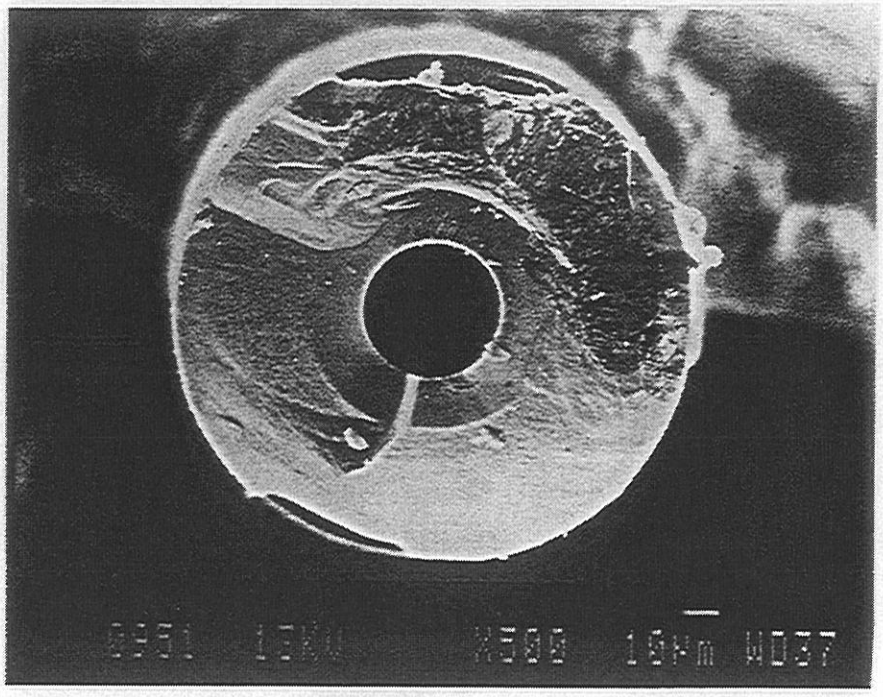

Fig. 11 : S.E.M. micrographs of fracture surfaces of SiC-based CVD filaments : (a) as received (b) after oxidation treatment

these unitary pores were bound together with a high temperature cement and the resulting assembly was hung up in a CVD/CVI reactor with the direction of the pores axis being perpendicular to the gas flow (fig.12).

4.2 - CVI experiments

The infiltration experiments were carried out in a hot wall CVD/CVI apparatus heated by r.f. induction (fig.13). The deposition chamber is a vertical cylindrical tube favorable to a laminar flow, with a large hot isothermal zone, coupled to a sensitive microbalance. It is equipped with accurate controlling systems for the monitoring of temperature, total pressure and various flow rates. MTS (which is liquid under standart conditions) is transported by bubbling the carrier gas H_2 in a bubbler vessel at a constant temperature. A good control of the MTS gas flow needs some additional devices, which are described elsewhere [34].

4.3 - Experimental results - Discussion

The CVI- experiments were performed during a sufficiently long time to close the pores entrances. The thickness profiles were determined by SEM observations on fracture sections operated at various levels in the model micropores (fig. 14). The studied experimental parameters are the temperature ($1073 \leq T \leq 1373$ K), the total pressure ($2 \leq P \leq 20$ kPa) and the aspect ratio ($90 \leq L/\Phi_0 \leq 300$).

4.3.1 - Influence of aspect ratio

The influence of the aspect ratio was experimentally studied under two different CVI conditions. The first investigation was peformed for T = 1073 K, P = 3 kPa, α = 3 and two values of pore length (L = 10 and 5 mm, corresponding to respective aspect ratios of 300 and 150). In spite of relatively favorable conditions, the SiC thickness profiles are not very homogeneous, as shown in figure 15. The volume fractions of infiltrated SiC are respectively 63 and 81 %. The second investigation, for T = 1223 K, P = 10 kPa, α = 5 and three values of pore length (L = 10, 5 and 3 mm, i.e. L/Φ_0 = 300, 150 and 90), gives similar results with still less homogeneous profiles (fig. 16). In both sets of experiments, an increase of the aspect ratio leads to a degradation of the infiltration profile, which is qualitatively in agreement with the results of the model (fig. 5).

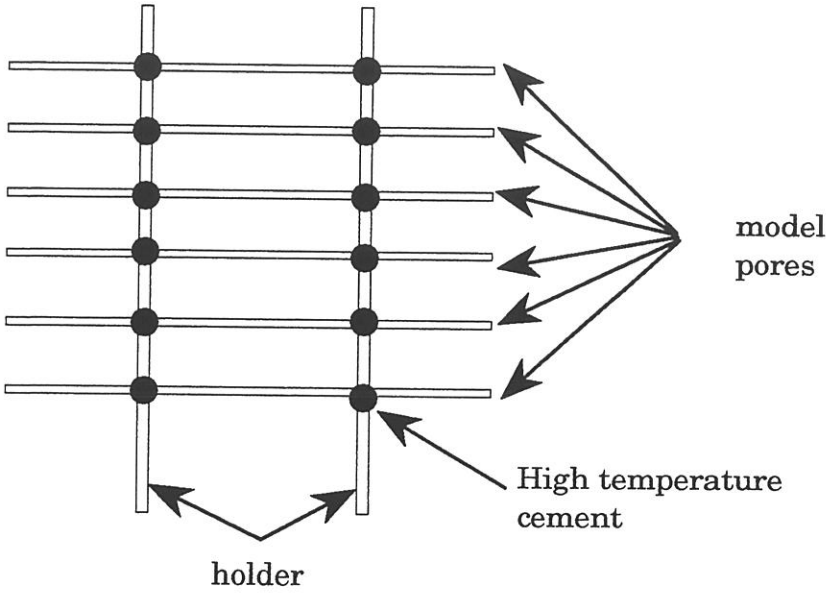

(a)

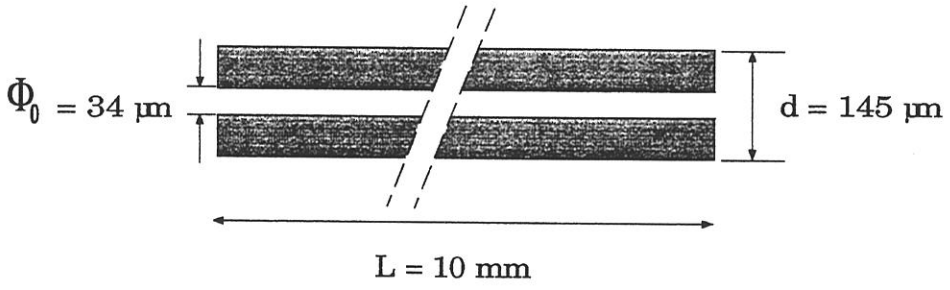

(b)

Fig. 12 : Model samples for experimental determination of silicon carbide thickness profiles along a model cylindrical pore :

(a) model pore assembly

(b) pore geometry

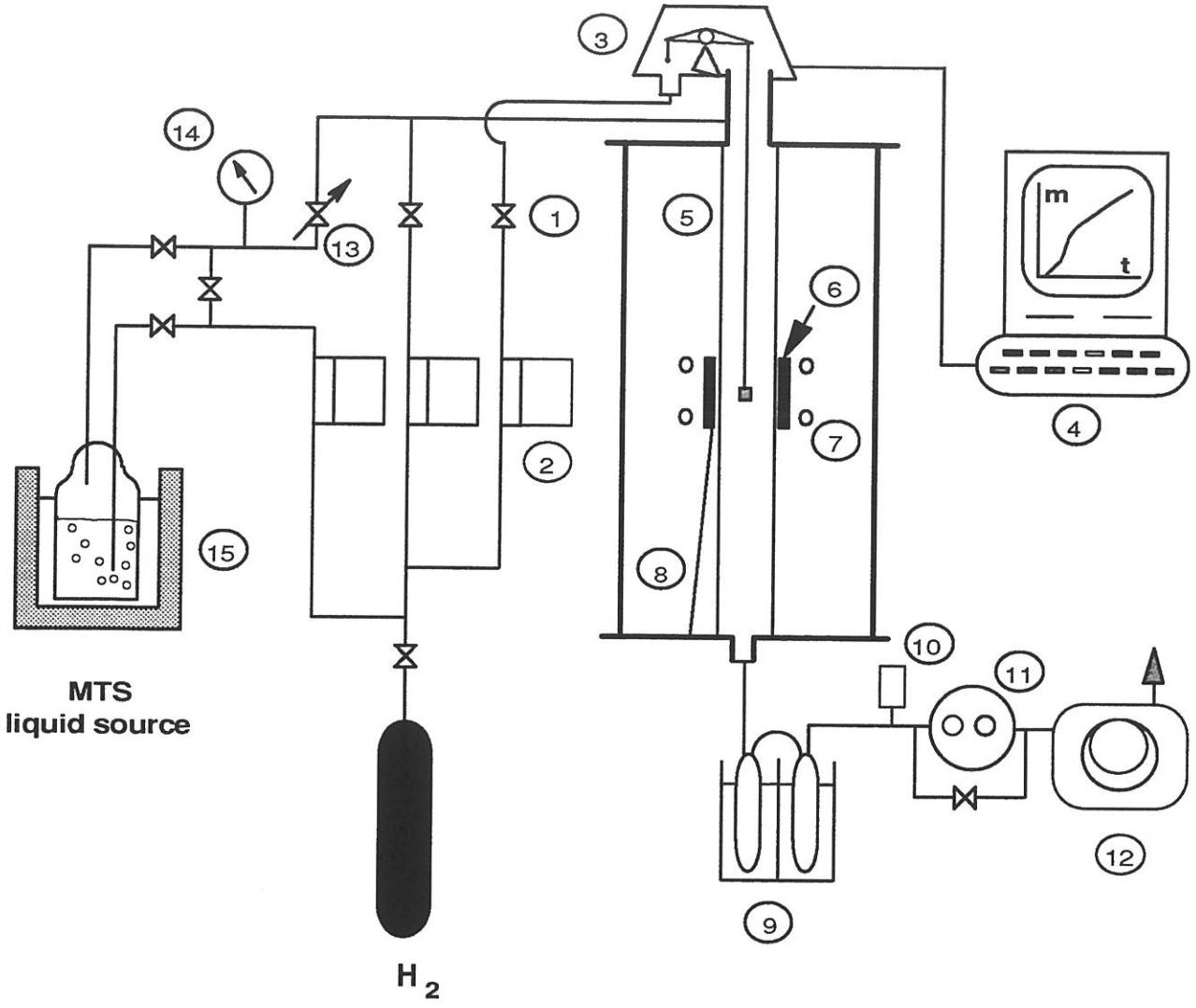

1 - Shutt-off valve
2 - Mass flowmeter
3 - Microbalance
4 - Microcomputer
5 - Silica tubular reactor
6 - Susceptor
7 - R.F. coil
8 - Thermocouple
9 - Liquid nitrogen trap
10 - Pressure sensor
11 - Pressure controller
12 - Vacuum pump
13 - Adjusting valve
14 - Manometer (P°)
15 - Thermostated bath ($P°_{MTS}$)

Fig. 13 : Schematics of the apparatus used for CVD/CVI of SiC-based ceramics

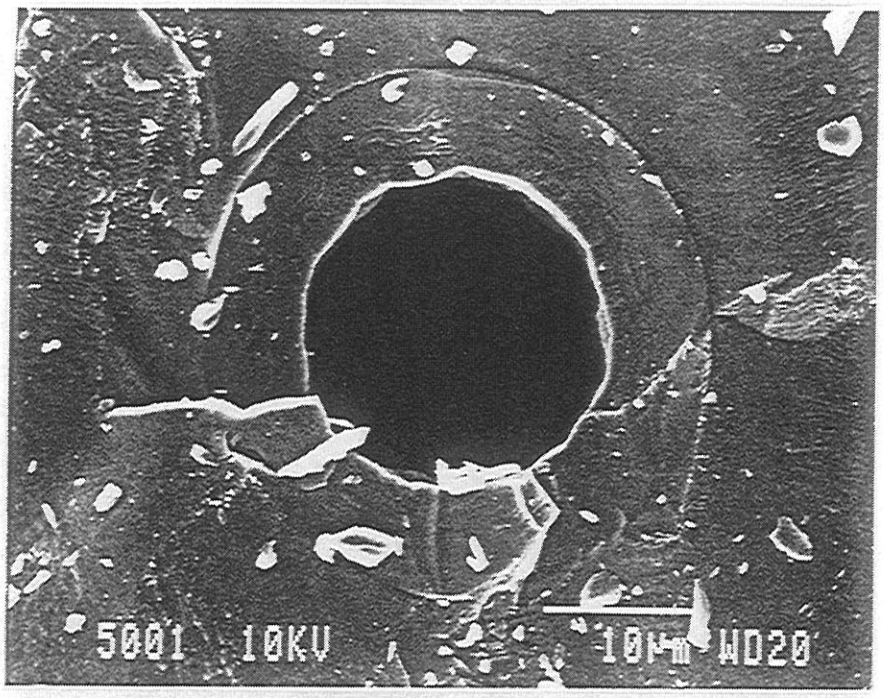

(a)

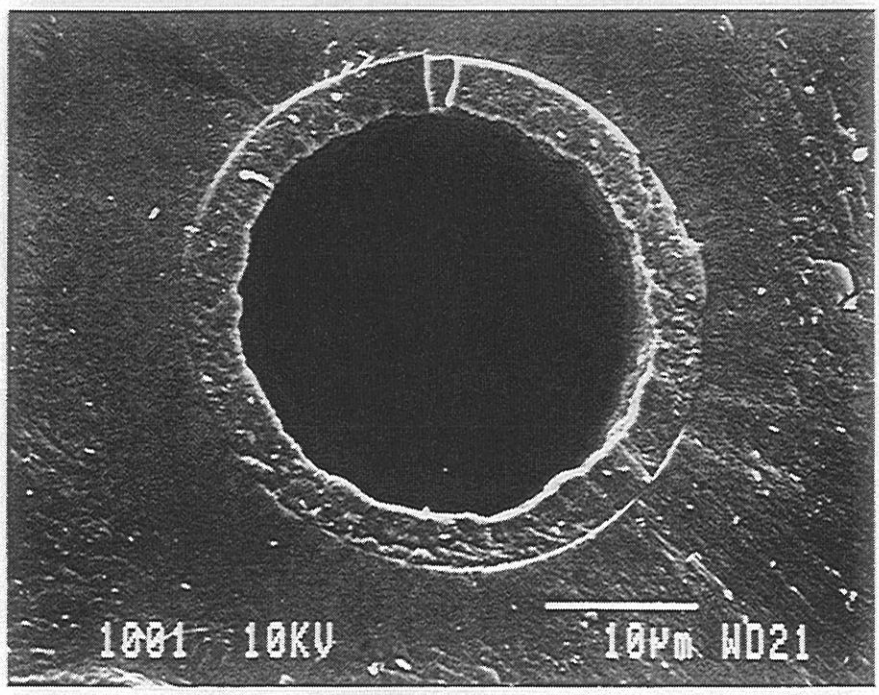

(b)

Fig. 14: SEM micrographs of fracture sections operated at various level on model pores infiltrated by SiC (a) at 1.5 mm and (b) at 5 mm far from the pore entrance.

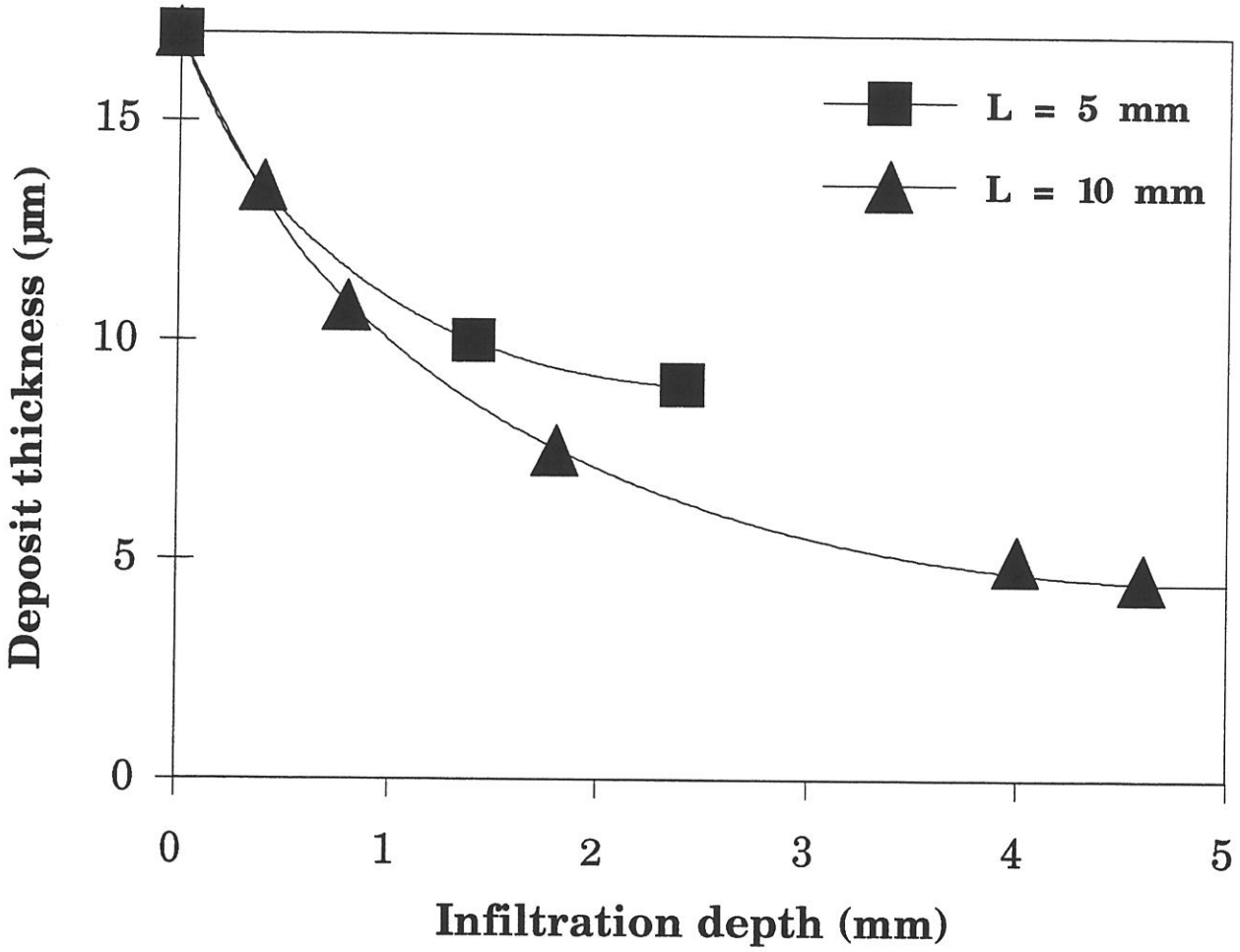

Fig. 15 : Calculated (full line) and experimental (markers) thickness profiles along a cylindrical pore for silicon carbide infiltrations with : T =1073 K, P = 3 kPa, Φ_0 = 34 µm, L = 10 and 5 mm, α = 3

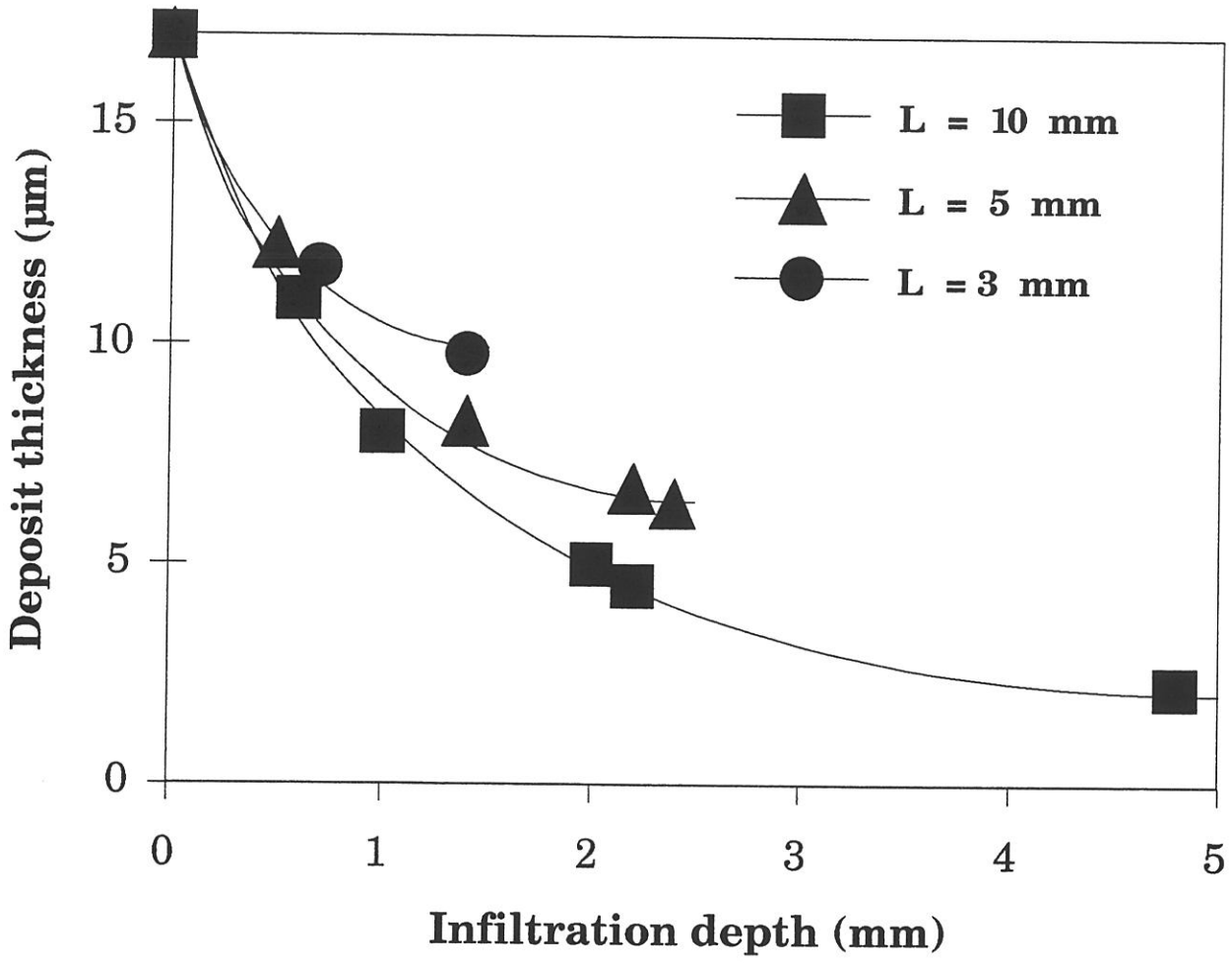

Fig. 16 : Calculated (full line) and experimental (markers) thickness profiles along a cylindrical pore for silicon carbide infiltrations with : T = 1223 K, P = 10 kPa, Φ_0 = 34 µm, L = 10, 5 and 3 mm, α = 5

Nevertheless, according to the kinetic law defined in 2.1.2 (equation (3)) for the deposition of SiC, the theoretical profiles calculated from the presently model are much more optimistic than the experimental ones, with a volume fraction of infiltrated SiC higher than 99 %. As previously mentioned, the assumption stated in 2.1 about the chemical system (i.e. the heterogeneous reaction of MTS) is not valid and one (or even several) intermediate unknown species X, homogeneously produced, must be considered as the actual source of SiC deposit at the entrance of the pore. The concentration of the species X is probably much lower than the initial concentration of MTS because the decomposition of MTS yields, besides X, several other species which do not react heterogeneously. So the rate of the deposition reaction can be expressed at the pore entrance :

$$\vartheta = k_{s1}(T)\, C_{MTS,\,0} = k_{s2}(T)\, C_{X,\,0} \qquad (14)$$

where $C_{MTS,0}$ is the MTS concentration at the pore entrance according to the hypotheses of 2.1(i.e. defined by equation (9))

$C_{X,0}$ is the actual X concentration at the pore entrance,

$k_{s1}(T)$ is the kinetic constant of equation (3),

$k_{s2}(T)$ is a new kinetic constant more convenient to represent the deposition chemical process.

The kinetic constant $k_{s2}(T)$ can be expressed as a function of $k_{s1}(T)$:

$$k_{s2} = \frac{C_{MTS\,,\,0}}{C_{X,\,0}}\; k_{s1} \qquad (15)$$

with $C_{MTS,\,0} > C_{X,\,0}$

The value of this ratio has been determined in order to fit one experimental profile of the first investigation (fig. 15). The chosen value of 30 seems very suitable since it leads for both aspect ratios to calculated profiles very close to the experimental ones. In addition, the same procedure, permitted to fit very well the three experimental infiltration profiles of the second investigation (fig. 16). These results show that the present model can accurately predict the influence of the aspect ratio on the deposit profiles, when a convenient kinetic law for the heterogeneous reaction is available.

4.3.2 - Influence of total pressure

Figure 17 shows three thickness profiles measured after infiltrations at T = 1223 K, α = 5 and L = 10 mm, for three values of the total pressure

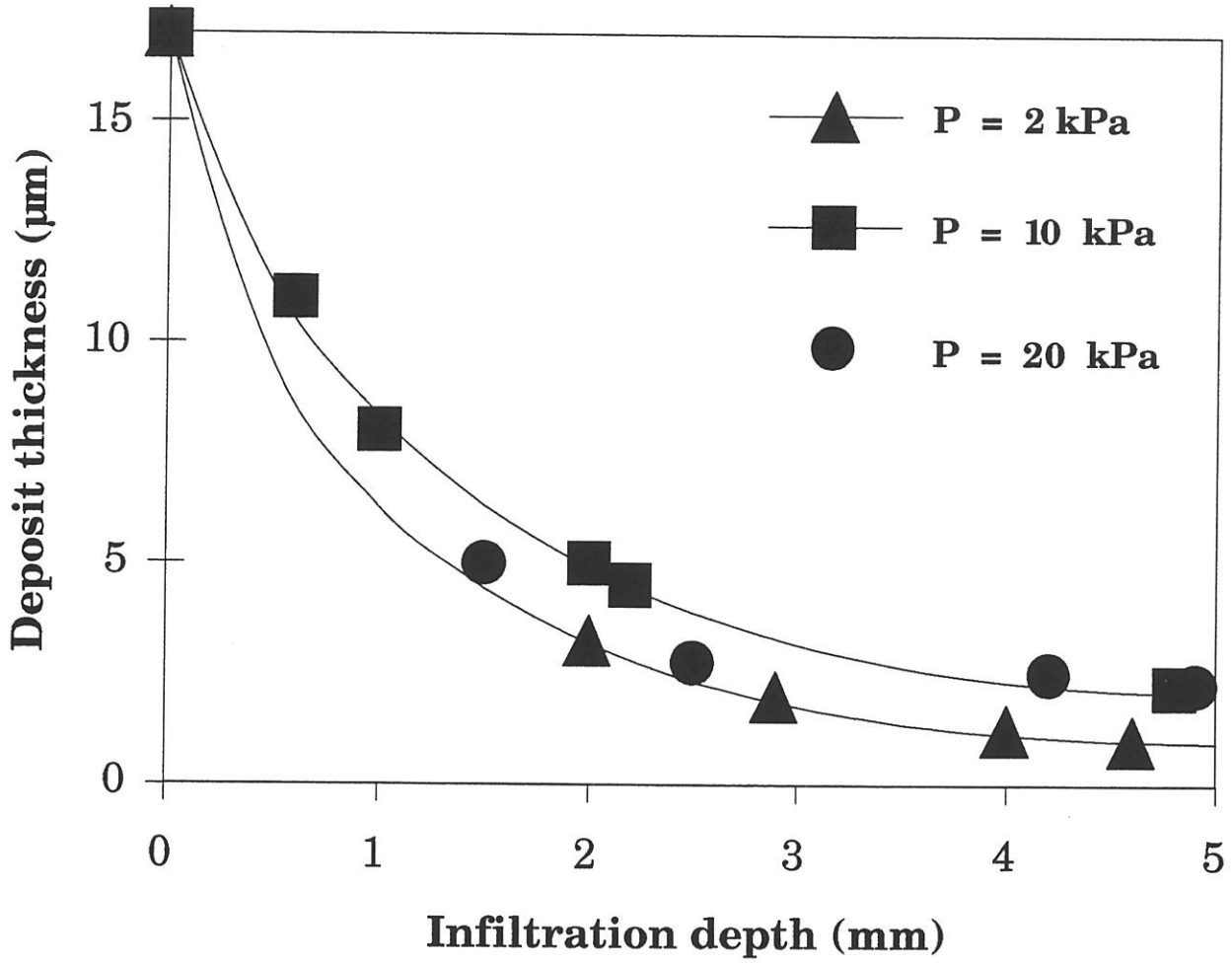

Fig. 17 : Calculated (full line) and experimental (markers) thickness profiles along a cylindrical pore for silicon carbide infiltrations with : T = 1223 K, P = 2, 10 and 20 kPa, Φ_0 = 34 µm, L = 10 mm, α = 5

P = 2, 10 and 20 kPa. Such conditions are faourable to mass transfers occurring within the pore by Fick diffusion. Under this type of mass transfer regime, the model predicts, with the kinetic law defined in 2.1.2, an improvement of the infiltration homogeneity when P is decreased. Nevertheless, these experimental profiles are observed to be almost independent of P, which is not in accordance with the previsions of the model (fig.2).

This behaviour could be explained on the basis of a Thiele modulus which does not depend on the total pressure. This condition would be achieved if the kinetic law is a first order law with respect to the intermediate X with a kinetic constant proportional to to P^{-1}. A kinetic law taking into account the inhibitor effect of HCl species, can be expressed by the following general expression :

$$\vartheta = \frac{k_1 C_X}{1 + k_2 C_{HCl}} \qquad (16)$$

This inhibitor effect of HCl was previously observed by Bessmann et al. [44]. On the other hand, Prébendé reported a clear decrease of SiC deposition rate under similar experimental conditions for a total pressure increasing from 3 to 15 kPa (fig. 18) [34].

HCl is a product of the homogeneous decomposition of MTS, ocurring outside the pore, e.g.according to the equation [34] :

$$CH_3SiCl_3 + H_2 \longrightarrow CH_4 + SiCl_2 + HCl \qquad (17)$$

So the HCl concentration at the pore entrance is close to the MTS concentration ($C_{MTS,0}$) defined by equation (9).

HCl is also a product of the heterogeneous deposition reaction in the pore. As suggested from figure 8b, the increase of the HCl concentration from the entrance ($C_{HCl,0}$) to the center of the pore is usually lower than the concentration of the source species at the pore entrance. The equation (15) evidences that the condition $k_{s2} >> k_{s1}$, required to get a good fitting between theoretical and experimental profiles, results in $C_{X,0} << C_{MTS,0}$. Consequently, the concentration of HCl is almost constant within the pore and the equation (16) can be rewritten as :

$$\vartheta(z,t) = \frac{k_1 C_X(z,t)}{k_2 C_{HCl,0}} \qquad (18)$$

$C_{HCl,0}$ being proportional to the initial concentration of MTS, i.e., for a constant

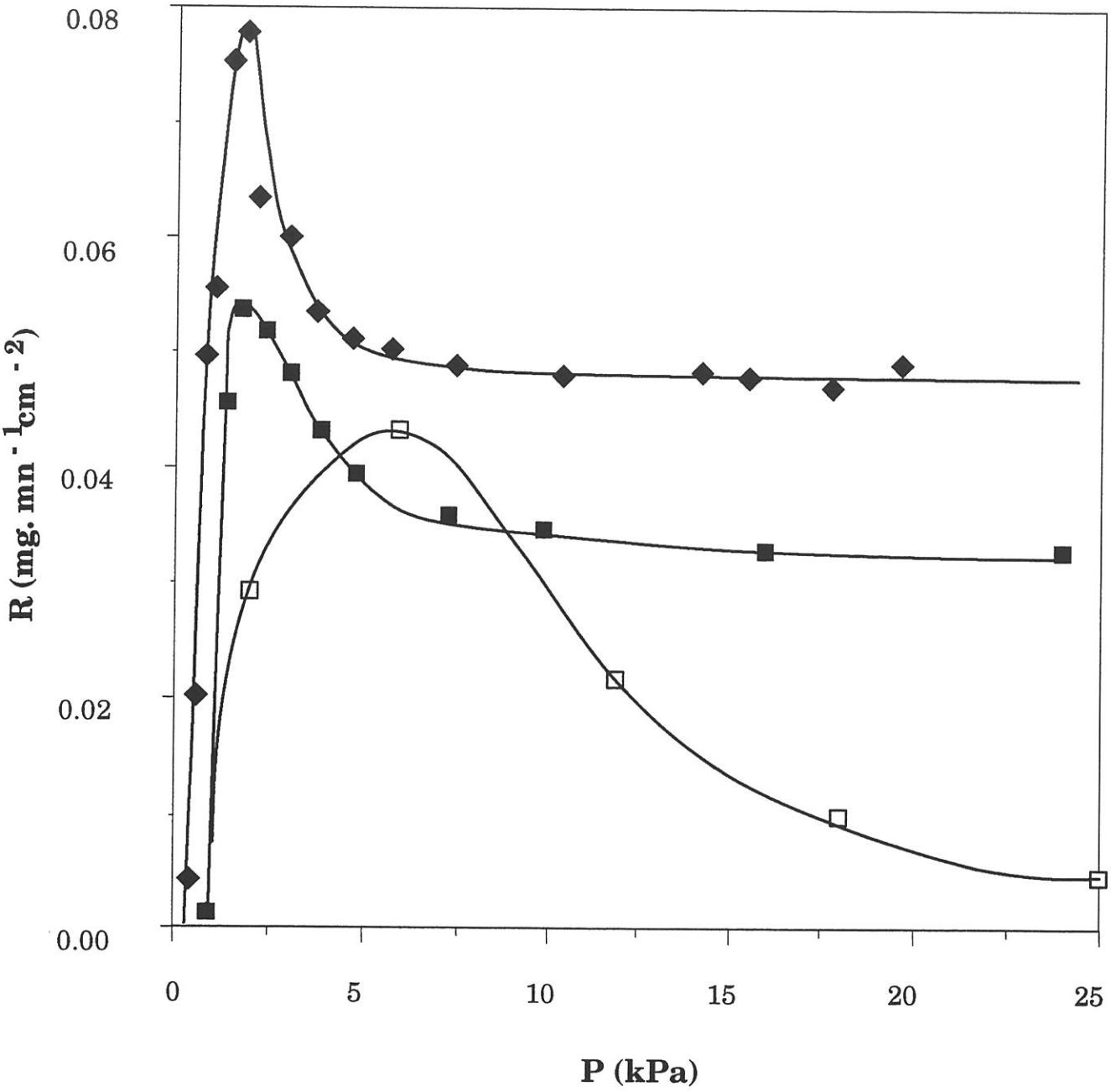

Fig. 18 : Variations of the growth rate of silicon carbide deposit from a MTS-H_2 gas mixture [34]

α ratio, proportional to the total pressure, the kinetic law (18) can be reduced to a first order law with respect to intermediate species X with a kinetic constant proportional to P^{-1} :

$$\vartheta(z,t) = \frac{k_3}{P} \quad C_X(z,t) \qquad (19)$$

With such a kinetic law for SiC deposition reaction, the independence of the infiltration profiles on the total pressure for the previously mentioned CVI conditions, could be predicted by the model.

4.3.3 - Influence of temperature

The experimental data shown in figure 19 for infiltrations performed at P = 20 kPa, α = 5, L = 10 mm and for T = 1223 and 1373 K, are in qualitative agreement with the profiles calculated by the model with the kinetic law defined in 2.1.2 (fig.1). A temperature increase results in a degradation of the infiltration profile.

However a steep thickness gradient is observed close to the pore entrance, over about 1 mm, and hereafter the profile is rather flat. These features, mainly observed at the highest temperature, are not accurately predicted by the model but can be explained on the basis of the inhibitor effect of HCl according to the kinetic law corresponding to equation (16). So, the increase of HCl concentration as a function of the infiltration depth close to the pore entrance, must be added to the decrease of the concentration of the intermediate source species X (assumed to be close, at the pore entrance, to the MTS concentration defined by equation (9)), both phenomena leading to a decrease of the heterogeneous reaction rate, particularly at high temperatures. As a consequence of this inhibitor effect, the thickness gradient is enhanced near the pore entrance compared to the theoretical profile calculated under the assumption of a first order kinetic law. Hereafter, the lower values of the heterogenous reaction rate result in rather low variations of the various gaseous species concentrations along the pore and an almost flat thickness profile.

5 - CONCLUSION

The CVI model for the infiltration of a straight cylindrical pore, described in part 1 [29], has been applied in the present contribution to the deposition of SiC-based

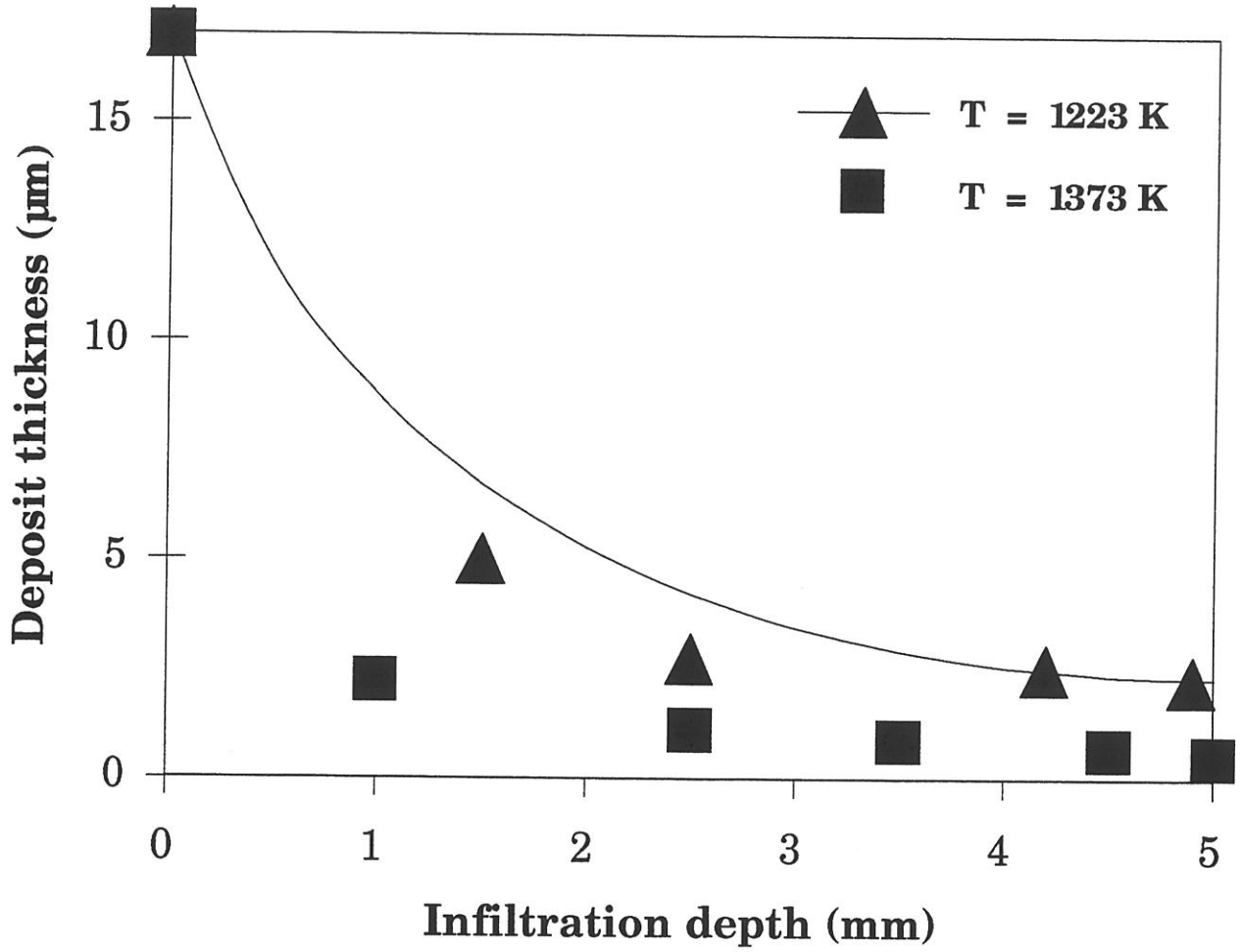

Fig. 19 : Calculated (full line) and experimental (markers) thickness profiles along a cylindrical pore for silicon carbide infiltrations with : T = 1223 and 1373K, P = 20 kPa, Φ_0 = 34 µm, L = 10 mm, α = 5

ceramics from MTS-H_2 mixtures.

On the basis of a simplified kinetic law, with a first order with respect to MTS, the model brings out the influence of various parameters on the CVI process. The infiltration homogeneity is highly improved by decreasing the pore aspect ratio (with constant diameter) and the temperature (due to the large activation energy of the kinetic process) and, in the case of Fick diffusion regime, by decreasing the total pressure and the pore diameter (with constant aspect ratio). Conversely, the composition of the gaseous phase (i.e. the ratio $\alpha = [H_2]/[MTS]$) and, in the case of Knudsen diffusion regime, the total pressure and the diameter have a very weak influence on the deposit thickness profiles.

The infiltration experiments carried out in model pores (34 µm in diameter and 10 mm in length) permitted to validate the CVI model by predicting accurately the influence of the aspect ratio, when suitable chemical kinetics data are considered. For instance, at relatively low temperatures and in order to take into account that the actual species which reacts heterogeneously is an intermediate species rather than MTS, the kinetic constant must be adjusted to a higher value in accordance with first order kinetics and a lower concentration of the intermediate. On the other hand, the experiments performed for various temperatures and total pressures have shown that a kinetic law more complex than a first order one must be considered, which includes an inhibitor effect of HCl species.

The investigations carried out in the present paper emphasize the importance of the kinetic data used in CVI models and particularly the need of a good knowledge of the homogeneous and heterogeneous chemical processes and the local kinetic laws, i.e with respect to the intermediate source species.

ACKNOWLEDGEMENTS

This works has been supported by EEC (EURAM program contract n° MAIE/ 0018/C) and jointly by the French Ministry of Research and Technology (MRT) and SEP through a grant given to one of the authors (R. F.).

REFERENCES

[1] J.A. Powell, L.G. Matus, Proc. First Int. Conf. on Amorphous and Crystalline Silicon Carbide (G.L. Harris and C.Y.-W. Yang, eds.), Springer-Verlag, Berlin/ Heidelberg, p. 2, 1989

[2] F. Christin, R. Naslain, C. Bernard, "A Thermodynamic and Experimental Approach of Silicon Carbide-CVD Application to the CVD Infiltration of Porous Carbon-Carbon Composites", Proc. 7th Int. Conf. CVD, Los Angeles, USA (1979), (T.O. Sedgwick et al., eds.), The Electrochem. Soc., Princeton, pp. 499-514, 1979

[3] R. Naslain, F. Langlais, R. Fedou, "The CVI-Processing of Ceramic Matrix Composites", Proc. 7th European Conf. CVD, Perpignan, France (1989), (M. Ducarroir et al., eds.), Colloque de Physique, Les Editions de Physique, Colloque C5, Suppl. N° 5, Vol 50, pp. 191-207, 1989

[4] P. Rai-Choudhury, N.P. Formigoni, J. Electrochem. Soc., Vol. 116, p. 1440, 1969

[5] J.E. Doherty, J. Metals, Vol. 28, p. 6, 1976

[6] R. Rampuch, L. Stobierski, Ceramungia Intern., Vol. 3, p. 43, 1977

[7] A. Suzuki, K. Furukawa, Y. Higashigaki, S. Harada, S. Nakajima, T. Inoguchi, J. Crystal Growth, Vol. 70, p. 287, 1984

[8] S. Motojima, N. Iwamori, T. Hattori, K. Kurosawa, J. Mater. Sci., Vol. 121, p. 1363, 1986

[9] Y. Furumura, M. Doki, F. Mieno, T. Eshita, T. Suzuki, M. Maeda, Proc. 10th Int. Conf. on CVD (G.W. Cullen, ed.), The Elecrochem. Soc., Pennington, p. 435, 1987

[10] Y. Avignal, M. Schieber, R. Levin, J. Crystal Growth, Vol. 24/25, p. 188, 1974

[11] F. Sibieude, G. Benezech, J. Mater. Sci., Vol. 23, N° 7, p. 1632, 1988

[12] H. Matsunami, K. Shibahara, N. Kuroda, W. Yoo, S. Nishino, Proc. Fisrt Int. Conf. on Amorphous and Crystalline Silicon Carbide, Vol. 3, N° 4, p. 443-448, 1957

[13] L.S. Hong, Y. Shimogaki, H. Komiyama, "Gas Phase Reaction in Synthesis of SiC Films by Low Pressure Vapor Deposition from Si_2H_6 and C_2H_8 at 873 K", Proc. 8th European Conf. on CVD, Glasgow (1991), (M.L. Hitchman and N.J. Archer, eds.), Journal de Physique IV, Les Editions de Physique, Colloque C2, Suppl. Journal de Physique II, Vol. 1, pp. 87-94, 1991

[14] T.D. Gulden, J. Am. Ceram. Soc., Vol. 51, p. 424, 1968

[15] J.J. Federer, Thin Solid Films, Vol. 40, p. 89, 1977

[16] K. Minato, K. Fukuda, J. Nucl. Mater., Vol. 149, p. 233, 1987

[17] F. Kobayaski, K. Ikawa, K. Iwamoto, J. Crystal Growth, Vol. 28, p. 395, 1975

[18] P. Tsui, K.E. Spear, Mat. Sci. Res., Vol. 17, p. 371, 1984

[19] M.G. SO, J.S. Chun, J. Vac. Sci. Technol., Vol. 6, p. 5, 1988

[20] B.S. Cartwright, P. Popper, Science of Ceramics 5, p. 473, 1970

[21] A.W.C. Van Kemenade, C.F. Stemfoort, J. Crystal Growth, Vol. 12, p. 13, 1972

[22] W.F. Knippenberg, G. Verspui, A.W.C. Van Kemenade, Proc. 3rd Int. Conf. on Silicon Carbide, Univ. of South Carolina Press, Columbia, p. 92, 1974

[23] K. Brennfleck, E. Fitzer, G. Schoch, M. Dietrich, Proc. 9th Int. Conf. on CVD, Cincinnati, USA (1984) (Mc D. Robinson et al., eds.), The Electrochem. Soc., Pennington, p. 649, 1984

[24] A.N. Kenigfest, Y.A. Davidov, V.S. Dergunova, A.P. Nabatnikov, G. Surskii, Fizika i Kimiya Obrabotki Materialov, Vol. 18, p. 76, 1984

[25] T. Kaneko, T. Onuko, H. Yumoto, J. Crystal Growth, Vol. 91, p. 599, 1988

[26] E. Fitzer and R. Gadow, "Fiber-Reinforced Silicon Carbide", Am. Ceram. Soc. Bull., Vol. 65, pp. 326-335, 1986

[27] J. Schlichting, Powder Metall. Int., Vol. 12, N° 3, p. 141, 1980

[28] J. Schlichting, Powder Metall. Int., Vol. 12, N° 4, p. 196, 1980

[29] R. Fedou, F. Langlais, R. Naslain; "A Modeling of the Isothermal/Isobaric Chemical Vapor Infiltration in a Straight Cylindrical Pore. Part. 1 Description of the Model", to be published

[30] J. Yeheskel, S. Agam, M.S. Darriel, "Mass Spectrometric Study of SiC-CVD from MTS (CH_3SiCl_3) and Hydrogen", Proc. 11th Int. Conf. on CVD (K.E. Spear, G.W. Cullen,eds.), The Electrochem. Soc., Pennington, pp. 699-702, 1990

[31] R. A. Svehla, NASA Tech. Rep. R-132, Lewis Research Center, Cleveland (OHIO), 1962

[32] E.R. Gilliland, Ind. Eng. Chem., Vol. 26, p. 681, 1934

[33] E. Fitzer, D. Hegen, Angew. Chem. Int. Ed. Engl., Vol. 18, p. 295, 1979

[34] C. Prebende, "Mécanismes Physico-Chimiques mis en jeu dans le Processus CVD d'Elaboration de Céramiques à base de Carbure de Silicium en Réacteur à Parois Chaudes", Thesis N° 347, University of Bordeaux I, 1989

[35] G.S. Fischman, W.T. Petuskey, J. Am. Ceram. Soc., Vol. 68, p. 185, 1985

[36] M.E. Aluko, Proc. First Int. Conf. on Amorphous and Crystalline Silicon Carbide (G.L. Harris and C.Y.-W. Yang, eds.), Stringer-Verlag, Berlin/Heidelberg, p. 51, 1989

[37] G. Schoch, W. Fritz, E. Fitzer, Tech. Rept EURAM Contract MAIE/0018/C, 1991

[38] J. Y. Rossignol, F. Langlais, R. Naslain, "A Tentative of Modelization of Titanium Carbide CVI within the Pore Network of Two-Dimensional Carbon-Carbon Composites Preforms", Proc. 9th Int. Conf. CVD, Cincinnati, USA (1984), (J. M. Blocher et al., eds.), The Electrochem. Soc., Pennington, pp. 596-914, 1984

[39] R. Fédou, E. Sipp, F. Rebillat, F. Langlais, R. Naslain, "A Modeling of the Isothermal/Isobaric Chemical Vapor Infiltration in a Straight Cylindrical Pore. Part 3 : Application to the CVI of Zirconia or Yttria", to be published

[40] J. Minet, F. Langlais, R. Naslain, "Chemical Vapor Infiltration of Zirconia within the Pore Network of Fibrous Ceramic Materials from $ZrCl_4$-H_2-CO_2 Gas Mixtures", Composites Sciences and Technology, Vol. 37, pp. 79-107, 1990

[41] L.C.J. de Haart, Y.S. Lin, K. J. De Vries, A.J. Burggraaf, "Modified CVD of Nanoscale Strucures in and EVD of Thin Layers on Porous Ceramic Membranes", Journal of the European Ceramic Society, Vol. 8, pp. 59-70, 1991

[42] C.H.J. Van Den Brekel, R.M.M. Fonville, P.J.M. Van Der Straten, G. Verspui, Proc. 8th Int. Conf. on CVD (J.M. Blocher et al., eds.), The Electrochem. Soc., Pennington, pp. 142-156, 1981

[43] M. Sasaki, A. Ohkubo, T. Hirai, "Gas Flow Simulation of Chemical Vapor Infiltration in a Vertical Hot-Wall Reactor", Journal de Physique IV, Colloque C2, Suppl. Journal de Physique II, Vol. 1, pp. 127-133, 1991

[44] T.M. Bessmann, B.W. Sheldon, M.D. Kaster, "Depletion Effects of SiC Deposition from Methyltrichorosilane", Journal of the American Ceramic Society (accepted)

CHAPITRE 3

Titre : A MODELING OF THE ISOTHERMAL/ISOBARIC CHEMICAL VAPOR INFILTRATION IN A STRAIGHT CYLINDRICAL PORE PART 3 : APPLICATION TO THE CVI OF ZIRCONIA OR YTTRIA

Submitted to the Journal of Materials Synthesis and Processing

A MODELING OF THE ISOTHERMAL/ISOBARIC CHEMICAL VAPOR INFILTRATION IN A STRAIGHT CYLINDRICAL PORE PART 3 : APPLICATION TO THE CVI OF ZIRCONIA OR YTTRIA

R. FÉDOU, E. SIPP(*), F. REBILLAT, F. LANGLAIS(**) and R. NASLAIN
Laboratoire des Composites Thermostructuraux (UMR 47 CNRS-SEP-UB1)
Domaine Universitaire, 3 Allée La Boétie
33600 Pessac (France)

ABSTRACT

The isothermal/isobaric chemical vapor infiltration of zirconia, from $ZrCl_4$-CO_2-H_2-Ar mixtures and yttrium oxide, from YCl_3-CO_2-H_2-Ar mixtures, along a straight cylindrical pore is studied according to a theoretical approach for both oxides and experimental approach for zirconia. A one dimensional model, utilizing kinetic laws established under well-controlled conditions and an iterative numerical procedure, are used to calculate the profiles of zirconia thickness and gaseous species concentrations along the pore axis at any given time and to study the effect of the main parameters on the infiltration homogeneity. For both cases, the total pressure, dilution ratio of the reactants with argon, pore aspect ratio as well as hydrogen partial pressure and, for the yttrium oxide infiltration, the YCl_3 partial pressure and temperature have an important effect on the profiles. Conversely, the effect of CO_2 partial pressure for both cases and, for zirconia infiltration, temperature (within the range 1200-1400 K) and $ZrCl_4$ partial pressure is more limited. For a given set of parameters, the profiles usually tend to become steeper near the pore entrance as the infiltration proceeds with the occurrence of a bottle neck phenomenon. For a critical time, the pore entrance is sealed by the deposit. Finally, few preliminary experiments performed on zirconia infiltration of model pores (34 µm in diameter and with an aspect ratio of 300) are used to validate the model.

KEY-WORDS: Zirconia, Yttrium Oxide, Chemical Vapor Infiltration, CVI, Modelling, Model Pore, Ceramic Matrix Composite, Kinetic Law

---

(*) Present adress : Alveo AG, Bruchstrasse 69, CH-6003 Luzern (Switzerland).
(**) to whom correspondence should be sent

1 - INTRODUCTION

Chemical vapor infiltration (CVI) is the most common processing technique used for the production at the plant level of ceramic matrix composites (CMCs). In this process, the ceramic matrix (e.g SiC) is formed as the result of a chemical reaction taking place between the various species of a gaseous precursor of that matrix (i.e CH_3SiCl_3 and H_2 for SiC) within the pore networks of a ceramic fiber preform heated at a moderate temperature ($\approx$ 1000 °C). In the original version of the CVI process, the mass transfers of the gaseous reactants and products in the pore network occur only by diffusion, the infiltration chamber being **isothermal and isobaric (ICVI)**. Under such conditions, temperature and total pressure should be maintened as low as possible in order to lower enough the deposition reaction kinetics (with respect to mass transfer) and to prevent an early sealing of the pore by the deposit (which is preferentially formed near the pore entrance). As a result, in ICVI the infiltration rate is rather slow (thus requiring infiltration durations of several hundreds of hours) and the composites often exhibit some residual porosity (incomplete densification). On the other hand : (i) a large number of preforms of complex and different shapes can be treated simultaneously and (ii) the ceramic fibers are undammaged during the composite processing (since it is performed at a low temperature). The feasability of the ICVI -processing of CMCs has been already established for a variety of matrices including carbon, carbides (SiC, B_4C, TiC), nitrides (BN, Si_3N_4) and oxides (Al_2O_3, ZrO_2)[1-6]. As far as we know, no detailed study on the processing of Y_2O_3-matrix CMC has been published. In order to increase the infiltration rate, assisted CVI-processes have been suggested in which a pressure gradient (PG-CVI) or/and a temperature gradient (TG-CVI) are applied to the preform. However, in all theses **forced-CVI (FCVI)** processes a specific tooling has to be applied to each preform up to the end of the infiltration with thus a significant loss of flexibility [7].

Regarding the long duration required to achieve the fabrication of CMCs by ICVI, it has been thought that theoretical modelling could be used to reduce the number of experiments necessary to work out the ICVI-parameters for any new preform or/and ceramic matrix. Several approaches have been already published [8-18]. Their objective is generally to calculate, for a given porous substrate (which is often a single straight cylindrical pore) and a set of CVI-parameters, the thickness profile of the infiltrated ceramic matrix assuming that the kinetic law of deposition of that ceramic is known for the gaseous precursors and CVI- conditions considered. An analysis of the results of the modelling studies already published and a comparison with

experimental data show that the availability of a proper kinetic law is a critical issue.

Recently, such a theoretical approach has been published by Fedou et al. for the infiltration of SiC (from a CH_3SiCl_3-H_2 precursor) in a straight cylindrical pore [19]. One of the advantages of this model lies in the fact that it is general, i.e it can be applied to any chemical system and it can use any given kinetic law. In the particular case of the infiltration of SiC, a kinetic law assuming an apparent reaction order of one with respect to CH_3SiCl_3, due to Schoch et al. was used [20]. The results of the calculations were used to study the effect of temperature, total pressure, pore diameter and aspect ratio on the thickness profile of the SiC-deposit along the pore. Finally, some calculated profiles were compared to profiles established experimentally for a model cylindrical straight pore (34 µm in diameter) and a rather good agreement between them was observed.

Zirconia is a refractory oxide which may have a high potential as matrix in CMCs for application in severe environments (i.e high temperatures and oxygen containing atmospheres). The feasability of processing of ZrO_2-matrix composites by ICVI has been established by Minet et al. [21]. However our knowledge in this field remains more limited than for the related SiC-matrix composites.

Yttrium oxide is also a refractory oxide with a melting point (T_f = 2410 °C) between alumina (T_f = 2050 °C) and zirconia (T_f = 2700 °C). Unlike zirconia, it does not exhibit a polymorphism, its crystal structure being of CaF_2-type up to T_f.

The objective of the present contribution is to show that Fedou model can be used to study the effects of the ICVI-parameters on the thickness profile of both ZrO_2 and Y_2O_3 respectively infiltrated from a gaseous $ZrCl_4$-CO_2-H_2-Ar and YCl_3-CO_2-H_2-Ar precursor, on the basis of a complex kinetic law wich has been recently proposed by Sipp et al. [22].

2 - THE ICVI-MODELING OF A STRAIGHT CYLINDRICAL PORE

2.1 - Hypotheses and calculation procedure

The model proposed by Fedou et al. for the infiltration of a pore with a ceramic deposited from a gaseous precursor, has been presented elsewhere [19,23]. It will be

sufficient here to recall the hypotheses which have been made, the basic equations being given in appendix.

(i) - The model pore is assumed to be initially cylindrical (diameter Φ_0; length L), and open at both ends. It is postulated that it remains straight and symmetrical with respect to its center during the infiltration process.

(ii) - The origin of time (t=0) is chosen as corresponding to the first mass transfer steady-state (assumed to be rapidly achieved with respect to the pore diameter variations). The infiltration process is considered as a series of quasi-steady-states of mass transfers.

(iii) - Since, in a fiber preform, the pores exhibit a high L/Φ_0 aspect ratio, a one dimensional theorietical approach is used, i.e the concentrations of the gaseous species are constant in a cross section of the pore and at any time t, they depend only on the axial coordinate z (defined as the distance from pore entrance). The pore profile at any time t is given by the variations of its diameter $\Phi(z,t)$ as a function of z. Since the pore is assumed to remain symmetrical, the study is limited to $0 \leq z \leq L/2$.

(iv) - The pore is isothermal, i.e the temperature in the pore is assumed to remain constant with respect to both time and space coordinates.

(v) - The mass transfers of the gaseous species along the pore are controlled by diffusion (Fick and Knudsen types), the forced convection being negligible in small pores (however, convection terms arising from mole number changes in the chemical reactions, are considered but can become also negligible when the reactants are highly diluted).

(vi) - No homogeneous reaction occurs in the pore during the infiltration process.

The differential equations, expressing the mass conservation (see appendix), are solved according to an iterative procedure and a numerical method utilizing finite differences, the first calculation being performed for the pore of constant initial diameter (i.e for $\Phi(z,t) = \Phi_0$). At each iteration, a concentration profile for each gaseous species i, $C_i(z,t)$ and a pore diameter profile $\Phi(z,t)$ are calculated along the pore and used in the next step. This iterative procedure is stopped when the pore entrance becomes sealed by the deposit, i.e when $\Phi(0,t) = 0$. In the following, the results of calculations

which have been performed for the infiltration of pure zirconia from $ZrCl_4$-CO_2-H_2-Ar and yttria from YCl_3-CO_2-H_2-Ar, are mainly presented as oxide thickness profiles for an infiltration duration t_c corresponding to $\Phi(0,t)=0$.

The calculations of the oxide deposit profiles and of the gaseous species composition profiles along the pore require three kinds of data : (i) the kinetic laws corresponding to the deposition of both oxides, expressed in terms of molar fluxes of the gaseous reactants (named ϑ), (ii) the diffusion coefficients of the various species in the gas phase and (iii) the molar volume of the deposit (named V_s) (see appendix 1).

2.2 - Kinetics laws

The kinetics corresponding to the deposition of both ZrO_2 and Y_2O_3 have been established by E. Sipp in a specially designed CVD-apparatus which has been described elsewhere [26]. The deposition rates were measured in-situ with a microbalance. All the flow rates (for H_2, CO_2, Ar, HCl, Cl_2 (only for the zirconia deposition)) where measured with mass flowmeters. In both cases, the deposition results from the hydrolysis of the chloride ($ZrCl_4$ or YCl_3). The water is produced by the reduction of carbon dioxide adsorbed at the substrate surface with hydrogen at high temperature.

2.2.1 - Kinetic laws for zirconia deposition

As discussed elsewhere [22], the deposition of zirconia from $ZrCl_4$-CO_2-H_2-Ar gas mixtures is assumed to occur according to the following reactions :

$$2\ H_{2(g)} + 2\ CO_{2(g)} \leftrightarrow 2\ H_2O_{(g)} + 2\ CO_{(g)} \quad (1)$$

$$ZrCl_{4(g)} + 2\ H_2O_{(g)} \rightarrow ZrO_{2(s)} + 4\ HCl_{(g)} \quad (2)$$

or by combining (1) and (2) :

$$ZrCl_{4(g)} + 2\ CO_{2(g)} + 2\ H_{2(g)} \rightarrow ZrO_{2(s)} + 2\ CO_{(g)} + 4\ HCl_{(g)} \quad (3)$$

with $\Delta G^{0,R(2)}(1200) = -184\ kJ.mol^{-1}$ and $\Delta G^{0,R(3)}(1200) = -190\ kJ.mol^{-1}$ (the gaseous reactants are $ZrCl_4$, CO_2 and H_2 whereas the gaseous products which are formed simultaneously with the zirconia deposit are CO and HCl). The kinetics corresponding to the deposition of ZrO_2 according to the overall equation (3) have been established

within various ranges of temperature, total pressure and gas phase composition. The flow rate of $ZrCl_4$ (generated from direct chlorination of zirconium chips set in a graphite crucible) was accurately derived from the weight loss of the zirconium bed continuously recorded with a millibalance.

Two different activation energy values were calculated from Arrhenius plots and the apparent partial orders were observed to be : (i) equal to zero with respect to HCl, Cl_2 and Ar and (ii) different from 0 for $ZrCl_4$, CO_2 and H_2. In the particular case of H_2, two different reaction orders were observed depending on the hydrogen partial pressure considered.

On the basis of these experimental data, three different kinetic laws were established, for a total pressure ranging from 2 up to 5 kPa, corresponding to the following general equation :

$$R = k_o \exp\left(-\frac{E_a}{\boldsymbol{R}\,T}\right) P_{ZrCl4}^{n1}\, P_{CO2}^{n2}\, P_{H2}^{n3} \qquad (4)$$

where R is the reaction rate (in $kg.s^{-1}.m^{-2}$), k_0 the pre-exponential factor of the kinetic constant, E_a the apparent activation energy, $\boldsymbol{R}$ the perfect gas constant (8.32 $J.mol^{-1}.K^{-1}$), T the temperature (in K), P_{ZrCl4} , P_{CO2} and P_{H2} the partial pressures of the reactants (in Pa), n_1 , n_2 and n_3, the reactions orders with respect to $ZrCl_4$, CO_2 and H_2. The values of k_0, E_a, n_1, n_2 and n_3 are listed in table I for the three kinetic laws within their P ; T and P_{H2} validity domains. The species $ZrCl_4$ is supposed to react itself at the surface, and the rate of H_2O production assumed to be fast with respect to the deposition reaction rate involving $ZrCl_4$ (i.e the reduction of adsorbed CO_2 with hydrogen (1) is not the limiting step for the overall reaction (3)).

2.2.2 - Kinetic law for yttrium oxide deposition

Few studies have been published up to now on the CVD of Y_2O_3 or other yttrium-based compounds [24-26]. Recently, E. Sipp has performed a detailed study of the kinetics of Y_2O_3 deposition from YCl_3-CO_2-H_2-Ar mixture [27], with the following main results : the deposition is assumed to occur according to the overall two reactions:

$$3\ H_{2(g)} + 3\ CO_{2(g)} \leftrightarrow 3\ H_2O_{(g)} + 3\ CO_{(g)} \qquad (5)$$

$$2\ YCl_{3(g)} + 3\ H_2O_{(g)} \rightarrow Y_2O_{3(s)} + 6\ HCl_{(g)} \qquad (6)$$

or by combining (5) and (6) :

Validity temperature and pressure ranges	k_0 $kg.s^{-1}m^{-2}Pa^{-\Sigma n_i}$	E_a $kJ.mol^{-1}$	n_1 $ZrCl_4$	n_2 CO_2	n_3 H_2
T < 1523 K	$1.0\ 10^{-11}$	39.5 ±1	1	0.5	2.0
1523 < T < 1823 K P_{H2} < 0.5 kPa	$6.8\ 10^{-12}$	154 ±2	1	0.5	2.3
1523 < T < 1823 K 0.5 < P_{H2} < 0.7 kPa	$1.0\ 10^{-11}$	154 ±2	1	0.5	0.5

Table I: **Numerical values of k_0, E_a, and apparent partial reaction orders for the three kinetics laws for the deposition of ZrO_2, according to [22]**

$$2\ YCl_{3(g)} + 3\ CO_{2(g)} + 3\ H_{2(g)} \rightarrow Y_2O_{3(s)} + 3\ CO_{(g)} + 6\ HCl_{(g)} \qquad (7)$$

The flow rate of YCl_3 (generated by direct vaporization) was accurately derived from the weight loss of the YCl_3 bed continuously recorded with a millibalance. The kinetic law corresponding to the deposition of Y_2O_3 according to the overall equation (7) proposed by E. Sipp is :

$$R = k_0 \exp\left(-\frac{E_a}{\boldsymbol{R}\,T}\right) P_{YCl3}^{2}\ P_{CO2}^{1}\ P_{H2}^{2} \qquad (8)$$

where R is the reaction rate (in $kg.s^{-1}.m^{-2}$), k_0 the pre-exponential factor of the kinetic constant, E_a the apparent activation energy, $\boldsymbol{R}$ the perfect gas constant (8.32 $J.mol^{-1}.K^{-1}$), T the temperature (in K), P_{YCl3} , P_{CO2} and P_{H2} the partial pressures of the reactants (in Pa). The validity domain of this kinetic is defined by : (i) $[CO_2]_{in}$ / $[YCl_3]_{in} > 9$ and $1 \leq [H_2]_{in} / [CO_2]_{in} \leq 5$, where $[\ i\ ]_{in}$ stands for concentration of species i introduced in the CVD/CVI apparatus, (ii) $T \leq 1373$ K, (iii) a total flow rate between 3 and 6 $l.mn^{-1}$ in standard conditions and (iv) a total pressure of about 4 kPa. Under such conditions, E_a = 616 $kJ.mol^{-1}$ and k_0 = 7.37 10^7 $kg.m^{-2}.s^{-1}Pa^{-5}$. The species YCl_3 is supposed to react at the substrate surface, and the rate of H_2O production assumed to be fast with respect to the deposition reaction rate involving YCl_3 (i.e the reduction of adsorbed CO_2 with hydrogen (5) is not the limiting step for the overall reaction represented by equation (7)).

2.3- Diffusion coefficients

As shown in appendix 1, the effective diffusion coefficients D_i were calculated, for each species i, by taking into account both the Knudsen diffusion coefficient $D_{i,K}$ and the Fick diffusion coefficient $D_{i,F}$ (equation A3).

The Knudsen coefficient $D_{i,K}$ of a species i in a pore diameter Φ was calculated, on the basis of the gas kinetics theory, according to the following equation :

$$D_{i,K} = \frac{\Phi}{3}\left[\frac{8\,\boldsymbol{R}\,T}{\pi M_i}\right]^{1/2} \qquad (9)$$

where $\boldsymbol{R}$ is the perfect gas constant and M_i is the molar mass of species i (expressed

in $kg.mol^{-1}$).

The Fick diffusion coefficient $D_{i,F}$ of a species i in a gas mixture whose composition is defined by molar fractions x_i and x_j (with j # i) was calculated according to the equation A4 (see appendix 1) from the various $D_{i,j}$ binary diffusion coefficients.

The $D_{i,j}$ binary diffusion coefficients were calculated according to the following equation :

$$D_{i,j} = 5.876\ 10^{-24}\ \frac{T^{3/2}}{P\ \sigma_{i,j}^{2}\ \Omega_D}\left[\frac{1}{M_i}+\frac{1}{M_j}\right]^{1/2} \qquad (10)$$

where $D_{i,j}$ is expressed in $m^2.s^{-1}$, T in Kelvin, P in Pa, M_i in $kg.mol^{-1}$, $\sigma_{i,j}$ (collision diameter) in m and Ω_D (collision integral) is dimensionless. The $\sigma_{i,j}$ is expressed by :

$$\sigma_{i,j} = \frac{\sigma_i + \sigma_j}{2} \qquad (11)$$

The values of Ω_D are extrapolated from Hirschfelder table [28] and $kT/\varepsilon_{i,j}$ values (where $\varepsilon_{i,j}$ is the maximum attractive energy between two molecules and k the Boltzmann constant) with :

$$\frac{\varepsilon_{i,j}}{k} = \left[\frac{\varepsilon_i}{k}\cdot\frac{\varepsilon_j}{k}\right]^{1/2} \qquad (12)$$

The values of σ_i and ε_i/k for H_2, CO, CO_2, HCl, Ar are taken from [29] and listed in table II. Those for $ZrCl_4$ and YCl_3 have been estimated according to a procedure described in appendix 2, and are also shown in table II.

3 - RESULTS OF THE CALCULATIONS

As already mentioned, the calculations which were performed according to the model presented in section 2.1 and in appendix 1 (with the data presented in section 2.2) give the gas phase composition in the pore and the pore diameter for any given values of space-time coordinates (z,t) and infiltration conditions (i.e temperature, total pressure, feed gas composition and initial pore dimensions).

A CVI-experiment is usually performed under conditions which maintain the pores open as long as possible in order to achieve a low residual porosity. Therefore,

Species i	σ_i [nm]	$\frac{\varepsilon_i}{k}$ [K]
H2	0.2827	59.7
CO	0.3690	91.7
CO2	0.3941	195.2
HCl	0.3339	344.7
Ar	0.3542	93.3
$ZrCl_4$	0.6100	1363.2
YCl_3	0.5269	2047.0

Table II: Values of σ_i and $\frac{\varepsilon_i}{k}$ chosen for the calculation of Ω_D

in the following sections, the emphasis will be put on the effect of the CVI parameters on the **ZrO_2 and Y_2O_3 thickness profiles** calculated for **a critical time t = t_c** corresponding to the pore entrance sealing by the deposit. These profiles could be regarded as limits. In addition, a few examples of in-pore gas phase composition profiles will be presented and discussed as well as a few examples of thickness profiles for short infiltration durations (i.e $t << t_c$).

3.1 - Effect of the infiltration parameters on the oxide deposit profiles along the pore (at $t = t_c$)

3.1.1 - Temperature

As already mentioned, ICVI-experiments are usually performed at temperatures as low as possible, temperature being known to have a very strong effect on the infiltration homogeneity [19,30]. For both oxides, a first series of calculations has been run for two different feed gas compositions and for a pore 100 µm in diameter and 10 mm in length (such a pore is actually observed in 2D fiber preforms commonly used as starting material for the preparation of many labaratory-scale CMC specimens [31]).

The figures 1 and 2 show the influence of temperature respectively on the calculated ZrO_2 and Y_2O_3 thickness profiles, at $t = t_c$. For zirconia infiltration, the first kinetic law (see table I) is assumed to be valid within the temperature range 1173 K < T < 1373 K.

For a given feed gas composition, an effect of temperature on the thickness profile (at $t = t_c$) is observed for the both oxides. For **zirconia infiltration**, this effect remains **rather moderate**, particularly when the reactants are highly diluted with argon, whereas for **yttria infiltration**, this effect is **very important**. As previously reported by many authors for the CVI of carbides (i.e SiC, B_4C or TiC), the best results in terms of thickness homogeneity are obtained for the **lowest temperature** value [12,30,31]. These results are consistent with the conclusions drawn by Minet et al. in their experimental study of the ICVI of zirconia in various complex fiber preforms [21].

The effect of temperature on the deposit thickness profile is much weaker for zirconia (within the 1173-1373 K temperature range) and stronger for yttria than for the carbide matrices. This is obviously related to the different values of the corresponding apparent activation energies. In their modelling of the ICVI of SiC (deposited from CH_3SiCl_3-H_2 mixtures), Fedou et al. [19] have used a kinetic law with E_a = 225

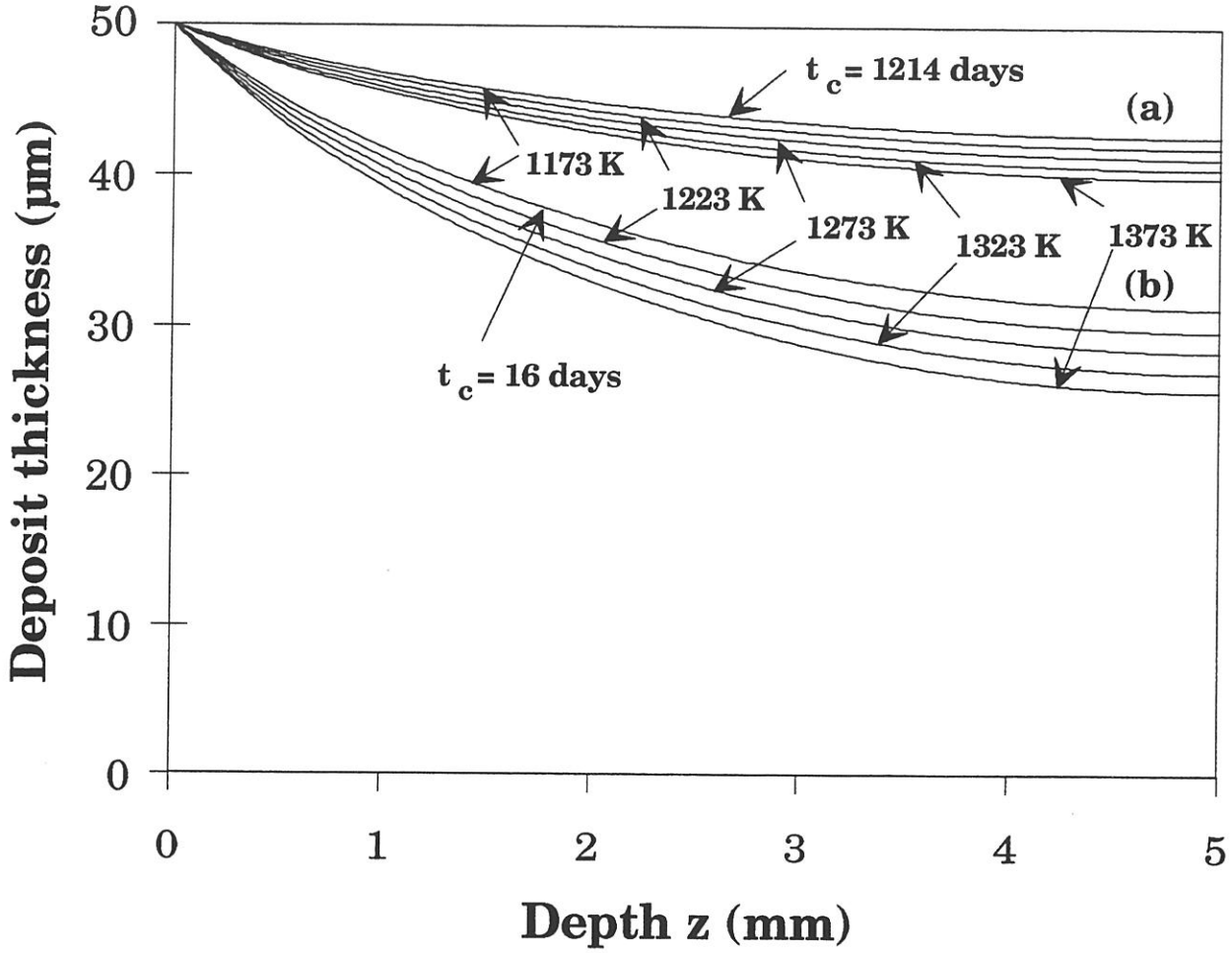

Fig. 1 : Influence of temperature on the calculated thickness profiles of zirconia deposit obtained from a $ZrCl_4$ - H_2 - CO_2 - Ar gas mixture for P = 2 kPa, Φ_0 = 100 µm, L/Φ_0 = 100,
(a) : α_{H2} = 30, α_{CO2} = 10, α_{ZrCl4} = 1, α_{Ar} = 1200,
(b) : α_{H2} = 0.3, α_{CO2} = 0.1, α_{ZrCl4} = 1, α_{Ar} = 12,
where α_i = [i]/[$ZrCl_4$] and [i] stands for concentration of the species i in the feed gas

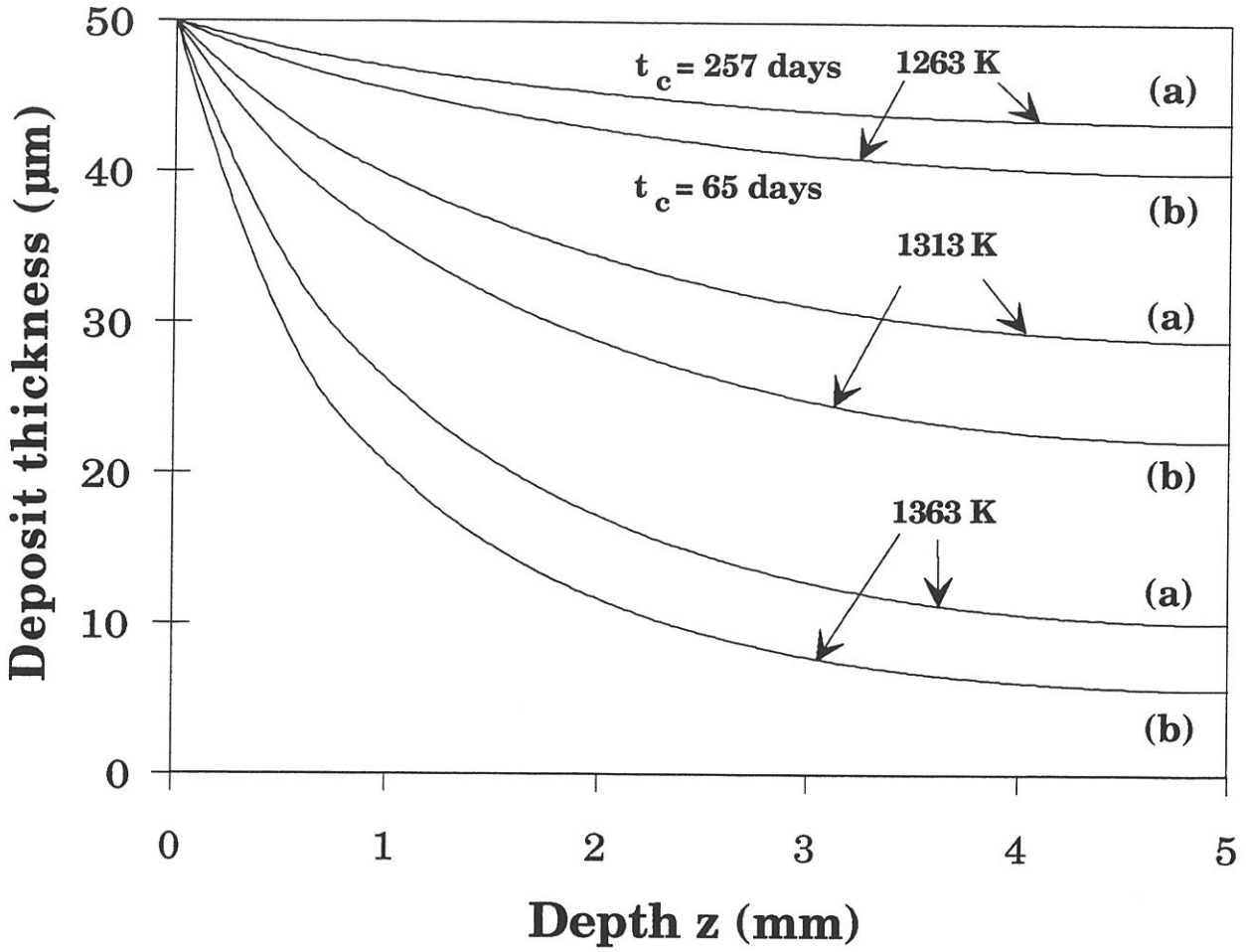

Fig. 2 : Influence of temperature on the calculated thickness profiles of yttrium oxide deposit obtained from a YCl_3 - H_2 - CO_2 - Ar gas mixture for P = 4 kPa, Φ_0 = 100 µm, L/Φ_0 = 100,
(a) : α_{H2} = 30, α_{CO2} = 10, α_{YCl3} = 1, α_{Ar} = 250,
(b) : α_{H2} = 15, α_{CO2} = 5, α_{YCl3} = 1, α_{Ar} = 125,
where α_i = [i]/[YCl_3] and [i] stands for concentration of the species i in the feed gas

$kJ.mol^{-1}$ [20], whereas the activation energy used here for zirconia is only E_a = 39.5 $kJ.mol^{-1}$ and for yttria 616 $kJ.mol^{-1}$. For zirconia infiltration, results rather close to those reported for SiC would be obtained in the 1523-1823 K range where the apparent activation energy is 154 $kJ.mol^{-1}$ (table I).

It is worthy of note that both zirconia and yttria thickness profiles calculated for the lowest temperatures are not as flat as they are for infiltration of SiC from CH_3SiCl_3-H_2 [19]. This feature could be related to the difference between the diffusion coefficients of the source species, i.e $ZrCl_4$ for zirconia, YCl_3 for yttria and CH_3SiCl_3 for SiC [19], the latter being higher than the formers.

The critical times t_c corresponding to the feed gas composition leading to the best infiltration homogeneity, are very long for the pore considered here, i.e 1214 days at 1173 K for zirconia and 257 days at 1263 K for yttria, owing to the law deposition rate of the oxides. They can be significantly lower, i.e t_c = 16 days at 1173 K for zirconia and t_c = 65 days at 1263 K for yttrium oxide, when a reactant-rich feed gas composition is used ((b) in fig. 1 and 2). However, under such conditions the infiltration homogeneity is not so good.

3.1.2 - Total Pressure

Zirconia thickness profiles at T = 1173 K and yttria profiles at T = 1363 K, corresponding to various total pressures (ranging from 2 to 5 kPa) are shown in fig. 3 and 4 for the same model pore (Φ_0 = 100 µm, L = 10 mm). It clearly appears that, in both cases, total pressure has a **very strong effect** on the infiltration homogeneity. It is even more pronounced than for the infiltration of SiC from CH_3SiCl_3-H_2 mixtures. As an example, the profile variations observed for zirconia when P is increased only from 2 to 5 kPa is similar to that reported by Naslain et al. for SiC when P is raised from 2 to 100 kPa for the same temperature and pore dimensions [30]. This feature could be related to the difference that exists between the kinetic laws : the overall reaction orders are 3.5 for zirconia (table I), 5.0 for yttria (see equation (8)) and only 1.0 for SiC [20]).

3.1.3 - Feed gas composition

Since in the kinetic laws represented by equation (8) with the data shown in table I, the apparent partial reaction orders with respect to $ZrCl_4$, YCl_3, CO_2 and H_2 are different from zero, it was anticipated that both oxide thickness profiles along the pore should depend on the feed gas composition. Thus, a new series of calculations

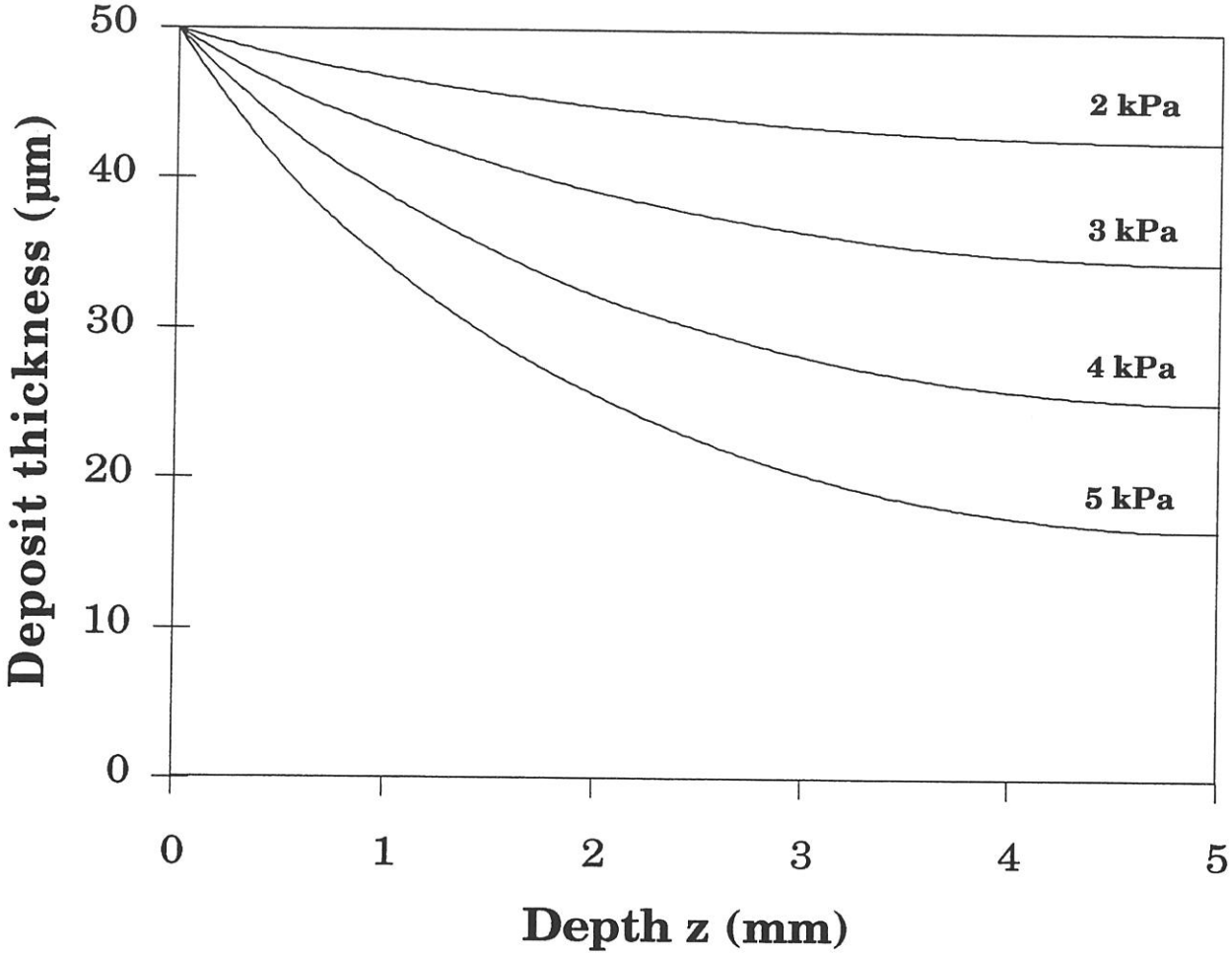

Fig. 3 : Influence of total pressure on the calculated thickness profiles of zirconia deposit obtained from a $ZrCl_4$ - H_2 - CO_2 - Ar gas mixture for T =1173 K, Φ_0 = 100 µm, L/Φ_0 = 100, α_{H2} = 30, α_{CO2} = 10, α_{ZrCl4} = 1, α_{Ar} = 1200, where α_i = [i]/[$ZrCl_4$] and [i] stands for concentration of the species i in the feed gas

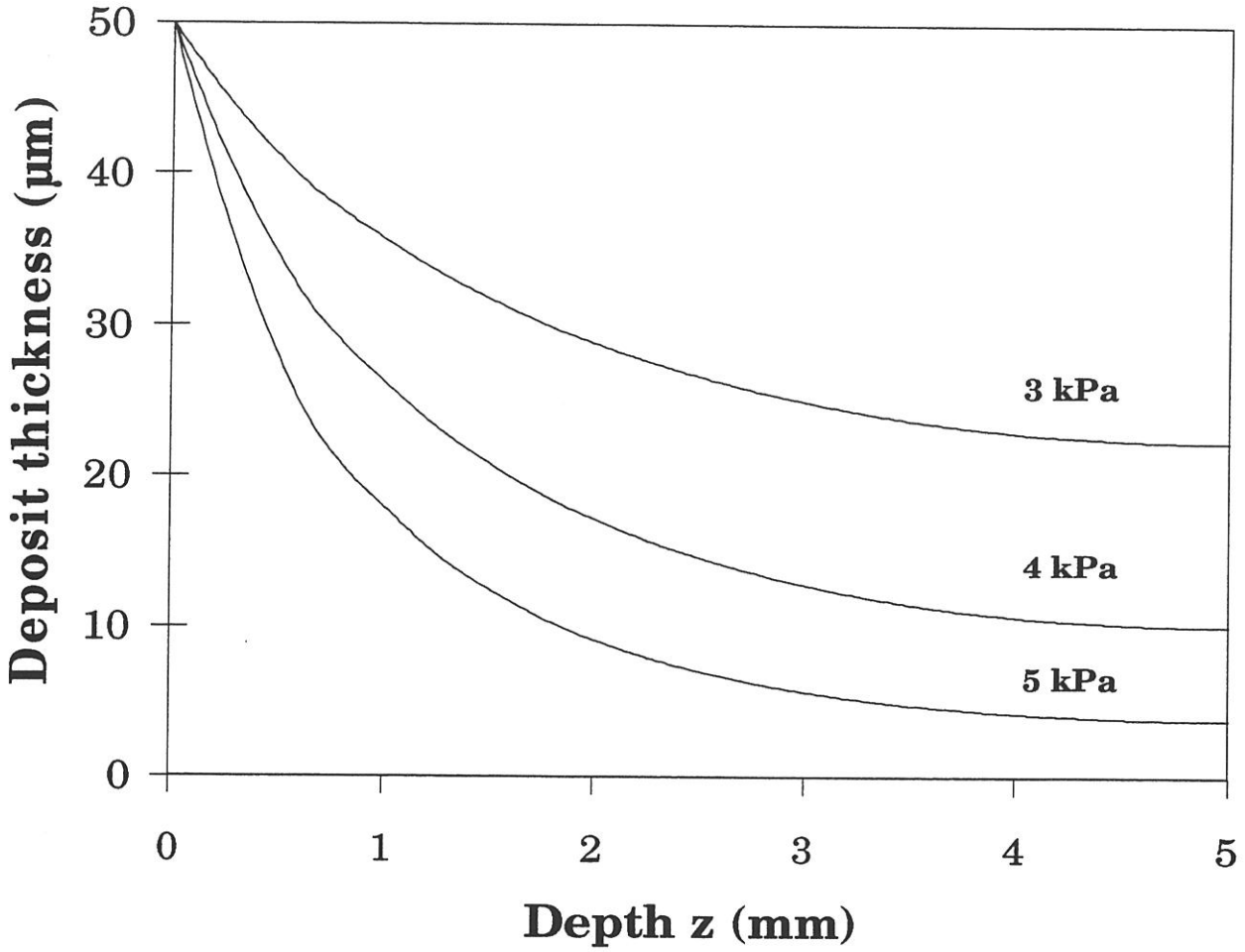

Fig. 4 : Influence of total pressure on the calculated thickness profiles of yttrium oxide deposit obtained from a YCl_3 - H_2 - CO_2 - Ar gas mixture for T =1363 K, Φ_0 = 100 µm, L/Φ_0 = 100, α_{H2} = 30, α_{CO2} = 10, α_{YCl3} = 1, α_{Ar} = 250, where α_i = [i]/[YCl_3] and [i] stands for concentration of the species i in the feed gas

was run in order to study the effect of the gas composition (out of the pore) on the infiltration homogeneity. The results are shown in figures 5 to 12.

Generally speaking, increasing the concentration of a species i (with i = $ZrCl_4$, YCl_3, CO_2 or H_2) in the feed gas tends to increase the oxide thickness gradient along the pore. This effect for CO_2 is the weakest since its apparent partial reaction order is the lowest in the deposition kinetics laws of both oxides (only equal to 1/2 for zirconia and 1.0 for yttria) (figures 7 and 8). For zirconia infiltration, the effect of $ZrCl_4$ (n_1 = 1), is moderate (fig.5). As a consequence, increasing the concentration of CO_2 for both oxides or $ZrCl_4$ for zirconia in the feed gas does not lower significantly the critical time value. Conversely, the effect of hydrogen for both oxides and YCl_3 for yttrium oxide is more important (fig. 6, 9 and 10) since the apparent order with respect to these species is high, i.e of about 2 except for law 3 (table I). As a result, increasing the partial pressure of hydrogen for both oxide and YCl_3 for yttrium oxide in the feed gas strongly reduces the critical time (as an example, for zirconia, it falls from 1214 to 24 days when α_{H2} is multiplied by 10). It is anticipated that the effect of hydrogen on the infiltration homogeneity of zirconia along the pore would be much weaker and comparable to that of CO_2 if the kinetic law 3 is used, since n_3 would fall from 2 to 0.5 (table I).

As shown in fig. 11 and 12, the effect of a dilution of the reactant species with argon on the infiltration homogeneity of both oxides is as dramatic as that of hydrogen although the apparent partial reaction order with respect to argon is nil. This strong effect of argon is purely a dilution effect since the calculations were performed at constant total pressure, i.e increasing the amount of argon in the feed gas reduces simultaneously all the partial pressures of the reactants. Therefore the effect of dilution by argon is comparable to that of decreasing total pressure under experimental conditions where kinetic effect is predominant with respect to Fick diffusion effect (coefficient inversely proportional to total pressure).

3.1.4 - Pore aspect ratio

The effect of the pore aspect ratio on the infiltration homogeneity of the pore was studied by calculating the oxides thickness profiles along pores with L/Φ_0 aspect ratio ranging from 10 to 1000 (i.e all the pores have the same diameter Φ_0 = 100 µm, the pore length L being varied from 1 to 100 mm). The results are shown in fig. 13 and 14. Since the pore length L is different from one pore to another, a reduced depth abscissa, defined as z/L is used.

The calculations clearly show that the pore aspect ratio L/Φ_0 has a very strong

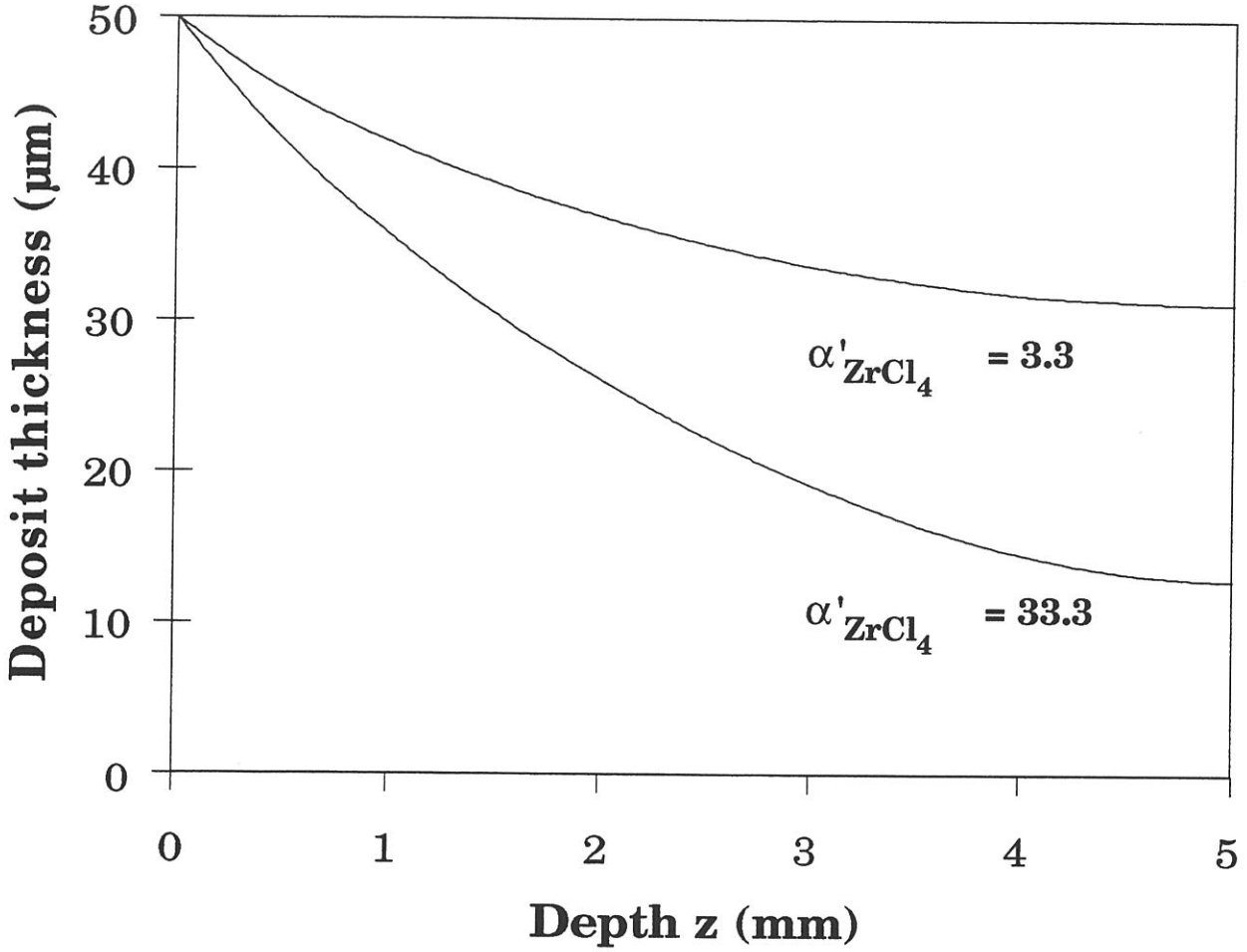

Fig. 5 : Influence of $ZrCl_4$ concentration on the calculated thickness profiles of zirconia deposit obtained from a $ZrCl_4$ - H_2 - CO_2 - Ar gas mixture for T =1173 K, P = 2 kPa, Φ_0 = 100 µm, L/Φ_0 = 100, α'_{H2} = 1, α'_{CO2} = 0.3, α'_{Ar} = 40, where $\alpha'_i = [i]/[H_2]$ and [i] stands for concentration of the species i in the feed gas

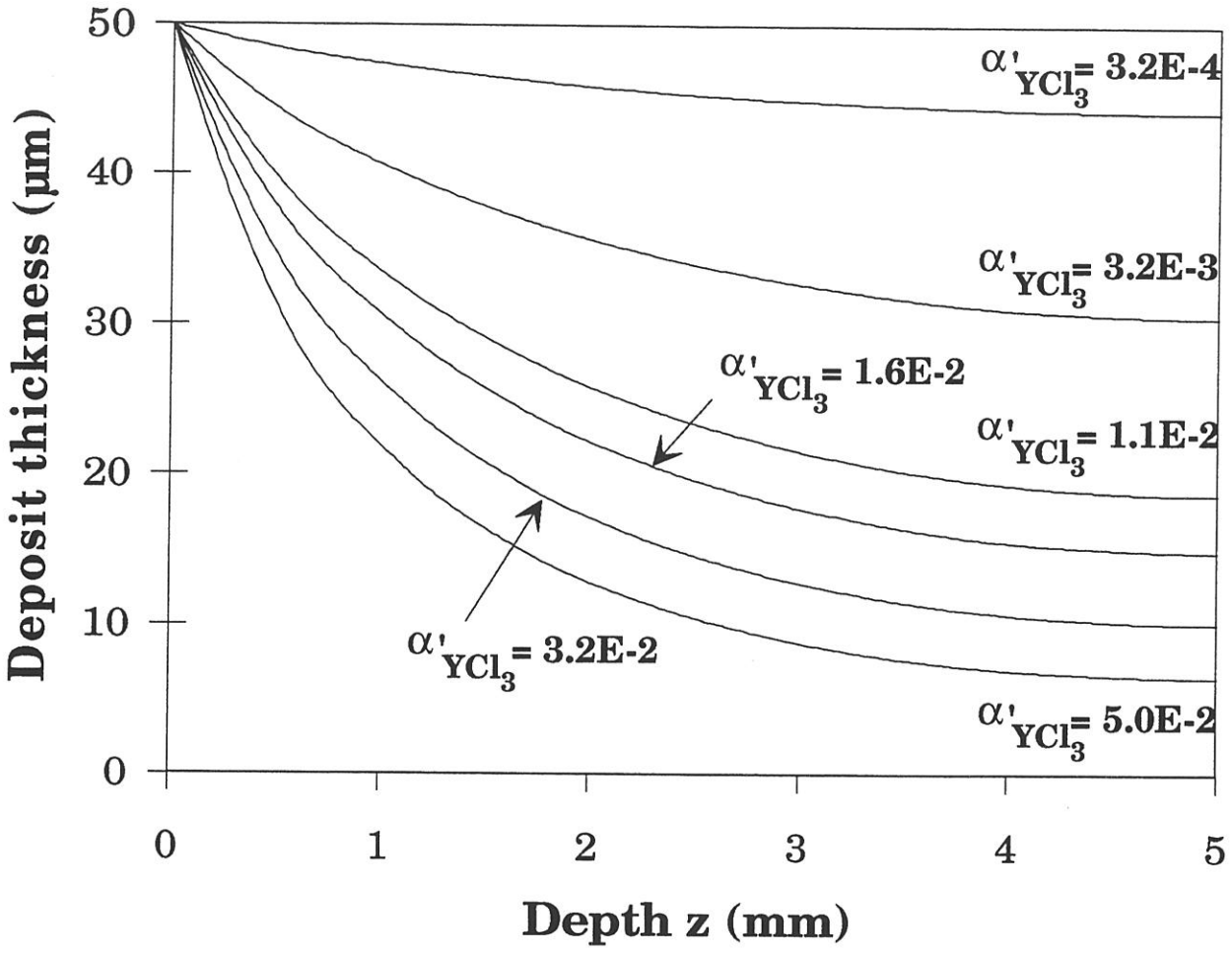

Fig. 6 : Influence of YCl_3 concentration on the calculated thickness profiles of yttrium oxide deposit obtained from a YCl_3 - H_2 - CO_2 - Ar gas mixture for T =1363 K, P = 4 kPa, Φ_0 = 100 µm, L/Φ_0 = 100, α'_{H2} = 1, α'_{CO2} = 0.333, α'_{Ar} = 8, where $\alpha'_i = [i]/[H_2]$ and [i] stands for concentration of the species i in the feed gas

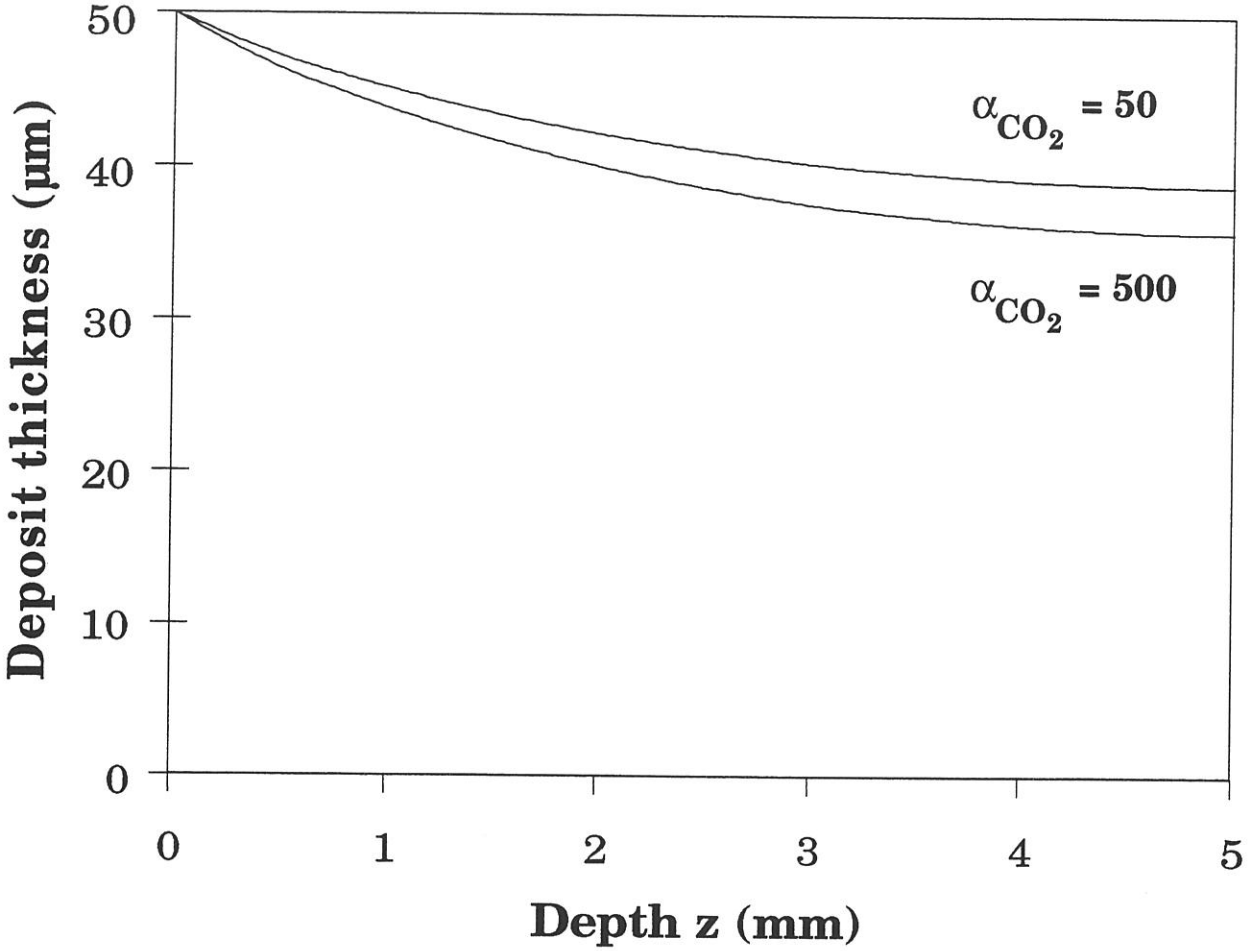

Fig. 7 : Influence of carbon dioxide concentration on the calculated thickness profiles of zirconia deposit obtained from a $ZrCl_4$ - H_2 - CO_2 - Ar gas mixture for T =1173 K, P = 2 kPa, Φ_0 = 100 µm, L/Φ_0 = 100, α_{H2} = 30, α_{ZrCl4} = 1, α_{Ar} = 1200, where α_i = [i]/[$ZrCl_4$] and [i] stands for concentration of the species i in the feed gas

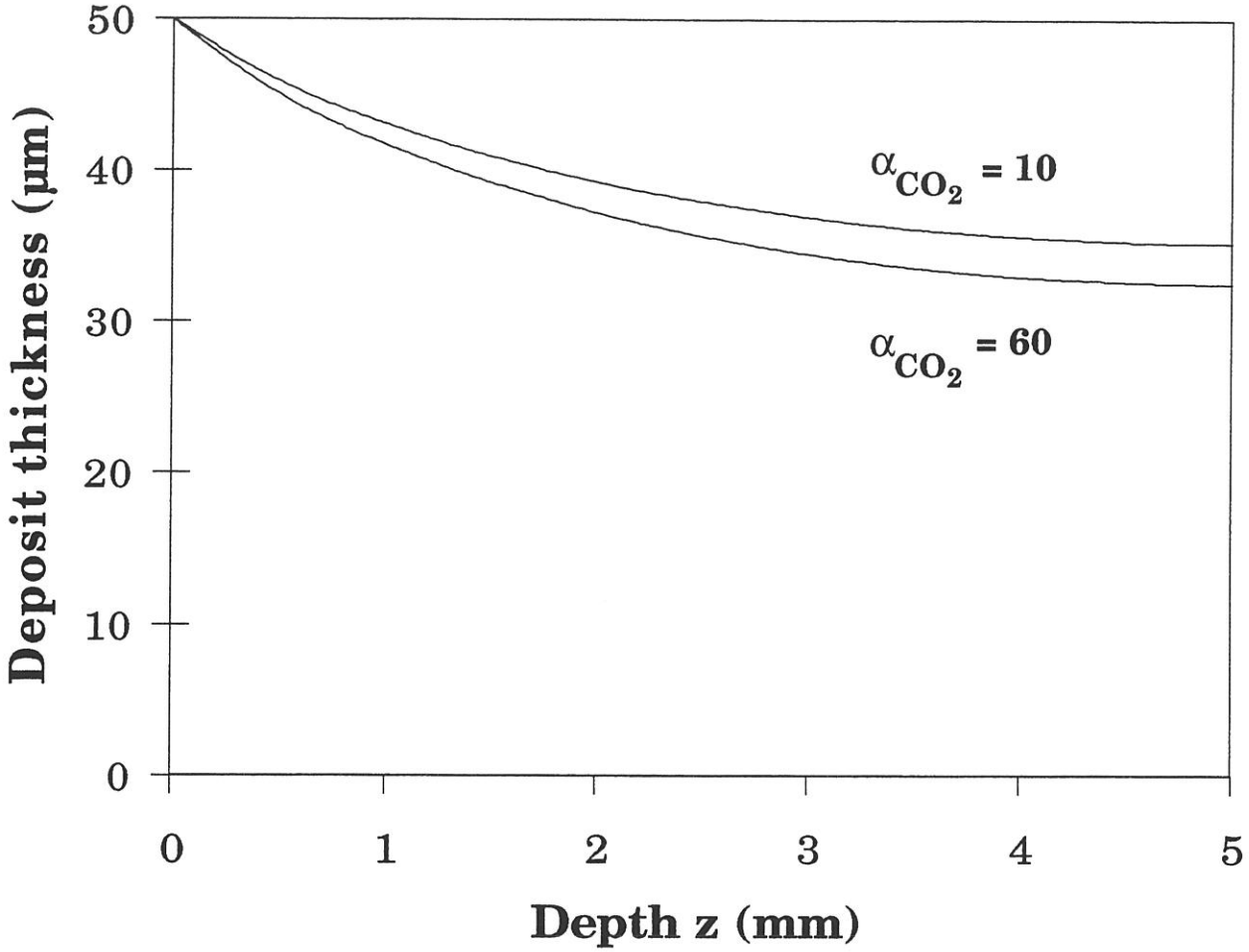

Fig. 8 : Influence of carbon dioxide concentration on the calculated thickness profiles of yttrium oxide deposit obtained from a YCl_3 - H_2 - CO_2 - Ar gas mixture for T =1363 K, P = 4 kPa, Φ_0 = 100 µm, L/Φ_0 = 100, α_{H2} = 1, α_{YCl3} = 1, α_{Ar} = 250, where α_i = [i]/[YCl_3] and [i] stands for concentration of the species i in the feed gas

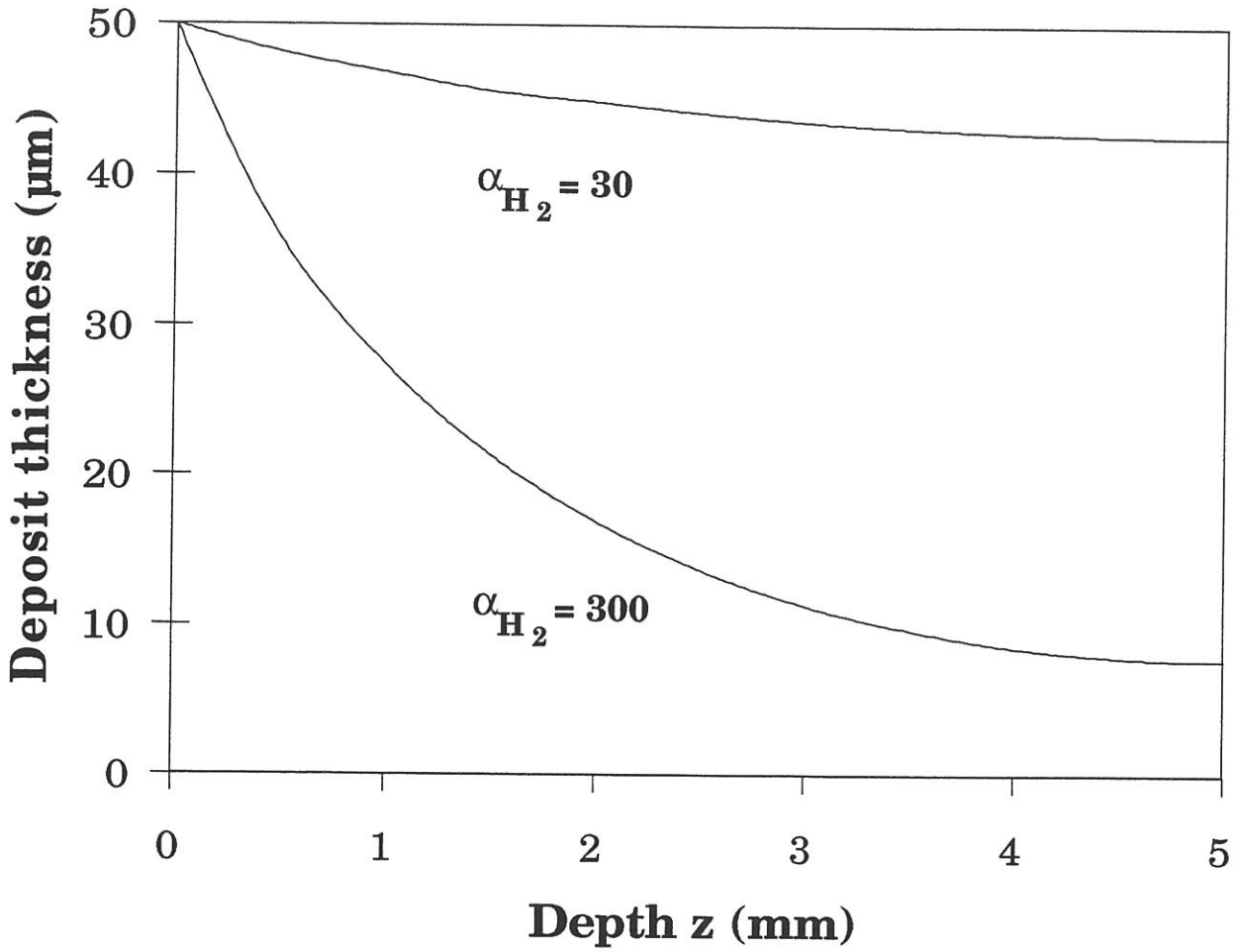

Fig. 9 : Influence of hydrogen concentration on the calculated thickness profiles of zirconia deposit obtained from a $ZrCl_4$ - H_2 - CO_2 - Ar gas mixture for T =1173 K, P = 2 kPa, Φ_0 = 100 µm, L/Φ_0 = 100, α_{CO2} = 10, α_{ZrCl4} = 1, α_{Ar} = 1200, where α_i = [i]/[$ZrCl_4$] and [i] stands for concentration of the species i in the feed gas

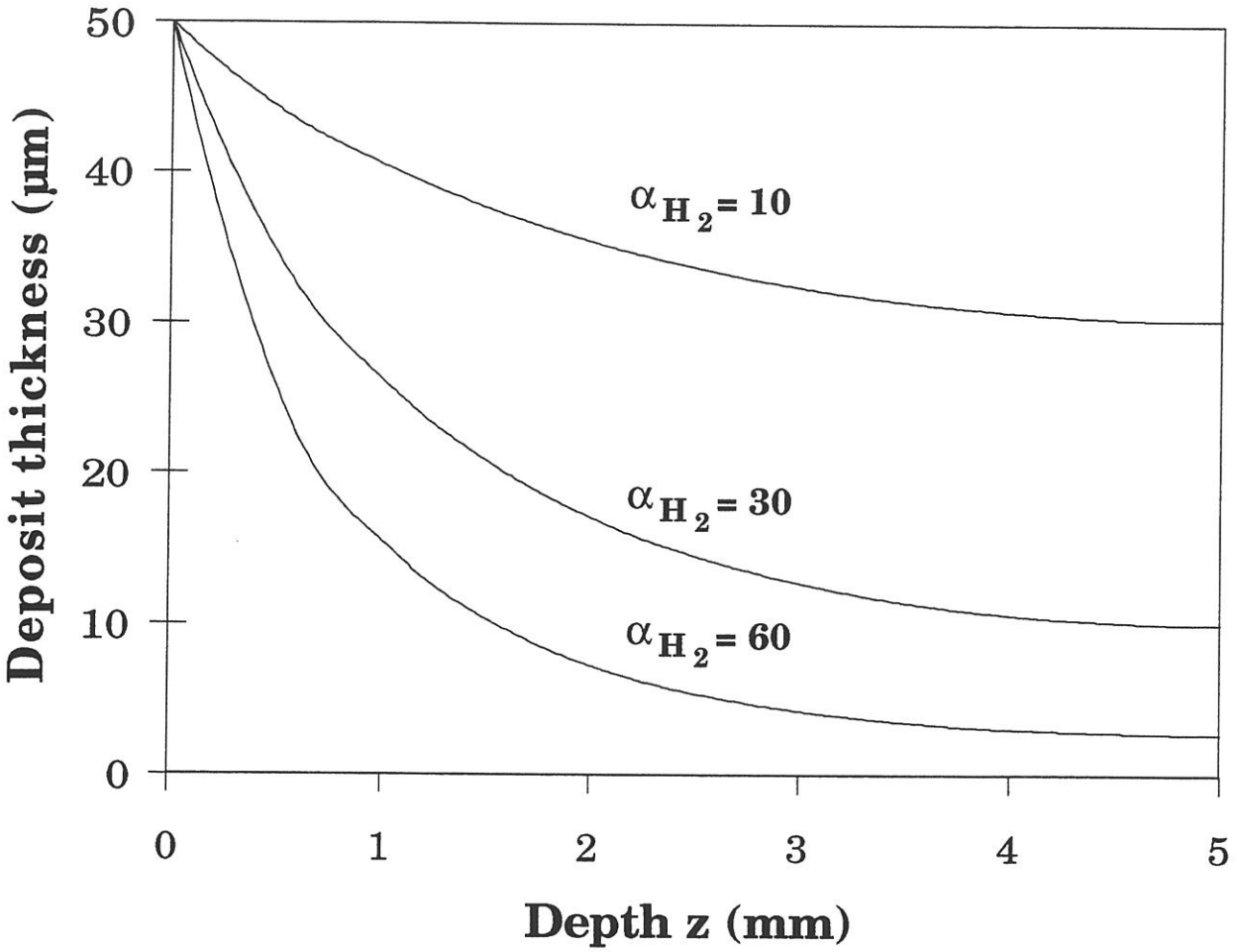

Fig. 10 : Influence of hydrogen concentration on the calculated thickness profiles of yttrium oxide deposit obtained from a YCl_3 - H_2 - CO_2 - Ar gas mixture for T =1363 K, P = 4 kPa, Φ_0 = 100 µm, L/Φ_0 = 100, α_{CO2} = 10, α_{YCl3} = 1, α_{Ar} = 250, where α_i = [i]/[YCl_3] and [i] stands for concentration of the species i in the feed gas

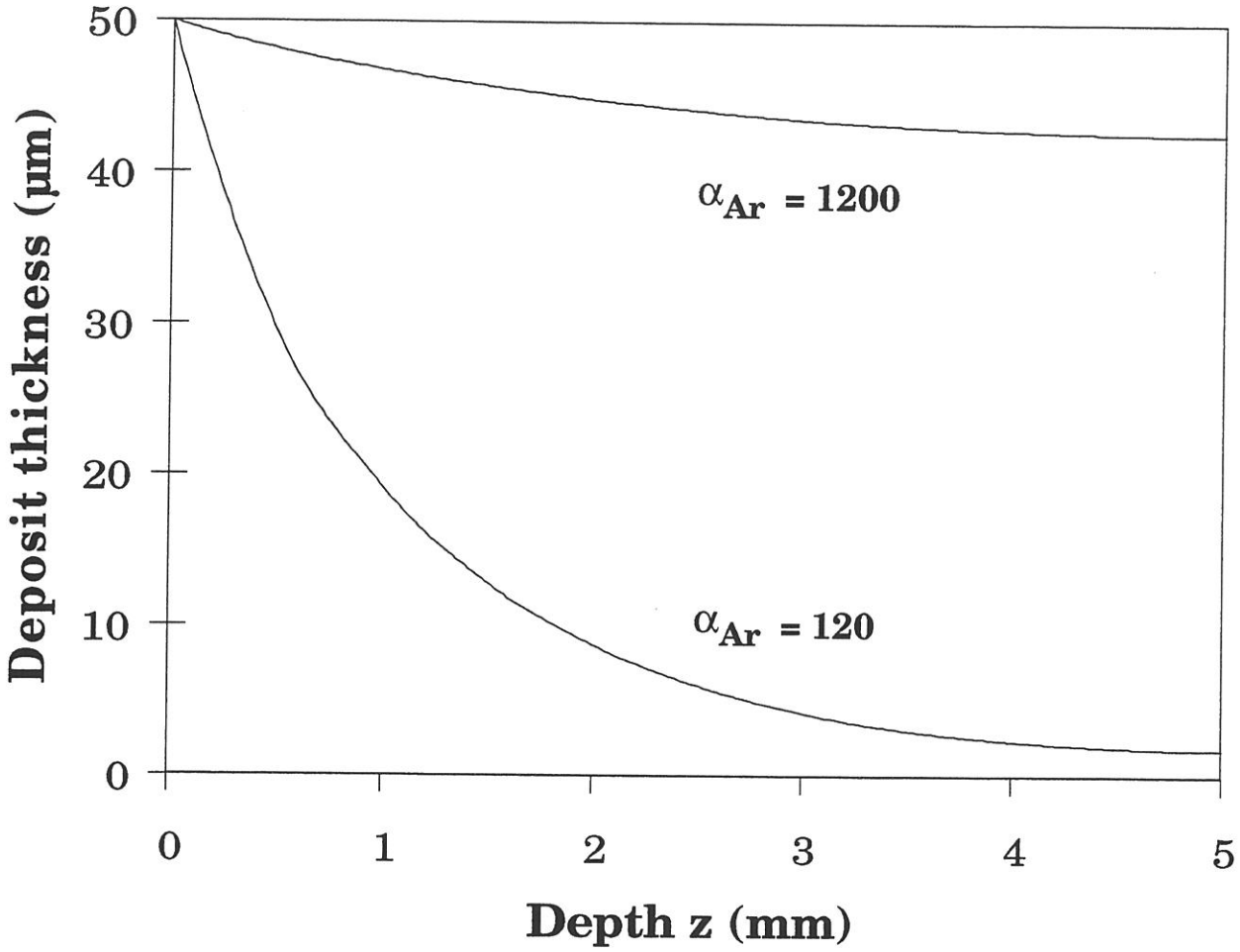

Fig. 11 : Influence of argon concentration on the calculated thickness profiles of zirconia deposit obtained from a $ZrCl_4$ - H_2 - CO_2 - Ar gas mixture for T =1173 K, P = 2 kPa, Φ_0 = 100 µm, L/Φ_0 = 100, α_{H2} = 30, α_{CO2} = 10, α_{ZrCl4} = 1, where α_i = [i]/[$ZrCl_4$] and [i] stands for concentration of the species i in the feed gas

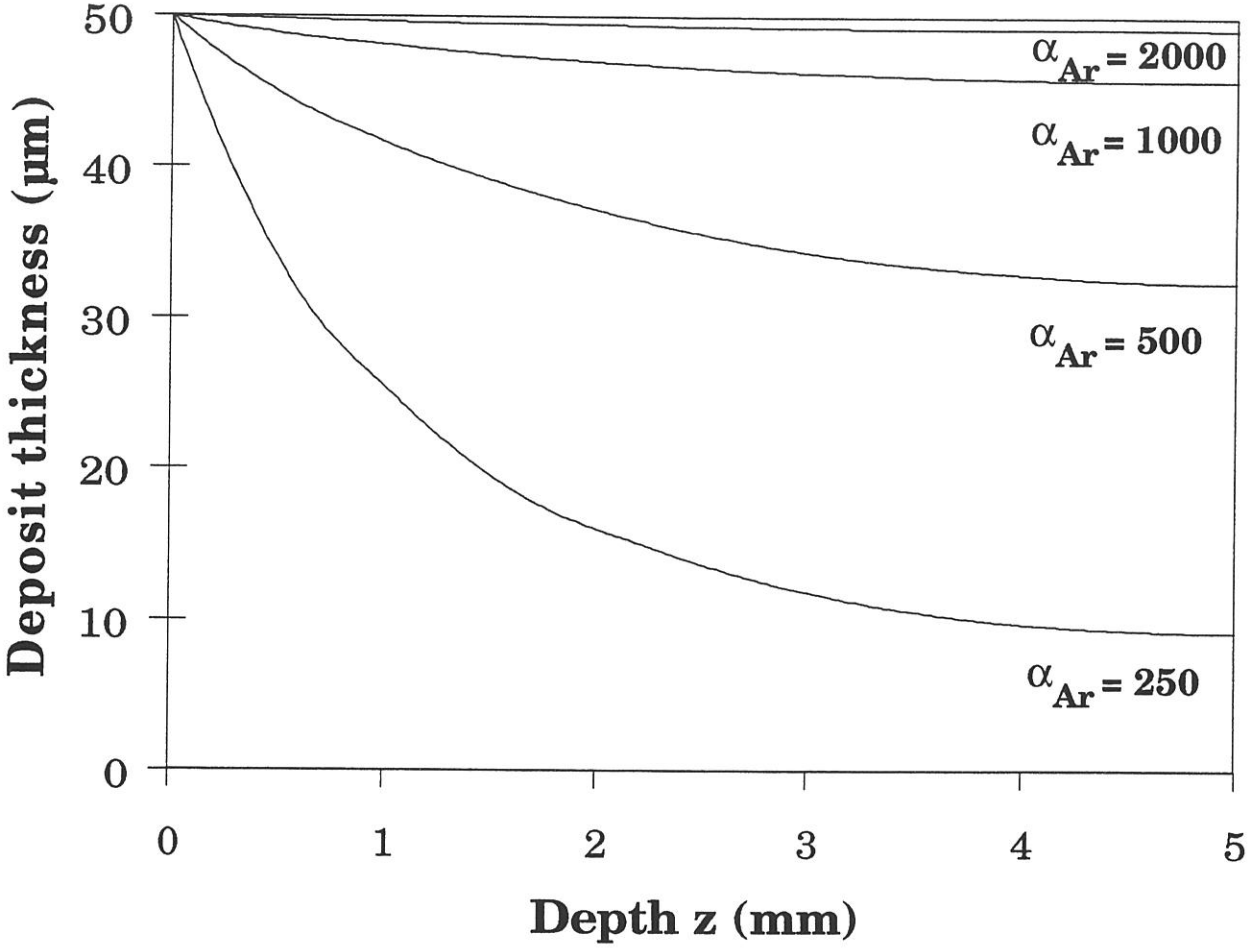

Fig. 12 : Influence of argon concentration on the calculated thickness profiles of yttrium oxide deposit obtained from a YCl_3 - H_2 - CO_2 - Ar gas mixture for T =1363 K, P = 4 kPa, Φ_0 = 100 µm, L/Φ_0 = 100, α_{H2} = 30, α_{CO2} = 10, α_{YCl3} = 1, where α_i = [i]/[YCl_3] and [i] stands for concentration of the species i in the feed gas

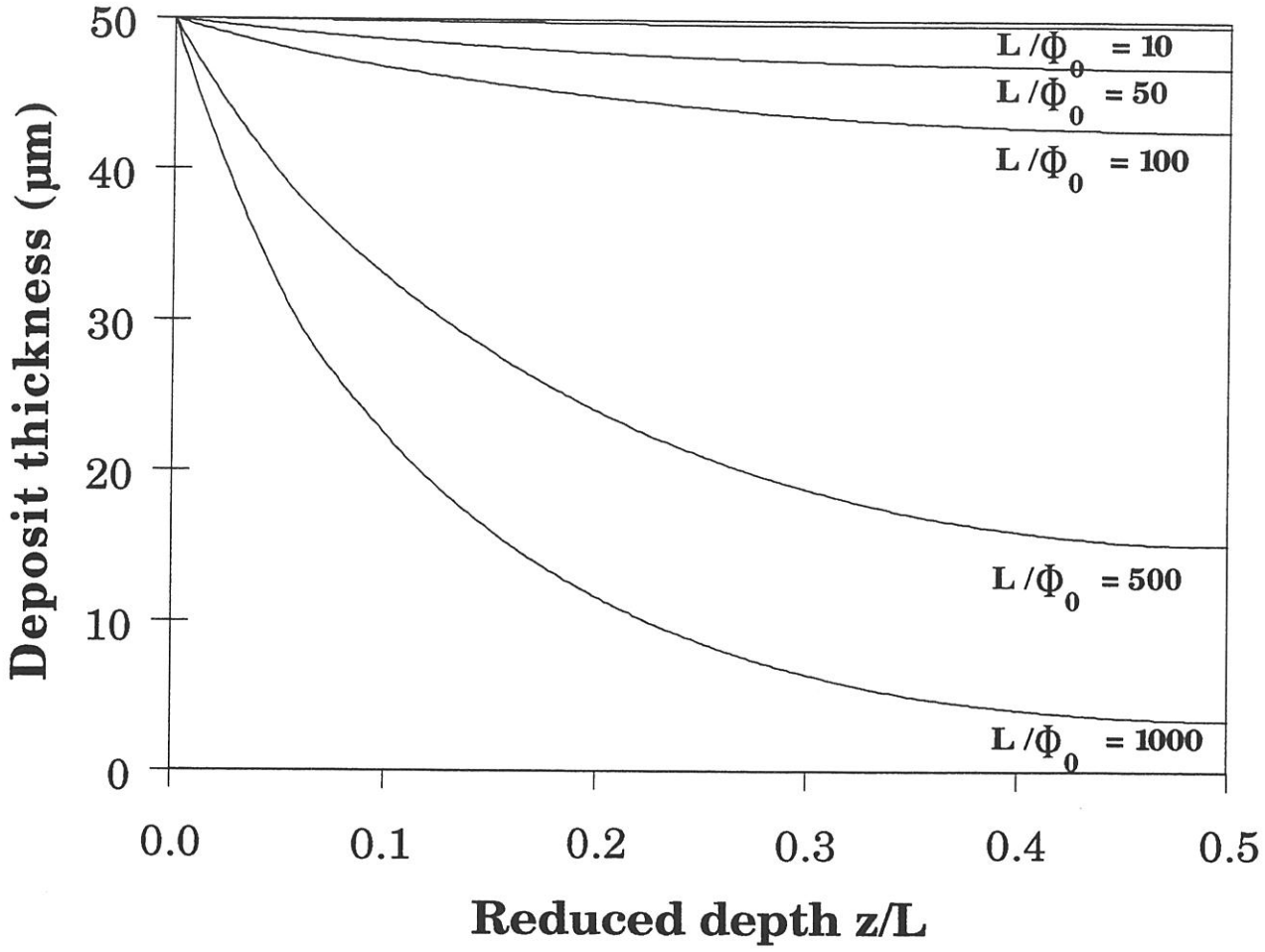

Fig. 13 : Influence of the aspect ratio on the calculated thickness profiles of zirconia deposit obtained from a $ZrCl_4$ - H_2 - CO_2 - Ar gas mixture for T =1173 K, P = 2 kPa, Φ_0 = 100 µm, α_{H2} = 30, α_{CO2} = 10, α_{ZrCl4} = 1, α_{Ar} = 1200, where α_i = [i]/[$ZrCl_4$] and [i] stands for concentration of the species i in the feed gas

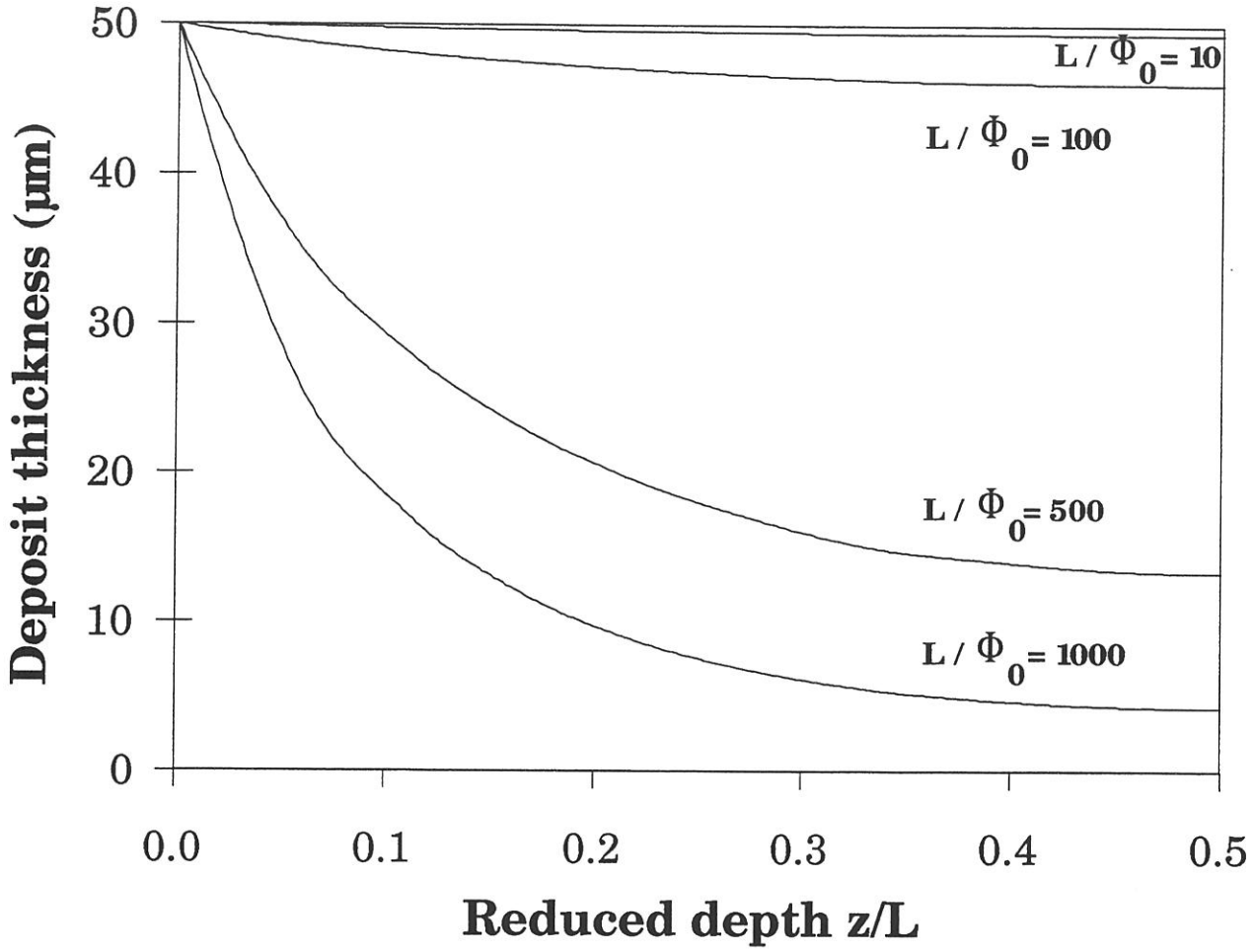

Fig. 14 : Influence of the aspect ratio on the calculated thickness profiles of yttrium oxide deposit obtained from a YCl_3 - H_2 - CO_2 - Ar gas mixture for T =1363 K, P = 4 kPa, Φ_0 = 100 µm, $\alpha_{H2} = 10$, $\alpha_{CO2} = 10$, $\alpha_{YCl3} = 1$, $\alpha_{Ar} = 400$, where $\alpha_i = [i]/[YCl_3]$ and [i] stands for concentration of the species i in the feed gas

effect on the infiltration homogeneity. This effect remains rather limited when L/Φ_0 is increased from 10 to 100 but it becomes dramatic when L/Φ_0 is raised from 100 to 1000. Under this latter condition, the zirconia deposit tends to be limited to the vicinity of the pore entrance. A similar result has been already reported by Fedou et al. for the infiltration of SiC (deposited from CH_3SiCl_3-H_2) in a straight cylindrical pore of same diameter [19]. It is also consistent with a well experimentally established feature of the CVI-processing of CMC according to which, in a given fiber preform (i.e with a given length), the pores of large diameter (i.e pores with low aspect ratio) are much easily infiltrated in a fiber preform than those with small diameters (i.e pores with high aspect ratio).

3.2 - Concentration profiles along the pore in the gas phase

As already mentioned, the model which has been presented in section 2.1 and in appendix, yields also the concentrations of the gaseous species in the pore as a function of space-time coordinates. These data can be used to draw the concentration profiles along the pore of any species i, in the gas phase, at any t value (e.g $t = t_c$ that is to say when the pore entrance becomes sealed by the deposit).

Some examples of such profiles are shown in fig. 15 and 16. Fig. 15 gives the concentration profiles of $ZrCl_4$, H_2, CO_2, CO and HCl for zirconia infiltration (fig. 15a) and the related zirconia thickness profile (fig. 15b) for a pore of medium size (Φ_0 = 34 µm) corresponding to the experimental study that will be discussed in section 4 (note that the concentrations of the gaseous species are shown on different scales). Fig. 16 gives the concentration profiles of YCl_3, H_2, CO_2, CO and HCl for yttria infiltration of a pore 100 µm in diameter.

For zirconia, the thickness profile (fig. 15b) exhibits a great thickness gradient : the chosen ICVI parameters make the infiltation difficult. Moreover since the calculations have been performed when t becomes equal to t_c, the entrance diameter of the pore is almost nil which explains that the occurrence of the source species $ZrCl_4$ is limited to the vicinity of the pore entrance (as a result of the mass transfer / chemical reaction competition). In a similar manner, the reaction products CO and HCl (see equation (3)) have almost constant concentrations along the pore axis except near the pore entrance where these concentrations are nil (boundary limit conditions). Finally, H_2 and CO_2, which are in large excess in the feed gas have uniform concentrations all along the pore. For yttria, the thickness profile (fig. 16b) is more flat than for zirconia : the chosen ICVI parameters for yttria infiltration are better than for zirconia. It is the reason why the source YCl_3 species occurs more in depth

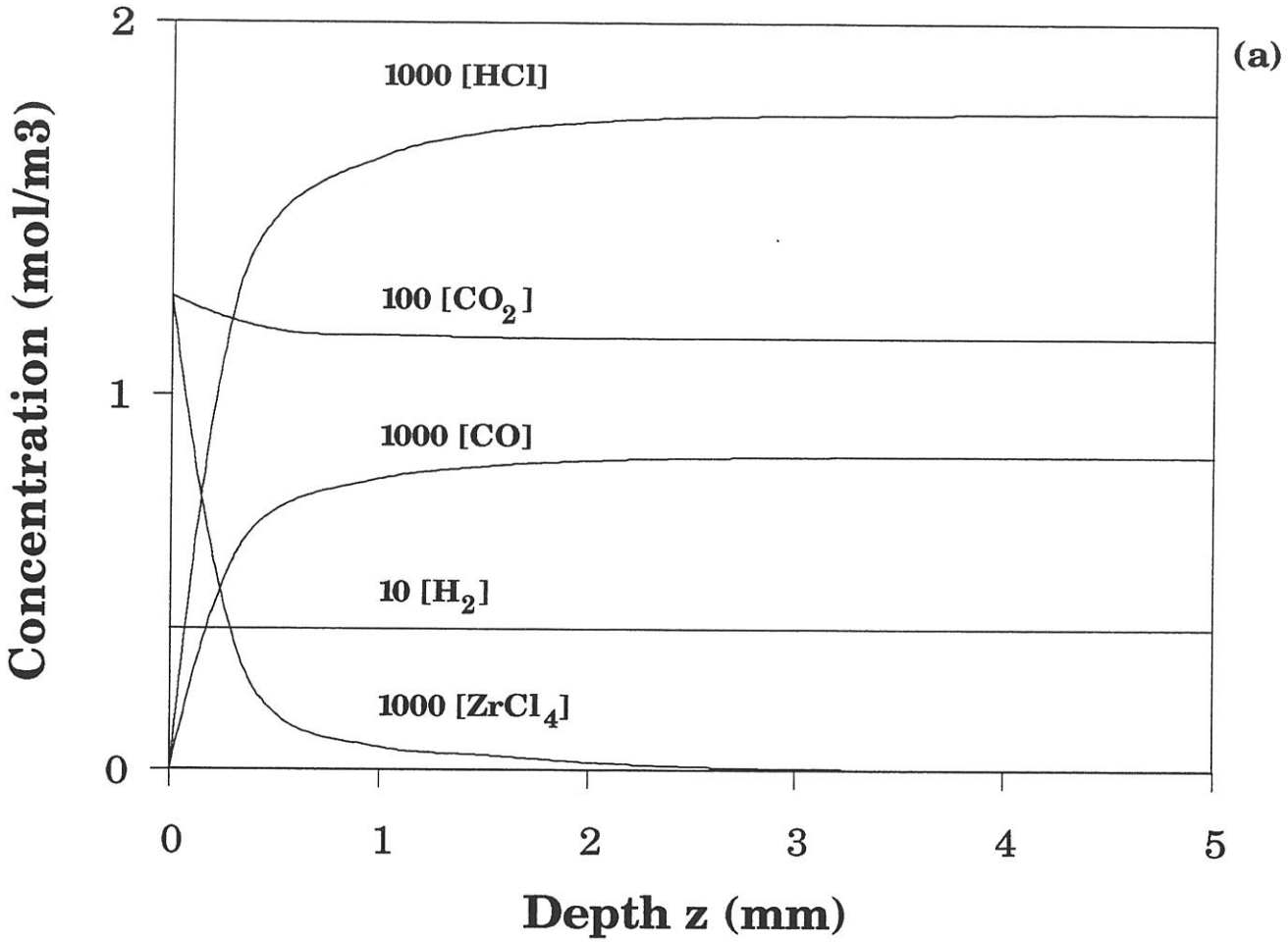

Fig. 15 : Calculated profiles along the pore axis for the infiltration of zirconia deposit obtained from a $ZrCl_4$ - H_2 - CO_2 - Ar gas mixture with T =1183 K, P = 2 kPa, Φ_0 = 34 µm, L = 10 mm, α_{H2} = 30, α_{CO2} = 10, α_{ZrCl4} = 1, α_{Ar} = 120, where α_i = [i]/[$ZrCl_4$] and [i] stands for concentration of the species i in the feed gas

(a) Concentrations of the gaseous species

(b) Zirconia deposit thickness

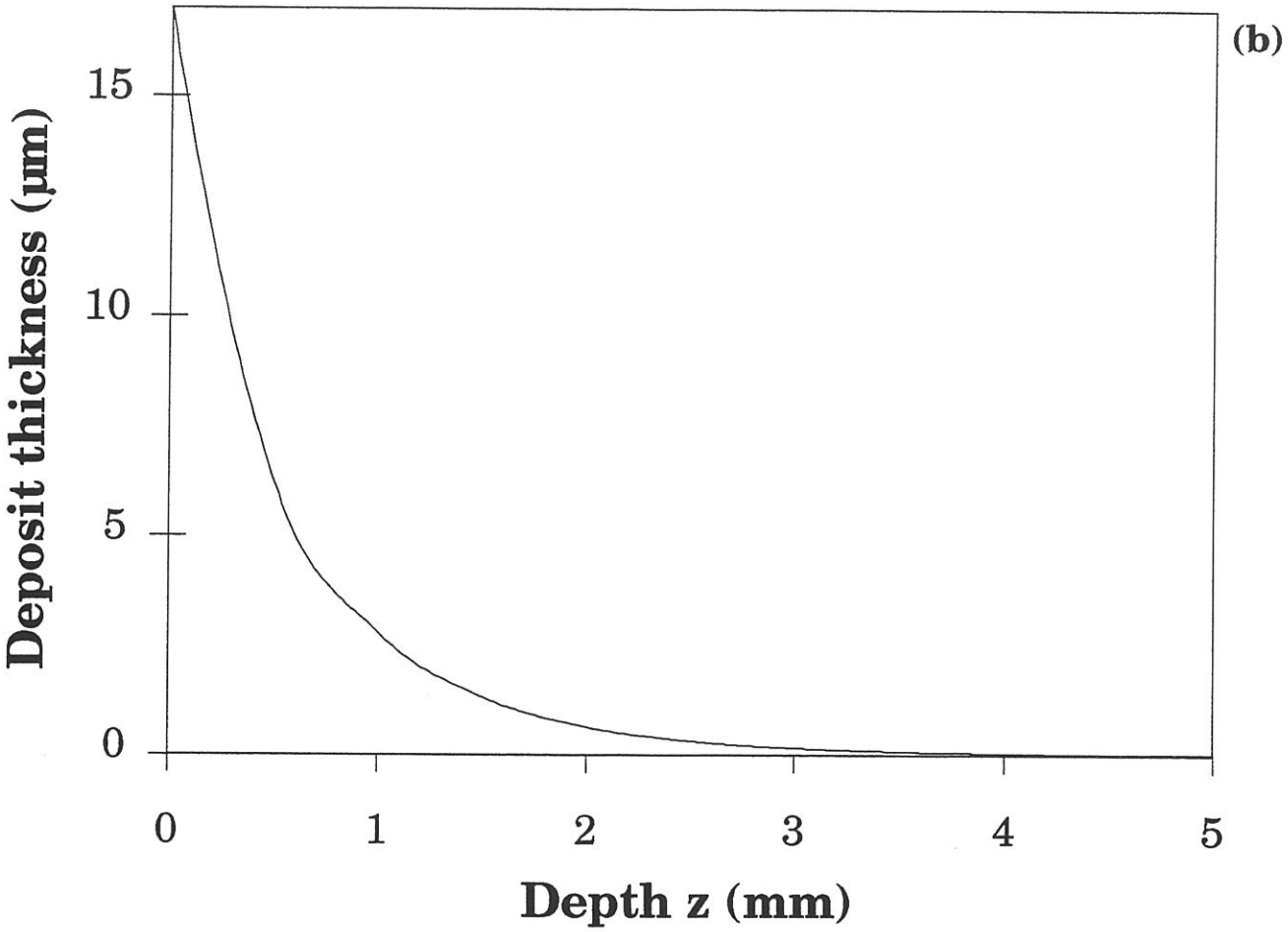

Fig. 15 : Calculated profiles along the pore axis for the infiltration of zirconia deposit obtained from a $ZrCl_4$ - H_2 - CO_2 - Ar gas mixture with T =1183 K, P = 2 kPa, Φ_0 = 34 µm, L = 10 mm, α_{H2} = 30, α_{CO2} = 10, α_{ZrCl4} = 1, α_{Ar} = 120, where α_i = [i]/[$ZrCl_4$] and [i] stands for concentration of the species i in the feed gas

(a) Concentrations of the gaseous species

(b) Zirconia deposit thickness

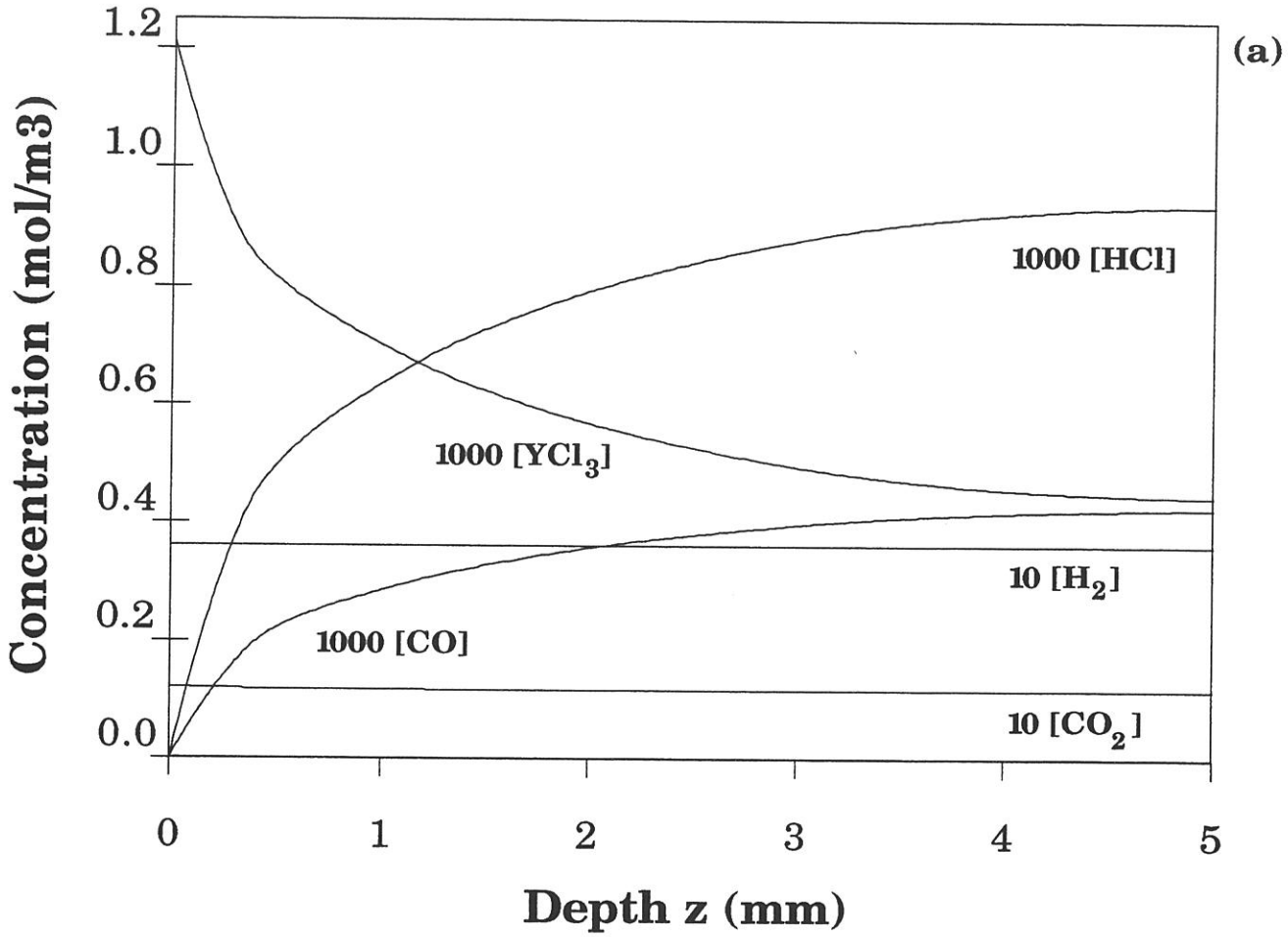

Fig. 16 : Calculated profiles along the pore axis for the infiltration of yttrium oxide deposit obtained from a YCl_3 - H_2 - CO_2 - Ar gas mixture with T =1363 K, P = 4 kPa, Φ_0 = 100 µm, L = 10 mm, α_{H2} = 30, α_{CO2} = 10, α_{YCl3} = 1, α_{Ar} = 250, where α_i = [i]/[YCl_3] and [i] stands for concentration of the species i in the feed gas

(a) Concentrations of the gaseous species
(b) Yttrium oxide deposit thickness

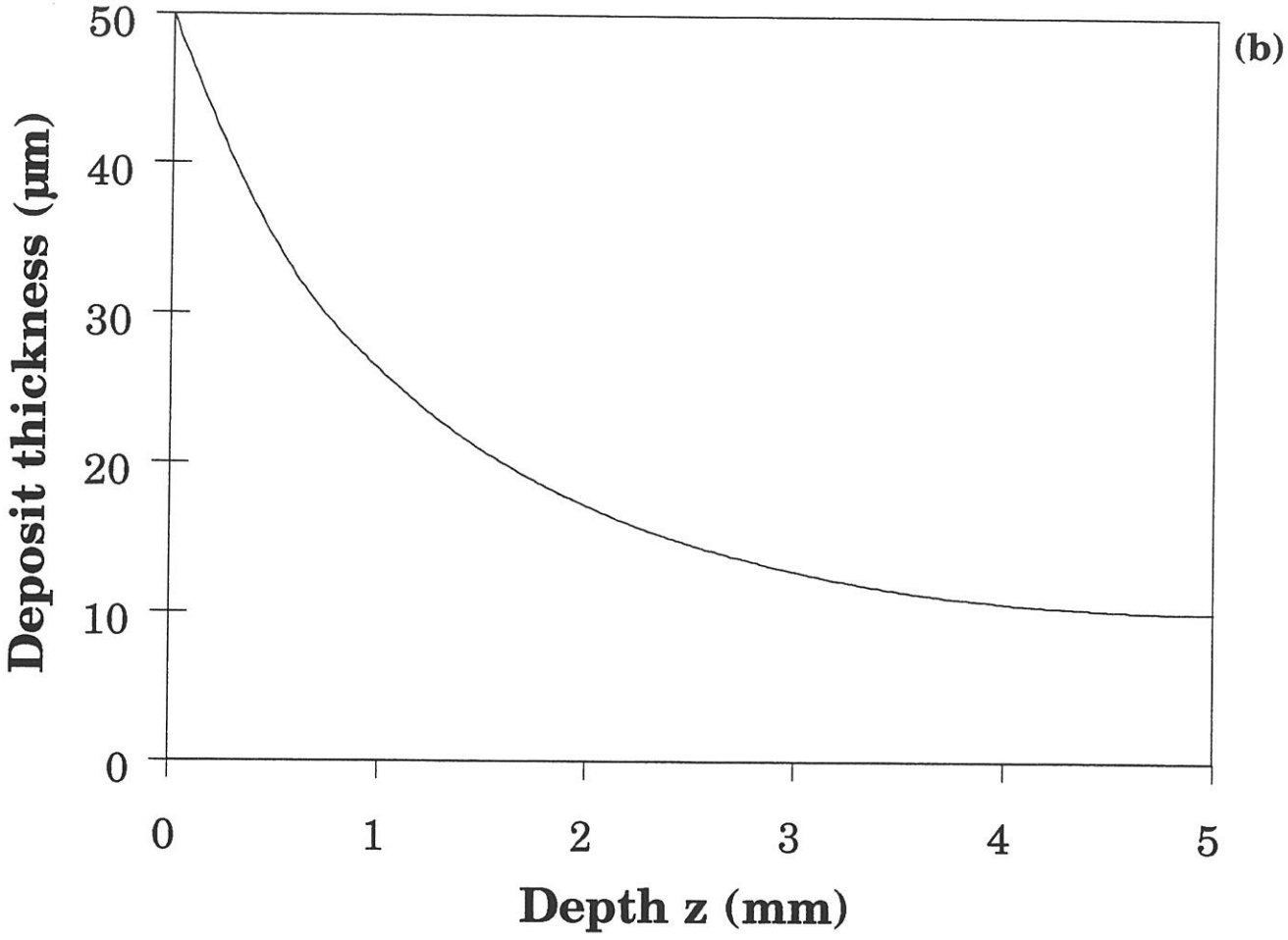

Fig. 16 : Calculated profiles along the pore axis for the infiltration of yttrium oxide deposit obtained from a YCl_3 - H_2 - CO_2 - Ar gas mixture with T =1363 K, P = 4 kPa, Φ_0 = 100 µm, L = 10 mm, α_{H2} = 30, α_{CO2} = 10, α_{YCl3} = 1, α_{Ar} = 250, where α_i = [i]/[YCl_3] and [i] stands for concentration of the species i in the feed gas

(a) Concentrations of the gaseous species
(b) Yttrium oxide deposit thickness

than $ZrCl_4$ species and the reaction products CO and HCl (see equation (7)) have not constant concentrations along the pore. Conversely, H_2 and CO_2 have uniform concentrations all along the pore, like for zirconia infiltration.

3.3 - Deposit thickness and species concentration profiles for $0 < t < t_c$

Up to now, all the results which have been discussed were related to the end of the pore infiltration, i.e to $t = t_c$. The model can also be used to calculate profiles (gaseous species concentrations and deposit thickness) at any time ranging from $t = 0$ (see the definition of the time origin in section 2.1) to $t = t_c$.

Examples of such calculations are shown in fig. 17 and 18 which emphasize how the **oxide deposit** is progressively formed in a pore of medium size (i.e 34 µm in diameter) for the first case and in a pore of large size (i.e 100 µm in diameter) for the second one as the infiltration duration is increased up to the pore sealing. As could be predicted, the thickness gradient near the pore entrance becomes steeper and steeper as the pore diameter at $z = 0$ is progressively reduced by the deposit.

Another example, related to the concentration of the gaseous phase species along the pore for zirconia infiltration is shown in fig. 19 for a pore of large diameter (Φ_0 = 100 µm and L = 10 mm) and infiltration conditions similar to those mentioned in fig. 15. Up to about $t = t_c/2$ (i.e as far as the pore entrance diameter is not too significantly reduced by the deposit), the diffusion of the reactants ($ZrCl_4$, CO_2 and H_2) in the pore and conversely that of the products (CO and HCl) in the opposit direction, are easy. As a result, the concentration profiles are rather flat for all the species. On the contrary when t is close or equal to t_c, a **bottle neck phenomenon** occurs near the pore entrance (whose diameter is close or equal to zero) : the center of the pore ($z = L/2$) is no longer fed with reactants and the reaction products no longer evacuated by diffusion.

4 - PRELIMINARY EXPERIMENTAL STUDY

Up to now and as far as we know, very few articles have been devoted to the experimental assessment of thickness profiles of ceramics deposited by CVI along model pores. This lack of work in this field might be related to the difficulties encountered in : (i) preparing model pores of well controlled geometries and (ii) measuring accurately in-pore thickness as low as one micrometer. Thickness profiles of SiC and TiC infiltrated by CVI in mm-size-diameter tubes were reported by Van Den Brekel et al. [11]. E.

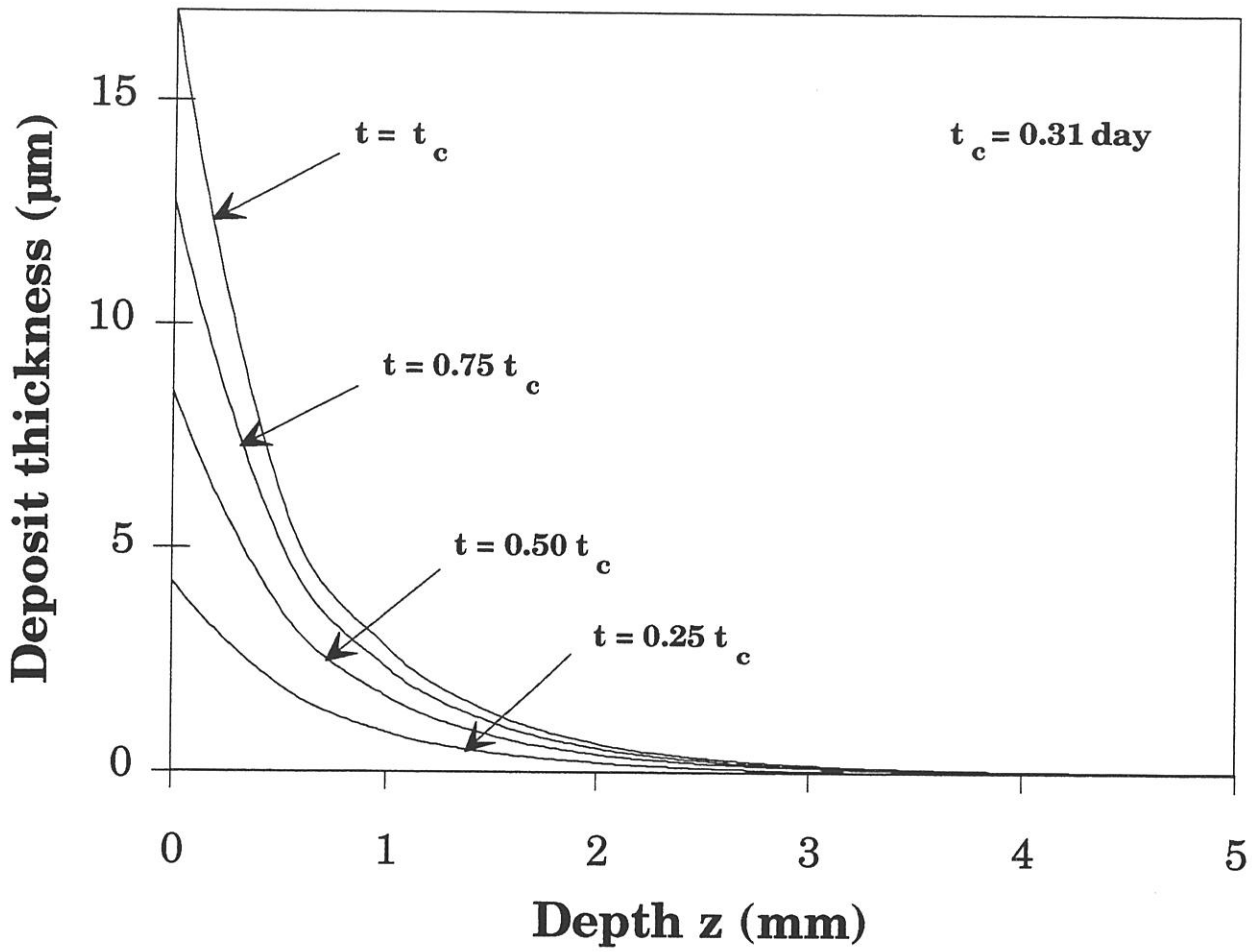

Fig. 17 : Calculated zirconia thickness profiles along the pore for various infiltration times (from t = 0 to t = t_c) with T =1183 K, P = 2 kPa, Φ_0 = 34 µm, L = 10 mm, α_{H2} = 30, α_{CO2} = 10, α_{ZrCl4} = 1, α_{Ar} = 120, where α_i = [i]/[$ZrCl_4$] and [i] stands for concentration of the species i in the feed gas

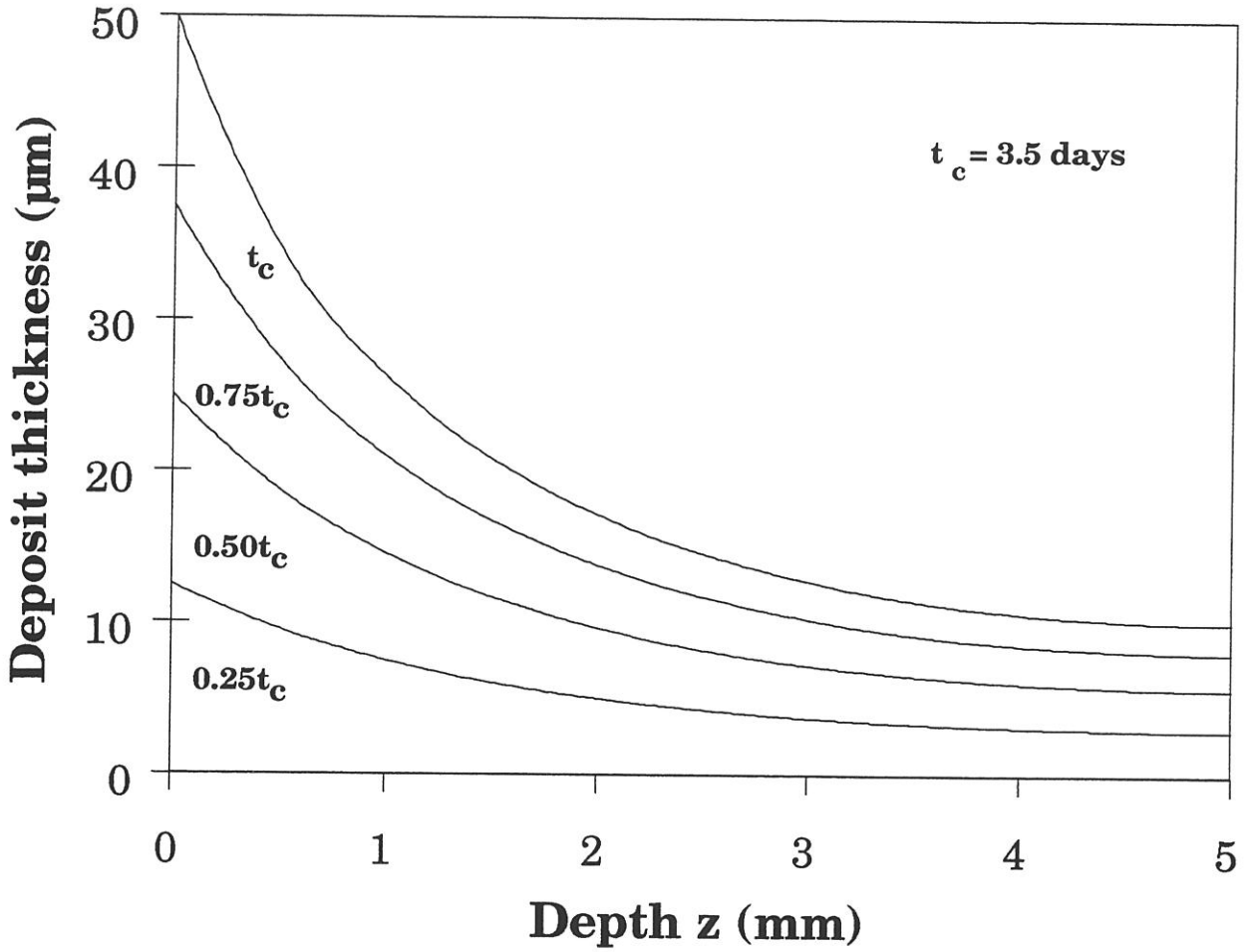

Fig. 18 : Calculated yttrium oxide thickness profiles along the pore for various infiltration times (from t = 0 to t = t_c) with T =1363 K, P = 4 kPa, Φ_0 = 100 µm, L = 10 mm, α_{H2} = 30, α_{CO2} = 10, α_{YCl3} = 1, α_{Ar} = 250, where α_i = [i]/[YCl_3] and [i] stands for concentration of the species i in the feed gas

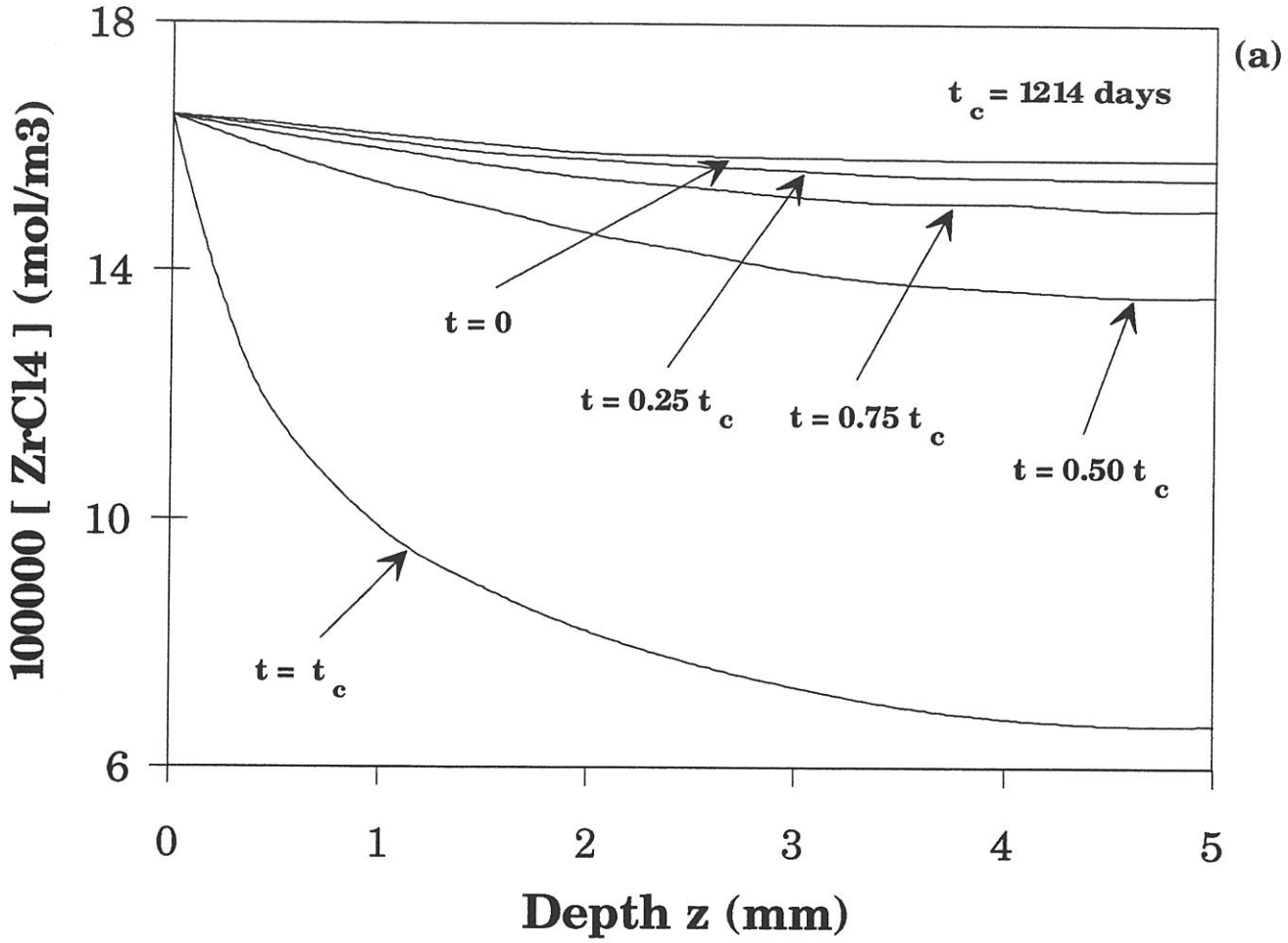

Fig. 19 : Concentration profiles of the gaseous species along the pore for zirconia infiltrations of increasing durations with T =1173 K, P = 2 kPa, Φ_0 = 100 µm, L/Φ_0 = 100, α_{H2} = 30, α_{CO2} = 10, α_{ZrCl4} = 1, α_{Ar} = 1200, where α_i = [i]/[$ZrCl_4$] and [i] stands for concentration of the species i in the feed gas
(a) $ZrCl_4$, (b) CO_2, (c) H_2, (d) CO, (e) HCl

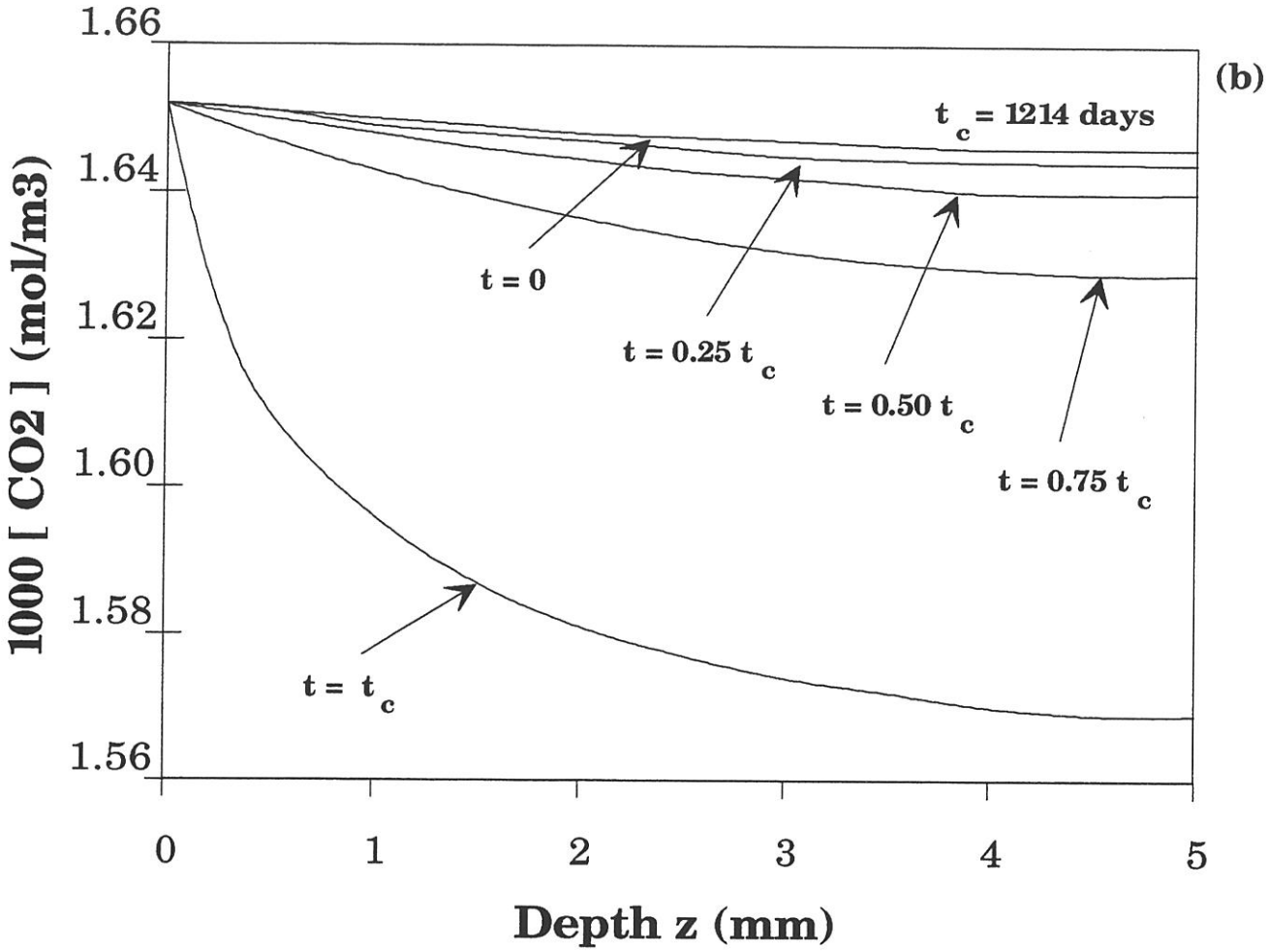

Fig. 19 : Concentration profiles of the gaseous species along the pore for zirconia infiltrations of increasing durations with T =1173 K, P = 2 kPa, Φ_0 = 100 µm, L/Φ_0 = 100, α_{H2} = 30, α_{CO2} = 10, α_{ZrCl4} = 1, α_{Ar} = 1200, where $\alpha_i = [i]/[ZrCl_4]$ and [i] stands for concentration of the species i in the feed gas
(a) $ZrCl_4$, (b) CO_2, (c) H_2, (d) CO, (e) HCl

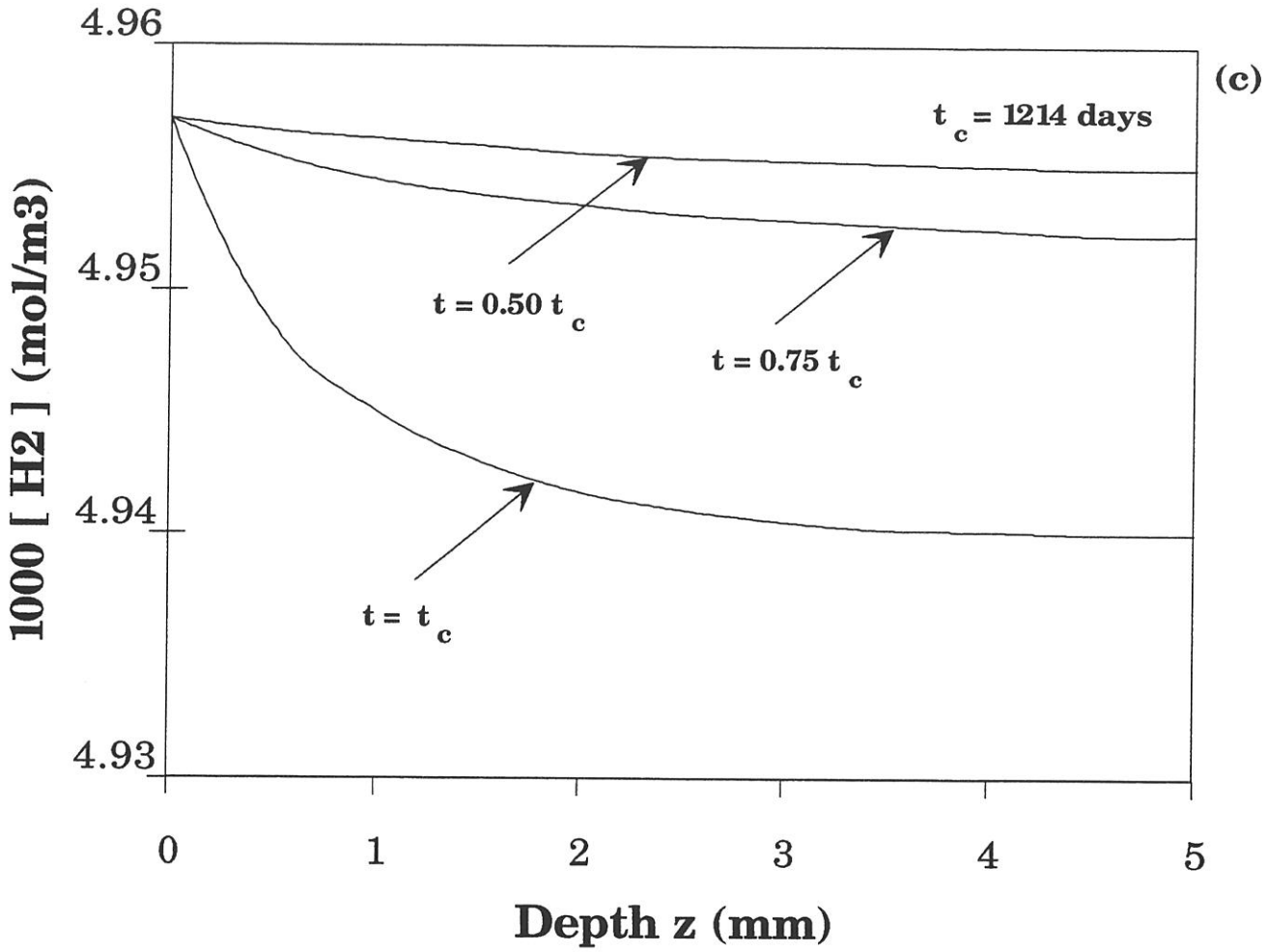

Fig. 19 : Concentration profiles of the gaseous species along the pore for zirconia infiltrations of increasing durations with T =1173 K, P = 2 kPa, Φ_0 = 100 µm, L/Φ_0 = 100, α_{H2} = 30, α_{CO2} = 10, α_{ZrCl4} = 1, α_{Ar} = 1200, where α_i = [i]/[$ZrCl_4$] and [i] stands for concentration of the species i in the feed gas
(a) $ZrCl_4$, (b) CO_2, (c) H_2, (d) CO, (e) HCl

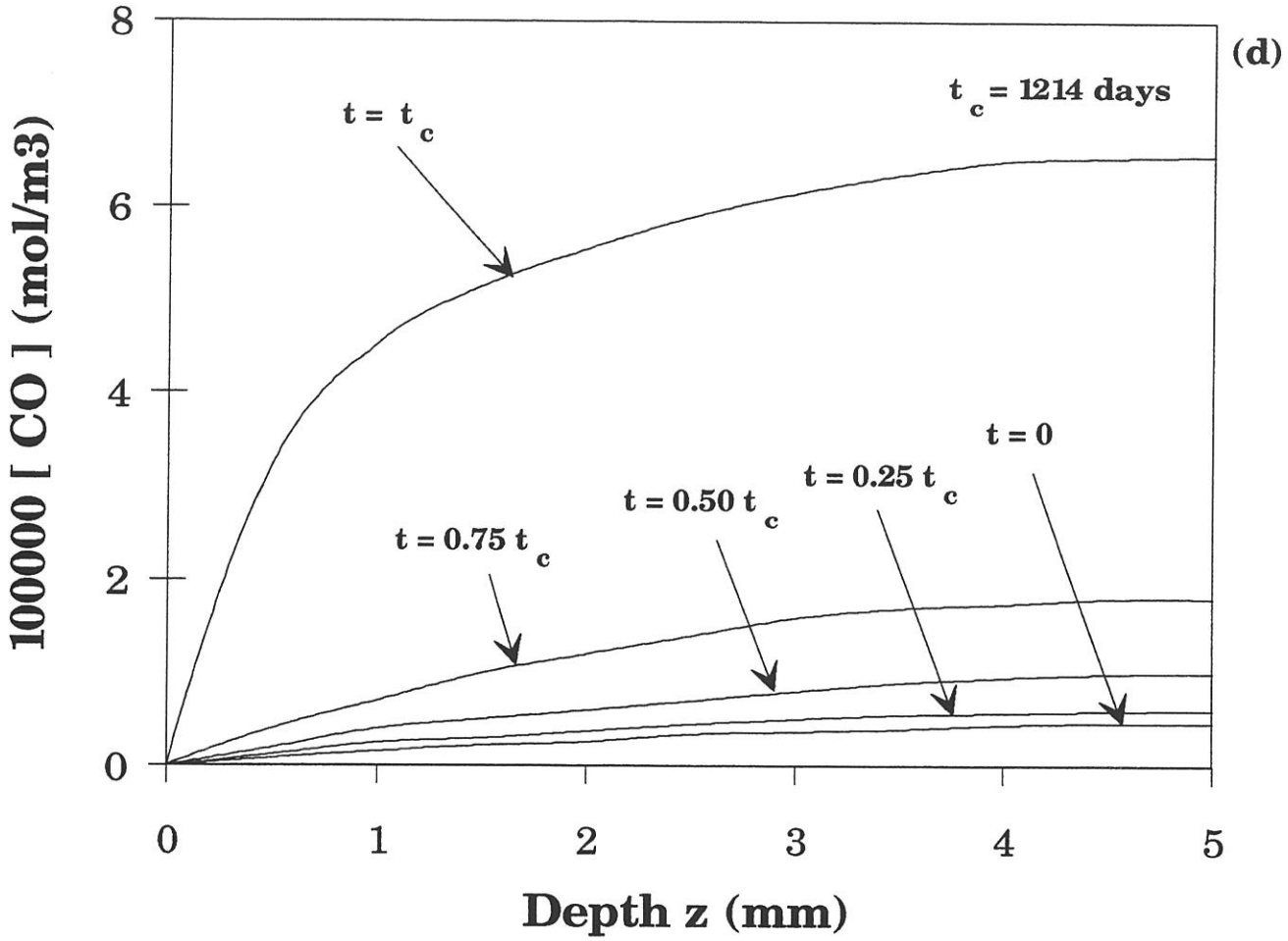

Fig. 19 : Concentration profiles of the gaseous species along the pore for zirconia infiltrations of increasing durations with T =1173 K, P = 2 kPa, Φ_0 = 100 µm, L/Φ_0 = 100, α_{H2} = 30, α_{CO2} = 10, α_{ZrCl4} = 1, α_{Ar} = 1200, where α_i = [i]/[$ZrCl_4$] and [i] stands for concentration of the species i in the feed gas
(a) $ZrCl_4$, (b) CO_2, (c) H_2, (d) CO, (e) HCl

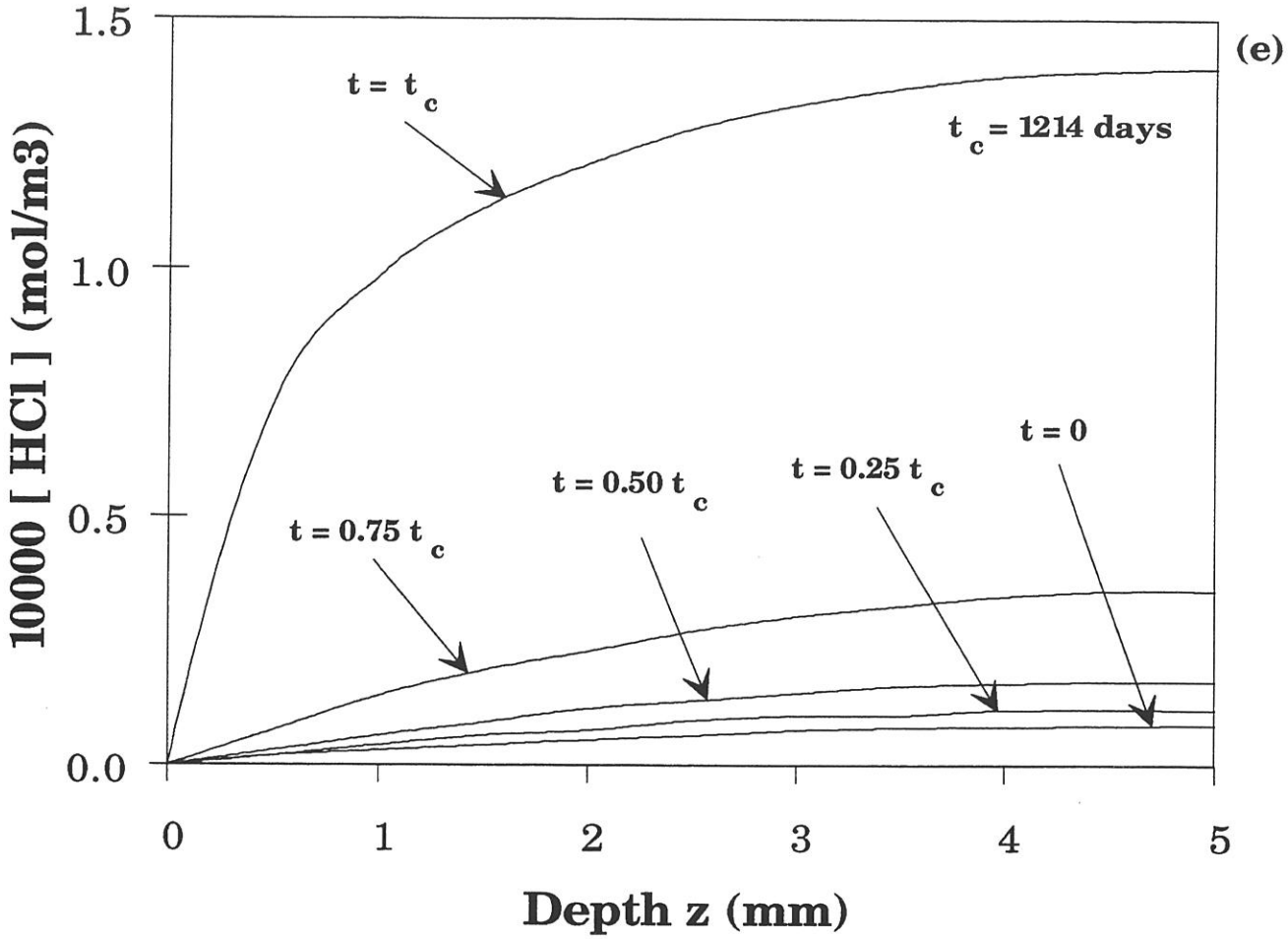

Fig. 19 : Concentration profiles of the gaseous species along the pore for zirconia infiltrations of increasing durations with T =1173 K, P = 2 kPa, Φ_0 = 100 µm, L/Φ_0 = 100, α_{H2} = 30, α_{CO2} = 10, α_{ZrCl4} = 1, α_{Ar} = 1200, where α_i = [i]/[$ZrCl_4$] and [i] stands for concentration of the species i in the feed gas
(a) $ZrCl_4$, (b) CO_2, (c) H_2, (d) CO, (e) HCl

Fitzer and D. Hegen [32] studied the thickness profiles of SiC deposited from CH_3SiCl_3-H_2 in holes drilled in graphite substrates (whose diameter ranged from 400 to 1000 µm and aspect ratio limited to a few tens). They also considered model pores, much smaller in diameter (i.e. with $1 < \Phi_0 < 20$ µm), present in sintered ceramics [32]. More recently, Fedou et al. used model straight cylindrical pores obtained after oxidizing the carbon core of SiC-CVD filaments(1) (145 µm in overall diameter). The advantage of this last model pore lies in the fact that : (i) the pore geometry is well defined (i.e it is almost a perfect straight cylinder with a smooth inner surface and a length which can be easily varied), (ii) the pore diameter, i.e about 34 µm, falls within the pore diameter spectrum of actual fiber preforms used for fabrication of many CMCs, (iii) this type of pore is well suited to the infiltration of SiC (no chemical or/and physical compatibility problems) [19]. In all cases, a rather good agreement between the calculated and measured thickness profiles were reported. Finally and as far as we know, no similar experiments have been performed for oxide infiltration.

4.1 - Experimental procedure

An experimental procedure similar to that reported by Fedou et al. for the SiC-thickness profiles was used here [19]. Segments of SiC-CVD filaments (145 µm in diameter and whose carbon core has a diameter of 34 µm), 10 mm in length, were submitted to an oxidation treatment at 800°C in air, in order to consume all the carbon core. This treatment yields model pores with an inner diameter of 34 µm and an aspect ratio L/Φ_0 of about 300. Several of these model pores were attached, parallel to each other, on two untreated filaments with a high temperature cement, as shown in fig. 20. The whole assembly was set on a pedestral in the isothermal zone of the CVD-apparatus which has been used by Sipp et al. to work out the kinetic laws related to the deposition of zirconia from $ZrCl_4$-CO_2-H_2-Ar mixtures [22]. Several CVI-experiments were performed under various conditions.

When a high enough amount of zirconia has been deposited, the model pores and their coating of zirconia were separated from the holder, embedded in an epoxy resin and polished (fig. 20). The thickness of in-pore zirconia deposit was measured along the pore axis (the origin of the abscissa being taken at one of the filament ends) directly on the micrograph.

(1) SCS-2 filaments from AVCO

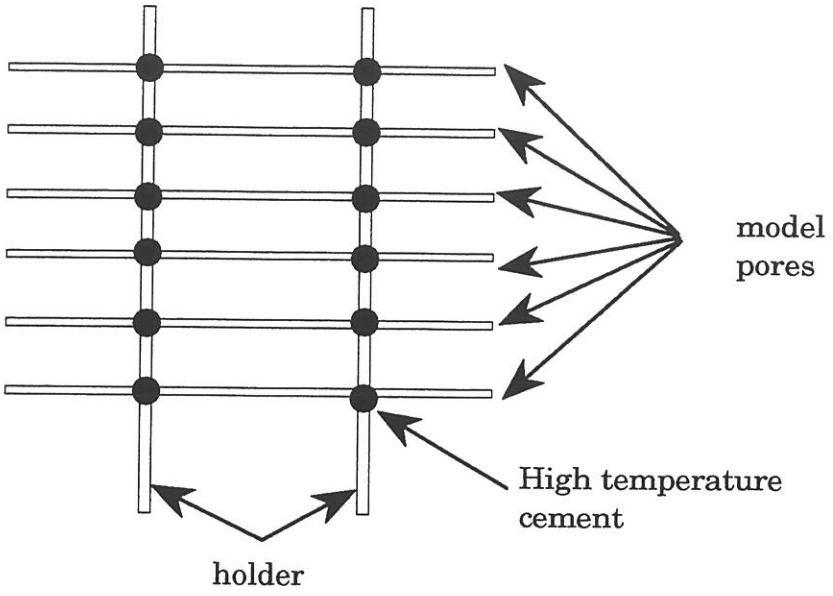

(a)

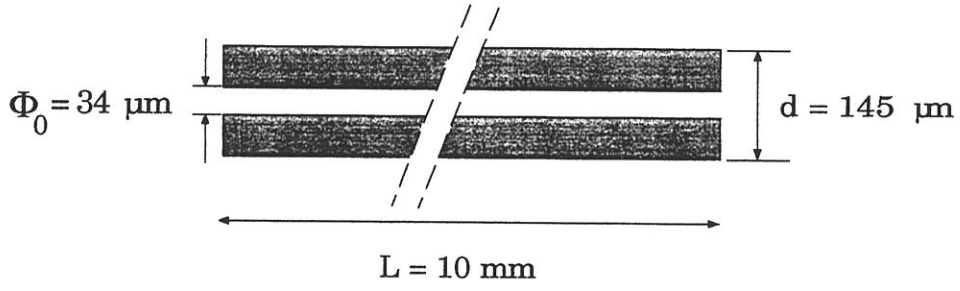

(b)

Fig. 20 : Experimental assessment of zirconia thickness profiles along a model straight cylindrical pore :

(a) model pore assembly
(b) pore geometry
(c) a model pore after zirconia CVI/CVD treatment,
(d) optical micrograph of a longitudinal section used to assess the ZrO_2 thickness profile

(c)

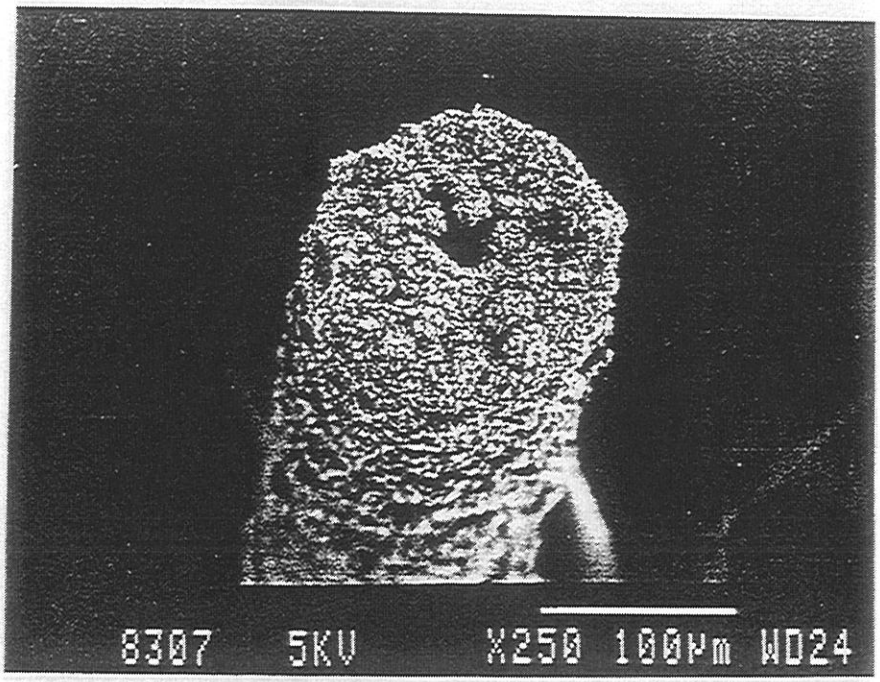

(d)

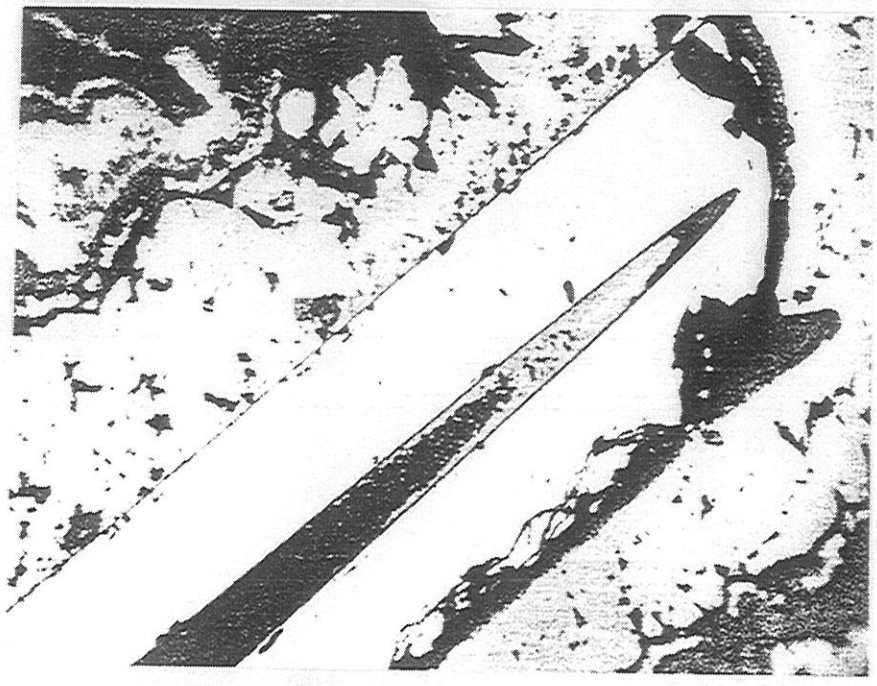

Fig. 20 : Experimental assessment of zirconia thickness profiles along a model straight cylindrical pore :

(a) model pore assembly
(b) pore geometry
(c) a model pore after zirconia CVI/CVD treatment,
(d) optical micrograph of a longitudinal section used to assess the ZrO_2 thickness profile

4.2- Preliminary results

A few infiltration experiments were performed under the following infiltration conditions : T = 1183 K; P = 2 kPa; Q_{ZrCl4} = 2 sccm ; Q_{CO2} = 20 sccm ; Q_{H2} = 60 sccm and Q_{Ar} = 240 sccm (i.e α_{CO2} = 10; α_{H2} = 30; α_{Ar} = 120) and t of the order of one hundred hours. The morphology of the pore after infiltration is shown in fig. 20c.

The pore entrance was observed to be sealed by the zirconia deposit, as predicted from the large infiltration duration with respect to the calculated value of t_c (respectively 100 hours and 8 hours). Moreover, no zirconia deposit was in the pore beyond a distance of about 400 µm from the pore initial entrance (a result in qualitative agreement with the high value of the model aspect ratio, i.e L/Φ_0 = 300). Finally, the zirconia deposit out or/and within the pore appears to be often rather porous probably due to the growth mechanism of zirconia (fig. 20 c-d).

Although the longitudinal polished sections were rarely perfectly diametral and parallel to the pore axis, the zirconia deposit thickness was tentatively measured for $0 < z < 400$ µm. the data are shown in fig.21.

4.3 - Discussion

From a comparison between the experimental and calculated profiles the following conclusions can be drawn :

(i) as predicted by the model, the preliminary experimental data show that there is a very steep gradient in the deposit thickness near the pore entrance, this gradient being steeper than the calculated gradient. The occurrence of such a steep gradient is obviously related to the high aspect ratio (i.e 300) which has been chosen for the model pore. The fact that the infiltration has been limited to 400 µm along the pore is also qualitatively consistent with the model. As shown in fig. 22, the diffusion of the reactants in the pore and that of the products out of the pore remain limited to the vicinity of the pore entrance whatever the infiltration time.

(ii) the fact that pore entrance is observed to be sealed by zirconia after a CVI experiment of about 100 hours is also consistent with the model since the value of the calculated critical time t_c is only of about 8 hours. Thus, the duration of the experiments (which were planned to yield sealed pores) could have been reduced.

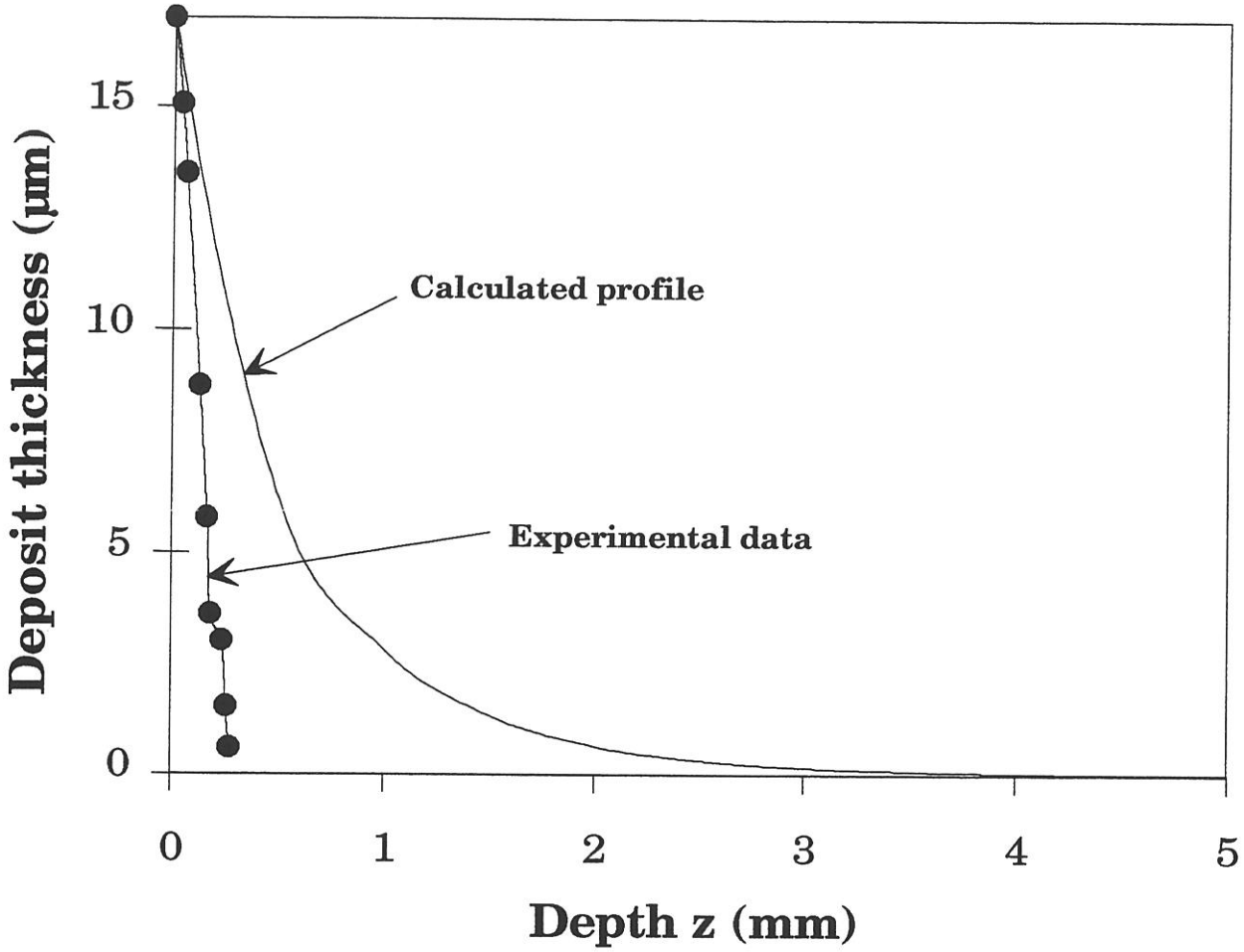

Fig. 21 : Calculated and measured zirconia thickness profiles along a pore model for T =1183 K, P = 2 kPa, Φ_0 = 34 µm, L = 10 mm, α_{H2} = 30, α_{CO2} = 10, α_{ZrCl4} = 1, α_{Ar} = 120, where $\alpha_i = Q_i/Q_{ZrCl4}$ and Q_i stands for flow rate of the species i in the feed gas

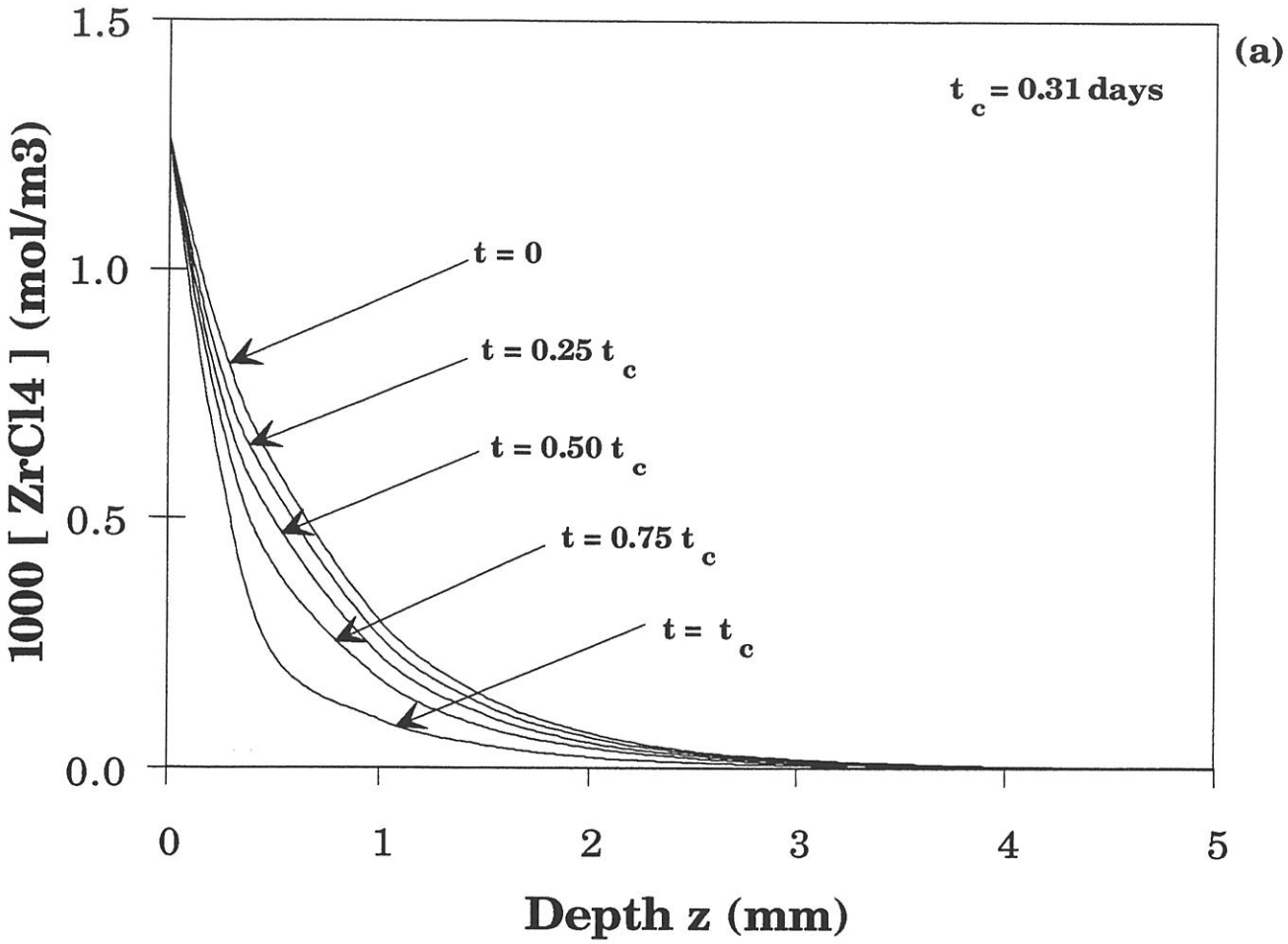

Fig. 22 : Concentration profiles of the gaseous species along the pore for zirconia infiltrations of increasing durations with T =1183 K, P = 2 kPa, Φ_0 = 100 µm, L/Φ_0 = 100, α_{H2} = 30, α_{CO2} = 10, α_{ZrCl4} = 1, α_{Ar} = 120, where α_i = [i]/[$ZrCl_4$] and [i] stands for concentration of the species i in the feed gas
(a) $ZrCl_4$, (b) CO_2, (c) H_2, (d) CO, (e) HCl

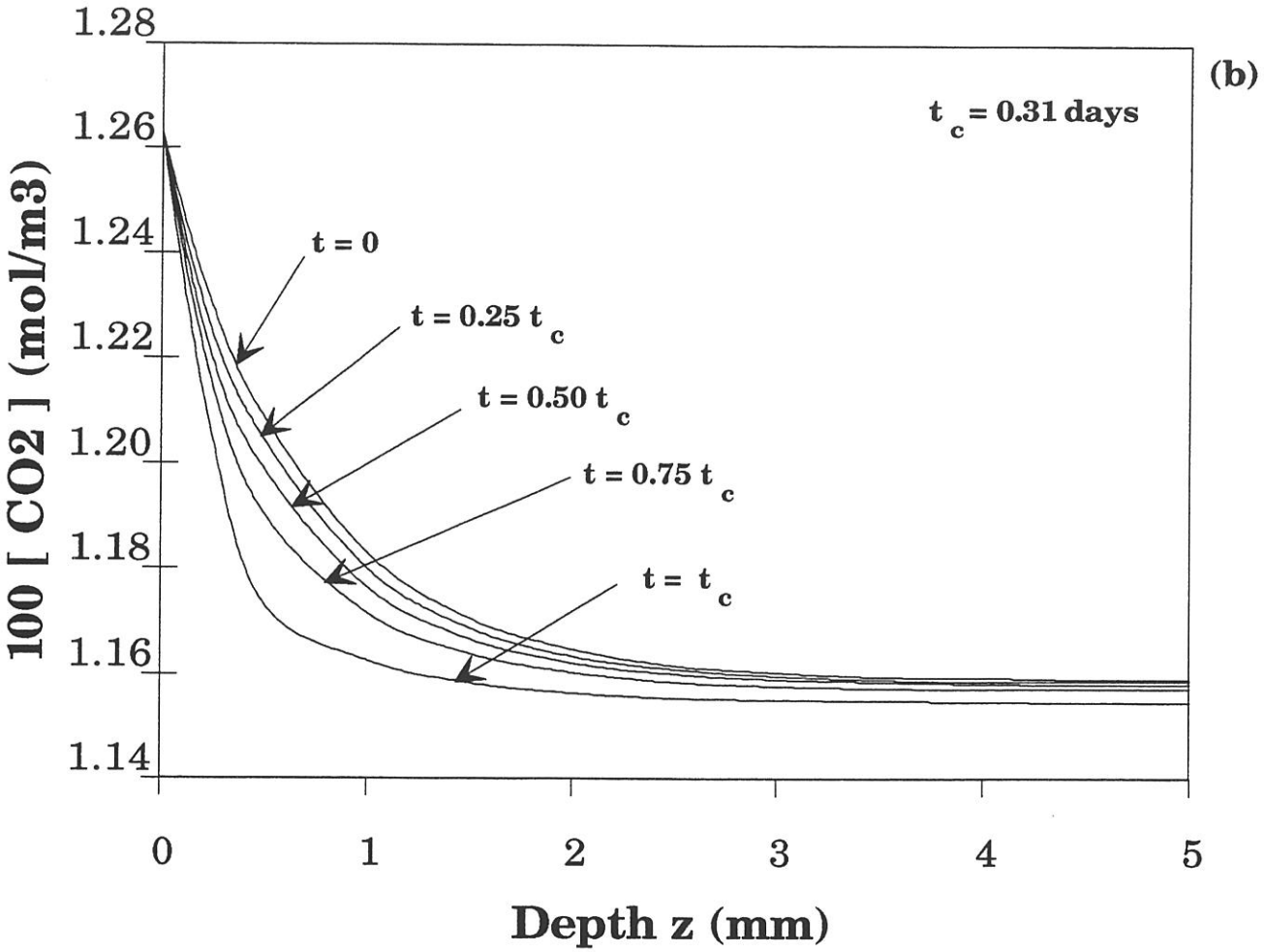

Fig. 22 : Concentration profiles of the gaseous species along the pore for zirconia infiltrations of increasing durations with T =1183 K, P = 2 kPa, Φ_0 = 100 µm, L/Φ_0 = 100, α_{H2} = 30, α_{CO2} = 10, α_{ZrCl4} = 1, α_{Ar} = 120, where α_i = [i]/[$ZrCl_4$] and [i] stands for concentration of the species i in the feed gas
(a) $ZrCl_4$, (b) CO_2, (c) H_2, (d) CO, (e) HCl

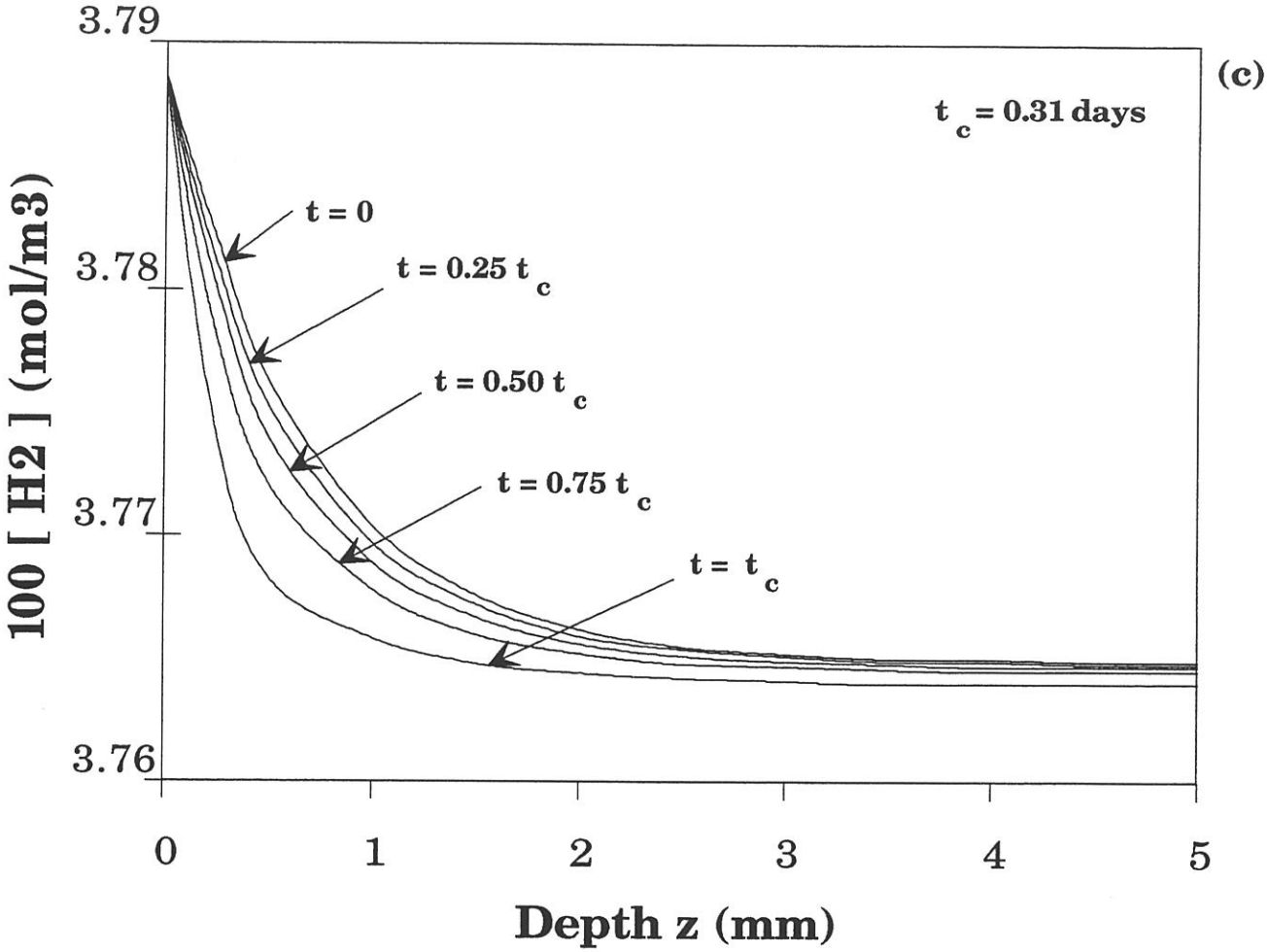

Fig. 22 : Concentration profiles of the gaseous species along the pore for zirconia infiltrations of increasing durations with T =1183 K, P = 2 kPa, Φ_0 = 100 µm, L/Φ_0 = 100, α_{H2} = 30, α_{CO2} = 10, α_{ZrCl4} = 1, α_{Ar} = 120, where α_i = [i]/[$ZrCl_4$] and [i] stands for concentration of the species i in the feed gas
(a) $ZrCl_4$, (b) CO_2, (c) H_2, (d) CO, (e) HCl

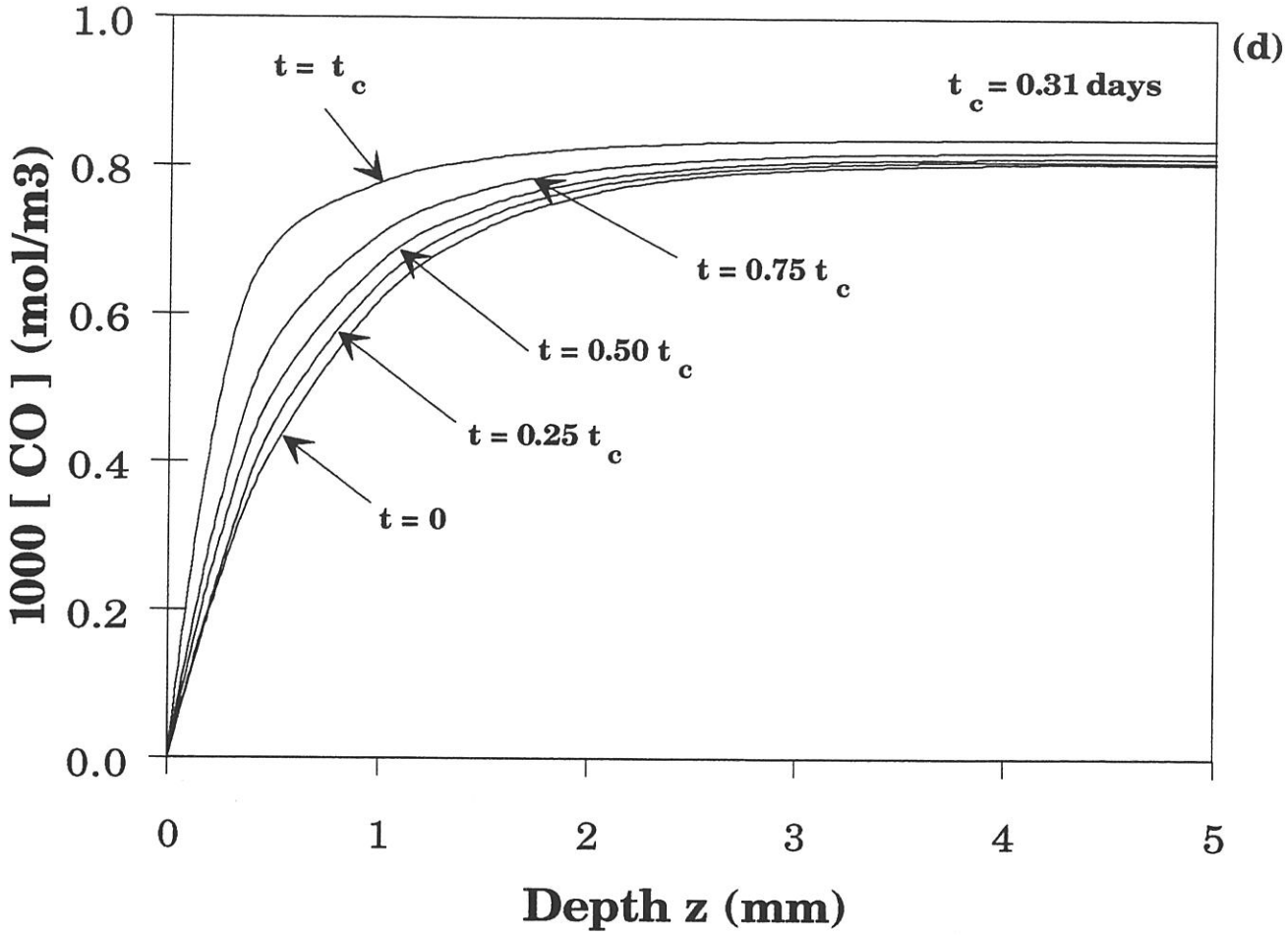

Fig. 22 : Concentration profiles of the gaseous species along the pore for zirconia infiltrations of increasing durations with T =1183 K, P = 2 kPa, Φ_0 = 100 µm, L/Φ_0 = 100, α_{H2} = 30, α_{CO2} = 10, α_{ZrCl4} = 1, α_{Ar} = 120, where α_i = [i]/[$ZrCl_4$] and [i] stands for concentration of the species i in the feed gas
(a) $ZrCl_4$, (b) CO_2, (c) H_2, (d) CO, (e) HCl

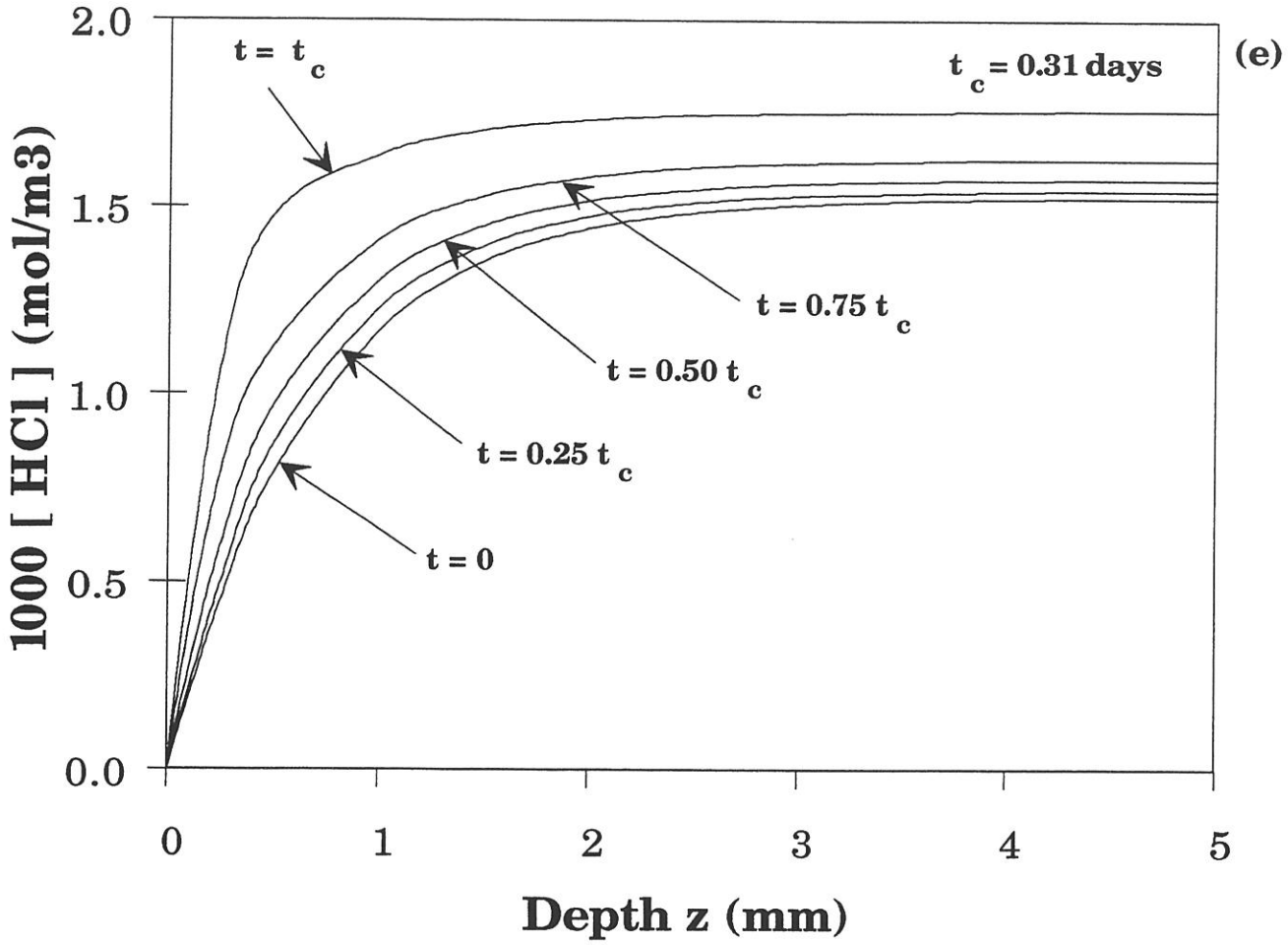

Fig. 22 : Concentration profiles of the gaseous species along the pore for zirconia infiltrations of increasing durations with T =1183 K, P = 2 kPa, Φ_0 = 100 µm, L/Φ_0 = 100, α_{H2} = 30, α_{CO2} = 10, α_{ZrCl4} = 1, α_{Ar} = 120, where α_i = [i]/[$ZrCl_4$] and [i] stands for concentration of the species i in the feed gas
(a) $ZrCl_4$, (b) CO_2, (c) H_2, (d) CO, (e) HCl

(iii) from a quantitative point of view, the main disagreement between the calculated and experimental profiles lies in the fact that the latter is steeper and remains almost linear. This disagreement may be, at least partly, related to the experimental procedure (see the micrograph shown in fig 20d) which could be improved because : (i) the polished section is not parallel to the revolution axis of the pore, involving errors in the experimental deposit thickness determination, (ii) the internal deposit is not dense, so the true density of the deposit is lower than the theorietical one, introduced in the model, and (iii) during the polishing, the internal zirconia deposit could be pulled out.

On the basis of the limited amount of experimental data presently obtained and of their limited accuracy, it seems too early to conclude whether or not the model (in its equations or/and numerical input data) will have to be modified. Nevertheless, it can be noticed that a validation of the model is proposed elsewhere in the case of SiC infiltration from CH_3SiCl_3-H_2 mixture [33] and carbon infiltration from C_3H_8 [34].

In the actual fiber preforms which have been used, e.g by Minet et al., to prepare zirconia-matrix composites according to the same CVI-process, less severe pore aspect ratios should be present since these authors have reported high volume fractions of infiltrated matrix and in some cases rather low residual porosities [21]. These features, apparently contradictory, could be explained by the fact that : (i) the pores in the actual preforms are highly interconnected and (ii) the pore spectrum consists of a variety of diameters, including pores of very large diameters (i.e 100 µm and more) even if the mean diameter is close to the diameter of the pore considered here.

More experiments on model porous substrates will be obviously necessary to validate properly the model or the data presented here, for zirconia infiltration. However, it is at least expected to be a useful tool for a better understanding of the phenomena involved in the CVI treatment of porous fiber bodies.

5 - CONCLUSION

A modelling of the infiltration of two oxides (zirconia and yttria) along a straight cylindrical pore (respectively from $ZrCl_4$-CO_2-H_2-Ar and YCl_3-CO_2-H_2-Ar mixtures), based on accurately established kinetic laws, has been used to calculate the profiles of gaseous species concentrations and deposit thickness along the pore axis for various infiltration times, pore aspect ratio and feed gas compositions, with the following main

conclusions :

(i) - the parameters whose effect on infiltration profiles of both oxides is the most important are : total pressure, dilution ratio of the reactants with argon, hydrogen partial pressure and pore aspect ratio. In the particular case of yttrium infiltration, the temperature and the YCl_3 partial pressure have such a great influence on the thickness profiles. When the dilution ratio of reactants with argon is decreased or when any other aboved-mentionned parameter is increased, the infiltration profiles move from rather flat curves (homogeneous infiltration) to curves which exhibit steep gradients near pore entrance (infiltration limited to the vicinity of the pore entrance),

(ii) - conversely, CO_2 partial pressure for both oxides, temperature and partial pressure of $ZrCl_4$ for zirconia have much lower effect on the infiltration profiles.

(iii) - for a given set of CVI-parameters, the deposit thickness profiles becomes steeper in the vicinity of the pore entrance, as time is increased giving rise to a **bottle neck phenomenon**. Finally, for a large enough time, refered to as a critical time t_c, the pore entrance becomes sealed by the deposit. The values of t_c depend on the CVI-parameters : it is very long (i.e several hundreds of days) for conditions yielding almost perfect homogeneous infiltration but very short (i.e a few hours) in the other case.

A few preliminary experiments were performed with zirconia infiltration of model straight cylindrical pores with a high aspect ratio (Φ_0 = 34 µm, L = 10 mm), in order to validate the model. Although some important features of the infiltration of zirconia predicted by the model were verified, it appears that more experiments, which could be performed on pores with lower aspect ratios, would be necessary.

ACKNOWLEDGEMENTS

The authors acknowledge the support that they received from Société Européenne de Propulsion (SEP) through a grant to E.S. and from both SEP and the French Ministery of Research through a grant to R.F.

APPENDIX 1 : Model for the ICVI of a straight cylindrical pore : Basic Equations [33]

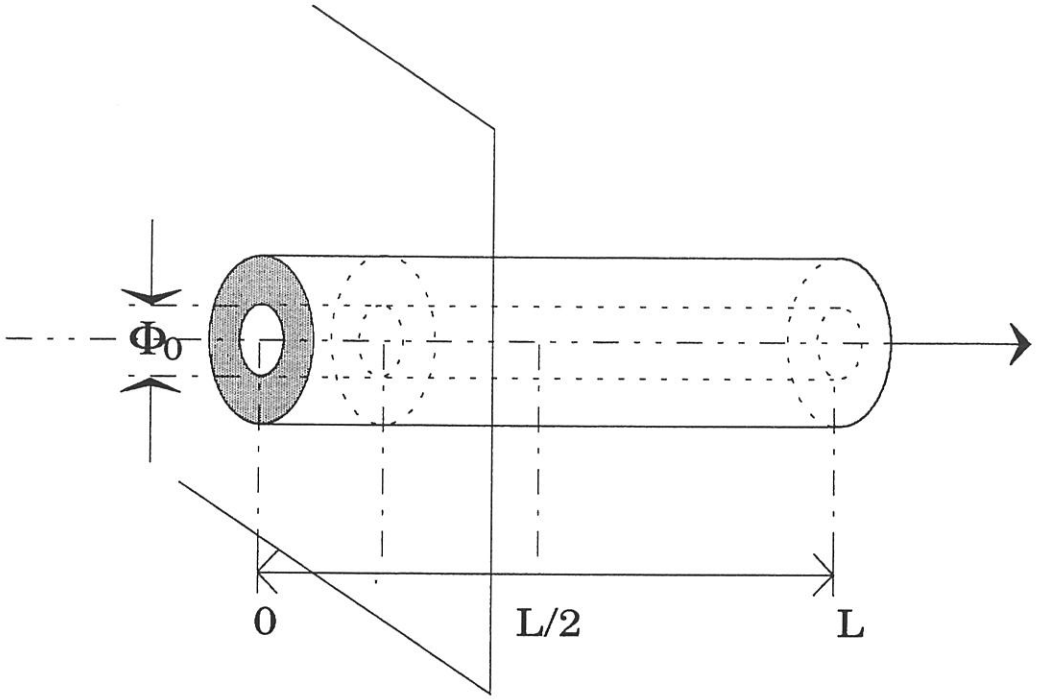

*** at steady state :**

$$D_i \frac{\partial^2 C_i}{\partial z^2} - \frac{\partial (x_i N)}{\partial z} + \frac{4 \nu_i \vartheta}{\Phi} = 0 \qquad (A1)$$

$$\frac{\partial \Phi}{\partial t} = -2 V_s \vartheta \qquad (A2)$$

$$\frac{1}{D_i} = \frac{1}{D_{i,F}} + \frac{1}{D_{i,K}} \qquad (A3)$$

$$\frac{1-x_i}{D_{i,F}} = \sum_{\substack{j=1 \\ j<>i}}^{n_g} \frac{x_j}{D_{i,j}} \qquad (A4)$$

*** boundary conditions :**

at z = L/2 (pore center)

$$\left[\frac{\partial C_i}{\partial z} \right]_{z=L/2} = 0 \qquad (A5)$$

$$\left[\sum_{i=1}^{n_g} N_i \right]_{z=L/2} = 0 \qquad (A6)$$

at z = 0 (pore entrance)

$$C_i(0,t) = C_{i,0} \qquad (A7)$$

APPENDIX 2 : Assessment of collision diameter and Lennard-Jones reduced energy of $ZrCl_4$ and YCl_3.

For almost all the usual gases, the collision diameter σ (in 10^{-10}m) and the Lennard-Jones energy ε (in J) can be found in the literature. For H_2, CO_2, CO and Ar the data are taken from [25]. In the case of zirconium chloride and yttrium chloride, these data are not available. Therefore, they must be assessed by several methods proposed in [32].

Assessment of $ZrCl_4$ data

a) σ estimation

The σ value can be estimated in using $SnCl_4$ data. The collision diameters of Zr and Sn can be deduced from their molar volumes at the melting point by the equation :

$$\sigma = V_{m,sol}^{1/3} \qquad \text{(A8)}$$

where $V_{m,sol}$ is the molar volume of the solid at its melting point (in $cm^3.mol^{-1}$).

For these solids, $V_{m,sol}(Zr) = 14\ cm^3.mol^{-1}$, whence $\sigma(Zr) = 2.95\ 10^{-10}$m, and $V_{m,sol}(Sn) = 16.26\ cm^3.mol^{-1}$, whence $\sigma(Sn) = 3.10\ 10^{-10}$m. The procedure consists in calculating the parameter k :

$$k = \frac{\sigma(SnCl_4)}{\sigma(Sn) + \sigma(Cl)} \qquad \text{(A9)}$$

Knowing that $\sigma(SnCl_4) = 6.202\ 10^{-10}$m and $\sigma(Cl) = 3.613\ 10^{-10}$m, the parameter k is equal to 0.924. The collision diameter of $ZrCl_4$ is then given by :

$$\sigma(ZrCl_4) = k[\ \sigma(Zr) + \sigma(Cl)\ ] = 6.06\ 10^{-10}\text{m}. \qquad \text{(A10)}$$

Another procedure uses the equation :

$$\sigma = 1.166 V_{b,liq}^{1/3} \qquad \text{(A11)}$$

where $V_{b,liq}$ is the molar volume of the liquid at its boiling point (in $cm^3.mol^{-1}$).

Approximating $V_{b,liq}$ to M/d_{liq} = 151 $cm^3.mol^{-1}$ (with M : molar mass and d_{liq} voluminal mass of the liquid), $\sigma(ZrCl_4)$ = 6.21 10^{-10}m is found. Values obtained by both methods are very close. Taking the mean value :

$$\sigma(ZrCl_4) = 6.10\ 10^{-10}\text{m}$$

b) ε/k estimation

Following the equation :

$$\varepsilon/k = 1.92\ T_{mp} \qquad \text{(A12)}$$

where T_{mp} is the melting point (in K)
k : Boltmann constant (1.38 10^{-23} $J.K^{-1}$)

In the case of $ZrCl_4$, T_{mp} = 710 K, so

$$\varepsilon/k(ZrCl_4) = 1363.2\ \text{K}$$

Assessment of YCl_3 data

a) σ estimation

In using the equation (A11), the voluminal mass of YCl_3 liquid at the boiling point (d_{bp} = 2.12 $g.cm^{-3}$) and M = 195.26 $g.mol^{-3}$:

$$\sigma(YCl_3) = 5.269\ 10^{-10}m$$

b) ε/k estimation

Following the equation :

$$\varepsilon/k = 1.15\ T_{mp} \qquad \text{(A13)}$$

where T_{mp} is the boiling point (in K)
k : Boltmann constant ($1.38\ 10^{-23}\ J.K^{-1}$),
it is found :

$$\varepsilon/k(YCl_3) = 2047\ K$$

REFERENCES

[1] F. Christin, R. Naslain, C. Bernard, "A Thermodynamic and Experimental Approach of Silicon Carbide-CVD Application to the CVD Infiltration of Porous Carbon-Carbon Composites", Proc. 7th Int. Conf. CVD, Los Angeles, USA (1979), (T.O. Sedgwick et al., eds.), The Electrochem. Soc., Princeton, pp. 499-514, 1979

[2] J.Y. Rossignol, R. Naslain, P. Hagenmuller, L. Heraud, "New Composite Materials with a Carbon-Titanium Carbide Hybrid Matrix for High Temperature Applications", ICCM IV, Tokyo, Japan (1982), (T. Hayashi et al., eds.), pp. 1227- 1237, 1982

[3] H. Hannache, F. Langlais, R. Naslain, "Kinetics of Boron Carbide Chemical Vapor Deposition and Infiltration", Proc. 5th European Conf. CVD, Uppsala, Sweden (1985), (J.O. Carlsson et al., eds.), Upssala Univ. Press, pp. 219-233, 1985

[4] H. Hannache, R. Naslain, C. Bernard, "Boron Nitride Chemical Vapor Infiltration of Fibrous Materials from BCl_3-NH_3-H_2 or BF_3-NH_3 Mixtures : a Thermodynamic and Experimental Approach", J. Less-Common Met., Vol. 95, pp. 221-246, 1983

[5] R. Colmet, R. Naslain, P. Hagenmuller, C. Bernard, "Thermodynamic and Experimental Analysis of Chemical Vapor Deposition of Alumina from $AlCl_3$- H_2-CO_2 Gas Phase Mixtures", J. Electrochem. Soc., Vol. 129, N° 6, pp. 1367- 1372, 1982

[6] J. Minet, F. Langlais, R. Naslain, "On the Chemical Vapor Deposition of Zirconia from $ZrCl_4$-H_2-CO_2-Ar Gas Mixture : II An Experimental Approach", J. Less-Common Met., Vol. 132, pp. 273-287, 1987

[7] T. M. Bessmann, R.A. Lowden, D.P. Stinton, T.L. Starr, "A Method for Rapid Chemical Vapor Infiltration of Ceramic Composites", Proc. 7th European Conf. CVD, Perpignan, France (1989), (M. Ducarroir et al., eds.), Colloque de Physique, Les Editions de Physique, Colloque C5, Suppl. N° 5, Vol 50, pp. 229-239, 1989

[8] E. W. Thiele, "Relation Between Catalytic Activity and Size of Particle", Ind. Eng. Chem., Vol. 31, N° 7, pp. 916-920, 1939

[9] E.E. Petersen, "Reaction of Porous Solid", AIChE Journal, Vol. 3, N° 4, pp. 443-448, 1957

[10] E. Fitzer and R. Gadow, "Fiber-Reinforced Silicon Carbide", Am. Ceram. Soc. Bull., Vol. 65, pp. 326-335, 1986

[11] C. H. J. Van Den Brekel, R. M. M. Fonville, P. J. M. Van Der Straten, G. Verspui, "CVD of Ni, TiN and TiC on Complex Shapes", Proc. 8th Int. Conf. CVD, Paris, France (1984), (Mc D. Robinson et al., eds.), The Electrochem. Soc., Pennington, pp. 142-156, 1984

[12] J. Y. Rossignol, F. Langlais, R. Naslain, "A Tentative of Modelization of Titanium Carbide CVI within the Pore Network of Two-Dimensional Carbon-Carbon Composites Preforms", Proc. 9th Int. Conf. CVD, Cincinnati, USA (1984), (J. M. Blocher et al., eds.), The Electrochem. Soc., Pennington, pp. 596-914, 1984

[13] M. F. Carolan, J. N. Michaels, "Chemical Vapor Deposition of Yttria Stabilized Zirconia on Porous Supports", Solid State Ionics, Vol. 25, pp. 207-216, 1987

[14] Y. S. Lin, K. J. De Vries, A. J. Burggraaf, "CVD Modification of Ceramic Membranes: Simulation and Preliminary Results", Proc. 7th European Conf. CVD, Perpignan, France (1989), (M. Ducarroir et al., eds.), Colloque de Physique, Les Editions de Physique, Colloque C5, Suppl. N° 5, Vol. 50, pp. 861-872, 1989

[15] T. L. Starr, "Modeling of Forced Flow/Thermal Gradient CVI", Proc. Int. Conf. on Wiskers-and-Fiber-Toughened Ceramics, Oak Ridge, USA (1988), (R. A. Bradley et al., eds), ASM International, Oak Ridge, pp. 243-252, 1988

[16] S. M. Gupte, J. A. Tsamopoulos, "Densification of Porous Materials by Chemical Vapor Infiltration", J. Electrochem. Soc., Vol. 136, N° 4, pp. 555-561, 1989

[17] N. H. Tai, T. W. Chou, "Analytical Modeling of Chemical Vapor infiltration in Fabrication of Ceramic Composites", J. Am. Ceram. Soc.,Vol. 72, N° 3, pp. 414-420, 1989

[18] S. Middleman, "The Interaction of Chemical Kinetics and Diffusion in the Dynamics of Chemical Vapor infiltration", J. Mater. Res. ,Vol. 4, N° 6, pp. 1515- 1524, 1989

[19] R. Fedou, F. Langlais, R. Naslain, "On the Modelling of the Chemical Vapor Infiltration of SiC-Based Ceramics in a Straight Cylindrical Pore", Proc. 11th Int. Conf. CVD, Seattle (1990), (K. E. Spear, C. W. Cullen, eds.), The Electrochem. Soc., Pennington, pp. 513-524, 1990

[20] G. Schoch, W. Fritz, R.E. Fitzer, Techn. Rept., EURAM Contract MAIE/0018/C, 1988

[21] J. Minet, F. Langlais, R. Naslain, "Chemical Vapor Infiltration of Zirconia within the Pore Network of Fibrous Ceramic Material from $ZrCl_4$-H_2-CO_2 Gas Mixtures", Composite Science and Technology, Special Issues on CMCs, Vol 37, pp. 79-107, 1990

[22] E. Sipp, F. Langlais, R. Naslain, "Kinetics of Deposition of Zirconia-based Ceramics from $ZrCl_4$-H_2-CO_2-Ar Gas Mixtures", High Performance Ceramic Films and Coatings, Proc. 7th CIMTEC- World Ceramic Congress, Montecatini Terme, Italy (1990), (P. Vincenzini, eds.), Elsevier, Amsterdam-Oxford-New-York-Tokyo, pp. 137-149, 1991

[23] R. Fédou, F. Langlais, R. Naslain, "A Modeling of the Isothermal/Isobaric Chemical Vapor Infiltration in a Straight Cylindrical Pore. Part. 1 Description of the Model", to be published

[24] J. L. Deschanvres, F. Cellier, G. Delabouglisse, "Thin Film of Ceramic Oxides by Modified CVD", Proc. 7th European Conf. CVD, Perpignan, France (1989), (M. Ducarroir et al., eds.), Colloque de Physique, Les Editions de Physique, Colloque C5, Suppl. N° 5, Vol. 50, pp. 695-705, 1989

[25] G. Wahl, S. Schosser, "Kinetic of Chlorination of Y and Zr and the Deposition of Y and Zr Oxides by Reaction of the Chlorides and Oxygen", Proc. 7th Int. Conf. CVD, Los Angeles, USA (1979), (T. O. Sedgwick and J. Watson, eds.), The Electrochem. Soc., Princeton, pp. 536-548, 1979

[26] K. Kamata, S. Matsumoto, Y. Shibata, "Yttrium (III) Oxide, Zirconium (IV) Oxide Films Prepared by Chemical Vapor Deposition", Yogyo Kyoskqi Shi, Vol. 90, pp. 46-47, 1982

[27] E. Sipp, "CVD/CVI de Céramiques à Base de Zircone Pure ou Stabilisée : Approche Thermodynamique et Expérimentale", Thesis N° 483, University of Bordeaux I, 1990

[28] J. O. Hirschfelder, R.B. Bird, E. L. Spotz, Chem. Revs., Vol. 44, pp. 205, 1949

[29] R. A. Svehla, NASA Tech. Rep. R-132, Lewis research Center, Cleveland (OHIO), 1962

[30] R. Naslain, F. Langlais, R. Fedou, "The CVI-Processing of Ceramic Matrix Composites", Proc. 7th European Conf. CVD, Perpignan, France (1989), (M. Ducarroir et al., eds.), Colloque de Physique, Les Editions de Physique, Colloque C5, Suppl. N° 5, Vol 50, pp. 191-207, 1989

[31] R. Naslain, F. Langlais, "CVD-Processing of Ceramic-Ceramic Composites Materials", Mater. Sci. Res., Vol. 20, pp. 145-164, 1986

[32] E. Fitzer, "Chemical Vapor Deposition - A Review of 25 Years Experience", Proc. 8th European Conf. CVD, Glasgow, Scotland (1991), (M.L. Hitchman, N.J. Archer., eds.), Journal de Physique IV, Les Editions de Physique, Colloque C2, N° 7, Suppl. Journal de Physique II, Vol 1, pp. 509-537, 1991

[33] R. Fédou, F. Langlais, R. Naslain, "A Modeling of the Isothermal/Isobaric Chemical Vapor Infiltration in a Straight Cylindrical Pore. Part. 2 Application to the CVI of SiC", to be published

[34] R. Fédou, P. Dupel, F. Langlais, R. Pailler, R. Naslain, "A Modeling of the Chemical Vapor Infiltration in a Straight Pore with a Rectangular Cross Section. Application to the CVI of Pyrocarbon ", to be published

[35] R. B. Bird, W. E. Stewart, E. N. Lightfoot, "Transport Phenomena", J. Wiley and Sons, eds., New York-Chichester-Brisbane-Toronto-Singapore, 1960

CHAPITRE 4

Titre : **A MODELING OF THE ISOTHERMAL ISOBARIC CHEMICAL VAPOR INFILTRATION IN A STRAIGHT PORE WITH A RECTANGULAR CROSS-SECTION - APPLICATION TO THE CVI OF PYROCARBON**

A MODELING OF THE ISOTHERMAL ISOBARIC CHEMICAL VAPOR INFILTRATION IN A STRAIGHT PORE WITH A RECTANGULAR CROSS-SECTION APPLICATION TO THE CVI OF PYROCARBON

R. FÉDOU, P. DUPEL, F. LANGLAIS(*), R. PAILLER and R. NASLAIN
Laboratoire des Composites Thermostructuraux (UMR 47 CNRS-SEP-UB1)
Domaine Universitaire 3, Allée La Boétie
33600 Pessac (France)

ABSTRACT : A modeling of the chemical vapor infiltration process in a straight pore with a rectangular cross-section, derived from a previously described model of the CVI in a straight cylindrical pore, is applied to the deposition of pyrocarbon from propane. This extension involves the same basic equations, the diameter of the cylindrical pore being replaced by the hydraulic diameter. A kinetic law with a first order with respect to C_3H_8 and an activation energy of 215 $kJ.mol^{-1}$is derived from preliminary kinetic study of the pyrocarbon CVD permits to state. The CVI model is validated by a good fit between the deposit thickness profiles along the pore calculated after adjustment of the kinetic data and experimental profiles measured for straight pores with various aspect ratios.

1 - INTRODUCTION

Carbon-carbon composite materials, consisting of carbon fibers embedded in a carbon matrix, are developed for their excellent thermomechanical properties. Their high fracture strength and stiffness, very low thermal expansion coefficient and good thermal shock and ablation resistance, have promoted their use for rocket nozzles and thermal shields of re-entry bodies. C-C composites are also used in brake disks owing to their excellent dynamic friction coefficient and medical prosthetic devices for their biocompatibility [1].

The matrix of these materials can be a coke when the fibrous substrate is impregnated by a liquid resin or a pitch, followed by a carbonization and a graphitization. It is a pyrocarbon when it is deposited by chemical vapor infiltration (CVI) from the

(*) to whom correspondence should be sent

thermal decomposition of a gaseous hydrocarbon. The second method yields C-C composites with a better quality (e.g. a density close to 2), but with a higher cost because the infiltration process when it is performed under isothermal/isobaric condition requires a long time, as previously reported for the CVI of various ceramic matrices : carbides (SiC, B_4C, TiC), nitrides (BN) or oxides (Al_2O_3, ZrO_2) [2-7].

Guidelines to decreasing the densification durations without degrading the quality of the composites, can be obtained by modeling the CVI process. Most of the already reported models provide a prediction of the deposit thickness profiles in a single straight cylindrical pore for given CVI conditions [8-18]. One of them, previously described in [19] and applied to SiC [20] and ZrO_2/Y_2O_3 [21], can be used for any chemical system with any kinetic law for the heterogeneous deposition reaction.

The purpose of the present contribution is to use the modeling proposed by Fédou et al. [19] for optimizing the process of pyrocarbon infiltration from C_3H_8. This contribution is not only an application of that model to a new chemical system, but it is also an extension of the model to a straight pore with a rectangular cross-section. This new pore geometry was chosen for practical reasons, i.e. in the experimental investigation, the thickness profiles can be more easily assessed along single axial section.

2 - THE MODEL

2.1 - Hypotheses

Before giving the consequences of a change in the pore geometry on the basic equations of the model which has been described in a detailed manner in [19], the stated assumptions will be recalled as follows :

(1) The pore is a straight open-ended pore with a length L, an initial rectangular cross-section (H_0 in height and W_0 in width). The gas phase composition is identical at both ends and constant during the infiltration process. The pore is supposed to remain symmetrical with respect to its center and thus the following study will be limited to one half of the pore (i.e. $0 \leq z \leq L/2$ where z is the axial coordinate defined as the distance from the nearest pore entrance).

(2) The infiltration is considered as a series of quasi-steady states, since mass transfers are very rapid with respect to the rate of variation of the pore geometry. The time origin ($t = 0$) is chosen as corresponding to the first mass transfer steady state.

(3) The whole pore is supposed to be isothermal during the infiltration process.

(4) No homogeneous reaction occurs within the pore.

(5) The concentrations of the gaseous species are constant in a cross-section of the pore. This hypothesis, which lowers the dimensionality of the problem (from 3D to 1D), can be justified by a large aspect ratio L/H_0 and the fact that the deposit thickness is the same on the four sides of the rectangular cross-section of the pore (H_0 = 320 µm and W_0 = 2 mm) (fig. 1). In the cylindrical pore, this homogeneity of thickness ca be explained by the symmetry with respect to the pore axis.

(6) The mass transfers of gaseous species within the pore are assumed to occur only by Fick and/or Knudsen diffusion, the forced convection phenomena being negligible in narrow pores. Nevertheless, the convection terms, which result from the mole number changes in the chemical reactions, are taken into account but can vanish when reactant species is highly diluted.

2.2 - Basic equations

For any time t and abscissa z, the cross-section of the pore is defined by its height H and its width W. According to hypothesis (5), the pore cross-section dimensions can be written :

$$W = W_0 - 2e \tag{1}$$

$$H = H_0 - 2e \tag{2}$$

where e is the deposit thickness. The geometry of the pore is totally defined by the constants H_0 , W_0 and by the function e (z, t) which represents the thickness profile for the time t.

As previously shown, the mass balance equations must be solved in order to describe the variations of the gas concentration and thickness profiles as a function of the experimental parameters [19]. The conservation equation for species i can be written in terms of molar flux :

$$\frac{\partial N_i}{\partial z} = \frac{\nu_i \vartheta \mathcal{P}}{\mathcal{A}} \tag{3}$$

where N_i is the absolute molar flux of species i (in $mol.m^{-2}s^{-1}$)

ν_i is the stoichiometric coefficient of species i in the heterogeneous reaction

(dimensionless)

ϑ is the rate of the heterogeneous reaction for the production of one mole of solid on a unit surface [22] (in mol. $m^{-2}s^{-1}$)

$\mathcal{P}$ is the perimeter of the pore cross-section (in m)

$\mathcal{A}$ is the area of the pore cross-section (in m^2)

For a cylindrical pore with a diameter $\Phi(z, t)$, equation (3) gives the following expression, reported in a previous paper [19] :

$$\frac{\partial N_i}{\partial z} = \frac{4 \nu_i \vartheta}{\Phi} \qquad (4)$$

For the pore with a rectangular cross-section, an equivalent diameter, referred to as the hydraulic diameter Φ_h, is defined by :

$$\Phi_h = \frac{4 \mathcal{A}}{\mathcal{P}} = \frac{2 W H}{W + H} \qquad (5)$$

By combining equations (3) and (5), a mass transfer equation similar to (4) is deduced :

$$\frac{\partial N_i}{\partial z} = \frac{4 \nu_i \vartheta}{\Phi_h} \qquad (6)$$

The variations versus time of the pore geometry can be expressed, as shown in appendix 1, by :

$$\frac{\partial B}{\partial t} = \frac{\partial W}{\partial t} = - 2 V_s \vartheta \qquad (7)$$

where V_s is the molar volume of the deposited solid (in $m^3\ mol^{-1}$).

In terms of deposit thickness, this equation becomes :

$$\frac{\partial e}{\partial t} = V_s \vartheta \qquad (8)$$

The various differential equations to be solved are given in appendix 2, together

with the boundary conditions according to hypotheses (1).

The mass conservation equations are solved by using an iterative procedure and a finite difference numerical method, the first calculation being carried out for the initial pore with a uniform cross-section (i.e. with e (z, 0) = 0). For each iteration, the concentration profiles of the various gas species C_i (z, t) and the thickness profiles e (z, t) are calculated and used in the following step. The computation of these profiles needs two kinds of data : the kinetic law of the deposition reaction and the diffusion coefficients of the various gas species.

2.3 - Data on the chemical system

2.3.1 - *The kinetic law*

The overall reaction which yields pyrocarbon deposit from propane as gaseous precursor, can be written as :

$$\frac{1}{3}\ C_3H_{8\,(g)} \longrightarrow C_{(s)} + \frac{4}{3}\ H_{2\,(g)} \qquad (9)$$

The chemical system considered in the present study includes both gaseous species C_3H_8 and H_2.

Under experimental conditions similar to those used for the pyrocarbon CVI experiments, a preliminary kinetic study was performed in order to deduce a deposition rate law to be compared to the data from the literature. The CVD/CVI apparatus is briefly described in appendix 3. The substrate was a graphite rectangular specimen 10 x 10 x 5 mm^3 in size. The growth rate was determined by measuring the deposit thickness on various sides of the substrate from optical micrographs. The flow rate was chosen high enough (200 sccm i.e. standard $cm^3\ mn^{-1}$) to favor a kinetic process controlled by the chemical reactions.

The apparent activation energy of the deposition process was determined by recording the logarithm of the growth rate as a function of the reciprocal temperature. For three values of the pressure (i.e. $P = P_{C3H8}$ = 0.8, 2.7 and 4.7 kPa) and temperatures ranging from 1300 to 1350 K, a linear plot (i.e. an Arrhenius type behavior) is observed (fig. 2), which means that the kinetic process is chemically controlled with an activation energy of 215 $kJ.mol^{-1}$. This value is higher than that obtained by Lee et al. for the same hydrocarbon precursor (172 $kJ.mol^{-1}$) [23] but rather close to those reported by

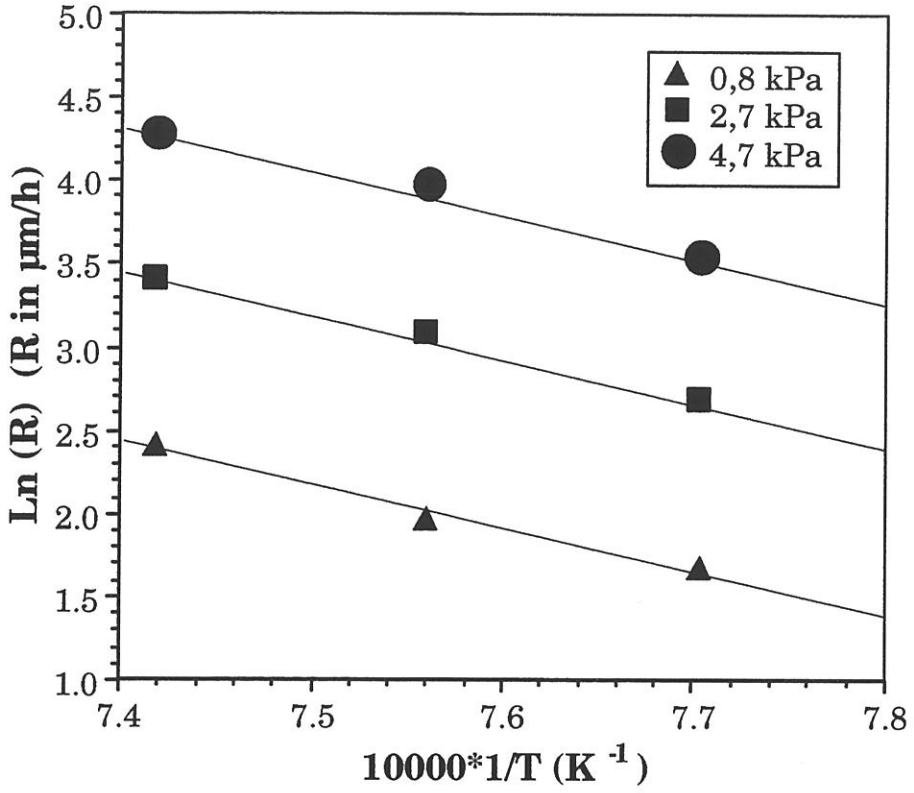

Fig. 2 : Arrhenius plots of the deposition rate of pyrocarbon for C_3H_8 a flow rate of 200 sccm and pressures of 0.8, 2.7 and 4.7 kPa.

Tesner for other precursors such as aromatics (230 $kJ.mol^{-1}$ for benzene, 243 for toluene, 239 for xylene, 222 for naphtalene and 218 for anthracene) [24]. According to several authors, the mechanisms of the pyrocarbon deposition involve very often intermediate species such as free radicals and/or aromatic molecules [24,25]. The present result could be explained on the basis of a kinetic process controlled by the chemical decomposition of aromatic intermediates.

The apparent reaction order with respect to the precursor species C_3H_8 was obtained by drawing the variations of the deposition rate versus pressure in a Ln-Ln plot. For three values of the temperature (1300, 1325 and 1350 K), these plots are almost linear and exhibit a slope very close to one (fig. 3). Such first order kinetics were previously found for several other saturated hydrocarbons (e.g. methane, ethane) or unsaturated ones (e.g. ethylene, propylene, benzene ...) [24].

On the basis of the experimental data, the following kinetic law can be proposed :

$$\frac{de}{dt} = k_{e0} \exp\left(-\frac{E_a}{\boldsymbol{R}T}\right) P \qquad (10)$$

where the growth rate is expressed in $\mu m.h^{-1}$
k_{eo} = 22 $\mu m.kPa^{-1}h^{-1}$
E_a = 215 $kJ.mol^{-1}$
$\boldsymbol{R}$ is the ideal gas constant (8.314 $J.mol^{-1}K^{-1}$)
P is the total pressure (in kPa).

2.3.2 - *The diffusion coefficients*

As shown in appendix 2, the effective diffusion coefficient D_i of a species i, is calculated by taking into account both Knudsen $D_{i,K}$ and Fick D_F diffusion coefficients (equation (A8)).

The Knudsen diffusion coefficient $D_{i,K}$ of a species i in a straight pore with a hydraulic diameter Φ_h can be calculated, according to the kinetic theory of gases, by :

$$D_{i,K} = \frac{\Phi_h}{3}\left[\frac{8\boldsymbol{R}T}{\pi M_i}\right]^{1/2} \qquad (11)$$

where M_i is the molar mass of species i (in $kg.mol^{-1}$).

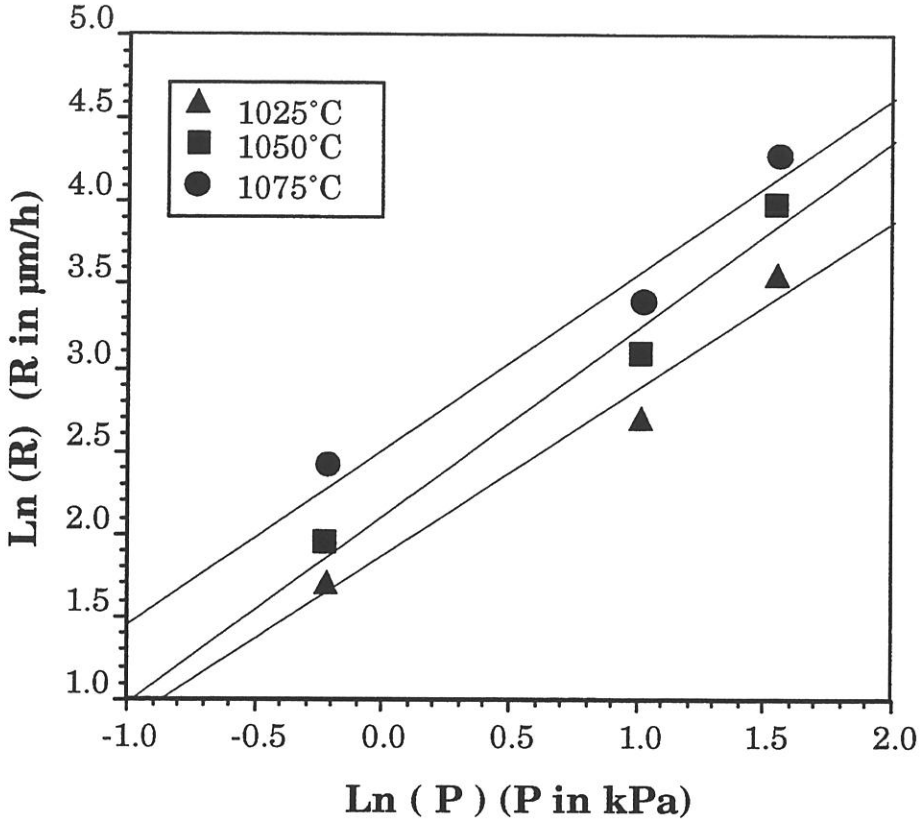

Fig. 3 : Variations of the deposition rate of pyrocarbon with C_3H_8 pressure in a Ln-Ln scale for a C_3H_8 flow rate of 200 sccm and temperatures of 1300, 1325 and 1350 K.

The equation (9) shows that H_2 is produced by the deposition reaction and consequently is present within the pore during the infiltration process, which involves a binary diffusion of propane through hydrogen. The Fick diffusion coefficient in a binary mixture does not depend on the mixture composition and can be derived from Hirschfelder expression :

$$D_{1,2} = 5.876\ 10^{-24} \frac{T^{3/2}}{P\ \sigma_{1,2}^{2}\ \Omega_D} \left[\frac{1}{M_1} + \frac{1}{M_2} \right]^{1/2} \qquad (12)$$

where $\sigma_{1,2}$ is the mean collision diameter (in m)

Ω_D is the Lennard-Jones collision integral (dimensionless)

$\sigma_{1,2}$ is calculated from

$$\sigma_{1,2} = \frac{\sigma_1 + \sigma_2}{2} \qquad (13)$$

Ω_D values can be obtained from Hirschfelder data [26] and $kT/\varepsilon_{1,2}$ values (where k is the Boltzman constant and $\varepsilon_{1,2}$ the maximum of attraction energy between both molecules) according to :

$$\frac{\varepsilon_{1,2}}{k} = \left[\frac{\varepsilon_1}{k} \cdot \frac{\varepsilon_2}{k} \right]^{1/2} \qquad (14)$$

For the present system (C_3H_8-H_2), the following data are used [27] :

σ_{C3H8} = 5.118 x 10^{-10} m

ε_{C3H8}/k = 273.1 K

σ_{H2} = 2.827 x 10^{-10} m

ε_{H2}/k = 59.7 K

3 - EXPERIMENTAL CVI STUDY

As shown in 2.2, the mass transfer equations to be solved are obtained by replacing the diameter Φ_0 of the cylindrical pore by the hydraulic diameter Φ_h of the pore with a rectangular cross-section. A first order kinetics of pyrocarbon deposition being assumed, the results previously reported for the CVI of SiC [20] are presently available. Similar influence of the various parameters (temperature, pressure and geometry of the pore)

on the infiltration profiles are found, with only shifts in the critical values of these parameters.

3.1 - Preparation of the model pores

Owing to the difficulty of preparing model pores with a well-controlled geometry and a high aspect ratio, and measuring accurately small deposit thicknesses, only a few papers have reported experimental profiles for ceramic obtained by CVI. The model cylindrical pores recently prepared by Fedou et al. exhibited a small diameter (i.e. Φ_0 = 34 µm, the diameter of the carbon core of the SCS SiC-CVD filaments), a rather high length (L ≈ 10 mm) and a smooth inner surface [20]. Conversely, the measurement of the deposit thickness along the pore (SEM observations on fracture sections operated at various levels) is not straightforward.

The presently used model pores are made from two plates placed side by side in order to form a substrate with the same shape than that of the substrate used in the CVD kinetic study (cf 2.3.1). The straight pores with rectangular cross-sections were obtained by machining grooves on one side of one plate. As shown in figure 4, each substrate includes three grooves with the same width (W_0 = 2 mm) and various depths (H_0 ≈ 60, 120 and 320 µm). The pore height is actually dependent on the tightening of both plates and the smoothness of their surface, which results in a possible error on H_0 of about 20 - 30 µm. Furthermore, the graphite exhibits some open microporosity. As a consequence, the three model pores are not rigorously independent, because an additional network of micropores occurs between them, whose volume fraction at the beginning of the infiltration is not negligible for the smallest model pore (i.e. that with H_0 ≈ 60 µm).

The practical interest of such pores is the easy assessement of the profiles of pyrocarbon deposit thickness by optical observations over the whole pore length, which needs only to cut axially the sample to embed it in a resin and to perform a conventional polishing.

3.2 - Experimental results - Discussion

Infiltration experiments were performed in the apparatus described in appendix 3 for a temperature T of 1323 K, various pressures (0.8 ≤ P ≤ 4.7 kPa) and flow rates (100 ≤ Q ≤ 400 sccm). A preliminary study shows that the pyrocarbon thickness profiles do not depend on the flow rate within the presently investigated range. This

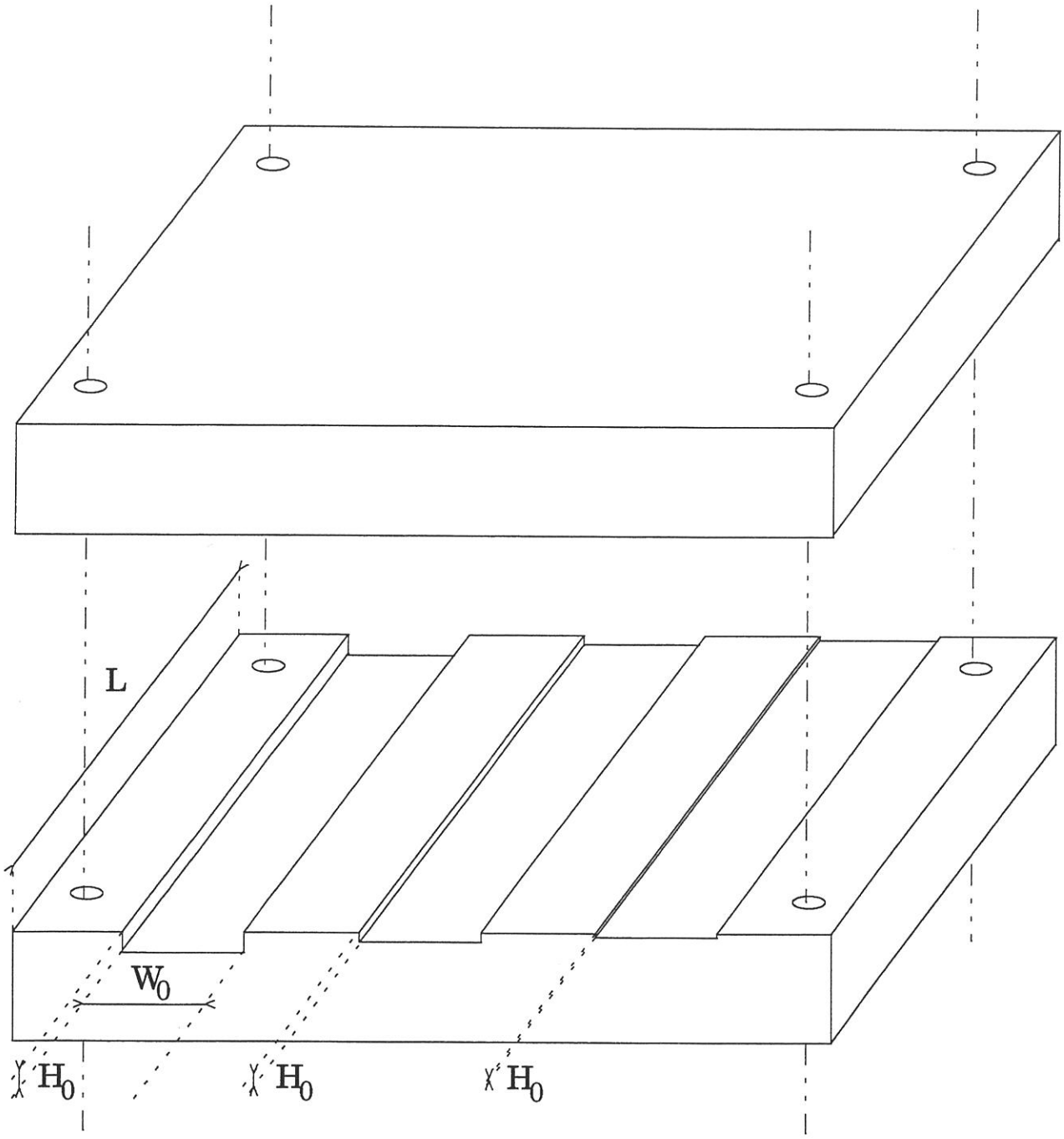

Fig. 4 : Schematics of the model graphite substrate including 3 pores, 20 mm in length, 2 mm in width and about 60, 120 and 320 μm in height.

result brings out that the infiltration process is not limited by the source species feed at the entrance of the pores, which justifies the boundary conditions (i.e. the constant concentrations at the pore ends during the densification).

Fig. 5 gives the infiltration profiles observed in the three kinds of pores for P = 4.7, 2.7 and 0.8 kPa. For the second and third pressure values (fig. 5b and 5c), the densification is stopped when the medium pore (i.e. of about 120 µm) is closed, while for the first pressure value (fig. 5a), it proceeds until closing the large pore. If the experimental profiles are compared for the medium pore (which is closed under the three conditions), the increase of pressure is found to improve slightly the homogeneity of the infiltration.

If the propane precursor species or an intermediate species resulting from a total and rapid decomposition of C_3H_8, is assumed to react at the pore surface (according to the kinetic law defined by equation (10) in 2.3.1), the present model foresees very flat infiltration profiles, with a volume fraction of infiltrated pyrocarbon higher than 99%. These results are not in agreement with the experiments. As previously shown for the CVI of SiC [20], the assumption on the chemical kinetics of pyrocarbon deposition is not valid and the concentration of one intermediate species X (i.e. the actual source species) at the pore entrance is probably much lower than the initial concentration of C_3H_8. As a consequence, the kinetic constant related to a new first order kinetic law with respect to X, must be chosen much higher than that of equation (10), according to the following expression :

$$k_{eo}\, C_{C3H8,0} = k'_{eo}\, C_{x,0} \qquad (15)$$

where k_{eo} is the preexponential factor of kinetic constant in equation (10),
k'_{eo} is a new kinetic factor which represents more conveniently the deposition chemical process,
$C_{C3H8,0}$ is the propane concentration at the reactor entrance,
$C_{x,0}$ is the concentration of the intermediate species X at the pore entrance.

A kinetic factor k'_{eo} of about 50 times k_{eo} seems suitable because it permits to fit the experimental profiles reported in figure 5a and b. The influence of the aspect ratio is well predicted by the model, particularly for the highest investigated pressure values.

Nevertheless, for the lowest pressure values, the experimental infiltration profiles are steeper than the predicted ones close to the pore entrance. This discrepancy can be explained by the inhibitor effect of H_2 (already reported to occur more strongly at

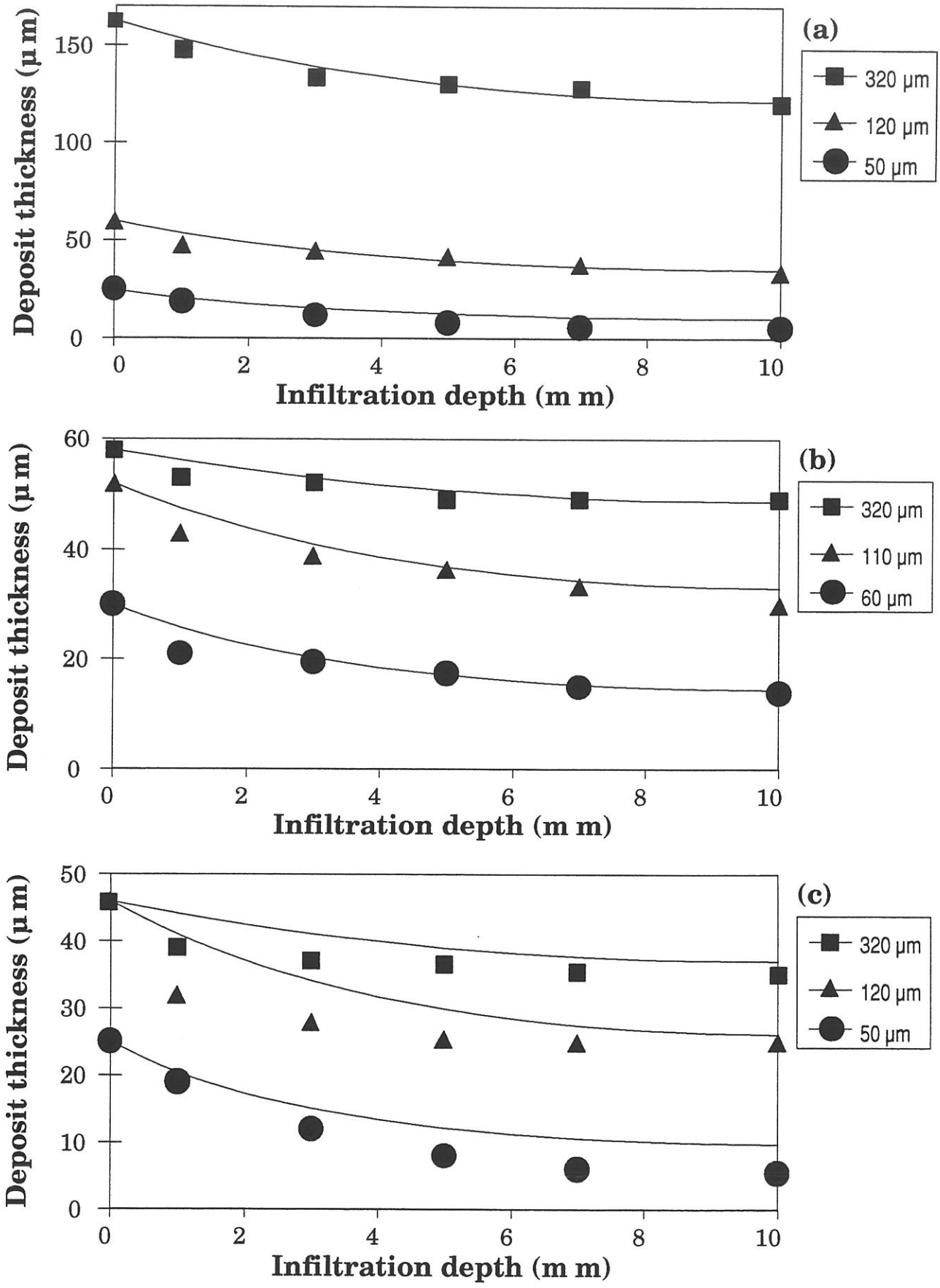

Fig. 5 : Experimental (markers) and calculated (full lines, with adjusted kinetic constant) profiles of pyrocarbon thickness along half-pores with rectangular cross-sections, 20 mm in length, 2 mm in width, 60, 120 and 320 µm in height for T = 1325 K and (a) P = 4.7 kPa, (b) P = 2.7 kPa, (c) P = 0.8 kPa

low pressure [28]) which is not taken into account in the presently used kinetic law. Hydrogen is produced by the pyrocarbon deposition reaction and is accumulated within the pore, as HCl does for the CVI of silicon carbide [20]. This feature can also justify the improvement of the infiltration homogeneity with an increase of pressure.

Another way to follow how the densification proceeds, is to plot the deposit thickness versus time, as shown in figure 6 for T = 1323 K, P = 3 kPa and Q = 300 sccm and for various infiltration depths from the entrance (z = 0) to the center (z = 10 mm) of the pore. The local growth rate is constant at the entrance while it decreases gradually within the pore as the infiltration proceeds and particularly after 50 h. This result confirms the prediction reported in a previous paper for the CVI of SiC in a cylindrical pore [20].

4 - CONCLUSION

The CVI model for the infiltration of a straight cylindrical pore, described in a previous paper [19], has been successfully extended to a straight pore with a rectangular cross-section and applied to a new chemical system (C_3H_8 precursor) which yields pyrocarbon deposition.

This extension needs only to replace the diameter of the cylindrical pore by the hydraulic diameter of the present pore (which can be expressed as a function of the perimeter and the area of the cross-section). The resulting model, based on a first order kinetic law for pyrocarbon deposition, gives the same qualitative influence of the various parameters on the quality of the infiltration [20].

If the chemical kinetics data are modified to take into account the decomposition of propane into reactive intermediate species, the CVI model is validated by fitting accurately most of the pyrocarbon thickness profiles measured for various aspect ratios. A still better fit could be obtained by using a kinetic law including the inhibitor effect of hydrogen.

For the substrate geometry of this study, the flux of the actual source species at the pore entrance does not limit the infiltration process which does not depend on the flow rate. This feature justifies the boundary conditions of constant concentrations at the pore ends. The assumption of constant gas concentration in any cross-section of the pore, which permits to build a 1D model, is also experimentally confirmed by the identical pyrocarbon thicknesses observed on the four sides of the rectangular pore.

ACKNOWLEDGEMENTS

The authors acknowledge the contribution of C. Robin-Brosse and J. Rey to the elaboration of the experimental procedure and the support that they received from both Société Européenne de Propulsion (SEP) and the French Ministery of Research through a grant to R.F. and P.D.

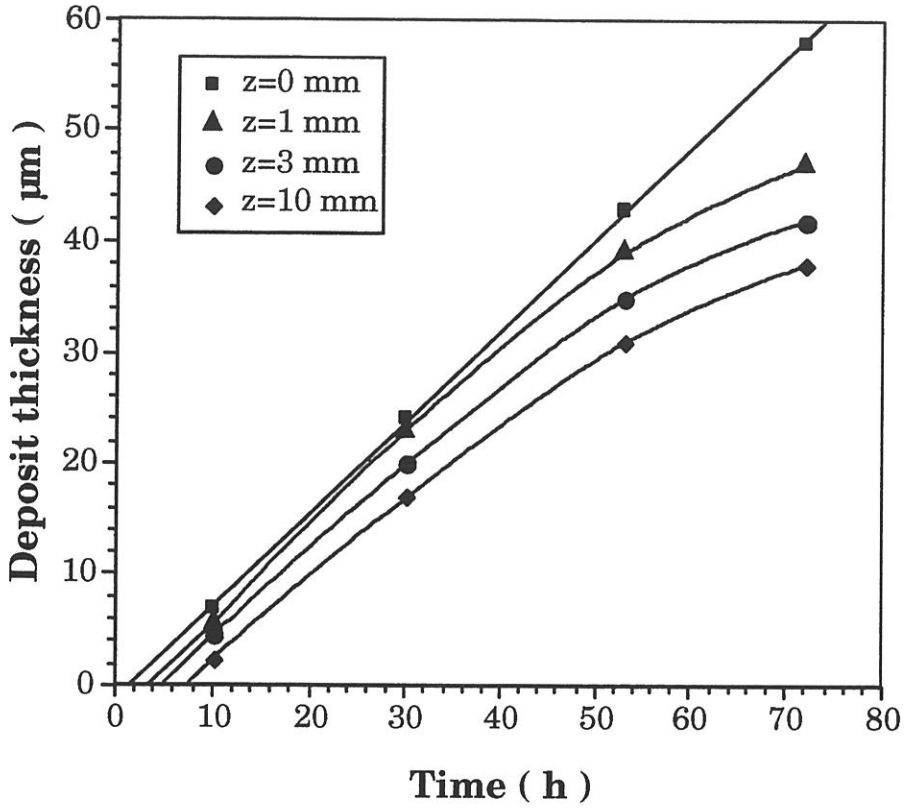

Fig. 6 : Experimental variations of the pyrocarbon deposit thickness with time at various infiltration depths in a rectangular pore 120 µm in height, for T = 1325 K and P = 3 kPa.

APPENDIX 1- Differential equation for the pore geometry change

The required equation results from a local treatment, by writing the volume of solid δV deposited on a thin shell of pore (δz in thickness) during the time δt :

$$\delta V = (W_t H_t - W_{t+\delta t} H_{t+\delta t}) \delta z \qquad (A1)$$

This volume can also be written as a function of the rate of the heterogeneous reaction ϑ and the molar volume of the deposited solid V_s :

$$\delta V = 2\vartheta \, \delta z \, \delta t \, V_s (W_t + H_t) \qquad (A2)$$

The equations (1) and (2) allow to write :

$$\frac{\partial B}{\partial t} = \frac{\partial W}{\partial t} \qquad (A3)$$

Thus equation (A1) can be developped as follows :

$$\delta V = [W_t H_t - (W_t + \frac{\partial H}{\partial t} \delta t) (H_t + \frac{\partial H}{\partial t} \delta t)] \delta z \qquad (A4)$$

whence

$$\delta V = - [(W_t + H_t) \frac{\partial H}{\partial t} \delta t + \left[\frac{\partial H}{\partial t} \right]^2 \delta t^2] \delta z \qquad (A5)$$

By combining (A2) and (A5) (neglecting the second order term in (A5)) with δt approaching zero, equation (7) is deduced :

$$\frac{\partial B}{\partial t} = \frac{\partial W}{\partial t} = - 2 V_s \vartheta \qquad (7)$$

APPENDIX 2 - Basic equations of the CVI model for a straight pore with a rectangular cross section [19]

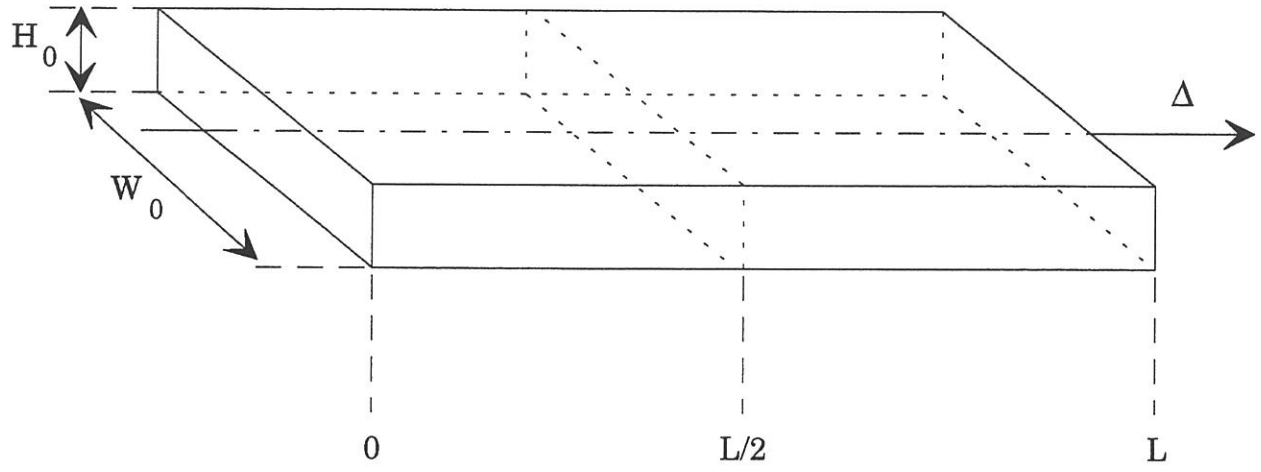

*** at steady state :**

$$D_i \frac{\partial^2 C_i}{\partial z^2} - \frac{\partial (x_i \mathbf{N})}{\partial z} + \frac{4 \nu_i \vartheta}{\Phi_h} = 0 \qquad \text{(A6)}$$

$$\frac{\partial B}{\partial t} = \frac{\partial H}{\partial t} = -2 V_s \vartheta \qquad \text{(A7)}$$

$$\frac{1}{D_i} = \frac{1}{D_F} + \frac{1}{D_{i,K}} \qquad \text{(A8)}$$

$$\mathbf{N} = \sum_{i=1}^{n_g} N_i \qquad \text{(A9)}$$

*** boundary conditions :**

at z = 0 (pore entrance) $\qquad C_i(0,t) = C_{i,0} \qquad$ (A10)

at z = L/2 (pore center) $\qquad \left[\frac{\partial C_i}{\partial z} \right]_{z=L/2} = 0 \qquad$ (A11)

$$(\mathbf{N})_{z=L/2} = 0 \qquad \text{(A12)}$$

APPENDIX 3 - Description of the CVD/CVI reactor

The deposition and infiltration experiments were performed in a hot wall CVD/ CVI reactor resistively heated and working under reduced pressures. The deposition chamber is a vertical cylindrical tube (27 mm in inner diameter) made of stainless steel, with a large isothermal zone. It is equipped with accurate controlling systems. The total pressure is maintained at a constant value between 0.5 and 25 kPa by a vacuum pump through a mechanical regulating system and a precise gauge. A mass flowmeter is used to control the C_3H_8 gas flow. The temperature is regulated with a thermocouple.

REFERENCES

[1] B. Broquere, B. Buttazzoni, J.-J. Choury, "Les composites Carbone-Carbone Leurs Applications Industrielles", in "Introduction aux Materiaux Composites" (R. Naslain ed.), Les Editions du CNRS, Institut des Materiaux Composites, Bordeaux, Vol. 2, pp. 405-438, 1985

[2] F. Christin, R. Naslain, C. Bernard, "A Thermodynamic and Experimental Approach of Silicon Carbide-CVD. Application to the CVD Infiltration of Porous Carbon-Carbon Composites", Proc. 7th Int. Conf. CVD, Los Angeles, USA (1979), (T.O. Sedgwick et al., eds.), The Electrochem. Soc., Princeton, pp. 499-514, 1979

[3] J.Y. Rossignol, R. Naslain, P. Hagenmuller, L. Heraud, "New Composite Materials with a Carbon-Titanium Carbide Hybrid Matrix for High Temperature Applications", in Proc. ICCM IV, Tokyo, Japan (1982), (T. Hayashi et al., eds.), pp. 1227- 1237, 1982

[4] H. Hannache, F. Langlais, R. Naslain, "Kinetics of Boron Carbide Chemical Vapor Deposition and Infiltration", Proc. 5th European Conf. CVD, Uppsala, Sweden (1985), (J.O. Carlsson et al., eds.), Upssala Univ. Press, pp. 219-233, 1985

[5] H. Hannache, R. Naslain, C. Bernard, "Boron Nitride Chemical Vapor Infiltration of Fibrous Materials from BCl_3-NH_3-H_2 or BF_3-NH_3 Mixtures : a Thermodynamic and Experimental Approach", J. Less-Common Met., Vol. 95, pp. 221-246, 1983

[6] R. Colmet, I. Lhermite-Sebire and R. Naslain, "Fibrous Alumina-Alumina Composite Materials Obtained according to a CVI Technique",Adv. Ceram. Mater., Vol. 138, N° 2, p. 221, 1982

[7] J. Minet, F. Langlais and R. Naslain, "Chemical Vapor Deposition of Zirconia within the Pore Network of Fibrous Ceramics Materials from $ZrCl_4$-H_2-CO_2-Ar Gas Mixtures", Composites Sciences and Technology, Vol. 37, pp. 79-107, 1990

[8] E. W. Thiele, "Relation Between Catalytic Activity and Size of Particle", Ind. Eng. Chem., Vol. 31, N° 7, pp. 916-920, 1939

[9] E.E. Petersen, "Reaction of Porous Solid", AIChE Journal, Vol. 3, N° 4, pp. 443-448, 1957

[10] E. Fitzer and R. Gadow, "Fiber-Reinforced Silicon Carbide", Am. Ceram. Soc. Bull., Vol. 65, pp. 326-335, 1986

[11] C. H. J. Van Den Brekel, R. M. M. Fonville, P. J. M. Van Der Straten, G. Verspui, "CVD of Ni, TiN and TiC on Complex Shapes", Proc. 8th Int. Conf. CVD, Paris, France (1984), (Mc D. Robinson et al., eds.), The Electrochem. Soc., Pennington, pp. 142-156, 1984

[12] J. Y. Rossignol, F. Langlais, R. Naslain, "A Tentative of Modelization of Titanium Carbide CVI within the Pore Network of Two-Dimensional Carbon-Carbon Composites Preforms", Proc. 9th Int. Conf. CVD, Cincinnati, USA (1984), (J. M. Blocher et al., eds.), The Electrochem. Soc., Pennington, pp. 596-914, 1984

[13] M. F. Carolan, J. N. Michaels, "Chemical Vapor Deposition of Yttria Stabilized Zirconia on Porous Supports", Solid State Ionics, Vol. 25, pp. 207-216, 1987

[14] Y. S. Lin, K. J. De Vries, A. J. Burggraaf, "CVD Modification of Ceramic Membranes: Simulation and Preliminary Results", Proc. 7th European Conf. CVD, Perpignan, France (1989), (M. Ducarroir et al., eds.), Colloque de Physique, Les Editions de Physique, Colloque C5, Suppl. N° 5, Vol. 50, pp. 861-872, 1989

[15] T. L. Starr, "Modeling of Forced Flow/Thermal Gradient CVI", Proc. Int. Conf. on Wiskers-and-Fiber-Toughened Ceramics, Oak Ridge, USA (1988), (R. A. Bradley et al., eds), ASM International, Oak Ridge, pp. 243-252, 1988

[16] S. M. Gupte, J. A. Tsamopoulos, "Densification of Porous Materials by Chemical Vapor Infiltration", J. Electrochem. Soc., Vol. 136, N° 4, pp. 555-561, 1989

[17] N. H. Tai, T. W. Chou, "Analytical Modeling of Chemical Vapor infiltration in Fabrication of Ceramic Composites", J. Am. Ceram. Soc.,Vol. 72, N° 3, pp. 414-420, 1989

[18] S. Middleman, "The Interaction of Chemical Kinetics and Diffusion in the Dynamics of Chemical Vapor infiltration", J. Mater. Res. ,Vol. 4, N° 6, pp. 1515- 1524, 1989

[19] R. Fédou, F. Langlais, R. Naslain, "A Modeling of the Isothermal/Isobaric Chemical Vapor Infiltration in a Straight Cylindrical Pore. Part. 1 : Description of the Model", to be published

[20] R. Fédou, F. Langlais, R. Naslain, "A Modeling of the Isothermal/Isobaric Chemical Vapor Infiltration in a Straight Cylindrical Pore. Part. 2 : Application to the CVI of SiC", to be published

[21] R. Fédou, E. Sipp, R. Rebillat, F. Langlais, R. Naslain, "A Modeling of the Isothermal/Isobaric Chemical Vapor Infiltration in a Straight Cylindrical Pore. Part. 3 : Application to the CVI of Zirconia or Yttria", to be published

[22] P. Molaës, J.C. Molaës, "Cinétique Chimique et Chimie Organique", Vuibert, Paris, 1985

[23] J.Y. Lee, J.H. Lee, W.S. Ryn, H.S. Kim, "A Study of the Properties of Pyrolytic Carbon deposited from Propane in a Tumbling and Stationnary Bed between 900 and 1230 °C", carbon, Vol. 21, N° 6, pp. 523-533, 1983

[24] P.A. Tesner, "Kinetics of pyrolytic carbon formation", Chemistry and Physics of Carbon (P.L. Walker, ed.), Vol. 19, Marcel Dekler, New York, 1979

[25] F. Trombel, J. Rappeneau, "Préparation des Pyrocarbones", Les Carbones II, Masson et Cie, Paris, 1965

[26] J. O. Hirschfelder, R.B. Bird, E. L. Spotz, Chem. Revs., Vol. 44, pp. 205, 1949

[27] R. A. Svehla, NASA Tech. Rep. R-132, Lewis research Center, Cleveland (OHIO), 1962

[28] M.L. Lieberman, "Chemical Vapor Deposition of Carbon : a Model to Relate Gas Phase Conditions to Structure of Deposit", Proc. 3thrd Int. Conf. on CVD, Hirsdale (F.A. Glasky, ed.), 1970, American Nuclear Society, Hirsdale, Illinois, pp. 488-495, 1970

CONCLUSION GÉNÉRALE

Ce travail s'inscrit dans le cadre de recherches visant à approfondir la connaissance des mécanismes impliqués dans l'élaboration des composites à matrice céramiques par dépôt chimique en phase vapeur (CVD/CVI) et à construire des modèles prévisionnels permettant d'améliorer la qualité et d'abaisser le coût des composites ainsi élaborés.

La présente étude a débuté au Laboratoire de Chimie du Solide, et s'est poursuivie au Laboratoire des Composites Thermostructuraux. Son principal objectif était de contribuer à la compréhension du couplage entre les mécanismes physiques (e.g. transferts de masse par diffusion de Fick et de Knudsen) et chimiques (réactions en phase homogène et hétérogènes) intervenant lors du procédé CVI. La diversité des préformes poreuses et la complexité de la géométrie du milieu poreux qu'elles forment nous a conduit à consacrer cette étude au cas de l'infiltration d'un pore rectiligne unique. La stratégie retenue a consisté à développer, dans un premier temps, un modèle d'infiltration d'un pore rectiligne cylindrique s'appuyant sur un nombre restreint d'hypothèses et pouvant intégrer n'importe quel système chimique et n'importe quelle cinétique hétérogène. Dans un deuxième temps, ce modèle a été appliqué à l'infiltration d'un tel pore par diverses céramiques, puis il a été adapté et appliqué au cas de l'infiltration d'un pore rectiligne à section droite rectangulaire par du pyrocarbone.

Une attention toute particulière a été donnée dans ce travail au développement d'études expérimentales permettant de valider le modèle et de quantifier avec précision l'infiltration dans des conditions aussi proches que possible de celle du modèle. Ces études nous ont conduit à utiliser des appareillages de CVD/CVI permettant un contrôle et une régulation précis des paramètres physiques d'infiltration.

Le **premier chapitre** s'attache à décrire le **modèle d'infiltration d'un pore rectiligne cylindrique** et sa **méthode de résolution**. Le modèle repose sur un faible nombre d'hypothèses justifiées par des raisons expérimentales ou théoriques. En particulier aucune hypothèse ne concerne les réactions hétérogènes : la cinétique de ces réactions est considérée au niveau local comme une fonction de la température et des concentrations de chaque espèce gazeuse. Les principales hypothèses consistent à supposer que (a) la concentration de chaque espèce gazeuse est constante suivant une section droite du pore, (b) l'infiltration se comporte, vis-à-vis des transfert de masse (i.e diffusion de Fick et de Knudsen), comme une succession d'états quasi-stationnaires, (c) le pore est symétrique par rapport à son centre et (d) la composition de la phase gazeuse aux extrémités du pore est constante au cours de l'infiltration.

L'hypothèse (a), permettant de passer d'un problème tridimensionnel à un problème unidimensionnel, est justifiée expérimentalement (chapitre 4). Quant à la deuxième hypothèse, elle se justifie de manière théorique (chapitre 1 et annexe C). Ce modèle se traduit par un système d'équations différentielles aux dérivées partielles non linéaires. La résolution est numérique et fait appel à la méthode des différences finies. Le modèle permet de calculer, à tous les stades de la densification et en particulier à la fin du processus lorsque le pore est bouché, les profils de concentration pour chaque espèce gazeuse et le profil en diamètre. Le modèle est validé numériquement par comparaison, dans des cas bien particuliers, à des modèles d'infiltration préexistants.

Le **deuxième chapitre** a pour objet d'appliquer le modèle au cas de l'**infiltration** d'un pore rectiligne cylindrique par **du carbure de silicium** déposé à partir du mélange CH_3SiCl_3 (MTS)-H_2, puis de le valider par une confrontation expérimentale. Une étude théorique a été menée sur la base d'une cinétique hétérogène simplifiée (supposée du premier ordre par rapport au MTS) en accord avec la réaction :

$$CH_3SiCl_{3(g)} \quad \text{----------} > \quad SiC_{(s)} + 3\ HCl_{(g)} \qquad (1)$$

La géométrie du pore est décrite par son diamètre initial et son facteur de forme, défini par le rapport de la longueur sur le diamètre initial du pore. Les paramètres influençant fortement l'infiltration sont la température (dont l'effet est directement lié à la forte énergie d'activation de la réaction), le facteur de forme et, lorsque la diffusion est régie par la diffusion de Fick, la pression totale et le diamètre initial du pore. L'homogénéité de l'infiltration s'améliore lorque l'un de ces facteurs diminue. Par contre, la composition de la phase gazeuse et, en régime de diffusion de Knudsen, le diamètre initial et la pression totale n'ont pas beaucoup d'influence sur les profils en épaisseur de dépôt. Lorsque la loi cinétique de dépôt est **simplement du premier ordre par rapport à la seule espèce source**, le modèle montre que l'**optimisation** de l'infiltration (en terme d'homogénéité et de vitesse de densification) consiste à se placer (i) à **basse température**, (ii) à une **pression totale aussi élévée que possible** tout en restant dans le domaine température/pression où la diffusion est **en régime de Knudsen**, et (iii) à une **composition relativement riche** en espèce source, de manière à diminuer le temps d'infiltration.

La deuxième partie de ce chapitre présente une description de la procédure expérimentale originale permettant de confronter le modèle à l'expérience. La principale difficulté a résidé dans l'obtention de pores dont la géométrie puisse être tant soit peu peu représentative de celle des pores présents dans les préformes fibreuses. La méthode retenue permet d'élaborer des pores rectilignes cylindriques en carbure de silicium

ayant une géométrie bien controlée (diamètre interne de 34 µm) et pouvant avoir des facteurs de forme très élevés (> 300). La détermination expérimentale des profils en épaisseur de dépôt fait appel à l'observation par microscopie électronique à balayage de sections de fractures effectuées à diverses abscisses le long du pore.

La comparaison entre les profils théoriques et expérimentaux réalisés à 800 °C permet de valider le modèle puisqu'il prévoit avec précision l'influence du facteur de forme sur le profil en épaisseur de dépôt. Cette comparaison met aussi en évidence que le schéma réactionnel (1) est beaucoup trop simple. Le MTS doit réagir en phase homogène avant de parvenir à l'entrée du pore. L'homogénéité de l'infiltration est très sensible à la cinétique des réactions de surfaces, et non pas à la cinétique apparente globale du processus de dépôt. Les réactions hétérogènes produisant le dépôt doivent faire intervenir un intermédiaire réactionnel dont la concentration est faible en comparaison de celle du MTS initialement introduit. Les expériences effectuées à diverses températures et pressions montrent de plus que **les lois cinétiques** régissant les réactions de surface **sont plus complexes qu'un simple loi du premier ordre**. En particulier, cette loi doit faire intervenir l'**effet inhibiteur de HCl** (expérimentalement constaté par divers auteurs). Ce chapitre met ainsi en exergue la nécessité de connaître les lois cinétiques des réactions hétérogènes au niveau local, i.e en fonction des espèces sources intermédiaires et des espèces produites (inhibition), et pour cela les lois cinétiques des réactions en phase homogène. Si l'étude cinétique par prise de masse ou détermination de la vitesse de croissance en épaisseur de dépôt à la surface d'un substrat est nécessaire, elle n'est donc pas suffisante. Il faut pouvoir disposer de moyens permettant une connaissance approfondie de la **composition de la phase gazeuse au voisinage de la surface de réaction** (accessible par analyse in situ, par spectrométrie Raman, Infra-Rouge, de masse ou par fluorescence). La loi cinétique du dépôt de carbure de silicium à partir du mélange MTS-H_2 n'étant pas strictement du premier ordre par rapport à une seule espèce source, les conclusions du modèle concernant l'optimisation ne peuvent pas totalement s'appliquer. En particulier, il semble que le comportement de la cinétique de la réaction de surface n'est pas linéaire par rapport à la pression totale et que son énergie d'activation est bien plus faible que l'énergie apparente d'activation du processus global de dépôt.

Le **troisième chapitre** démontre la capacité du modèle à prendre en compte des systèmes et des **réactions chimiques complexes**, en appliquant le modèle au cas de l'infiltration d'un pore rectiligne cylindrique par de la **zircône** (déposée à partir du mélange $ZrCl_4$-CO_2-H_2-Ar) et de l'**oxyde d'yttrium** (déposé à partir du mélange YCl_3-CO_2-H_2-Ar). Les systèmes chimiques impliqués dans ces infiltrations comporte de nombreuses espèces gazeuses et les lois cinétiques respectives de dépôt de la zircône

et de l'oxyde d'yttrium sont complexes :

$$ZrCl_{4(g)} + 2\ CO_{2(g)} + 2\ H_{2(g)} \rightarrow ZrO_{2(s)} + 2\ CO_{(g)} + 4\ HCl_{(g)} \quad (2)$$

$$R = k_o \exp\left(-\frac{E_a}{\boldsymbol{R}\,T}\right) P_{ZrCl4}^{1}\ P_{CO2}^{1/2}\ P_{H2}^{2} \quad (3)$$

$$2\ YCl_{3(g)} + 3\ CO_{2(g)} + 3\ H_{2(g)} \rightarrow Y_2O_{3(s)} + 3\ CO_{(g)} + 6\ HCl_{(g)} \quad (4)$$

$$R = k_o \exp\left(-\frac{E_a}{\boldsymbol{R}\,T}\right) P_{YCl3}^{2}\ P_{CO2}^{1}\ P_{H2}^{2} \quad (5)$$

L'étude théorique montre que pour les deux oxydes, les paramètres qui ont le plus d'influence sont la pression totale, le taux de dilution des réactifs dans l'argon et la pression partielle d'hydrogène. Dans le cas de l'infiltration de l'oxyde d'yttrium, la température et la pression partielle de YCl_3 ont aussi une grande influence. Lorsque le taux de dilution augmente ou lorsque l'un des paramètres cités ci-dessus diminue, l'homogénéité des profils en épaisseur de dépôt est améliorée. Contrairement au cas d'une simple cinétique du premier ordre, il n'y a pas de limitation de l'effet de la pression lorsque les transferts de masse s'effectuent en régime de Knudsen. Pour les deux oxydes, la pression partielle de CO_2 (réactif ayant l'ordre réactionnel le plus faible), et pour l'infiltration de la zircône, la pression partielle de ZrCl4 et la température (de par la faible énergie d'activation) n'ont qu'une légère influence. De manière générale, le modèle montre que l'**infiltration des oxydes** est **plus difficile que celle du carbure de silicium** (étudié au chapitre 2). En particulier, les vitesses de densification, nécessaires à l'obtention d'une bonne homogénéité des profils en épaisseur, peuvent être **très lentes** (le temps de fermeture d'un pore de 100 µm de diamètre est de plusieurs centaines de jours pour une bonne infiltration). La forte influence de la composition et la difficulté d'infiltration sont liées à la présence d'un ordre réactionnel total élevé (>3) et à la taille des molécules sources ($ZrCl_4$ et YCl_3) qui rend leur diffusion difficile. Cependant, si l'on possède des données précises sur les cinétiques hétérogènes locales, **le modèle peut apporter une aide précieuse à l'optimisation de l'infiltration** en terme de vitesse de densification pour une qualité d'infiltration donnée.

Le **quatrième chapitre** montre les possiblités d'extension du champ d'application

du modèle à d'**autres géométries de pore**. Ce chapitre traite en effet de la modélisation du procédé CVI dans un pore rectiligne à section droite rectangulaire et de l'application du modèle ainsi modifié au cas de l'infiltration d'un tel pore par du pyrocarbone déposé à partir de propane. En remplaçant le diamètre du pore cylindrique par le **diamètre hydraulique** (défini comme étant égal à 4 fois l'aire de la section droite du pore sur son périmètre), le modèle d'infiltration d'un pore cylindrique peut être directement étendu au cas du pore à section rectangulaire. Une brève étude cinétique expérimentale montre que le dépôt de pyrocarbone à partir du propane suit une loi cinétique du premier ordre par rapport au propane. Les pores modèles sont obtenus par usinage de rainures de faibles profondeurs sur la surface d'une plaque de graphite. En appliquant une autre plaque de graphite non rainurées sur la première, des pores rectilignes à section rectangulaire dont les hauteurs sont approximativement de 60, 120 et 320 µm sont obtenus. L'étude expérimentale de CVI montre que (i) l'hypothèse des concentrations constantes suivant une section droite du pore est vérifiée par l'observation d'une coupe transversale effectuée au centre d'un pore après infiltration (épaisseurs déposées identiques sur les 4 côtés de la section rectangulaire) et (ii) le choix des conditions aux limites (composition de la phase gazeuse à l'entrée du pore constante) est justifié par le fait que les profils en épaisseur d'infiltration sont indépendants du débit total gazeux dans le réacteur. La comparaison entre les profils expérimentaux et les profils théoriques obtenus à partir d'une loi cinétique du premier ordre par rapport au propane associé au schéma réactionnel suivant :

$$C_3H_{8(g)} \text{ ---------- > } 3\ C_{(s)} + 4\ H_{2(g)} \qquad (6),$$

aboutit à des conclusions similaires à celles du chapitre 2 : les réactions hétérogènes doivent faire intervenir une (ou des) espèce(s) intermédiaire(s) (issue(s) de réactions en phase homogène) présente(s) en faible quantité dans la phase gazeuse à l'entrée du pore. Le modèle parvient à simuler l'influence de la géométrie du pore. Les écarts observés dans certaines conditions entre profils expérimentaux et théoriques peuvent s'expliquer en partie par le rôle inhibiteur de l'hydrogène, constaté par plusieurs auteurs, mais qui n'a pas été examiné lors de l'étude cinétique préliminaire.

En résumé, la présente étude a permis d'apprécier de manière détaillée dans le cas d'un pore modèle simple l'influence sur la qualité de la CVI et la vitesse de densification, de nombreux paramètres géométriques et opératoires. Elle a montré d'autre part la nécessité de connaître les cinétiques hétérogènes au niveau local et donc la composition de la phase gazeuse dans la zone chaude (étude entreprise par F. Loumagne en collaboration avec un laboratoire de l'ONERA). Le but final de la

modélisation du procédé CVI est de prévoir le comportement vis-à-vis de la densification d'une préforme fibreuse réelle dans un réacteur de laboratoire, puis de tout un chargement de ces préformes dans un réacteur industriel. A cet effet une description géométrique préalable du réseau poreux complexe qu'elle constitue est nécessaire. Il faut de plus être capable de prévoir l'évolution de cette géométrie en fonction de l'épaisseur de dépôt sur la surface interne du réseau de pores, i.e en fonction du degré d'avancement de la densification. Le modèle présenté dans ce mémoire peut, dans son principe, être adapter à des structures plus complexes (e.g. représentation d'une préforme par une réseau équivalent de pores rectilignes), avec modification des conditions aux limites. En effet, l'importance de la surface interne des préformes fibreuses impose de considérer, aux extrémités des pores débouchants non plus des concentrations constantes, mais des flux molaires constants. Ces flux sont en fait limités par les phénomènes de transferts de matière à l'extérieur de la préforme. Une étape utlérieure pourrait prendre en compte le couplage entre les phénomènes d'infiltration se produisant à l'intérieur de la (ou des) préforme(s) et les divers transferts (masse, chaleur et quantité de mouvement) se produisant dans le réacteur à l'extérieur de celle(s)-ci.

ANNEXE A

Titre : DESCRIPTION DE L'INSTALLATION DE CVD POUR LES INFILTRATIONS DE CARBURE DE SILICIUM

ANNEXE A

DESCRIPTION DE L'INSTALLATION DE CVD POUR LES INFILTRATIONS DE CARBURE DE SILICIUM

1 - CHOIX DE L'INSTALLATION

1.1 - Objectifs

L'appareillage est destiné à modéliser les mécanismes physico-chimiques du dépôt et de l'infiltration du carbure de silicium par voie gazeuse (CVD/CVI) dans le système élémentaire Si-C-H-Cl. La géométrie du réacteur doit être simple et permettre de modéliser aisément les phénomènes de transfert. L'expérimentation cinétique doit être fiable et précise de manière à pouvoir étudier convenablement l'étude du processus à partir d'un système chimique complexe.

1.2 - Caractéristiques de l'installation

Le réacteur est de type :

- *LPCVD* (Low Pressure CVD), les cinétiques de dépôt étant contrôlées par les réactions chimiques seulement à basses pressions,

- *tubulaire cylindrique*, l'écoulement de la phase gazeuse étant de type laminaire et laminaire rampant,

- *à parois chaudes*, unr large zone isotherme évitant la convection naturelle du gaz,

- *vertical*, l'échantillon pouvant alors être suspendu à une microbalance.

La source utilisée au cours de cette étude pour le dépôt de carbure de silicium

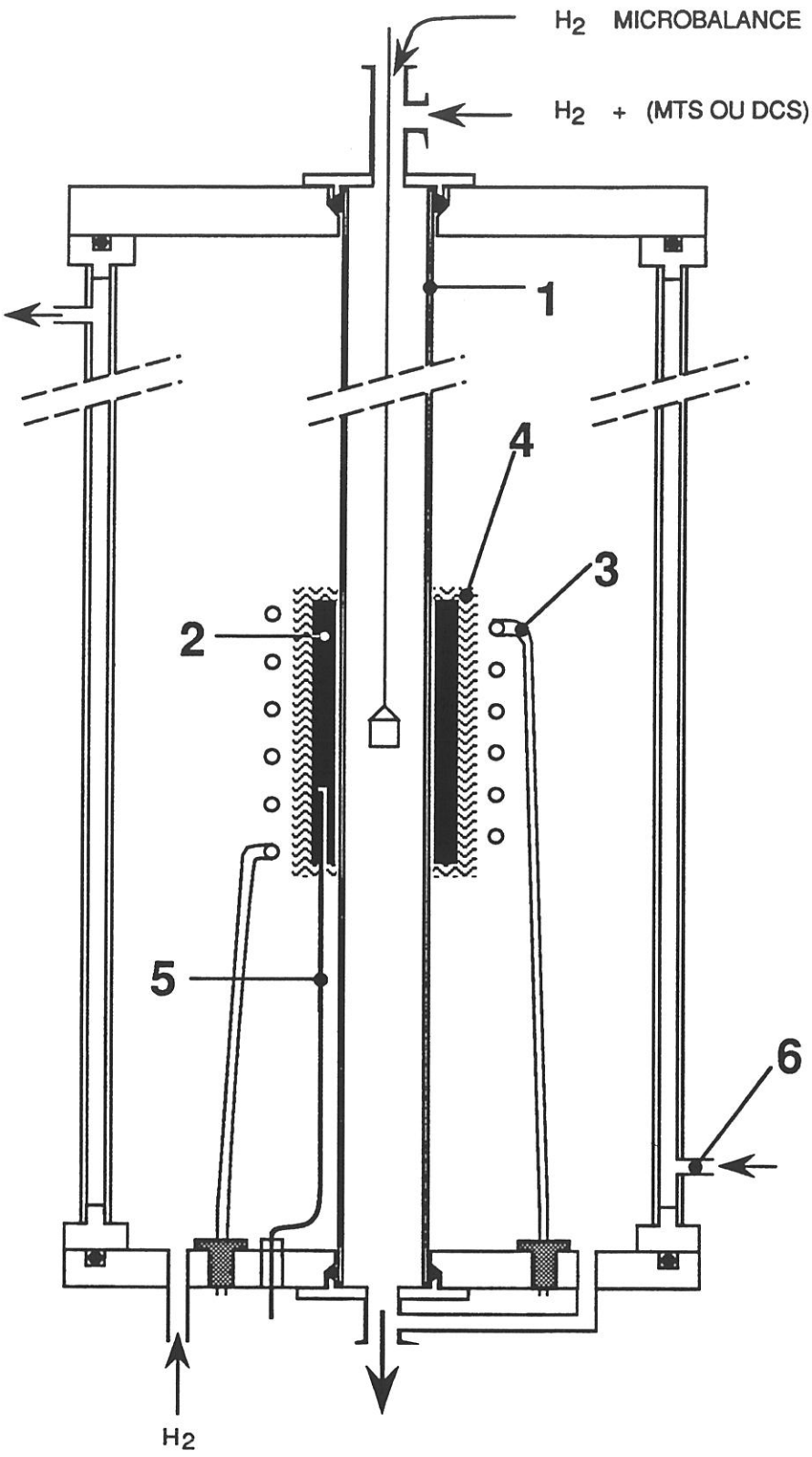

1 - Tube réacteur en silice
2 - Susceptor en graphite
3 - Spire inductrice
4 - Isolant
5 - Thermocouple
6 - Circulation d'eau de refroidissement

Fig. A1: Schéma du réacteur

est le CH_3SiCl_3 (méthyltrichlorosilane ou MTS) avec l'hydrogène comme gaz vecteur. Ce réacteur permet aussi de déposer du silicium, en utilisant comme source le SiH_2Cl_2 (Dichlorosilane ou DCS).

Les paramètres physiques expérimentaux imposés au cours d'une infiltration sont la température de la zone de réaction, la pression totale et les débits partiels des gaz injectés dans le réacteur. Ils doivent être mesurés et régulés indépendamment avec une grande précision.

Les évolutions de la masse de l'échantillon introduit dans le four peuvent être suivies grâce à une microbalance.

2 - DESCRIPTION DU REACTEUR

Le **tube réactionnel** dont les dimensions sont : diamètre d = 34 mm et hauteur h = 350 mm, est en silice vitreuse. Les valeurs des débits des gaz utilisés sont telles que la valeur du nombre de Reynolds est inférieur à 100 à température ambiante. La longueur du tube nécessaire à l'établissement d'un régime laminaire situé au-delà d'une zone de perturbation (ici l'entrée du réacteur) vaut alors l = 0.035 Re.d, soit ici 12 cm. Cette condition est largement vérifié, puisque la hauteur du tube en amont de la zone chaude du réacteur est de 25 cm. Les seules perturbations de l'écoulement du gaz sont l'échantillon et le fil qui le suspend dans le réacteur.

Le système de chauffage est du type inductif haute fréquence : l'inducteur est un solénoïde en cuivre et le susceptor un cylindre en graphite de 14 cm de haut. ce dernier est placé à l'extérieur du tube en silice, afin de ne pas perturber le flux gazeux. Une bonne isolation thermique externe assure le chauffage des parois du tube **par rayonnement** du susceptor.

Le tube du réacteur, isolé de l'extérieur par des joints étanches, est monté dans une **enceinte protectrice** en acier inoxydable, refroidie à l'eau (figure A1). Une circulation d'hydrogène dans l'enceinte et une sortie commune avec le tube réactionnel

assure une équipression.

3 - CONTROLE DES PARAMETRES PHYSIQUES EXPERIMENTAUX

La figure A2 représente l'ensemble de l'installation de CVD/CVI. Le contrôle des paramètres doit être rigoureux pour pouvoir modéliser les processus de CVD/ CVI étudié. Une partie du gaz vecteur de l'hydrogène traverse la microbalance afin de la protéger d'éventuelles rétrodiffusions de gaz corrosifs. Chaque débit partiel Q_X de gaz X est régulé. Dans le réacteur, la température T de la zone de réaction où se trouve l'échantillon est également régulé. Enfin, la pression totale P est régulée par un dispositif situé entre les pièges cryogéniques et la pompe à vide. L'installation permet de ne faire varier qu'un paramètre à la fois, ce qui permet d'analyser l'influence de chaque paramètre sur les cinétiques de dépôt ou sur l'infiltration.

3.1 - Pression totale

Un régulateur à membrane couplé à un capteur de pression permettent de maintenir une pression totale constante jusqu'aux vannes de régulation intégrées au débitmètres massiques des diverses conduites de gaz ou à la vanne manuelle de réglage en sortie du barbotteur à MTS. La gamme de pression utilisable est de $1 \leq P \leq 25$ kPa.

3.2 - Débits partiels

Des débitmètres massiques contrôlent et régulent les débits volumiques dans les conditions standarts (25 °C et 101.325 kPa) des gaz employés. La source utilisée pour le dépôt de carbure de silicium pose un problème pour le contrôle de son débit car le MTS est liquide dans les conditions normales de température et de pression son flux ne peut être maîtrisé directement avec un débitmètre comme on le fait avec

1 - Vanne d'arrêt
2 - Débitmètre massique
3 - Microbalance
4 - Microordinateur
5 - Tube réacteur en silice
6 - Susceptor
7 - Spire inductrice
8 - Thermocouple
9 - Pièges cryogéniques
10 - Capteur de pression
11 - Régulateur de pression à membrane
12 - Pompe primaire
13 - Vanne de régulation
14 - Manomètre
15 - Bain thermostaté

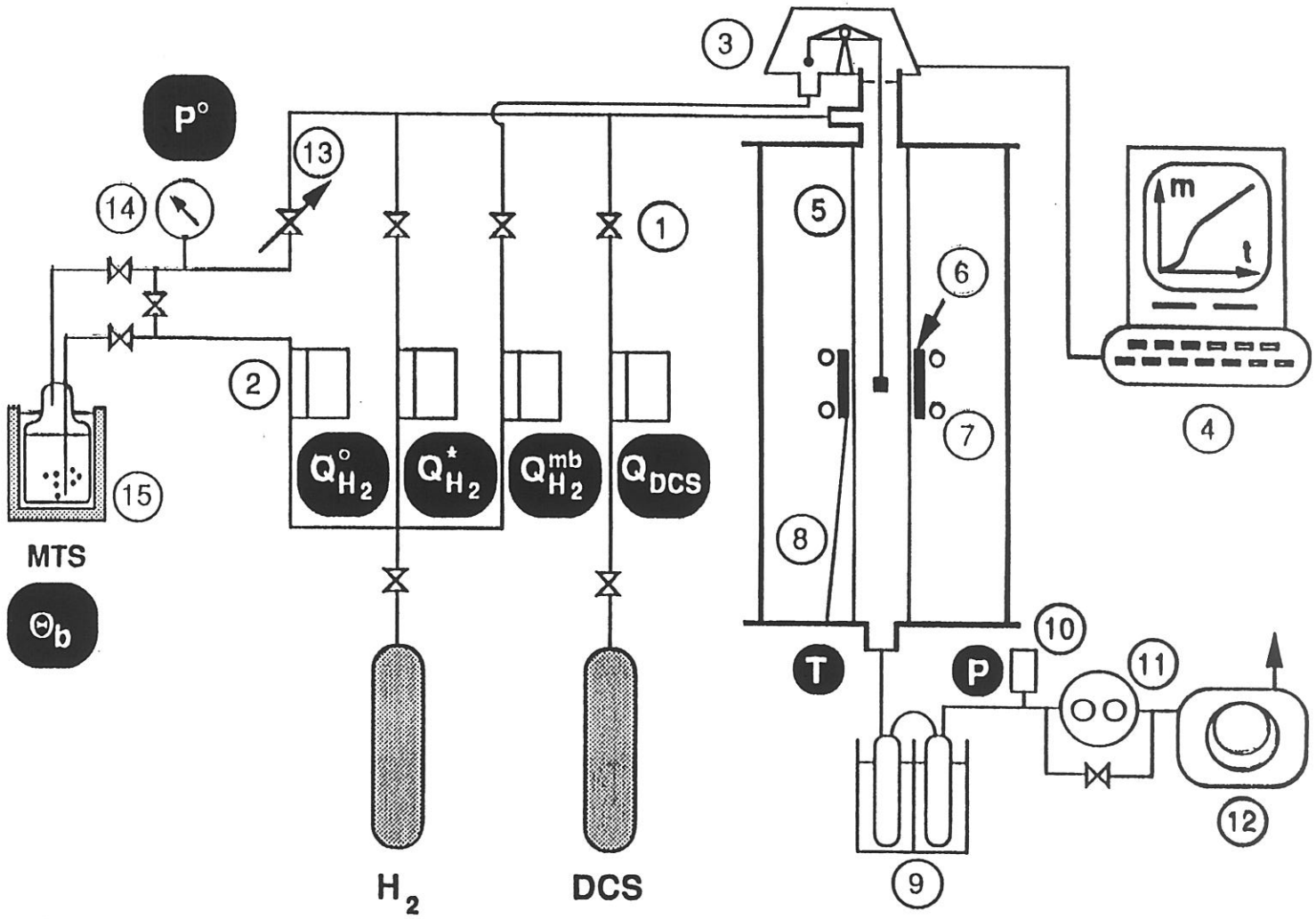

Fig. A2 : Schéma de principe de l'installation du réacteur CVD modèle

une source gazeuse (comme DCS). Un barbottage d'hydrogène dans le MTS conduit à une phase gazeuse dont la composition est connue dans l'hypothèse de la saturation (la pression partielle du MTS dans le mélange étant alors égale à la pression de vapeur du MTS, fonction de la tempéraure régulée du bain de MTS liquide). Afin d'avoir une composition relativement indépendante de la pression totale du réacteur, une vanne de réglage manuelle précise est placée entre le barbotteur au sein duquel la pression totale est P° et le réacteur dont lea pression totale est P. En amont de cette vanne, la température du bain Θ_b permet de connaître (grâce à la courbe pression vapeur saturante/température) la pression de vapeur saturante du MTS. On a donc les relations :

$$P^\circ = P^\circ_{MTS} + P^\circ_{H2} \qquad (A.1)$$

et

$$\alpha^\circ = Q^\circ_{H2}/Q_{MTS} = P^\circ_{H2}/P^\circ_{MTS} \qquad (A.2)$$

avec

P°_{MTS} : pression de vapeur saturante du MTS

P°_{H2} : pression d'hydrogène dans le barbotteur

Q°_{H2} : débit d'hydrogène passant dans le barbotteur

α° : rapport de dilution du MTS dans le barbotteur

Q_{MTS} : débit de MTS sortant du barbotteur

d'où

$$\alpha^\circ = (P^\circ - P^\circ_{MTS})/ P^\circ_{MTS} \qquad (A.3)$$

et

$$Q_{MTS} = Q^\circ_{H2}/ \alpha^\circ \qquad (A.4)$$

En aval de cette vanne, le mélange MTS + H_2 est dilué par de l'hydrogène dont le débit est Q'_{H2}. On calcule alors les grandeurs :

$$Q = Q_{MTS} + Q'_{H2} \qquad (A.5)$$

et

$$\alpha = Q_{H2}/Q_{MTS} = (Q'_{H2} + Q^{\circ}_{H2})/Q_{MTS} \qquad (A.6)$$

avec

Q : débit total passant dans dans le réacteur

Q_{H2} : débit total d'hydrogène passant dans le réacteur

α : rapport de dilution du MTS dans le réacteur

soient

$$\alpha = \alpha^{\circ} (1 + Q'_{H2} / Q^{\circ}_{H2}) \qquad (A.7)$$

$$Q = Q'_{H2} + Q^{\circ}_{H2}(1+1/ \alpha^{\circ}) \qquad (A.8)$$

ou inversement, si l'on veut imposer α et Q, on ajuste alors les débits partiels d'hydrogène :

$$Q^{\circ}_{H2} = \alpha^{\circ} Q/(1+ \alpha^{\circ}) \qquad (A.9)$$

$$Q'_{H2} = Q (\alpha - \alpha^{\circ})/(1+ \alpha) \qquad (A.10)$$

et le débit partiel de MTS est alors :

$$Q_{MTS} = Q /(1+ \alpha) \qquad (A.11)$$

Connaissant α, P et Q, on peut en déduire les pressions partielles P_{H2} et P_{MTS}, ainsi que les fractions molaires y_{H2} et y_{MTS}. En effet on a les relations :

$$P = P_{MTS} + P_{H2} \tag{A.12}$$

$$\alpha = P_{H2}/P_{MTS} \tag{A.13}$$

d'où :

$$P_{H2} = P\,\alpha / (1 + \alpha) \tag{A.14}$$

$$P_{MTS} = P / (1 + \alpha) \tag{A.15}$$

On en déduit les valeurs des fractions molaires des espèces :

$$y_{H2} = P_{H2}/P = \alpha / (1 + \alpha) = Q_{H2}/Q \tag{A.16}$$

$$y_{MTS} = P_{MTS}/P = 1 / (1 + \alpha) = Q_{MTS}/Q \tag{A.17}$$

3.3 - Température

Un régulateur de température assure une température T_R constante dans la zone réactionnelle grâce à un thermocouple placé dans le susceptor. La puissance nécessaire est fournie par un générateur HF de 6 kW. On étalonne régulièrement la température T réelle à l'intérieur du tube de silice à l'aide d'un autre thermocouple, avec un écoulement gazeux d'hydrogène dans des conditions Q_{H2} et P données (figure A3).

3.3.1 - *Profil thermique*

On régule à T_R fixe (par exemple 1000 °C), et on mesure T en fonction de z

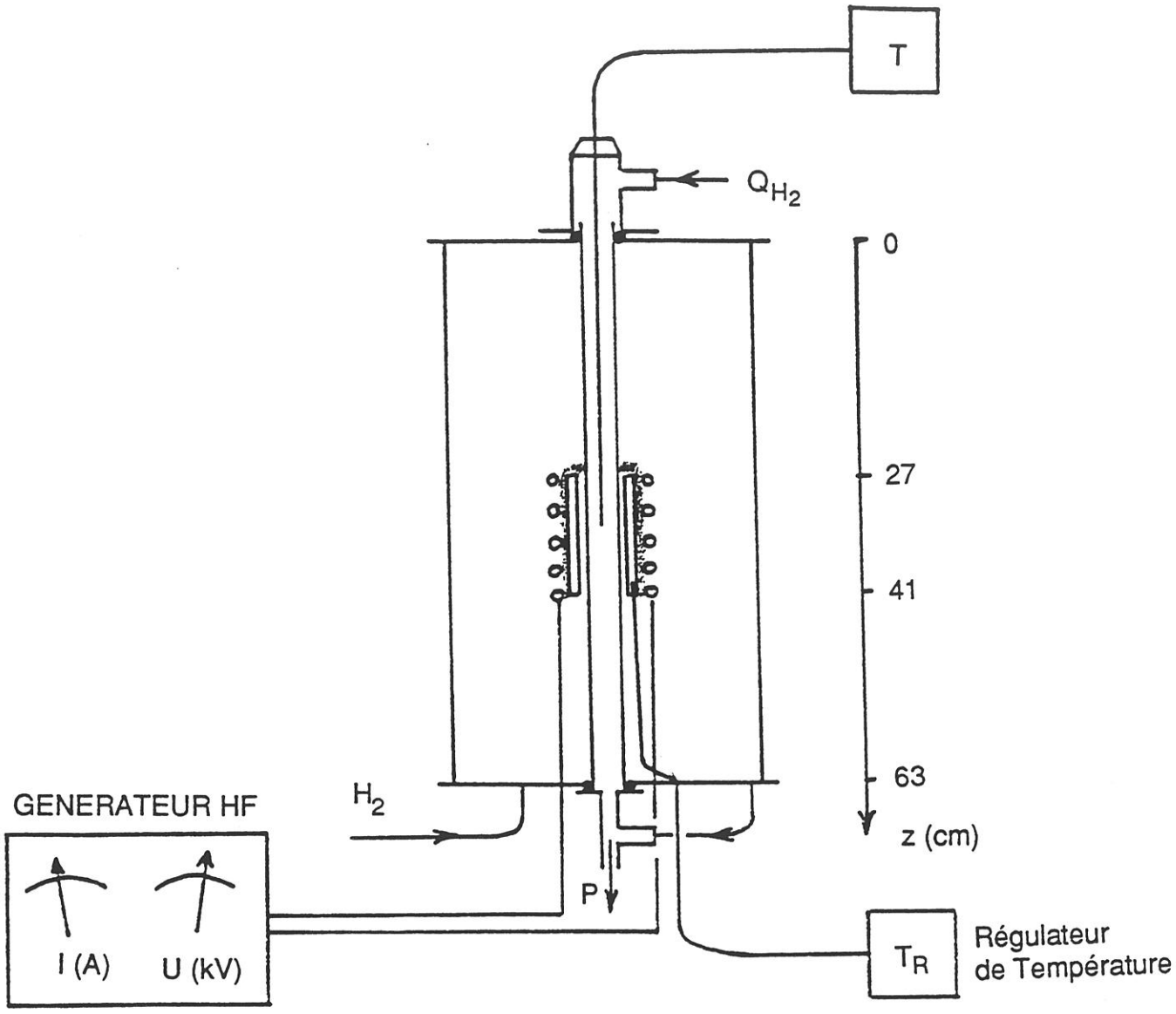

Fig. A3 : Schéma de principe du réacteur illustrant la mise au point thermique

suivant l'axe du tube. Le profil T(z) obtenu a une allure en "cloche" (Figure A4). Néanmoins une zone quasi-isotherme (à 5°C) d'une longueur de 3 cm est observée au niveau du milieu du susceptor. L'influence de P sur ce profil thermique est négligeable et un très fort débit d'hydrogène déplace légèrement le maximum de température vers le bas.

3.3.2 - *Etalonnage*

A la côte z_{max} (sommet du profil thermique), on mesure T en fonction de T_R.

On trouve pratiquement une relation linéaire entre T et T_R dans la gamme $800°C \leq T_R \leq 1200$ °C. L'écart entre T et T_R peut augmenter lorsque les parois du tube sont recouvertes d'une épaisseur de dépôt important.

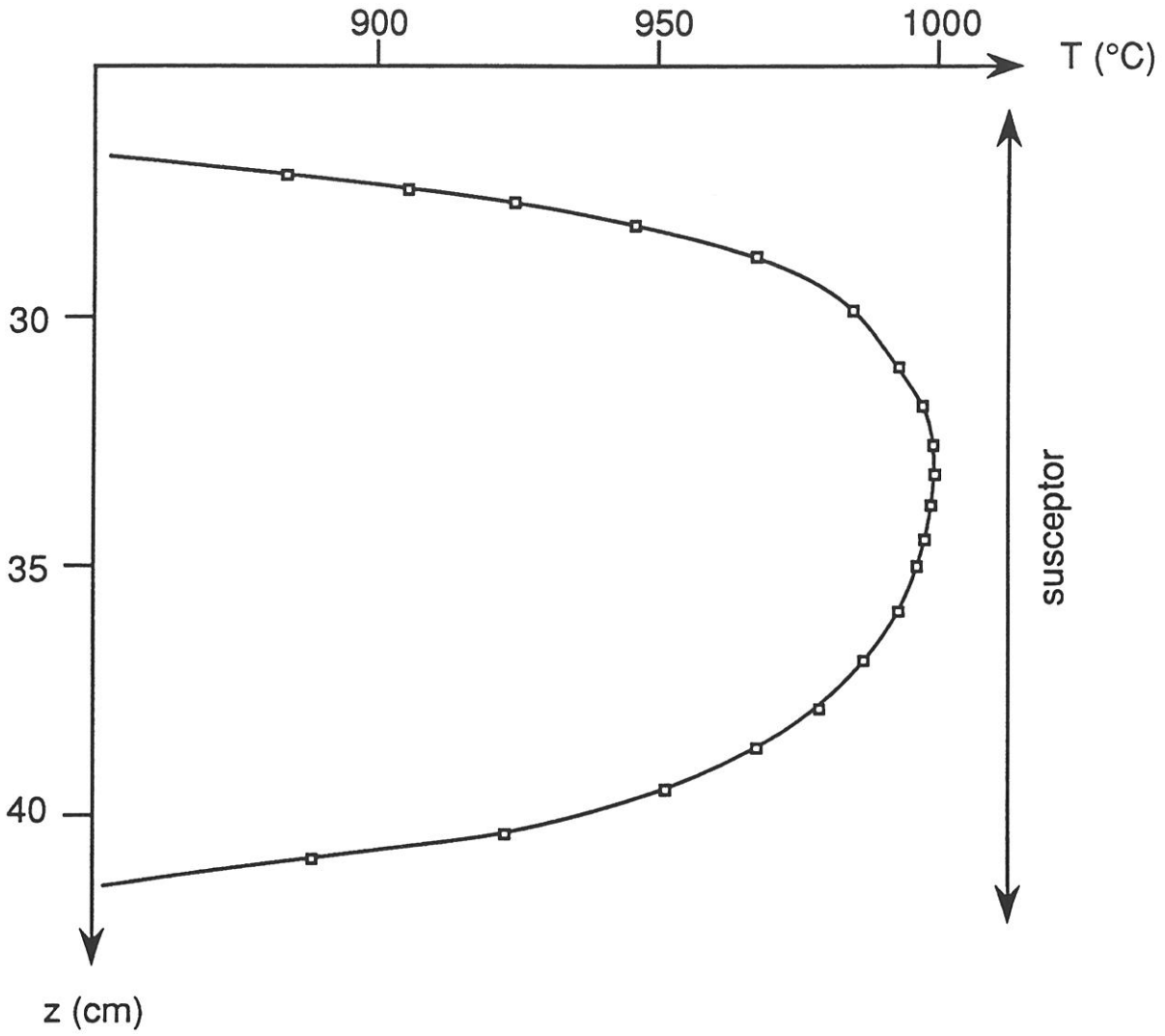

Fig. A4 : Profil de température à T_R=1000°C (P=2kPa, Q_{H_2} =200sccm) dans le réacteur (zone du susceptor)

ANNEXE B

Titre : **CALCUL DES COEFFICIENTS DE DIFFUSION**

ANNEXE B

CALCUL DES COEFFICIENTS DE DIFFUSION

1- LES DIFFERENTS MODES DE DIFFUSION DANS LES PORES

La diffusion est le mode de transport qui se produit en absence de convection (vitesse moyenne des particules composant le système nulle). Elle peut avoir pour origine des gradients de pressions partielles, de température, de concentration ou d'une force extérieure (champ électrique, champ magnétique).

Dans ce qui suit, on ne considèrera que la diffusion provoquée par un gradient de composition d'une phase gazeuse (i.e pression partielle ou concentration), dans un système isotherme, isobare et en absence de tout gradient de force extérieure.

Lorqu'un gaz contient plusieurs espèces de molécules dont les pressions partielles varient d'un point à un autre, le phénomène de diffusion qui apparait est un processus qui tend à diminuer les inégalités de composition, suivant ainsi le principe de Le Châtelier. L'explication physique de ce phénomène réside dans la théorie cinétique des gaz : de par l'agitation thermique, il y a davantage de molécules d'une espèce donnée qui se déplacent des régions riches en cette espèce que de molécules du même type en sens inverse. Le flux résultant pour chaque type de molécule va en sens inverse du gradient de composition, i.e dans la direction vers laquelle la composition chute le plus rapidement. La première loi de Fick indique de plus que ce flux est directement proportionnel au gradient de composition :

$$\vec{N_i} = -D_i \vec{\nabla} C_i \qquad (B.1)$$

avec J_i : flux de diffusion de l'espèce i en $mol.m^{-2}.s^{-1}$

D_i : coefficient de diffusion de l'espèce i en $m^2.s^{-1}$

C_i : concentration de l'espèce i en $mol.m^{-3}$

Puisque ce phénomène apparait alors qu'il n'y a pas de convection, on obtient :

$$\sum_i \vec{N}_i = \vec{0} \qquad \text{(B.2)}$$

Etudions plus précisement le cas de la diffusion dans un pore rectiligne cylindrique de longueur L et diamètre Φ, et ne considérons que la diffusion axiale (figure B.1). L'écriture de (B.1) se simplifie par la projection de N_i sur l'axe de symétrie du pore, orienté suivant z :

$$N_i = -D_i \frac{\partial C_i}{\partial z} \qquad \text{(B.3)}$$

Deux mécanismes différents de diffusion peuvent alors se présenter :

a) dans le cas le plus courant, la diffusion est limitée par les chocs incessants des molécules entre elles : c'est le régime moléculaire ou régime de Fick

b) si le libre parcours moyen des molécules (distance moyenne séparant deux chocs consécutifs d'une molécule avec une autre) devient grand devant la dimension moyenne de la section droite du pore (ici le diamètre du pore), la diffusion devient limitée par les chocs des molécules avec les parois internes du pore : c'est le régime de Knudsen.

Ce deuxième mode de diffusion n'apparaît que dans des conditions extrèmes (diamètre de quelque microns, haute température et basse pression) que l'on atteint en CVI.

Il existe des conditions pour lesquelles les deux mécanismes interviennent simultannément. Leur couplage obéit à la loi de Bosanquet [1-2] :

$$\frac{1}{D_i} = \frac{1}{D_{i,F}} + \frac{1}{D_{i,K}} \qquad \text{(B.4)}$$

avec D_i : coefficient de diffusion résultant du couplage des deux modes de diffusion (en $m^2.s^{-1}$)

$D_{i,F}$: coefficient de diffusion de Fick en ($m^2.s^{-1}$)

$D_{i,K}$: coefficient de diffusion de Knudsen (en $m^2.s^{-1}$)

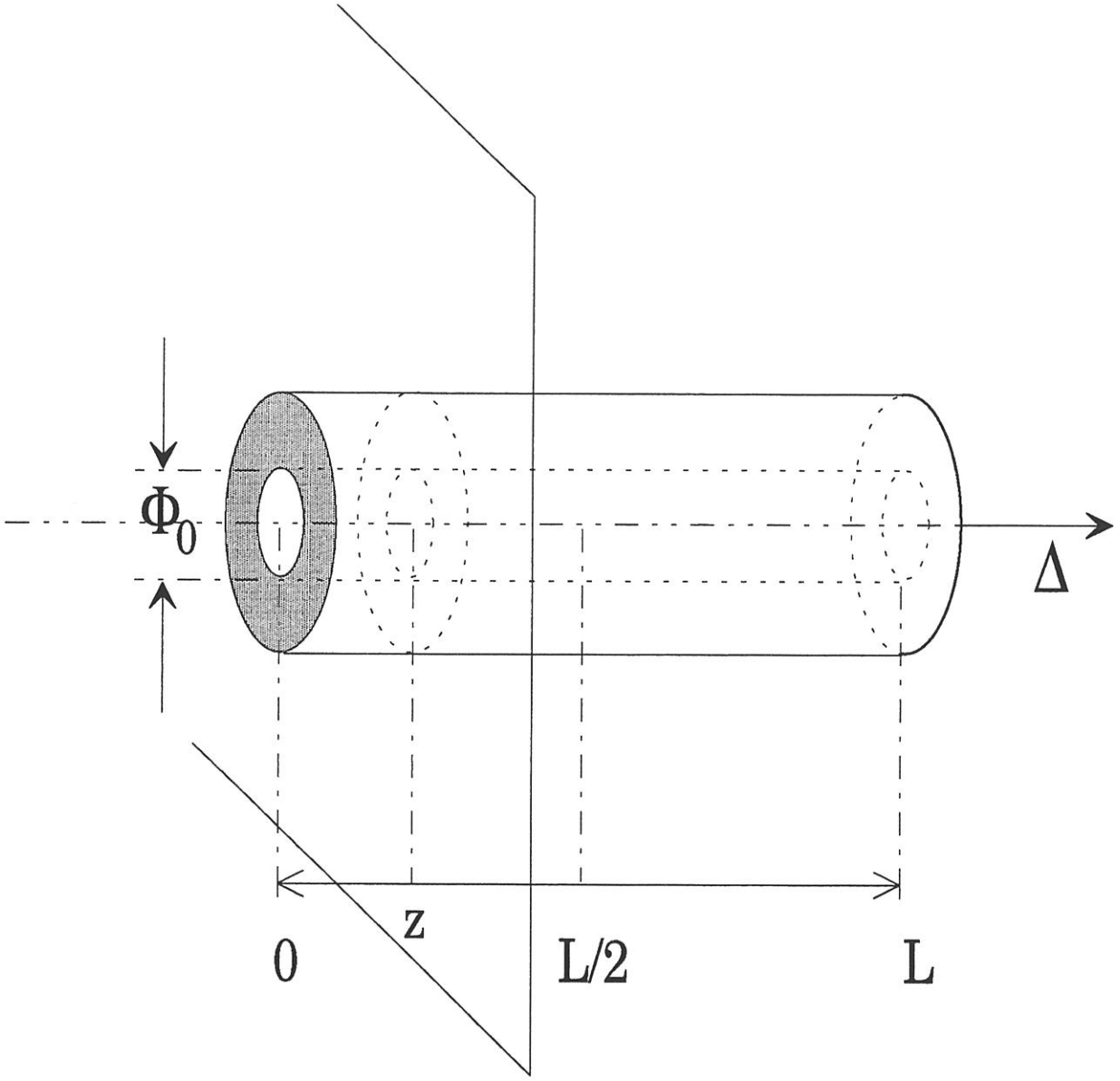

Figure B.1 : Représentation schématique d'un pore rectiligne cylindrique de diamètre Φ et de longueur L

2- ESTIMATION DES COEFFICIENTS DE DIFFUSION DE FICK

2.1- Estimation des coefficients de diffusion pour les mélanges binaires

Il existe de nombreuses méthodes de mesure des coefficients de diffusion dans les gaz, mais les mesures sont difficiles et encore peu précises [3]. En particulier, très peu de mesures des coefficients de diffusion à haute température ont été entreprises. Il faut donc la plupart du temps estimer ces coefficients.

2.1.1- Formule de Hirschfelder

En effectuant divers calculs à partir du potentiel de Lennard-Jones, afin de tenir compte des forces attractives et répulsives des molécules, Hirschfelder et al. [4-5] ont abouti à une formule permettant d'estimer les coefficients de diffusion de Fick pour un mélange binaire entre les espèces i et j :

$$D_{i,j} = 1.858\ 10^{-27} \frac{T^{3/2}}{P\ \sigma_{i,j}^{2}\ \Omega_D} \left[\frac{1}{M_i} + \frac{1}{M_j} \right]^{1/2} \qquad \text{(B.5)}$$

avec $D_{i,j}$: coefficient de diffusion (en $m^2.s^{-1}$)

T : température absolue (en K)

P : pression absolue (en atm)

M : masse molaire (en $g.mol^{-1}$)

$\sigma_{i,j}$: diamètre de collision moyen (en m)

Ω_D : Integrale de collision de Lennard-Jones, sans dimension

L'intégrale de collision est une fonction du facteur adimensionnel $T^* = kT/\varepsilon_{i,j}$ où k est la constante de Boltzman. Elle a été calculée pour de nombreux T^* par Hirschfelder, ce qui permet de la déterminer par interpolation linéaire (voi. Table B.1). Il est à noter que puisque Ω_D dépend de la température, $D_{i,j}$ n'est pas proportionnel à $T^{3/2}$.

$\sigma_{i,j}$ et $\varepsilon_{i,j}$ sont des constantes intervenant directement dans l'expression décrivant le potentiel de Lennard-Jones :

Liste des valeurs de l'intégrale de collision en fonction de $T^* = kT/\varepsilon$

Ω_D	T^*	Ω_D	T^*
000,30	2,6620	002,70	0,9770
000,35	2,4760	002,80	0,9672
000,40	2,3180	002,90	0,9576
000,45	2,1840	003,00	0,9490
000,50	2,0660	003,10	0,9406
000,55	1,9660	003,20	0,9328
000,60	1,8770	003,30	0,9256
000,65	1,7980	003,40	0,9186
000,70	1,7290	003,50	0,9120
000,75	1,6670	003,60	0,9058
000,80	1,6120	003,70	0,8998
000,85	1,5620	003,80	0,8942
000,90	1,5170	003,90	0,8888
000,95	1,4760	004,00	0,8836
001,00	1,4390	004,10	0,8788
001,05	1,4060	004,20	0,8740
001,10	1,3750	004,30	0,8694
001,15	1,3460	004,40	0,8652
001,20	1,3200	004,50	0,8610
001,25	1,2960	004,60	0,8568
001,30	1,2730	004,70	0,8530
001,35	1,2530	004,80	0,8492
001,40	1,2330	004,90	0,8456
001,45	1,2150	005,00	0,8422
001,50	1,1980	006,00	0,8124
001,55	1,1820	007,00	0,7896
001,60	1,1670	008,00	0,7712
001,65	1,1530	009,00	0,7556
001,70	1,1400	010,00	0,7424
001,75	1,1280	020,00	0,6640
001,80	1,1160	030,00	0,6232
001,85	1,1050	040,00	0,5960
001,90	1,0940	050,00	0,5756
001,95	1,0840	060,00	0,5596
002,00	1,0750	070,00	0,5464
002,10	1,0570	080,00	0,5352
002,20	1,0410	090,00	0,5256
002,30	1,0260	100,00	0,5130
002,40	1,0120	200,00	0,4644
002,50	0,9996	400,00	0,4170
002,60	0,9878		

Table B.1

$$\Psi_{i,j}(r) = 4\,\varepsilon_{i,j}\left[\left(\frac{\sigma_{i,j}}{r}\right)^{12} - \left(\frac{\sigma_{i,j}}{r}\right)^{6}\right] \qquad \text{(B.6)}$$

avec

$\Psi_{i,j}(r)$: énergie potentielle du système composé de deux molécules (en J)

$\varepsilon_{i,j}$: maximum de l'énergie d'attraction entre les deux molécules (en J)

$\sigma_{i,j}$: diamètre moyen de collision (en m)

r : distance séparant les deux molécules (en m).

Les constantes de Lennard-Jones pour le mélange binaire i,j peuvent être évaluées à partir des caractéristiques de chaque constituant pur, selon

$$\sigma_{i,j} = \frac{\sigma_i + \sigma_j}{2} \qquad \text{(B.7)}$$

$$\frac{\varepsilon_{i,j}}{k} = \left[\frac{\varepsilon_i}{k} \cdot \frac{\varepsilon_j}{k}\right]^{1/2} \qquad \text{(B.8)}$$

Enfin, pour chaque constituant, le diamètre de collision et la constante de force de Lennard-Jones sont disponibles dans des tables [6] ou peuvent être estimés par [7-8] :

$$\sigma = 0{,}833 * (V_c)^{1/3} \qquad \text{(B.9)}$$

ou

$$\sigma = 1{,}18 * (V_b)^{1/3} \qquad \text{(B.10)}$$

et

$$\frac{\varepsilon}{k} = 0{,}75\,T_c \qquad \text{(B.11)}$$

ou

$$\frac{\varepsilon}{k} = 1{,}15\,T_b \qquad \text{(B.12)}$$

ou

$$\frac{\varepsilon}{k} = 1{,}92\,T_m \qquad \text{(B.13)}$$

avec σ : diamètre de collision (en 10^{-10} m)

ε : maximum de l'énergie d'attraction entre deux molécules (en J)

k : constante de Boltzman (en $J.K^{-1}$)

V_c : volume molaire critique (en $cm^3.mol^{-1}$)

V_b : volume molaire au point d'ébulition normale (en $cm^3.mol^{-1}$)

T_c : température critique (en K)

T_b : température d'ébulition normale (en K)

T_m : température de fusion (en K).

C'est ainsi que de nombreuses valeurs de ε et σ ont été déterminées. Les valeurs que l'on peut trouver et qui nous interresse dans le cadre de cette étude sont rassemblées dans la table B.2.

Des constantes de Lennard-Jones sont aussi utilisées pour calculer la viscosité des gaz (théories très similaires). Bien que leur valeur diffère quelque peu des constantes de diffusion, on peut les utiliser faute de mieux.

Comparons les valeurs estimées par la formule de Hirschfelder et les valeurs mesurées pour le système hygrogène/argon à pression atmosphérique :
Les quatres valeurs expérimentales sont :

T = 242,2 K	$D_{mes} = 0{,}562\ 10^{-4}$ $m^2.s^{-1}$
T = 448 K	$D_{mes} = 1{,}76\ 10^{-4}$ $m^2.s^{-1}$
T = 806 K	$D_{mes} = 4{,}86\ 10^{-4}$ $m^2.s^{-1}$
T = 1069 K	$D_{mes} = 8{,}00\ 10^{-4}$ $m^2.s^{-1}$

D'après la table B.2, nous trouvons

$\sigma_{H2} = 2{,}827\ 10^{-10}$ m $\qquad$ $\sigma_{Ar} = 3{,}542\ 10^{-10}$ m

$(\varepsilon/k)_{H2} = 59{,}7$ K $\qquad$ $(\varepsilon/k)_{Ar} = 93{,}3$ K

soit

$\sigma = 3{,}185\ 10^{-10}$ m $\qquad$ $(\varepsilon/k) = 74{,}6$ K

Liste des valeurs du diamètre de collision σ et de la constante de force ε/k, utilisés dans la formule de Hirschfelder

Symbole	Nom	σ (10^{-10} m)	ε/k (K)
Ar	Argon	3,542	93,3
He	Helium	2,551	10,22
BF_3	Trifluorure de Bore	4,98	186,3
CH_4	Méthane	3,758	148,6
CO	Monoxyde de carbone	3,690	91,7
CO_2	Dioxyde de carbone	3,941	195,2
C_3H_8	Propane	5,118	273,1
HCl	Chlorure d'hydrogène	3,339	344,7
HF	Fluorure d'hydrogène	3,148	330,0
H_2	Hydrogène	2,827	59,7
H_2O	Eau	2,641	809,1
NH_3	Ammoniac	2,900	558,3
$ZrCl_4$	Térachlorure de Zirconium	6,100	1363,2
YCl_3	Trichlorure d'Yttrium	5,269	2047,0

Table B.2

Pour T = 242,2 K, kT/ε = 3,24 d'où par interpolation à partir de la table B.1 , on trouve Ω_D = 0,92954 , ce qui donne $D_{est} = 0{,}538\ 10^{-4}\ m^2.s^{-1}$, soit une erreur de -4%.

De même pour les autres températures

T = 448 K $D_{est} = 1{,}55\ 10^{-4}\ m^2.s^{-1}$, soit une erreur de -12%,
T = 806 K $D_{est} = 4{,}13\ 10^{-4}\ m^2.s^{-1}$, soit une erreur de -15%,
T = 1069 K $D_{est} = 6{,}55\ 10^{-4}\ m^2.s^{-1}$, soit une erreur de -18%.

Cette comparaison est représentative de la qualité de l'estimation des coefficients de diffusion. Elle est en général très bonne à température ambiante (<= 5%), mais se dégrade pour les températures plus élevées (domaine qui nous intéresse). Cet écart s'explique par le fait que les coefficients de diffusion sont expérimentalement proportionnels à T^n, n variant suivant les systèmes de 1,2 à 2,0 : pour des températures élevées, la qualité de la prédiction passe par une bonne adéquation entre les exposants théoriques et expérimentaux de la température.

A hautes températures, la formule de Hirschfelder et les formules qui vont suivre, doivent être simplement considéré comme des moyens d'estimer l'ordre de grandeur des coefficients de diffusion.

2.1.2 Formules semi-empiriques

Lorsque les constantes ε et σ d'une molécule ne peuvent être estimées, on peut toujours employer des equations semi-empiriques.

La première proposée par Fuller et al. [9-10] provient d'un affinement de résultats expérimentaux :

$$D_{i,j} = \frac{10^{-9}\, T^{3/2}}{P\left((\Sigma v)_i^{1/3} + (\Sigma v)_j^{1/3} \right)^2} \left[\frac{1}{M_i} + \frac{1}{M_j} \right]^{1/2} \qquad \text{(B.14)}$$

avec $D_{i,j}$: coefficient de diffusion (en $m^2.s^{-1}$)

T : température absolue (en K)

M : masse molaire (en $g.mol^{-1}$)

(Σv) : volume de diffusion (en m^3.kgmol soit 10^{-3} $cm^3.mol^{-1}$)

Quelques volumes moléculaires de diffusion sont donnés dans la table B.3. Pour les autres, il faut calculer le volume moléculaire en sommant les volumes atomiques de tous les atomes composant la molécule (volumes atomiques listés dans la table B.3). Le nombre de volumes atomiques donnés par la table reste limité (en particulier manquent Si, B, Zr, Y, F ...)

Comparaison entre les valeurs mesurées et estimées pour le système hygrogène/ argon à pression atmosphérique pour les températures de T = 242,2 K; T = 448 K; T = 806 K et T = 1069 K. D'après la table B.3,

$(\Sigma v)_{H2}$ = 7,.07 $cm^3.mol^{-1}$ et $(\Sigma v)_{Ar}$ = 20,1 $cm^3.mol^{-1}$, d'où

T = 242,2 K $D_{est} = 0{,}5008\ 10^{-4}\ m^2.s^{-1}$, soit une erreur de -11%,

T = 448 K $D_{est} = 1{,}47\ 10^{-4}\ m^2.s^{-1}$, soit une erreur de -16%,

T = 806 K $D_{est} = 4{,}11\ 10^{-4}\ m^2.s^{-1}$, soit une erreur de -15%,

T = 1069 K $D_{est} = 6{,}73\ 10^{-4}\ m^2.s^{-1}$, soit une erreur de -17%.

Une deuxième formule semi-empirique dérivant de la théorie cinétique des gaz a été proposée par Gilliland [11] la proposa en 1934 :

$$D_{i,j} = 4.300\ 10^{-7} \frac{T^{3/2}}{P\left(v_i^{1/3} + v_j^{1/3}\right)^2} \left[\frac{1}{M_i} + \frac{1}{M_j}\right]^{1/2} \qquad \text{(B.15)}$$

avec $D_{i,j}$: coefficient de diffusion (en $m^2.s^{-1}$)

T : température absolue (en K)

M : masse molaire (en $g.mol^{-1}$)

v : volume molaire au point d'ébulition normale (en $cm^3.mol^{-1}$)

Les valeurs de v sont directement obtenues par la table B.4 ou par sommation des volumes atomiques (listés dans cette table) de tous les atomes composant la molécule.

Liste des volumes de diffusion pour quelques molécules simples se rapportant à cette étude, pour utilisation de l'équation de Fuller

Symbole	Nom	Σv ($cm^3.mol^{-1}$)
H_2	Hydrogène	7,07
He	Helium	2,88
Ar	Argon	16,1
CO	Monoxyde de carbone	18,9
CO_2	Dioxyde de carbone	26,9
H_2O	Eau	12,7
NH_3	Ammoniac	14,9

Liste de quelques volumes de diffusion atomiques se rapportant à cette étude, pour utilisation de l'équation de Fuller

Symbole	Nom	v ($cm^3.mol^{-1}$)
H	Elément hydrogène	1,98
C	Carbone	16,5
O	Oxygène	5,48
N	Elément Azote	5,69
Cl	Element chlore	19,5

Table B.3

Liste des volumes molaires au point d'ébulition normale pour quelques molécules se rapportant à cette étude, en vue de l'utilisation de l'équation de Gilliland

Symbole	Nom	v ($cm^3.mol^{-1}$)
H_2	Hydrogène	14,3
CO	Monoxyde de carbone	30,7
CO_2	Dioxyde de carbone	34,0
H_2O	Eau	18,9

Liste des volumes atomique permettanr de calculer le volume molaire au point d'ébulition normale pour les molécules se rapportant à cette étude, en vue de l'utilisation de l'équation de Gilliland

Symbole	Nom	v ($cm^3.mol^{-1}$)
H	Elément hydrogène	3,7
C	Carbone	14,8
O	Oxygène	12,8
N	Elément Azote	15,6
	Dans amine primaire	10,5
F	Fluor	8,7
Cl	Chlore terminal comme dans R-Cl	21,6
Cl	Chlore median comme dans R-CHCl-R'	24,6
Si	Silicium	32,0

Table B.4

Comparaison entre les valeurs mesurées et estimées pour le système hygrogène/ ammoniac à pression atmosphérique :

Les cinq valeurs expérimentales sont :

$T = 263$ K $\quad D_{mes} = 0{,}580\ 10^{-4}\ m^2.s^{-1}$

$T = 298$ K $\quad D_{mes} = 0{,}78\ 10^{-4}\ m^2.s^{-1}$

$T = 358$ K $\quad D_{mes} = 1{,}09\ 10^{-4}\ m^2.s^{-1}$

$T = 473$ K $\quad D_{mes} = 1{,}86\ 10^{-4}\ m^2.s^{-1}$

$T = 533$ K $\quad D_{mes} = 2{,}15\ 10^{-4}\ m^2.s^{-1}$

D'après la table B.4, nous trouvons

$v_{H2} = 14{,}3\ cm^3.mol^{-1}$ et $v_{NH3} = (10{,}5 + 3*3{,}7) = 21{,}6\ cm^3.mol^{-1}$,

soit en aplliquant (B.14) :

$T = 263$ K $\quad D_{est} = 0{,}505\ 10^{-4}\ m^2.s^{-1}$, soit une erreur de -14%

$T = 298$ K $\quad D_{est} = 0{,}609\ 10^{-4}\ m^2.s^{-1}$, soit une erreur de -22%

$T = 358$ K $\quad D_{est} = 0{,}801\ 10^{-4}\ m^2.s^{-1}$, soit une erreur de -27%

$T = 473$ K $\quad D_{est} = 1{,}22\ 10^{-4}\ m^2.s^{-1}$, soit une erreur de -35%

$T = 533$ K $\quad D_{est} = 1{,}46\ 10^{-4}\ m^2.s^{-1}$, soit une erreur de -32%

L'écart est sensiblement important car le coeffichient de diffusion expérimental varie jusqu'à 473 K en T^2, puis a tendance à revenir à $T^{3/2}$ pour la plus haute température. On peut donc penser qu'il y aura un rattrapage vers des températures plus élevées.

2.2- Estimation des coefficients de diffusion pour un mélange gazeux à multicomposants

Pour les gaz, les coefficients de diffusion binaire de Fick $D_{i,j}$ sont normalement supposés indépendant de la composition de la phase gazeuse. Avec cette approximation, la diffusion moléculaire d'une espèce i suivant l'axe z du pore, dans un mélange gazeux comportant n_g constituants, est décrite par la formule de Stephan-Maxwell

[7] :

$$\frac{\partial C_i}{\partial z} = \sum_{j=1}^{n_g} \frac{1}{D_{i,j}} \left(x_i N_j - x_j N_i \right) \qquad \text{(B.16)}$$

avec C_i : concentration de l'espèce i (en $mol.m^{-3}$)

N_j : flux molaire absolu de l'espèce j (en $mol.m^{-2}.s^{-1}$)

x_j : fraction molaire de l'espèce j, sans dimension

Le flux molaire absolu de l'espèce i peut aussi s'écrire sous la forme :

$$N_i = -D_{i,F} \frac{\partial C_i}{\partial z} + x_i \sum_{j=1}^{n_g} N_j \qquad \text{(B.17)}$$

avec $D_{i,F}$: coefficient de diffusion moléculaire effectif de l'espèce i dans le mélange gazeux (en $m^2.s^{-1}$)

Dans cette expression, le premier terme représente le flux de diffusion pure, et le second est le flux d'entrainement ou flux de Stephan. En combinant (B.16) et (B.17), on obtient :

$$D_{i,F} = \frac{N_i - x_i \sum_{j=1}^{n_g} N_j}{\sum_{j=1}^{n_g} \frac{x_i N_j - x_j N_i}{D_{i,j}}} \qquad \text{(B.18)}$$

Cette dernière formule montre que D dépend à la fois de la composition et des flux locaux, ce qui la rend difficile à utiliser.

Si les gradients de composition ne sont sont pas trop important, on peut utiliser une équation approchante, en supposant que chaque espèce i diffuse à travers un mélange gazeux stagnant ($N_j = 0$ pour $j \neq i$) de sorte qu'en mettant (B.18) sous la forme :

$$D_{i,F} = \frac{N_i - x_i N_i - x_i \sum_{\substack{j=1 \\ j<>i}}^{n_g} N_j}{\sum_{j=1}^{n_g} \frac{x_i N_j - x_j N_i}{D_{i,j}}} \qquad (B.19)$$

on puisse écrire :

$$\frac{1-x_i}{D_{i,F}} = \sum_{\substack{j=1 \\ j<>i}}^{n_g} \frac{x_j}{D_{i,j}} \qquad (B.20)$$

3- ESTIMATION DES COEFFICIENTS DE DIFFUSION DE KNUDSEN

Considérons un pore rectiligne de périmètre H, de section A variables et de longueur L. Appliquons aux extrémités de ce pore une différence de concentration en une espèce gazeuse i, dans des conditions physiques telles que le libre parcours moyen des molécules i soit largement supérieur à H. Dans ces conditions, Knudsen a montré [12] que :

$$N_{i,o} A_o = - N_{i,L} A_L = - \frac{4}{3} \frac{v_a}{\int_0^L \frac{H}{A^2} dz} (C_{i,L} - C_{i,0}) \qquad (B.21)$$

avec $N_{i,0}$: flux molaire absolu de l'espèce i à l'entrée du pore, projeté sur l'axe Δ (fig. AI.1) (en $mol.m^{-2}.s^{-1}$)

A : aire de la section droite du pore (en m^2)

P : périmètre de la section droite du pore (en m)

$C_{i,0}$: concentration de l'espèce i à l'entrée du pore (en $mol.m^{-3}$)

v_a : vitesse moyenne des molécules de l'espèce i (en $m.s^{-1}$).

Sous forme locale, cette équation se traduit par :

$$N_i = -\frac{4}{3} v_a \frac{H}{A} \frac{\partial C_i}{\partial z} \qquad (B.22)$$

L'equation (B.22) est similaire à la première loi de Fick (B.1), de sorte que l'on puisse assimiler ce mode de transport à une diffusion avec le coefficient de diffusion $D_{i,K}$ suivant :

$$D_{i,K} = \frac{4}{3} v_a \frac{H}{A} \qquad (B.23)$$

avec $D_{i,K}$: coefficient de diffusion de Knudsen de l'espèce i (en $m^2.s^{-1}$).

La théorie cinétique des gaz permet de calculer v_a uniquement en fonction de la température du gaz et de sa masse molaire :

$$v_a = \left[\frac{8 \boldsymbol{R} T}{\pi M_i}\right]^{1/2} \qquad (B.24)$$

avec T : température du gaz (en K)

$\boldsymbol{R}$: constante des gaz parfait (8.314 $J.mol^{-1}.K^{-1}$)

M_i : masse molaire de l'espèce i (en $kg.mol^{-1}$)

La quantité définie par 4 fois le rapport de la surface de la section droite sur son périmètre s'appelle la diamètre hydraulique, et sera noté Φ_h (en m). Dans le cas d'un pore rectiligne cylindrique, où la section droite est un disque de diamètre Φ (en m), on obtient $\Phi_h = \Phi$, de sorte que le coefficient de diffusion de Knudsen s'écrive :

$$D_{i,K} = \frac{\Phi}{3} \left[\frac{8 \boldsymbol{R} T}{\pi M_i}\right]^{1/2} \qquad (B.25)$$

Pour un pore rectiligne dont la section droite est un rectangle de hauteur h et de largeur l (en m), le coefficient de diffusion de Knudsen se calcule par :

$$D_{i,K} = \frac{2hl}{3(h+l)} \left[\frac{8 \boldsymbol{R} T}{\pi M_i} \right]^{1/2} \qquad (B.26)$$

Dans le cas particulier où l >> h (pore formé par deux surface plane très rapprochées), $D_{i,K}$ devient

$$D_{i,K} = \frac{2h}{3} \left[\frac{8 \boldsymbol{R} T}{\pi M_i} \right]^{1/2} \qquad (B.27)$$

Enfin, si l'on considère un pore rectiligne dont la section est carrée (h=l), de coté a (en m), le coefficient de diffusion devient :

$$D_{i,K} = \frac{a}{3} \left[\frac{8 \boldsymbol{R} T}{\pi M_i} \right]^{1/2} \qquad (B.28)$$

Ainsi, pour la diffusion de Knudsen, un pore cylindrique de diamètre Φ est équivalent à un pore de section carré de coté a=Φ.

Exemple de calcul

Considérons d'une part la diffusion en régime de Knudsen de l'espèce $TiCl_4$ dans un pore cylindrique de diamètre Φ , et d'autre par la diffusion de Fick de $TiCl_4$ dans un mélanbe binaire avec CH_4. La masse molaire de $TiCl_4$ étant de 189,9 10^{-3}kg.mol^{-1}, on obtient :

$$D_K = 3{,}520\ \Phi\ T^{1/2} \qquad (B.29)$$

En appliquant la formule de Hirschfelder, on obtient :

$$D_F = 2{,}43\ 10^{-9}\ P^{-1}\ T^{3/2} \qquad (B.30)$$

La transition entre le régime de diffusion de Fick et de Knudsen est régie par l'équation suivante résultant de l'égalité des deux coefficients :

$$\Phi P = 6{,}90\ 10^{-9}\ T \qquad (B.31)$$

Trois types de transition peuvent survenir :

- transition en pression :

Lorsque l'on passe des hautes pressions vers les basses pressions, on passe du régime de Fick au régime de Knudsen. C'est ainsi que, pour une température de 1273 K et un pore de 100 µm, le régime de Knudsen prédomine pour des pressions inférieures à 9 kPa.

- transition en diamètre :

Lorsque l'on passe des pores à diamètre élevé vers des pores à faible diamètre, on passe du régime de Fick au régime de Knudsen. C'est ainsi que, pour une température de 1273 K et une pression de 5 kPa, le régime de Knudsen prédomine pour les pores dont le diamètre est inférieur à 180 µm.

- transition en température :

On peut trouver des conditions particulières pour lesquelles une transition en température est envisageable : lorsque l'on passe des basses températures vers les hautes températures, on passe du régime de Fick au régime de Knudsen. C'est ainsi que, pour un pore dont le diamètre est de 100 µm et pour une pression de 8 kPa, le régime de Knudsen prédomine pour les températures supérieures à 1160 K.

REFERENCES

[1] C.H. Bosanquet; British T.A. Rept. BR 507; 1944

[2] R.B. Evans, G.M. Watson, E.A. Mason; "Gaseous diffusion in porous media at uniform pressure"; J. Chem. Phys.; Vol. 35; N° 6; 1961

[3] J. Salvinien, B. Brun, J. Appell; "Mesure des coefficients de diffusion , Séparation chimique", Les Techniques de l'Ingénieurs; p. 1515

[4] J.O. Hirschfelder, R.B. Bird, E.L. Spotz; Chem. Rev.; Vol. 44; p. 205; 1949

[5] J.O. Hirschfelder, C.F. Curtis, R.B. Bird; "Molecular Theory of Gases and Liquids"; Wiley; New York; 1954

[6] R. A. Svehla; NASA Tech. Rep. R-132; Lewis research Center; Cleveland (OHIO); 1962

[7] R.B. Bird, W.E. Stewart, E.N. Lightfoot; "Transport Phenomena"; J. Wiley et Sons eds.; 1960

[8] R.C. Reid, J.M. Prausnitz, B.E. Poling; "The properties of gases and liquids", 4th ed.; Mac Graw Hill Book company eds; 1987

[9] E.N. Fuller, P.D. Schettler, J.C. Giddings; "A New Method for prediction of binary gas-phase diffusion coefficients"; Ind. Eng. Chem.; Vol. 56; N° 5; 1966

[10] E.N. Fuller, P.D. Schettler, J.C. Giddings; Ind. Eng. Chem.; Vol. 58; N° 19; 1966

[11] E.R. Gilliland ; Ind. Eng. Chem.; Vol. 26; N° 681; 1934

[12] M. Knudsen; "The Kinetic Theory of Gases", 3rd ed.; Wiley; New York; 1950

ANNEXE C

JUSTIFICATION DE L'HYPOTHESE DU REGIME QUASI-STATIONNAIRE POUR LES TRANSFERTS DE MASSE

Une des justification de cette hypothèse est basée sur une publication de E.E. Petersen [1]. Ce dernier s'est proposé d'aborder l'attaque d'un solide poreux (graphite) par un gaz (monoxyde de carbone) en modélisant plus particulièrement l'attaque d'un pore cylindrique sur la base des hypothèses suivantes :

- le pore est initialement un cylindre de rayon r_0 et de longueur égale à 2L
- les transferts de matière interviennent uniquement sous la forme de diffusion de Fick
- la réaction hétérogène se produisant à la surface interne du pore est une réaction irréversible d'ordre un par rapport à l'espèce réactive
- le pore est symétrique par rapport à son centre et la concentration du gaz réactif (dilué dans un gaz vecteur) aux deux extrémités du pore (constante sur toute la section droite et au cours du temps) est égale à C_0.

L'équation générale à résoudre est :

$$\frac{\partial C}{\partial t} = \frac{D}{r^2} \frac{\partial}{\partial z} \left(r^2 \frac{\partial C}{\partial z} \right) - \frac{2k}{r} C \qquad (C.1)$$

avec D : coefficient de diffusion du réactif dans le mélange binaire constitué par le réactif et le gaz vecteur (en $m^2.s^{-1}$),

k : constante de la cinétique hétérogène du premier ordre (en m.s-1),

r : rayon du pore (en m),

z : distance ou profondeur d'infiltration (en m).

En utilisant les coordonnées réduites, à savoir la concentration réduite Ψ, la distance réduite η, le temps adimensionnel τ, le rayon réduite ξ et le module de Thiele α, définis par :

$$\Psi = \frac{C}{C_0} \qquad (C.2)$$

$$\eta = \frac{x}{L} \qquad (C.3)$$

$$\tau = \frac{Dt}{L^2} \qquad (C.4)$$

$$\alpha = \sqrt{\frac{2k\,L^2}{r_0}} \qquad (C.5)$$

$$\xi = \frac{r}{r_0} \qquad (C.6)$$

l'équation (C.1) s'écrit :

$$\frac{\partial \Psi}{\partial \tau} = \frac{1}{\xi^2} \frac{\partial}{\partial \eta} \left(\xi^2 \frac{\partial \Psi}{\partial \eta} \right) - \alpha^2 \frac{\Psi}{\xi} \qquad (C.7)$$

Pour des temps courts (τ petit), la géométrie est supposée ne pas beaucoup évoluer, de sorte que (C.7) devienne :

$$\frac{\partial \Psi}{\partial \tau} = \frac{\partial^2 \Psi}{\partial \eta^2} - \alpha^2 \Psi \qquad (C.8)$$

Les conditions aux limites se mettent sous la forme :

$$\left[\Psi \right]_{\eta = 0} = 1 \qquad \text{(C.9)}$$

$$\left[\frac{\partial \Psi}{\partial \eta} \right]_{\eta = 1} = 0 \qquad \text{(C.10)}$$

La condition initiale choisie par E. Petersen, consistant à supposer qu'au départ, il n'y a pas d'espèce réactive dans le pore, s'écrit comme suit :

$$\left[\Psi(\tau=0) \right]_{\eta > 0} = 0 \qquad \text{(C.11)}$$

E. Petersen propose la solution suivante :

$$\Psi(\tau, \eta) = \frac{\mathrm{ch}[\, \alpha\, (\, 1-\eta\,)\,]}{\mathrm{ch}[\, \alpha\,]} - \frac{4}{\pi} \sum_{n=0}^{\infty} \frac{(-1)^n \exp\left[- \dfrac{\alpha^2 - (2n+1)^2\pi^2}{4}\, \tau \right] \cos\left[\dfrac{(2n+1)\,(1-\eta)\pi}{2} \right]}{(2n+1)\left[1 + \dfrac{4}{(2n+1)^2\pi^2} \right]} \qquad \text{(C.12)}$$

Dans l'équation (C.12), le terme en sommation ne converge pas lorsque n tend vers l'infini. De plus, pour $\tau = 0$ et $\eta = 1$, l'équation se réduisant à :

$$\Psi(0, 1) = \frac{1}{\mathrm{ch}[\, \alpha\,]} - \frac{4}{\pi} \sum_{n=0}^{\infty} \frac{(-1)^n}{(2n+1)\left[1 + \dfrac{4}{(2n+1)^2\pi^2} \right]} \qquad \text{(C.13)}$$

ne satisfait pas à la condition initiale (équation (C.11)). L'équation (C.12) ne peut donc pas être solution du système d'équations (C.8) à (C.11).

Cette conclusion a conduit à rechercher une solution à ce système, en utilisant la méthode des transformées de Laplace. La solution proposée est la suivante :

$$\Psi(\tau, \eta) = \frac{\mathrm{ch}[\,\alpha\,(1-\eta)\,]}{\mathrm{ch}[\,\alpha\,]} - \frac{4}{\pi} \sum_{n=0}^{\infty} \frac{(-1)^n (2n+1) \exp\left[-\left(\alpha^2 + \frac{(2n+1)^2\pi^2}{4}\right)\tau\right] \cos\left[\frac{(2n+1)(1-\eta)\pi}{2}\right]}{\alpha^2 + \frac{(2n+1)^2\pi^2}{4}} \qquad \text{(C.14)}$$

Il a été vérifié numériquement pour de nombreuses valeurs de α, que cette solution satisfasse la condition initiale.

Le premier terme de l'équation (C.14) représente le profil en concentration à l'état stationnaire (i.e pour $\tau \to \infty$), la géométrie du pore restant constante. L'équation (C.14) permet d'apprécier le temps qu'il faut attendre pour s'approcher de ce profil à une erreur ε près. En particulier, on peut regarder l'écart des valeurs des concentrations pour $\eta = 1$:

$$\Psi(\tau, \eta) = \frac{\mathrm{ch}[\,\alpha\,(1-\eta)\,]}{\mathrm{ch}[\,\alpha\,]} + \varepsilon \qquad \text{(C.15)}$$

L'équation (C.14) montre que la convergence de cette équation est accélérée lorsque α augmente. Le cas α proche de zéro est donc le plus défavorable à l'hypothèse du régime stationnaire. Pour l'infiltration, ce cas correspond au cas d'un profil très plat pour la concentration de l'espèce source ($\Psi_{\eta=1} \approx \Psi_{\eta=0}$), et donc à une infiltration aisée.

L'utilisation de (C.14) donne les résultats suivants :

$\alpha = 10^{-2}$ $\quad \Psi(3)_{\eta=1} = 1,0 - 8\ 10^{-4} + \ldots .$

$\alpha = 1$ $\quad \Psi(2)_{\eta=1} = 0,65 - 9\ 10^{-4} + \ldots .$

$\alpha = 10^{-2}$ $\quad \Psi(0,2)_{\eta=1} = 9.10^{-5} - 3,9\ 10^{-11} + \ldots .$

Dans les conditions les plus défavorables, le profil en concentration est égal à 10^{-3} près du profil stationnaire au bout de $\tau = 3$. Cela correspond, dans le cas, par exemple de l'infiltration de carbure de silicium à partir du mélange MTS-H_2 à des temps inférieurs à 10 s. Au cours de cette durée, la géométrie de pore ne s'est pratiquement pas modifiée. Par conséquance, le découplage des variables de temps et d'espace dans la modélisation de l'infiltration d'un pore rectiligne est acceptable.

REFERENCE

[1] E.E. Petersen, "Reaction of Porous Solid", ALChE Journal, Vol. 3, N° 4, pp. 443-448, 1957

ANNEXE D

METHODE DES DIFFERENCES FINIES

Cette méthode est très souvent utilisée et se trouve décrite dans de nombreux ouvrages [1,2]. Soit une fonction f multivariable. Soit x l'un de ces variables. Cette fonction peut être développé en série de Taylor autour du point x_0 :

$$f(x_0+h) = f(x_0) + h\left[\frac{\partial f}{\partial x}\right]_{x_0} + h^2/2\left[\frac{\partial^2 f}{\partial x^2}\right]_{x_0} + \ldots \qquad (D.1)$$

Lorsque l'on discrétise cette fonction suivant des valeurs de x régulièrement espacé par un intervalle h, la méthode consiste à faire une approximation sur les dérivées partielles par rapport à la variable x. Les approximations utilisées dans ce mémoire sont :

- dérivée partielle par une différence à droite :

$$\left[\frac{\partial f}{\partial x}\right]_{x_0} = \frac{f(x_0+h) - f(x_0)}{h} \qquad (D.2)$$

- dérivée seconde partielle sur trois point :

$$\left[\frac{\partial^2 f}{\partial x^2}\right]_{x_0} = \frac{f(x_0+h) + f(x_0-h) - 2f(x_0)}{h^2} + \varepsilon(h^2) \qquad (D.3)$$

avec $\varepsilon(h)$ et $\varepsilon(h^2)$, erreur d'ordre un et d'ordre deux engendrées par l'approximation.

REFERENCES

[1] M. Sibony, J.-Cl. Mardon "Analyse Numérique I - Systèmes Linéaires et Non Linéaires", Hermann, Paris, 1988

[2] M. Sibony, J.-Cl. Mardon "Analyse Numérique II - Aproximations et Equations Différentielles", Hermann, Paris, 1988

ANNEXE E

METHODE DU GRADIENT

Cette annexe décrit de manière générale une des méthodes mathématiques intervenant dans le calcul des profils en concentration pour chacune des n_g espèces gazeuses à un instant t donné.

La résolution du système d'équations différentielles partielles non linéaires, permettant d'obtenir ces profils, se transforme, après avoir discrétiser le pore en n_z intervalles réguliers de longueur Δz, appliquer la méthode des différences finies et utiliser l'algorithme décrit dans le chapitre 1, en une recherche de valeurs propres d'une application $\mathcal{A}$:

$$\mathcal{A}(\underline{x}) = \underline{x} \qquad \text{(E.1)}$$

avec $\mathcal{A}$: application de E -> E

$\underline{x}$: élément de E.

E est un espace à n dimensions de réels. Dans le cadre de cette étude, E est une espace de réels positifs à $n_g*(n_z+1)$ dimensions ou un élement représente la concentration de l'espèce i (i=1, ... , n_g) à la côte $p\Delta z$ (p=0, ... , n_z).

D'après Sibony et J.-Cl. Mardon [1,2], si l'application $\mathcal{A}$ vérifie les relations suivantes, quelquesoient $\underline{x}$ et $\underline{y}$ appartenant à E :

$$\text{a) } (\mathcal{A}(\underline{x})-\mathcal{A}(\underline{y}), \underline{x}-\underline{y}) \geq C \; || \; \underline{x} - \underline{y} \; ||^2 \qquad C > 0 \qquad \text{(E.2)}$$

avec (,) : produit scalaire dans E

|| || : norme associé au produit scalaire

et

$$\text{b) } || \; \mathcal{A}(\underline{x})-\mathcal{A}(\underline{y}) \; || \leq M \; || \; \underline{x} - \underline{y} \; || \qquad M > 0 \qquad \text{(E.3)}$$

alors, pour tout $\underline{b}$ appartenant à E, l'équation

$$\mathcal{A}(\underline{x}) = \underline{b} \qquad \text{(E.4)}$$

admet une solution unique et peut se résoudre par approximations succéssives suivant la méthode du gradient. La recherche des valeurs propres de l'application est équivalente à l'équation (E.4). En effet, l'équation (E.1) peut s'écrire en posant:

$$\mathcal{A}' = A - I \qquad \text{(E.5)}$$

avec I : application identité sur E,

sous la forme:

$$(\mathcal{A}' - I)\,(\underline{x}) = \underline{0} \qquad \text{(E.6)}$$

avec $\underline{0}$: élément nul de E.

La méthode du gradient permet de résoudre (E.4) en utilisant la suite $(\underline{x}_n)$ définie par les itérations :

$$\underline{x}_{n+1} = \underline{x}_n - \rho_0 \,(\, \mathcal{A}(\underline{x}_n) - b \,) \qquad \text{(E.7)}$$

Cette suite converge avec $\underline{x}_0$ et ρ_0 convenablement choisis, ρ_0 étant le facteur d'amortissement ($0 < \rho_0 < 1$).

La procédure du gradient consiste alors à :

i) initialiser $\underline{x}_0$ et choisir ρ_0

ii) appliquer (E.7) jusqu'à ce que le critère de convergence soit atteint.

REFERENCES

[1] M. Sibony, J.-Cl. Mardon "Analyse Numérique I - Systèmes Linéaires et Non Linéaires", Hermann, Paris, 1988

[2] M. Sibony, J.-Cl. Mardon "Analyse Numérique II - Aproximations et Equations Différentielles", Hermann, Paris, 1988

ANNEXE F

Proceedings of the 11th International Conference on CVD, Seattle (K.E. Spear and C.W. Cullen editors), The Electrochemical Society, Pennington (1990)

ON THE MODELING OF THE CHEMICAL VAPOR INFILTRATION OF SiC-BASED CERAMICS IN A STRAIGHT CYLINDRICAL PORE

R. FEDOU, F. LANGLAIS and R. NASLAIN

Laboratoire des Composites Thermostructuraux (UMR 47 CNRS-SEP-UB1), Europarc, 1-3, Avenue Léonard de Vinci, F-33600 Pessac

A chemical vapor infiltration technique is used to densify porous fiber preforms for the preparation of ceramic matrix composites. The proposed numerical modeling is based on Fick and Knudsen diffusive mass transfer in a straight cylindrical pore, including any chemical system and kinetic law. The model is applied to the deposition of SiC-based ceramics from CH_3SiCl_3/H_2 and gives concentration and deposit thickness profiles along the pore at any stage of the densification. The influence of various parameters is shown and compared to preliminary experimental results.

1- INTRODUCTION

The chemical vapor infiltration (CVI) processing of ceramic matrix composites (CMC) is based on the densification of refractory fibrous preforms (e.g. made of carbon, silicon carbide or alumina fibers) by a deposit resulting from a heterogeneous gas-solid chemical reaction taking place within the pore network of the preform. This technique was successfully applied to various refractory matrices such as carbides (SiC, B_4C, TiC), a nitride (BN) and oxides (Al_2O_3, ZrO_2) [1-7]. The choice of convenient infiltration conditions, even in the case of the largely studied SiC matrix, is still empirical owing to the complexity of the actual porous substrates and chemical systems. A thorough study of the infiltration mechanisms with a view to build-up previsional models seemed to be necessary in order to optimize both the homogeneity of CVI-processed composites and the densification kinetics. Such an approach obviously needs the use of model porous substrates. The single straight cylindrical pore, already selected in a few models recently published, was also chosen in the present work [8-13,15-17].

Most recent publications in this field are based on older work carried out by Thiele in the field of theoretical studies on the efficiency of porous catalysts [8]. This author

evolved a 1-D model taking into account the diffusive transfers and the chemical reaction occurring in a cylindrical pore with a constant radius. The analytical solving of mass balance equations in the steady state, resulted in concentration profiles and effective reaction rates as a function of a dimensionless number (i.e. ratio between kinetics constant and diffusion coefficient), presently referred to as the Thiele modulus. The same kind of approach was used for etching chemical reactions, such as gasification of graphite by CO_2. As an example, the model proposed by Peterson permitted to foresee the increase in radius of a cylindrical pore [9]. This author validated the quasi steady-state hypothesis, which assumes that mass transfer is very rapid with respect to variations of the pore geometry.

As far as the more recent CVI modeling is concerned, Fitzer calculated, for the first time, theoretical infiltration depths on the basis of limit values of the Thiele modulus by assuming, as in catalysis, that the infiltration efficiency is given by the ratio between the deposition rate within the pore and the deposition rate at the pore entrance [10]. Van den Brekel et al. proposed a 2-D analytical modeling of the CVD process in a macroscopic cylindrical tube whose radius was assumed not to depend on time [11]. They considered, on the one hand, chemical reactions with orders close to one and, on the other hand, mass transfer occurring only by Fick diffusion. Rossignol et al. has applied this model to CVI in a microscopic cylinder [4]. They introduced Knudsen diffusion, and assumed : (i) reaction order equal to one and (ii) a cylindrical geometry of the pore with a time dependent radius. The last model, applied to the infiltration of various ceramics (SiC and Al_2O_3 for composites, ZrO_2 (Y_2O_3) for electrolytes [12] or porous membranes [13]), dealt with 1-D or quasi 1-D calculations, under the hypothesis of the quasi steady state, taking into account Knudsen diffusion. A few authors introduced in the equation of mass conservation the convection term originating from either mole number variation related to the chemical reaction [8, 13] or forced flow in the porous substrate [14]. In most studies, only the heterogeneous chemical reactions were considered and assumed to be first order with respect to the precursor species [14-17]. However, Lin et al. have shown in their model the influence of reaction orders ranging between 0 and 2, on the deposition profiles [13]. Lastly, Middleman proposed an analytical modeling including, besides the heterogeneous reaction, an homogeneous reaction resulting in the formation of an intermediate species [17].

In most of the previously mentioned models, the variations of the pore geometry during the infiltration process were sometimes pointed out but usually they were not taken into account in the calculations. Nevertheless, the Knudsen diffusion coefficient, and consequently the Thiele modulus, depend on the pore radius, which varies as a

function of both time and spatial coordinates along the pore. The aim of the present contribution was to derive a model which includes : (i) the pore geometry variations, (ii) any chemical mechanisms and (iii) gaseous precursors not necessarily diluted. The influence of the parameters, such as temperature, total pressure and geometry of the pore, was studied for a relatively simple chemical system in order to validate the model and a first experimental comparison is proposed.

2- THEORETICAL MODEL

2.1- Hypotheses

(1) The cylindrical model pore (Φ_0 in diameter and L in length) is assumed to remain straight during the infiltration process. It is open-ended and symmetrical with respect to its center.

(2) The time origin (t = 0) is chosen as corresponding to the first mass transfer steady state, which is supposed to be set up very rapidly with respect to variations of the pore diameter. The infiltration process is considered as a series of quasi-steady states.

(3) Due to the high L/Φ_0 aspect ratio of the studied pore, the model considers only the axial direction. As a consequence, the concentrations of the gaseous species are constant in a cross-section of the pore and, at any time t, depend only on the axial coordinate z (which is defined as the distance from the pore entrance). The pore profile at time t is given by its diameter as a function of z : Φ (z, t). The symmetry of the pore permits study of only the half-pore defined by $0 \leq z \leq L/2$.

(4) The temperature is assumed to be constant not only versus time but also in the whole pore volume.

(5) Mass transfer is only controlled by diffusion processes, forced convection being negligible in small pores. Nevertheless, the convection terms, which result from the mole number changes in the chemical reactions, are considered, but can become zero when the reactive species are highly diluted.

(6) No homogeneous reaction occurs within the pore.

2.2- Basic equations

The time variations of the concentration profiles for the various gaseous species and the deposit thickness profiles can be investigated by solving the mass balance

equations for each species. The conservation equation for species i, resulting from the z-component of the general vector equation of mass transfer in cylindrical coordinates (hypothesis (3)), can be expressed in terms of molar units as follows [18] :

$$\frac{\partial c_i}{\partial t} + \frac{\partial N_i}{\partial z} = R_i \qquad (1)$$

where c_i is the concentration of species i (in mole m^{-3})
N_i is the absolute molar flux of species i (in mole $m^{-2}s^{-1}$)
R_i is an algebraic production term : a source or sink term if the i-species is produced or consumed (in mole $m^{-3}s^{-1}$)

In the hypothesis (2) of steady state, this equation is obviously simplified :

$$\frac{\partial N_i}{\partial z} = R_i \qquad (2)$$

According to hypothesis (5), the absolute molar flux includes a pure diffusion term and a convective term (which is positive if the deposition chemical reaction consumes gaseous molecules and negative in the opposite case) :

$$N_i = -D_i \frac{\partial c_i}{\partial z} + x_i \sum_j N_j \qquad (3)$$

where D_i is the diffusion coefficient of species i (in m^2s^{-1})
x_i is the molar fraction of species i

The term R_i can be deduced from a local treatment, by writing the conservation of mole number of species i over a thin shell of pore (Δz in thickness and $\pi\Phi^2/4$ in section) :

$$\left|\begin{array}{c}\text{Rate of consumption of i}\\ \text{by chemical reaction on the}\\ \text{pore surface}\end{array}\right| = (\text{rate of i in}) - (\text{rate of i out}) \qquad (4)$$

$$\text{i.e.} \quad \nu_i \vartheta \pi\Phi \Delta z = \left(N_i^{in} - N_i^{out} \right) \frac{\pi \Phi^2}{4} \qquad (5)$$

where ν_i is the stoechiometric coefficient of species i in the surface reaction
ϑ is the kinetics of the deposition reaction (in mole $m^{-2}s^{-1}$)

By taking the limit as Δz approaches zero, we obtain a new expression of equation (2) :

$$\frac{\partial N_i}{\partial z} = \frac{4 \nu_i \vartheta}{\Phi} \tag{6}$$

which becomes by using equation (3) :

$$D_i \frac{\partial^2 c_i}{\partial z^2} - \frac{\partial}{\partial z} \left(x_i \sum_j N_j \right) + \frac{4 \nu_i \vartheta}{\Phi} = 0 \tag{7}$$

The diameter of the studied pore can be very small, particularly when the densification is almost achieved. In this case, Knudsen diffusion can replace Fick diffusion. As a consequence, an overall diffusion coefficient must be taken into account, according to Bosanquet definition [19] :

$$\frac{1}{D_i} = \frac{1}{D^\circ_i} + \frac{1}{D_{i,K}} \tag{8}$$

where $D_{i,K}$ is the Knudsen diffusion coefficient of species i

D°_i is the Fick diffusion coefficient of species i in the gaseous mixture,

with $\frac{1}{D^\circ_i} = \frac{1}{1-x_i} \sum_{j <> i} \frac{x_j}{D_{ij}}$ (D_{ij} : binary Fick diffusion coefficient)

The coefficient $D_{i,K}$ and the chemical reaction term being dependent on the pore diameter, the differential equation (7) must be solved with another one which gives the diameter variations versus time for the position z.

$$\frac{\partial \Phi}{\partial t} = - 2 V_s \vartheta \tag{9}$$

where V_s is the molar volume of the deposited solid S

2.3- Boundary conditions

At the pore entrance, the concentration c_i is assumed to be constant and controlled

by the phenomena occurring outside the pore

$$c_i(0,t) = c^\circ_i \tag{10}$$

At the center of the pore, the symmetry assumes

$$\left[\frac{\partial c_i}{\partial z} \right]_{z=L/2} = 0 \tag{11}$$

$$\left(\sum_j N_j \right)_{L/2} = 0 \tag{12}$$

2.4- Solving method

A first iterative procedure, performed with a constant initial diameter $\Phi(z, 0) = \Phi_0$, results in the first steady state, i.e. the first concentration profile c_i (z, 0). The total molar flux $\sum_j N_j$ (z, 0) is calculated for this initial pore by summing equation (7) over all the chemical species. The diffusion coefficients D_i(z, 0), which depend on the pore diameter Φ and the concentration c_i, are calculated according to (8). Then, by solving successively equations (7) and (9), the new profiles of concentration $c_i(z, t_1)$ and of pore diameter $\Phi(z, t_1)$, are obtained. On the basis of these values of c_i and Φ, the previous calculation procedure is performed again. This procedure is stopped when the pore entrance is closed (i.e. $\Phi(0, t) = 0$). The differential equations are solved with a numerical method using finite differences.

3- SIMULATION RESULTS

The model, which is available for any chemical system and kinetic law, can be applied to the deposition of SiC from CH_3SiCl_3 (MTS)/H_2 precursor, according to the overall heterogeneous equation :

$$CH_3SiCl_{3(g)} \text{ ------> } SiC_{(s)} + 3HCl_{(g)} \tag{13}$$

Up to now, the chemical mechanism involved in this CVD system is not yet totally clarified [20-23]. As a consequence, a simplified chemical model, assuming a reaction

order of one with respect to CH_3SiCl_3, is introduced in the computation procedure. The kinetic law, taken from Schoch et al., is chosen as follows [24] :

$$\vartheta = k_0 \exp(-E/(\boldsymbol{R}T))\, c_{MTS} \qquad (14)$$

with $k_0 = 49\ ms^{-1}$ and $E = 225\ kJ\ mole^{-1}$

A first validation was made by comparing the results obtained from the present model to those of the Rossignol model [4]. The deposition profiles were found to be similar, with only a slight shift towards a less homogeneous infiltration for the Rossignol model. This shift could be attributed to the Rossignol hypothesis of a cylindrical pore with a diameter equal to the entrance diameter (i.e. always lower than the actual average diameter), which results in an over-estimated aspect ratio L/Φ and a worse infiltration profile.

3.1- Deposition profiles

The results of the simulation are presented as deposit thickness profiles in a half pore at the end of the densification process, i.e. when the pore entrance is closed.

Figure 1 shows the influence of temperature on the calculated profiles, for a total pressure of 20 kPa , an initial pore diameter of 100µm and an initial aspect ratio of 100. The infiltration should be homogeneous at 800°C, while at 1100°C the model foresees only a very thin deposit at the center of the pore. This result is qualitatively similar to those presented in previous work [4, 10, 25].

The influence of total pressure is shown in figure 2 for a temperature of 950°C and the same pore geometry. A decrease of the total pressure from 100 kPa to 10 kPa should drastically improve the infiltration homogeneity (as previously reported), but a further decrease should not be very usefull. This latter feature can be explained by assuming that, as the pressure decreases, the mass transfers occur more and more by Knudsen diffusion and the effect of pressure on (i) the reaction rate and (ii) the diffusive mass transfer are balanced.

The deposit thickness is drawn in figure 3 as a function of the reduced infiltration depth (i.e. z/L) for various values of the initial aspect ratio L/Φ_0, a temperature of 950°C, a total pressure of 0.1 kPa and an initial diameter of 100µm. The results of the calculations show a rapid improvement of the deposition profile as L/Φ_0 decreases and a very homogeneous infiltration for an aspect ratio of 10. In figure 4, the deposition profiles are shown as reduced thickness $(\Phi_0 - \Phi)/2\Phi_0$ versus reduced depth (z/L) for

various initial pore sizes, a temperature of 1000°C, a total pressure of 20 kPa and an initial aspect ratio of 100. The model predicts a better infiltration for small pores.

The influence of the geometry of the pore, presented in figures 3 and 4, was not studied in previous work. It can be analysed on the basis of the Thiele modulus, which results from the analytical solution of mass balance equations in the case of a reaction order of one [17]. The concentrations within the pore are more homogeneous with a smaller Thiele modulus, which is defined as :

$$\sqrt{\frac{kL^2}{D\Phi_0}} = \frac{L}{\Phi_0}\sqrt{\Phi_0}\sqrt{\frac{k}{D}} \qquad (15)$$

where k is the kinetic rate constant of the deposition reaction. Equation (15) describes, besides the chemical, k, and physical, D, kinetic factors, two geometrical parameters : (i) the aspect ratio L/Φ_0 with a constant diameter and (ii) the diameter Φ_0 with a constant aspect ratio. The Thiele modulus is decreased, i.e. the infiltration is better, when (i) L/Φ_0 is decreased, as reported in figure 3, and (ii) Φ_0 is decreased, as observed in figure 4. The latter result is not valid under conditions of Knudsen diffusion which results in removing the factor $(\Phi_0)^{1/2}$ (for small pore diameters $\leq$ 1 µm).

3.2- HCl concentrations

HCl is a species produced in the overall reaction of SiC deposition from CH_3SiCl_3/H_2 precursor (equation 13). The HCl concentration can be an important parameter in the deposition kinetic law, HCl reacting probably as inhibitor. Even if it is not yet introduced in the experimental kinetic law, it was interesting to assess its occurrence within the pore. The present model permits to calculate its concentration profile for various infiltration conditions at any stage of the densification.

Table 1 shows the influence of temperature on the HCl reduced concentration (i.e. $C_{HCl}(z)/C_{MTS}(0)$) at the center of the pore (z = L/2) before closing the pore entrance (e.g. for t = 0.75 t_c, where t_c is the closing time).

This concentration increases with the infiltration temperature, which is a probable consequence of the thermal activation of the chemical reaction kinetics.

HCl reduced concentration rises also with increasing total pressure, as shown in table 2. This result can be explained by assuming that, during the densification, HCl molecules are less easily evacuated from the pore at relatively high pressures, because

of a steeper deposit gradient close to the entrance. Thus, there would be a greater accumulation effect as total pressure increases.

The influence of the pore diameter at a constant value of the aspect ratio, (L/Φ_0 = 100), a temperature of 1100°C, a total pressure of 20 kPa and a time $t = 0.75\ t_c$, is shown in table 3. When the pore diameter decreases from 100 µm to 10 µm, the HCl reduced concentration decreases, which is probably due to the better deposit profile decreasing the accumulation effect. From 10 µm to 1µm, the occurrence of Knudsen diffusion cancels the influence of the pore diameter on the infiltration profile and results in a constant HCl reduced concentration.

From a general point of view, the previous calculations suggest that the quality of the infiltration profile in the cylindrical pore is improved when the reduced concentration of HCl produced within the pore is decreased.

4- EXPERIMENTAL RESULTS - DISCUSSION

4.1- Preparation of the model pores

The preparation route, used to obtain straight cylindrical pores, starts with cylindrical SiC-based CVD filaments (*), which are made of (i) a carbon core (32 µm in diameter), (ii) a pyrocarbon coating (about 2 µm in diameter) and (iii) a 53 µm SiC-deposit. Pieces of these filaments 1 cm in length were subjected to a controlled oxidation at 800°C in air for about 100 h, which resulted in the consumption of the carbon core and pyrocarbon film, leaving a microscopic tube with an inner diameter of 34 µm. These samples were briefly characterized by optical and scanning electron microscopy (SEM) and the pores found to be very regular, with a smooth inner surface (fig. 5). Several of these unitary tubes were sealed together and hung in a CVD/CVI reactor with the direction of the pores axis being perpendicular to the gas flow.

4.2- CVI experiments

The infiltration experiments were carried out in a hot wall CVI-apparatus heated by r.f. induction. The deposition chamber is a vertical cylindrical tube favorable to a laminar flow, with a large hot isothermal zone, coupled to a sensitive microbalance.

(*) SCS-2 from AVCO

It has been described in more detail elsewhere [26]. It is equipped with accurate controlling systems for the regulation of temperature, total pressure and flow rates. Due to its liquid state under the standard conditions, MTS is transported by bubbling the carrier gas H_2 in a bubbler vessel at a constant temperature. A good control of the MTS gas flow needs some additional devices, which are described in another paper [23].

4.3- Experimental profiles

The first experimental investigation dealt with the influence of temperature on the actual deposition profile in the model pores described above. The CVI experiments were performed during a sufficiently long time to close the pore entrances. The thickness profiles were determined by SEM observations on fracture sections operated at various levels in the model micropores. Figure 6 shows two profiles for two temperatures, a total pressure P = 20 kPa, an α ratio $P_{H2}/P_{MTS} = 5$ and a total flow rate Q = 100 sccm. The infiltration is found better at 950°C than at 1100°C which is consistent with the theoretical results (fig. 1). Nevertheless a marked thickness gradient is observed close to the pore entrance, over about 1 mm, and hereafter the profile is rather flat.

A comparison between theoretical and experimental deposition profiles is shown in figure 7. The deviation of the experimental profile with respect to the calculated profile could be explained by HCl which is concentrated within the pore as calculated above (cf. 3.2) and acts as an inhibitor (it should be recalled that HCl was not present in the kinetic law, cf equation 14, used in the present calculations). This would be consistent with a kinetic law for the SiC deposition process involving a negative order with respect to HCl species. The large amount of HCl in the pore can influence not only the kinetics of the deposition (i.e. the infiltration profile), but also the chemical composition of the deposit (e.g. a pure SiC deposit could occur as well as SiC + Si or SiC + C codeposits depending on the position in the pore). Further experiments on these model pores as a function of time, total pressure and initial composition, including chemical analysis of the deposits, are in progress to validate the present model, which should be eventually run with more realistic kinetic laws.

ACKNOWLEDGEMENTS

The authors wish to thank Dr C. Prébendé for his valuable advice, especially for the experimental CVD investigations. This work was financially supported by EEC

(EURAM Program, contract n° MAIE/0018/C) as well as by Educational French Ministry (MENJS) and SEP via a grant to R. Fedou.

REFERENCES

1- F. CHRISTIN, R. NASLAIN and C. BERNARD, Proc. 7th Int. Conf. CVD (T.O. Sedwick and H. Lydtin, eds.), The Electrochem. Soc., Princeton (1979) 499-514

2- E. FITZER, D. HAGEN and J. STROHMEIER, Rev. Int. Hautes Temper. Refract., **17** (1980) 23

3- H. HANNACHE, F. LANGLAIS and R. NASLAIN, Proc. 5th European Conf. CVD (J.O. Carlson and J. Lindström, eds.), Uppsala (1985) 219-233

4- J.Y. ROSSIGNOL, F. LANGLAIS and R. NASLAIN, Proc. 9th Int. Conf. CVD (Mc D. Robinson et al., eds.), The Electochem. Soc., Pennington (1984) 596-514

5- H. HANNACHE, R. NASLAIN and C. BERNARD, J. Less-Common Met., **95** (1983) 221

6- R. COLMET, I. LHERMITTE-SEBIRE and R. NASLAIN, Adv. Ceram. Mater., **138**/2 (1986) 221

7- J. MINET, F. LANGLAIS and R. NASLAIN, Composites Sci. Technology, **37** (1990) 79-107

8- E.W. THIELE, Ind. Eng. Chem., **31**/7 (1939) 916

9- E.E. PETERSEN, A.I. Ch. E. Journal, **3**/4 (1957) 443

10- E. FITZER and R. GADOW, Am. Ceram. Soc. Bull, **65** (1986) 326

11- C.H.J. VAN DEN BREKEL, R.M.M. FONVILLE, P.J.M. VAN DER STRATEN and G. VERSPUI, Proc. 8th Int. Conf. CVD (Blocher J.M. et al., eds.), The Electrochem. Soc., Pennington (1981) 142-156

12- M.F. CAROLAN and J.N. MICHAELS, Solid State Ionics, **25** (1987) 207

13- Y.S. LIN, K.J. DE VRIES and A.J. BURGGRAAF, Proc. 7th European Conf. CVD (M. Ducarroir et al., eds.), Les Editions de Physique, Colloque C5, supplément au n° 5, **50** (1989) 861-872

14- T.L. STARR, Proc. Int. Conf. on Whisker-and Fiber-Toughened Ceramics (R.A. Bradley et al., eds.) ASM International, Oak Ridge (1988) 243-252

15- S.M. GUPTE and J.A. TSAMOPOULOS, J. Electrochem. Soc. **136** (1989) 555

16- N.H. TAI and T.W. CHOU, J. Am. Ceram. Soc., **72** (1989) 414

17- S. MIDDLEMAN, J. Mater. Res., **4** (1989) 1515

18- R.B. BIRD, W.E. STEWART and E.N. LIGHTFOOT, Transport Phenomena, J. Wiley and sons, New York (1960)

19- P.C. CARMAN, L'écoulement des gaz à travers les milieux poreux, traduit par J. Machefer, P.U.F. (19361)

20- G.S. FISCHMAN and W.T. PETUSKEY, J. Am. Ceram. Soc., **68** (1985) 185

21- M.E. ALUKO, Proc. First Int. Conf. on Amorphous and Crystalline Silicon Carbide, G.L. Harris and C.Y.-W. Yang, eds.,Springer-Verlag, Berlin/Heidelberg (1989) 51

22- C. PREBENDE, F. LANGLAIS, R. NASLAIN and C. BERNARD, submitted to J. Electrochem. Soc.

23- C. PREBENDE, F. LANGLAIS and R. NASLAIN, submitted to J. Electrochem. Soc.

24- G. SCHOCH, W. FRITZ and E. FITZER, Techn. Rept., EURAM Contract MAIE/ 0018/C (1988)

25- R. NASLAIN, F. LANGLAIS and R. FEDOU, J. Physique, Colloque C5, **50** (1989) 191-207

26- F. LANGLAIS, C. PREBENDE and C. BERNARD, accepted for publication in J. Crystal Growth

TEMPERATURE (°C)	REDUCED HCl CONCENTRATION at z = L/2
1100	1.30
1000	1.12
900	0.87
850	0.76
800	0.65

Table 1 : Reduced HCl concentration at z = L/2 calculated for various temperatures under the following conditions Φ_0 = 100 µm, L/Φ_0 = 100, P = 20 kPa and t = t_c

PRESSURE (kPa)	REDUCED HCl CONCENTRATION at z = L/2
100	0.96
50	0.76
20	0.52
2	0.20
0.2	0.15

Table 2 : Reduced HCl concentrations (at z = L/2) for various total pressures calculated under the following conditions Φ_0 = 100 µm, L/Φ_0 = 100, T = 900°C and t = 0.75 t_c

DIAMETER (μm)	REDUCED HCl CONCENTRATION at z = L/2
100	1.35
10	1.16
1	1.16

Table 3 : Reduced HCl concentration at z = L/2 calculated for various pore diameters under the following conditions $L/\Phi_0 = 100$, T = 1100°C, P = 20 kPa and $t = t_c$

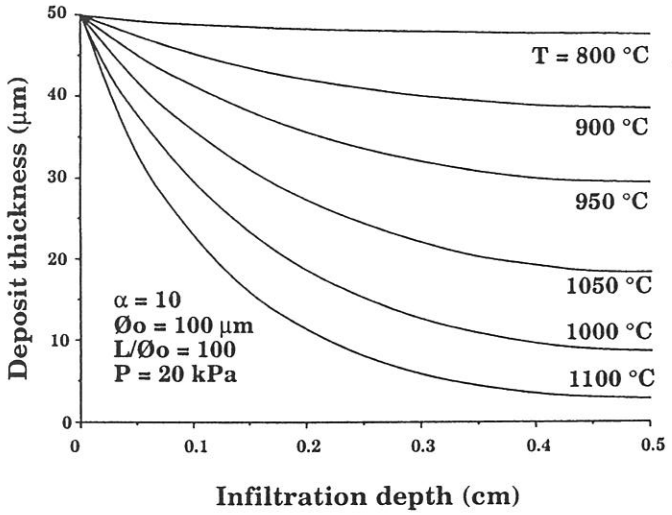

Fig. 1- Influence of temperature on the calculated thickness profiles of deposits obtained from a mixture of MTS and hydrogen

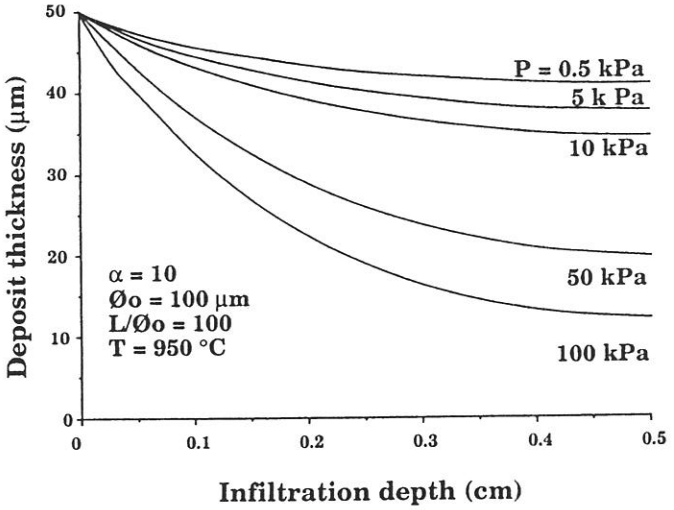

Fig. 2- Influence of total pressure on the calculated thickness profiles of deposits obtained from a mixture of MTS and hyrogen

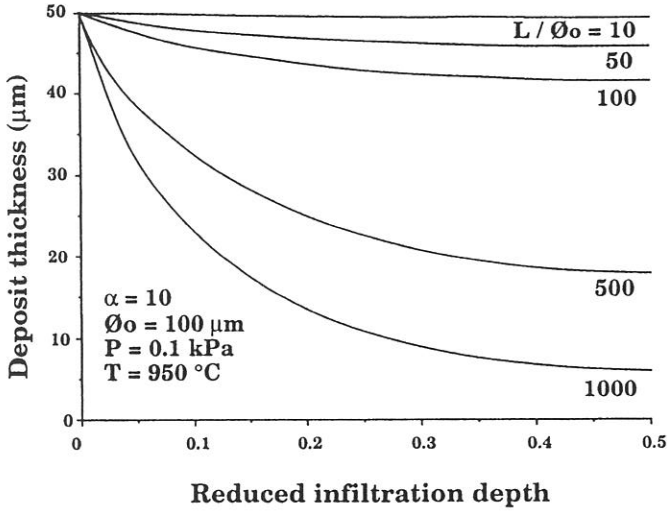

Fig. 3- Influence of the aspect ratio $L/Ø_o$ on the calculated thickness profiles of deposits obtained from a mixture of MTS and hyrogen

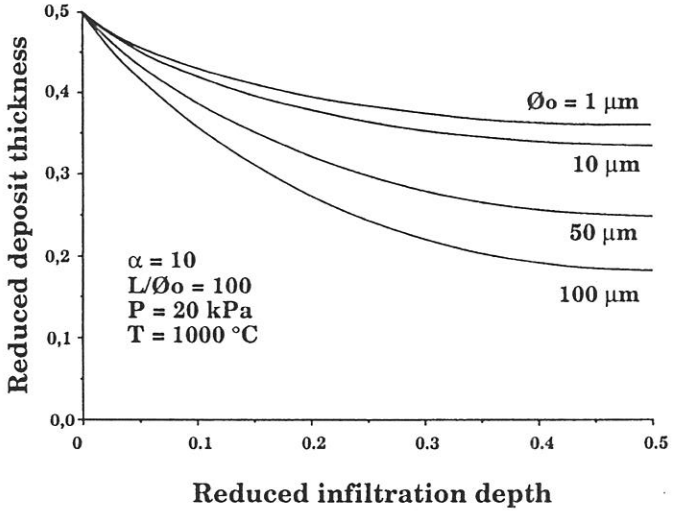

Fif. 4- Influence of the diameter $Ø_o$, with $L/Ø_o$ being constant, on the calculated thickness profiles of deposits obtained from a mixture of MTS and hydrogen

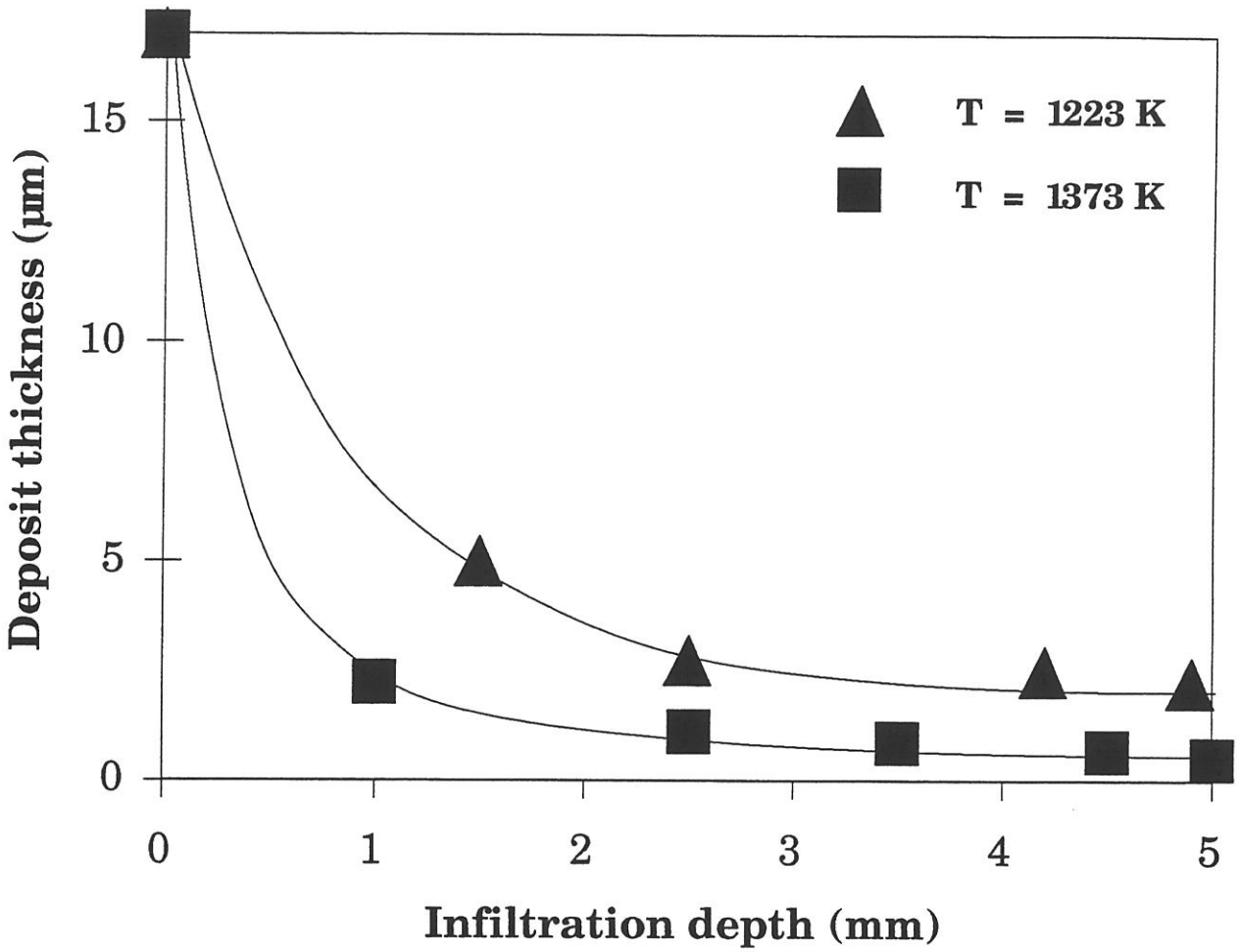

Fig. 6- Experimental thickness profiles of a SiC-based deposit measured in a cylindrical pore open at both ends for the following conditions : Φ_0 = 34 µm, L = 1 cm, P = 20 kPa, $\alpha = P_{H2}/P_{MTS}$ = 5, Q = 100 sccm

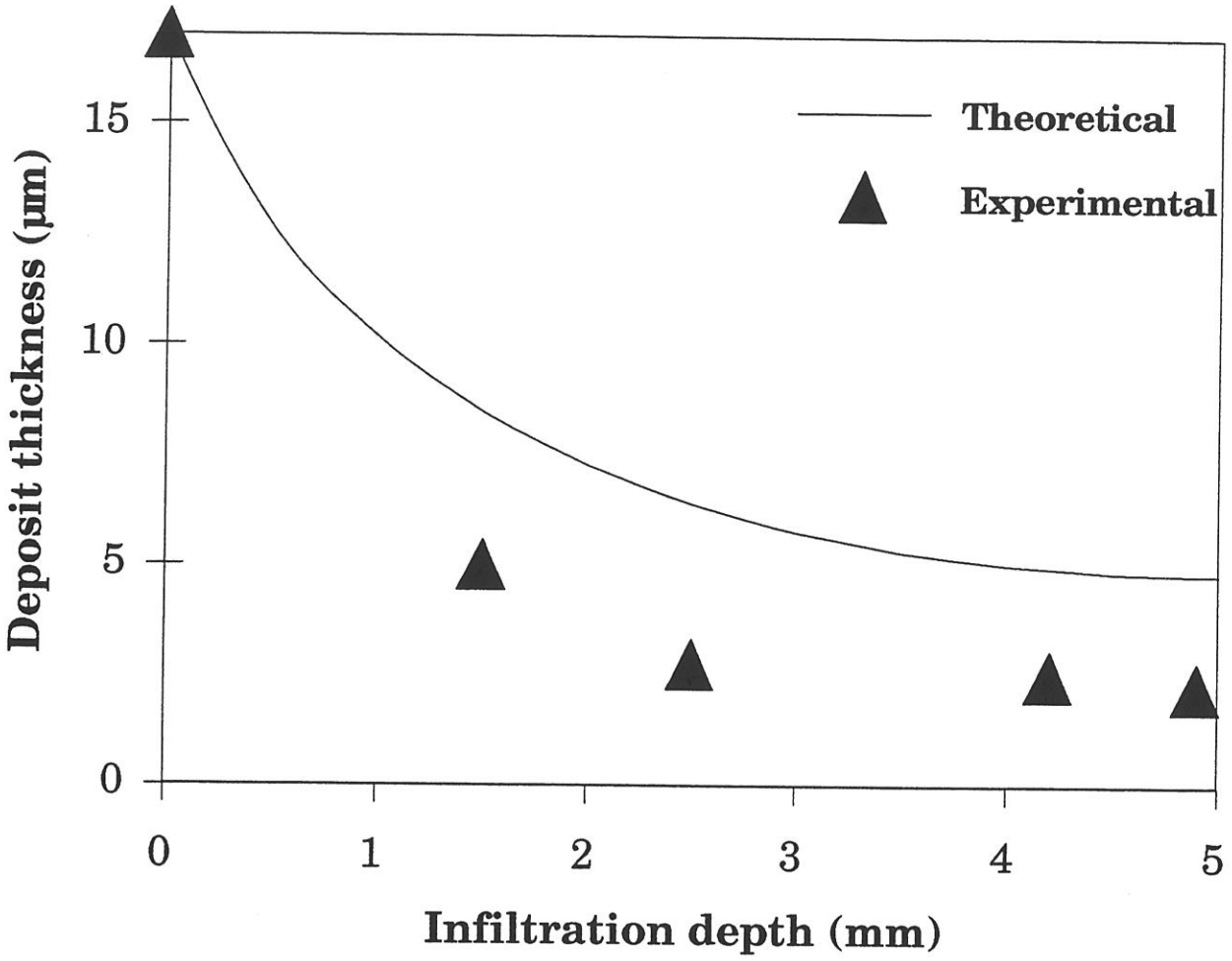

Fig. 7- Comparison between calculated (solid line) and experimental thickness profiles of a SiC-based deposit obtained under the following conditions : T = 950°C, P = 19 kPa, $\alpha = P_{H2}/P_{MTS} = 5$, Q = 100 sccm